Motile Cilia Dysfunction: Characterising Zebrafish *prpf8* and *pierce1/pierce2* Mutants with Left/Right Axis Defects

A thesis submitted to the University of Manchester for the degree of Doctor of Philosophy in the Faculty of Biology, Medicine and Health

2022

Dale W Maxwell

School of Biological Sciences, Division of Evolution, Infection and Genomics

Contents

Word count = 57480

List of Figures

List of videos

Video 3.1 - WT KV Motile Cilia

Video 3.2 - *cph* KV Motile Cilia

Video 3.3 - WT KV GFP Motile Cilia

Video 3.4 - cph KV GFP Motile Cilia

Video 3.5 - WT Pronephric Duct Motile Cilia

Video 3.6 - cph Pronephric Duct Motile Cilia (15fps)

Video 3.7 - cph GFP Pronephric Duct Motile Cilia (15fps)

Video 3.8 - WT Otic Vesicle Motile Cilia

Video 3.9 - cph Otic Vesicle Motile Cilia

Video 3.10 - Prpf8 Cilia Co-localisation Z Stack

Video 4.1 - tbMO KV Motile Cilia

Video 4.2 - tbMO KV Motile Cilia With Tracked Particle

Video 4.3 - tbMO Pronephric Duct Motile Cilia

Video 4.4 - tbMO Nasal Placode Motile Cilia

Video 5.1 - p1p2 Knockout KV Motile Cilia

Video 5.2 - p1p2 Knockout p1 Rescue KV Motile Cilia

Video 5.3 - p1p2 Knockout p2 Rescue KV Motile Cilia

Video 5.4 - p1p2 Knockout Pronephric Duct Motile Cilia

Video 5.5 - p1p2 Knockout Nasal Placode Motile Cilia

List of Abbreviations

aa : Amino Acid

adRP : Autosomal Dominant Retinitis Pigmentosa

A-P : Anterior - Posterior

Arf : ADP-ribosylation factor

BBS : Bardet-Biedl Syndrome

BMP : Bone Morphogenic Protein

BSA : Bovine Serum Albumin

Ca^{2+} : Calcium ion

Cerl2: Cerberus-like protein 2

CHD : Congenital Heart Disease

CNS : Central Nervous System

cph : Cephalophŏnus

dpf : Days Post Fertilisation

ENU: N-ethyl-N-nitrosourea

FGF: Fibroblast growth factor

Foxj1: forkhead box j1

GDP : Guanine Di-Phosphate

GFP: green fluorescent protein

GTP : Guanine Tri-phosphate

Hh : Hedgehog

hpf : Hours Post Fertilisation

IF : Immunofluorescence

IFT : Intraflagellar Transport

Igu : Iguana

iPSC : Induced Pluripotent Stem Cell

KV : Kupffer's Vesicle

L/R : Left/Right

Lft1 : Lefty1

Lft2 : Lefty2

LPM : Lateral Plate Mesoderm

mNEC : Mouse Nasal Epithelial Cells

mz : Maternal Zygotic

PBDT : PBS BSA DMSO Triton-X

PBS : Phospho buffered Saline

PBT : PBS Triton-X

PCD : Primary Cilia Dyskinesia

PCP : Planar Cell Polarity

PCR : Polymerase Chain Reaction

PFA : Paraformaldehyde

Pitx2: pituitary homeobox 2

Pkd2: polycystin 2

PRPF : Pre-mRNA Processing Factor

Ptc1 : Patched1

PTW : PBS Tween

qPCR : Quantitive Polymerase Chain Reaction

RA: Retinoic Acid

RNAi : Ribonucleic Acid Interference

RNP: Ribonucleoprotein

RP : Retinitis Pigmentosa

RPE : Retinal Pigment Epithelium

RT-PCR : Reverse Transcription Polymerase Chain Reaction

s : Somite

sbMO : Splice Blocking Morphant

Shh : Sonic Hedgehog

Smo : Smoothened

snRNA: small nuclear RNA

snRNP: small nuclear ribonucleoprotein

Spaw : Southpaw

SS : Splice Site

tbMO : Translation Blocking Morphant

TBS : Tris Buffered Saline

TEM : Transmission Electron Microscopy

US : Usher Syndrome

UTR : Un-Translated Region

WISH : Whole Mount in situ Hybridisation

WT : Wild Type

Abstract

The vast majority of multicellular eukaryotes show some form of symmetry, whether this be radial or bilateral. In vertebrates, bilateral symmetry is apparent at the whole organism level, however internal organs have a defined left and right sidedness in placement and internal symmetry. In mammals, the left/right body axis is defined early in development in an organ called the Embryonic Node. The analogous laterality organ is the Kupffer's Vesicle in teleost fish. In this project I characterise two zebrafish mutants which exhibit defects in laterality establishment; one which contains a premature stop codon in the spliceosomal gene *prpf8* and another which contains null mutations in *pierce1* and *pierce2*, two genes with currently unknown function.

Preliminary investigations into these *prpf8* and *pierce1*/2 mutants observed a high percentage of unlooped hearts, indicative of problems in left/right axis formation. I investigated Kupffer's Vesicle to determine whether the cilia in this structure are present and functional. Subsequently, I examined key laterality marker genes to elucidate the downstream effects on cardiac laterality caused by the KV cilia perturbation. Additionally, for the *prpf8* mutant fish I investigated why mutation of a protein involved in the key processes of splicing would have such detrimental effects on cilia morphology and function by examining Prpf8 protein localisation in both *prpf8* mutant and Prpf8 knockdown fish models. My findings indicate that Prpf8 plays a significant role in ciliogenesis, with mutants and knockdowns exhibiting global cilia defects. The reason for this, as of yet, is still unclear. However, I present strong preliminary data that show prpf8 localises to cilia axonemes, suggesting a direct mechanism for Prpf8-cilia protein interaction. In contrast, I also present data showing an increase in mis-splicing of *arl13b*, a critical cilia gene, in multiple Prpf8 mutant models, suggesting a more indirect, spliceosomal role for Prpf8 in causing cilia dysfunction.

With regard to the *pierce1/pierce2* double mutant, I show that loss of both these proteins is critical for cilia motility in the KV, and that rescue of either one of the genes rescues cilia motility and restores correct heart looping directionality.

This project has wide reaching implications on the understanding and possible diagnosis of a range of conditions including heterotaxy related congenital heart disease as well as primary cilia dyskinesia and Retinitis Pigmentosa.

Declaration

No portion of the work referred to in the thesis has been submitted in support of an application for another degree or qualification of this or any other university or other institute of learning

Copyright Statement

i. The author of this thesis (including any appendices and/or schedules to this thesis) owns certain copyright or related rights in it (the “Copyright”) and s/he has given the University of Manchester certain rights to use such Copyright, including for administrative purposes.

ii. Copies of this thesis, either in full or in extracts and whether in hard or electronic copy, may be made only in accordance with the Copyright, Designs and Patents Act 1988 (as amended) and regulations issued under it or, where appropriate, in accordance with licensing agreements which the University has from time to time. This page must form part of any such copies made.

iii. The ownership of certain Copyright, patents, designs, trademarks and other intellectual property (the “Intellectual Property”) and any reproductions of copyright works in the thesis, for example graphs and tables (“Reproductions”), which may be described in this thesis, may not be owned by the author and may be owned by third parties. Such Intellectual Property and Reproductions cannot and must not be made available for use without the prior written permission of the owner(s) of the relevant Intellectual Property and/or Reproductions.

iv. Further information on the conditions under which disclosure, publication and commercialisation of this thesis, the Copyright and any Intellectual Property and/or Reproductions described in it may take place is available in the University IP Policy (see http://documents.manchester.ac.uk/DocuInfo.aspx?DocID=2442 0), in any relevant Thesis restriction declarations deposited in the University Library, the University Library’s regulations (see http://www.library.manchester.ac.uk/about/regulations/) and in the University’s policy on Presentation of Theses.

Acknowledgements

First and foremost, my biggest thanks go to my supervisor Dr Kathryn Hentges. Thank you, Kathy, for always being supportive and optimistic even when my experiments were continually failing. Thank you for always having your office door both physically and metaphorically open and taking the time to listen to my silly questions or frustrated rants. I don't think I could have completed this PhD without you as my supervisor. Finally thank you for laughing when I told you I accidentally sacrificed the male mouse and thought my PhD was over.

I would also like to convey a huge amount of gratitude to my co-supervisor Prof Sudipto Roy. Sudipto, you continually pushed me to be a better scientist both in terms of laboratory expertise as well as in mindset. Thank you for encouraging me to do more than I thought I could. The time I spent in your lab in Singapore was the highlight of my PhD. I'm still not convinced the universe doesn't physically exist though.

I would also like to thank my other co-supervisor Prof Raymond O'Keefe. Ray, thank you for letting me borrow your restriction enzymes in times of need. I'd also like to thank you for being especially friendly and approachable whether it be to talk about confusing results or just for a general chat.

A special mention goes to Dheeraj, Qiu Tao, Lucy, Hui Li, Lu Hao, Charlie, Yan Ling, Stelios, Caroline and all other members of the Roy lab who made my time working there a positive and fun experience. I wouldn't have remained sane without you.

Additionally, I'd also like to thank Wasay, Huw and Katherine for their continued technical expertise, support and friendship over these last four year.

I cannot convey my thanks enough to all members of the Singapore Wanderers Rugby Club. Thank you for providing me with a release for my stress each Tuesday, Thursday and Saturday. Thank you for always being available for a beer no matter the time or place. I can honestly say the two years spent playing and socialising with you lot made my PhD a much more bearable undertaking. Though, I'm still recovering from that one Suffer Saturday I did.

Penultimately, I'd like to thank my family for their support throughout this project. Thank you for always picking up the phone to listen to me complain or ask questions I could've Googled. Thank you paying for my drinks in bars I couldn't afford in Singapore.

Finally, I owe a huge thanks to my partner Alicia. Thank you for pulling me over to your table at the 1st year postgrad ball. Thank you for putting up with me being 6000 miles away for two years and only seeing each other through a phone for one of those years. This PhD would have been a lot duller without you doing it by my side. Most importantly, thank you for always letting me have the last McNugget.

This thesis is dedicated to the memory of my grandpa,

Alan Brown,

who never got to see me start my PhD, but would be immensely proud to see me finish it.

Chapter 1: Introduction

1.1 Establishment of the Left/Right Axis

Bilaterally symmetric organisms account for around 99% of all animals (Finnerty, 2005). Animals that exhibit bilateral symmetry tend to be externally symmetric on the sagittal plane, dividing the body down the middle into the left and right, with one of each pair of limbs or sensory organs being on either side. Parts of the anatomy that do not come in pairs, such as the nose and mouth, are placed on the midline and thus still exhibit bilateral symmetry. However, on the inside, it is more complex. Most internal organs are asymmetric, either being placed on the left or right side of the body e.g. the heart or liver respectively. Organs that do form in the centre tend to be asymmetric in themselves e.g. the stomach and lungs (Gee, 1998). Although the internal body plan is asymmetric, organogenesis still relies on the precise establishment of the overall left/right (L/R) axis for correct development of asymmetric organs as well as their correct placement within the organism.

Due to this innate need for developing organs to a have pre-defined left and right, establishment of the L/R axis is one of the earliest events in embryo development. *Situs solitus* is the term used to describe the canonical development of the L/R axis, however errors in establishment of the L/R axis can lead to a myriad of organ *situs* defects. One such defect is the absolute mirroring of the usual body plan, where the left is now the right and vice versa. This condition is known as *situs inversus totalis* and surprisingly, when occurring as an isolated condition, does not lead to further health issues (NIH, 2015; Blum and Ott, 2018). Conversely, *situs ambigus,* also referred to as heterotaxy, is the term used to describe the random placement of the organs in regards to their L/R positioning. This condition may result from a proportion of the organs displaying mirrored L/R axis placement in comparison to the rest of the organism, or indeed parts of an individual organ being mirrored while the rest of the organ maintains correct L/R orientation. Unlike *situs inversus totalis*, *situs ambigus* is associated with a multitude of further health complications, one of the most common being congenital heart disease (CHD) (Ramsdell 2005; Kathiriya 2000). CHD is the most common cause of non-infectious neonatal death (Hoffman and Kaplan, 2002). Defects in the establishment of the L/R axis are corelated with a significantly increased risk of developing CHD, with 3% of all CHD cases resulting from heterotaxy (Zhu et al., 2006). Furthermore, 30% of deaths are associated with heterotaxy linked CHD, making it one of the most severe forms of CHD (Bowers et al., 1996).

The mechanism behind the establishment of the L/R axis was unknown up until a few decades ago when a ciliated structure termed the node was discovered in mouse embryos (Sulik et al., 1994; Bellomo et al., 1996). Surgical or genetic ablation of this pit resulted in the development of severe L/R axis defects (Ang and Rossant, 1994; Davidson et al., 1999). The node is a concave pit of cells in which anticlockwise (when viewed dorsally) fluid flow is proposed to be the factor that breaks the L/R symmetry (Nonaka et al., 1998; Hamada, 2016). This anticlockwise fluid flow has been shown to be critical for correct

establishment of the L/R axis as its removal causes the randomisation of the L/R axis, with artificial reversal of this fluid flow causing situs inversus (Nonaka et al., 2002). The mechanism behind the breaking of L/R symmetry can be dissected into 3 main phases; establishment of the anticlockwise flow, sensing the fluid flow, and transfer of this asymmetry into the lateral plate mesoderm (LPM) (Hamada, 2016).

Within the node cavity, each cell has a long single motile cilium (see 1.1) which beats radially in an anticlockwise direction, thus producing the anticlockwise fluid flow (Nonaka et al., 1998). Indeed, nodal fluid flow was disrupted in mouse mutants for key motile cilia genes, causing defects in L/R axis establishment (Okada et al., 1999; Watanabe et al., 2003). The role for motile cilia in the production of nodal fluid flow is also conserved to humans as conditions such as Kartagener Syndrome, which results from a loss of functional cilia, frequently presents with L/R axis defects (Norris and Grimes, 2012). These motile monocilia within the node are located at the posterior of each cell and also possess a slight tilt towards to posterior of the node. This localisation and tilt of the motile cilia within the node has been proposed to be regulated by the planar cell polarity (PCP) pathway (Nonaka et al., 2005) with defects in this pathway resulting in L/R axis defects (Mahaffey et al., 2013). These findings demonstrate that motile cilia anticlockwise rotational beating as well as correct localisation and tilt are required to produce the anticlockwise fluid flow necessary for correct L/R axis establishment.

As well as the motile radially beating cilia at the base of the cavity within the node, there are also non-motile primary cilia which extend from the crown cells surrounding the pit. Recent studies suggest that these immotile primary cilia act as the sensors of fluid flow within the node (Yoshiba et al., 2012). Indeed, Kif3a knockout mouse embryos, which lack all cilia, exhibited L/R axis defects. However when expression of Kif3a was restored to just the crown cell, resulting in formation of these non-motile primary cilia, the mouse embryos were able to respond to artificially induced fluid flow suggesting these cilia are required for sensing of flow (Takeda et al., 1999; Yoshiba et al., 2012).

There are two main models to explain how the nodal fluid flow is sensed. Firstly, it has been suggested that the embryos sense the fluid flow via the mechanical force of the fluid movement bending the primary cilia – termed the mechanosensory model. Secondly, that the fluid flow transports an unknown signalling molecule or morphogenic factor to the left side of the node thus setting up a gradient that may be sensed – termed the chemosensor model (Yoshiba and Hamada, 2014). In regards to the first model, the mechanical movement of the primary cilia due to the nodal flow has been proposed to induce a calcium (Ca^{2+}) increase within the crown cells. This increase in Ca^{2+} is then proposed to elicit a downstream signalling cascade which induces gene expression changes that define the left and the right. (McGrath et al., 2003). Indeed, the transmembrane Ca^{2+} channel protein Pkd2 is essential for correct L/R establishment and has been associated with the Ca^{2+} concentration spike on the left side of the node in

response to nodal fluid flow (Pennekamp et al., 2002; McGrath et al., 2003). Since Pkd2 is expressed in both node pit cells as well as in crown cells, its function in sensing fluid flow remained unclear. Work by Yoshiba et al. (2014) utilising a Pkd2 knockout mouse and systematically restoring Pkd2 expression to either the pit cells, crown cells or the whole node, found that restoration of Pkd2 to pit cells did not rescue normal L/R establishment. However, specifically restoring expression of Pkd2 in crown cells was sufficient to rescue correct L/R axis development. Furthermore, Pkd2 specifically localises to cilia within the node suggesting it plays a critical role in the sensing and thus Ca^{2+} response to nodal fluid flow (Norris and Grimes, 2012; Yoshiba and Hamada, 2014).

However, further work has failed to demonstrate a specifically left or right sided Ca^{2+} increase in response to fluid flow. Additionally, it has been demonstrated that mechanical movement of the primary cilia on crown cells is not sufficient to cause a Ca^{2+} response (Yoshiba and Hamada, 2014; Delling et al., 2016). These findings suggest that the Ca^{2+} concentration increase is not an immediate response to mechanosensing by primary cilia in crown cells and may point to an alternative mechanism for flow sensing. Indeed, the chemosensing model would explain why it only takes a very small number of rotating cilia for correct establishment of the L/R axis (Shinohara et al., 2012) as the force generated by such few motile cilia would be too weak to be sensed by primary cilia along the edge of the node. It was initially proposed that sonic hedgehog and retinoic acid filled vesicles within the node acts as the determinant for L/R asymmetry (Tanaka et al., 2005). However, currently no signalling molecule or morphogen involved in establishment of the L/R axis has been identified within the node (Hamada, 2020). How the anticlockwise fluid flow within the node is directly sensed is still inconclusive, however it is clear that the Pkd2 protein and the Ca^{2+} response play an indispensable role, possibly as intermediaries between flow sensing and downstream L/R gene expression targets (Yoshiba and Hamada, 2014; Delling et al., 2016; Hamada, 2020).

The downstream genetic target of this enigmatic signalling pathway is *Cerl2* (Schweickert et al., 2010; Shinohara et al., 2012). The presence of *Cerl2* mRNA is initially bilateral around the node, however becomes asymmetric with higher levels on the right side as anticlockwise fluid flow increases, with left sided *Cerl2* mRNA being degraded (Kawasumi et al., 2011)(Figure 1.1). *Cerl2* is the first gene to be asymmetrically expressed within the developing embryo and mouse mutants of *Cerl2* display randomisation of L/R axis establishment (Marques et al., 2004). Higher *Cerl2* expression on the right side of the node acts to inhibit the activity of NODAL on that side, possibly by inhibiting the formation of a NODAL:GDF1 heterodimer (Tanaka et al., 2007; Hamada, 2020).

NODAL is the fundamental molecule involved in the establishment of the L/R axis (Collignon et al., 1996). Initially, *Nodal* is expressed bilaterally but expression is eventually restricted to the left side of the node due to the inhibitory effects of CERL2 on the right. Left

sided expression of *Nodal* is involved in a positive feedback loop which further upregulates *Nodal* expression (Marques et al., 2004). The left sided expression of *Nodal* within the crown cells of the node then induces the expression of *Nodal* in the left Lateral Plate Mesoderm (LPM). The expression of *Nodal* in the LPM, in turn, causes the downstream expression of other L/R related genes (Saijoh et al., 2003). Mice which express *Nodal* on the right of the LPM exhibit *situs inversus* (Yokoyama et al., 1993). In order to restrict *Nodal* expression to the left LPM, NODAL induces the expression of *Lefty1* and *Lefty2* in the midline and left LPM respectively. LEFTY1 and LEFTY2 act as inhibitors of *Nodal,* ensuring *Nodal* expression remains asymmetrically expressed on the left (Burdine and Schier, 2000). As the expression of *Nodal* determines the left side of the embryo, mouse mutants which lack *Nodal* display right side isomerism, whereas mutants for *Lefty1*/2 display left isomerism as NODAL is able to diffuse across the midline resulting in bilateral expression (Meno et al., 1998, 2001; Shiratori and Hamada, 2006).

As *Nodal* is only expressed in a comparatively short developmental window (~6 hours) there must be other downstream genes that translate this biochemical breaking of symmetry into anatomical asymmetry. Of these downstream genes, one of the best characterised is *Pitx2.* PITX2 is a transcription factor required for the development of a multitude of organs, including the heart (Shiratori et al., 2001). Like *Nodal, Pitx2* is asymmetrically expressed on the left (Figure 1.2). Unlike *Nodal, Pitx2* expression persists until much later stages in development(Burdine and Schier, 2000). Absence of PITX2 results in defects in L/R organogenesis but, because PITX2 determines the left side of the organ, most viscera display right isomerism (Liu et al., 2001). Interestingly, mice that either lacked *Pitx2* expression completely or displayed symmetric *Pitx2* expression, did not exhibit alterations in heart looping directionality even though other laterality defects were present (Shiratori and Hamada, 2006).

Although the mechanism behind L/R establishment discussed so far has been in relation to mammals, there is considerable conservation of this laterality mechanism across all vertebrates (Hamada and Tam, 2014). The zebrafish equivalent of the mammalian node is Kupffer's Vesicle (KV) and is found at the posterior of the embryo in the developing tail bud at around 14 hours post fertilisation (hpf) (Essner et al., 2005). The outline of L/R axis establishment described above is almost identical for zebrafish, with the zebrafish equivalent of *Nodal* being *southpaw* (*spaw)* and equivalent of *Cerl2* being *dand5*. Additionally, the motile ciliated cells within the KV are clustered around the anterior of the pit rather than the posterior as in the mouse node (Hamada and Tam, 2014). The main difference between mouse and zebrafish models in terms of embryo laterality establishment is in the conversion from biochemical gene expression signals to organogenesis. In zebrafish *spaw* mutants, directional looping of the heart is somewhat unaffected suggesting this breaking of L/R symmetry in the heart is *spaw* independent (Noël et al., 2013). In

support of this hypothesis, work by Ocaña et al., (2017) proposes the bone morphogenetic protein (BMP) Prrx1 forms a right sided expression that controls heart asymmetry in zebrafish. The *prrx1* expression in the right LPM and the *spaw*/*pitx2* expression in the left LPM seem to function together resulting in reciprocal repression to control heart looping directionality in zebrafish (Hamada, 2020). This is in opposition to mouse data which shows *Prrx1* knockout does not affect heart asymmetry (Bergwerff et al., 2000). As stated, although there are finer differences between the establishment of asymmetric organogenesis in mouse and zebrafish models, the fundamental mechanism which establishes the L/R axis of the whole organism remains the same.

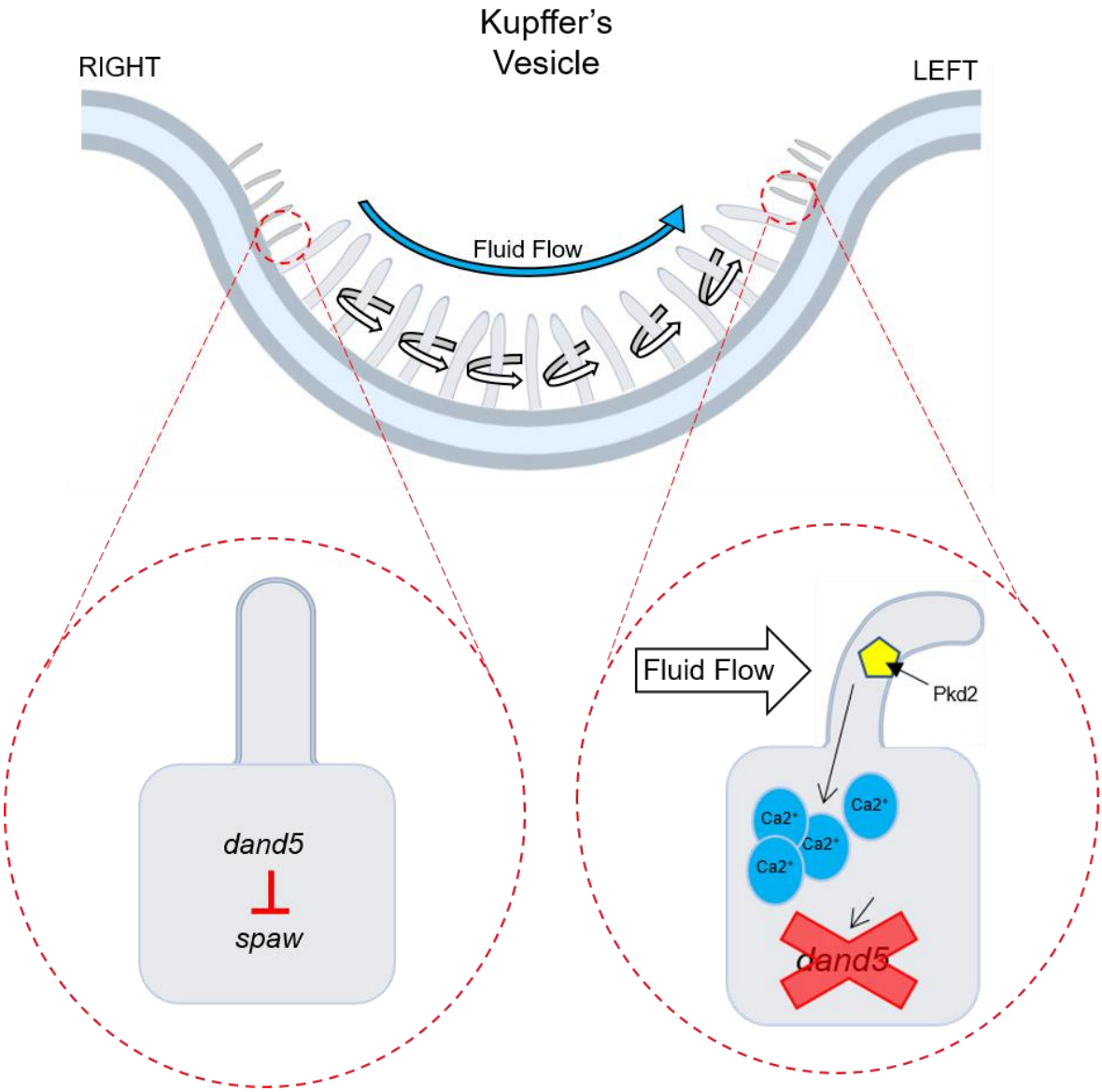

Figure 1.1: Anticlockwise Cilia Beating Generates KV Fluid Flow.
Diagram depicting the leftward fluid flow in the KV generated by anticlockwise (when viewed dorsally) beating of motile cilia. Fluid flow is sensed by immotile cilia, which then causes a calcium increase mediated by Pkd2. *dand5* mRNA is degraded on the left causing higher *dand5* expression on the right which inhibits *spaw*.

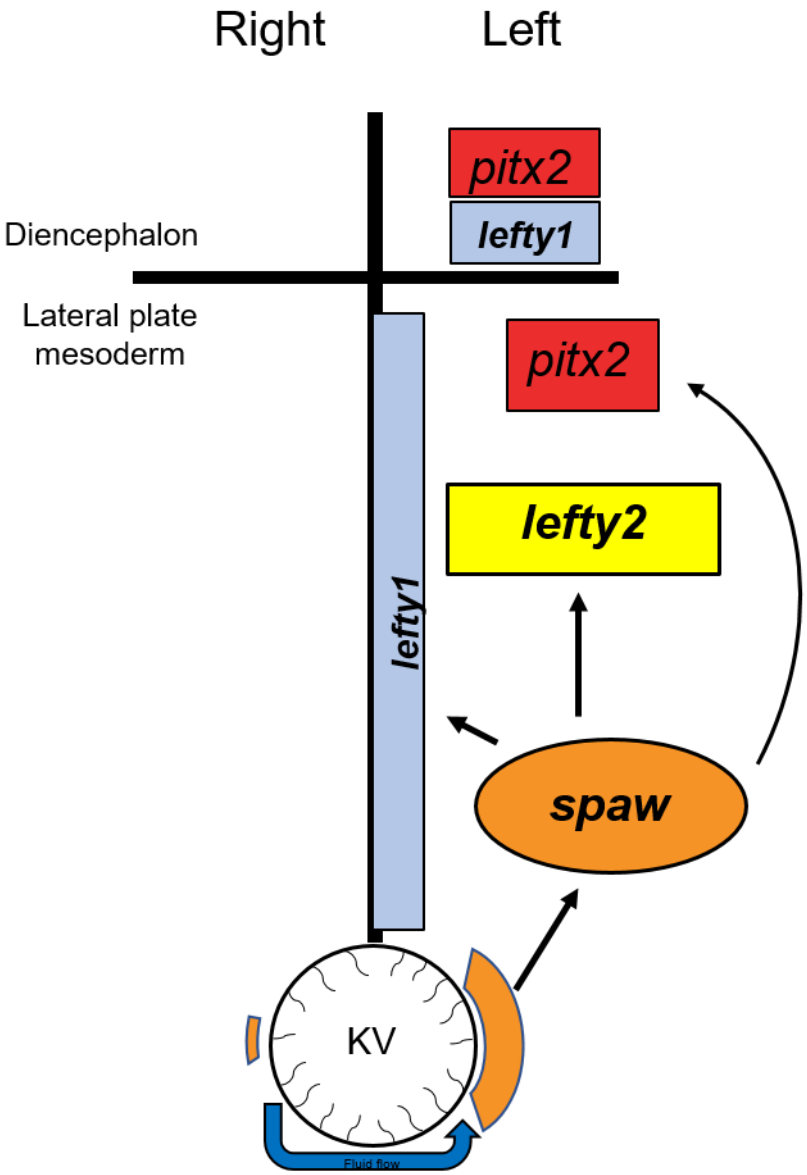

Figure 1.2: Expression Patterns of Genes Involved in Laterality Establishment
Diagram depicting the expression pathway of genes critical to the formation of the L/R axis. Un-inhibited *spaw* at the left of the KV induces left sided *spaw* expression in the LPM through an unknown mechanism. Spaw then induces the expression of *lefty1* in the midline and *lefty2* in the left heart precursor cells at the anterior of the LPM, thus restricting *spaw* to the left LPM. Spaw then induces *pitx2* in the left LPM and left diencephalon.

1.1.2 Looping of the Zebrafish Heart

By 48hpf the heart of a zebrafish is positioned on the left, however to get to this position correct jogging and looping of the heart must take place. At 19hpf heart precursor cells migrate and fuse forming a symmetrical cone down the midline of the developing embryo (Glicman Holtzman et al., 2007; Grant et al., 2017). As this cone rotates, the posterior end stretches and moves over to the left of the embryo – termed cardiac jogging (Stainier et al., 1993). This jogging is controlled by the expression of *spaw,* with left sided *spaw* expression causing leftward jogging, right sided *spaw* causing right sided jogging and bilateral or absent *spaw* causing jogging to fail and the hear tube to remain on the mid line (Baker et al., 2008; Medeiros De Campos-Baptista et al., 2008). After leftward heart jogging is complete, at roughly 30hpf, the heart tube begins to loop rightwards forming a short of S-shaped tube that is offset to the left (Desgrange et al., 2018). Defects in *spaw* expression can produce hearts that are looped to the left or stay in the midline, however work by (Noël et al., 2013) suggest that looping and sidedness of *spaw* expression are independent (Figure 1.3). Further work by Grimes et al., (2020) has demonstrated that although the heart looping is indeed independent of *spaw* sided expression, direction of looping is heavily dependent on jogging directionality. Grimes et al., (2020) found that left sided *spaw* expression and thus leftward jogging always resulted in rightward looping, however midline jogging caused by absent or bilateral *spaw* also resulted in rightward looping roughly 50% of the time. Furthermore, right sided jogging resulted in right sided looping only 50-60% of the time (Grimes et al., 2020). This work demonstrated that there is indeed a correlation between *spaw* expression, and by extension the L/R axis, and heart looping directionality, but that rightwards looping of the heart is the default in most scenarios

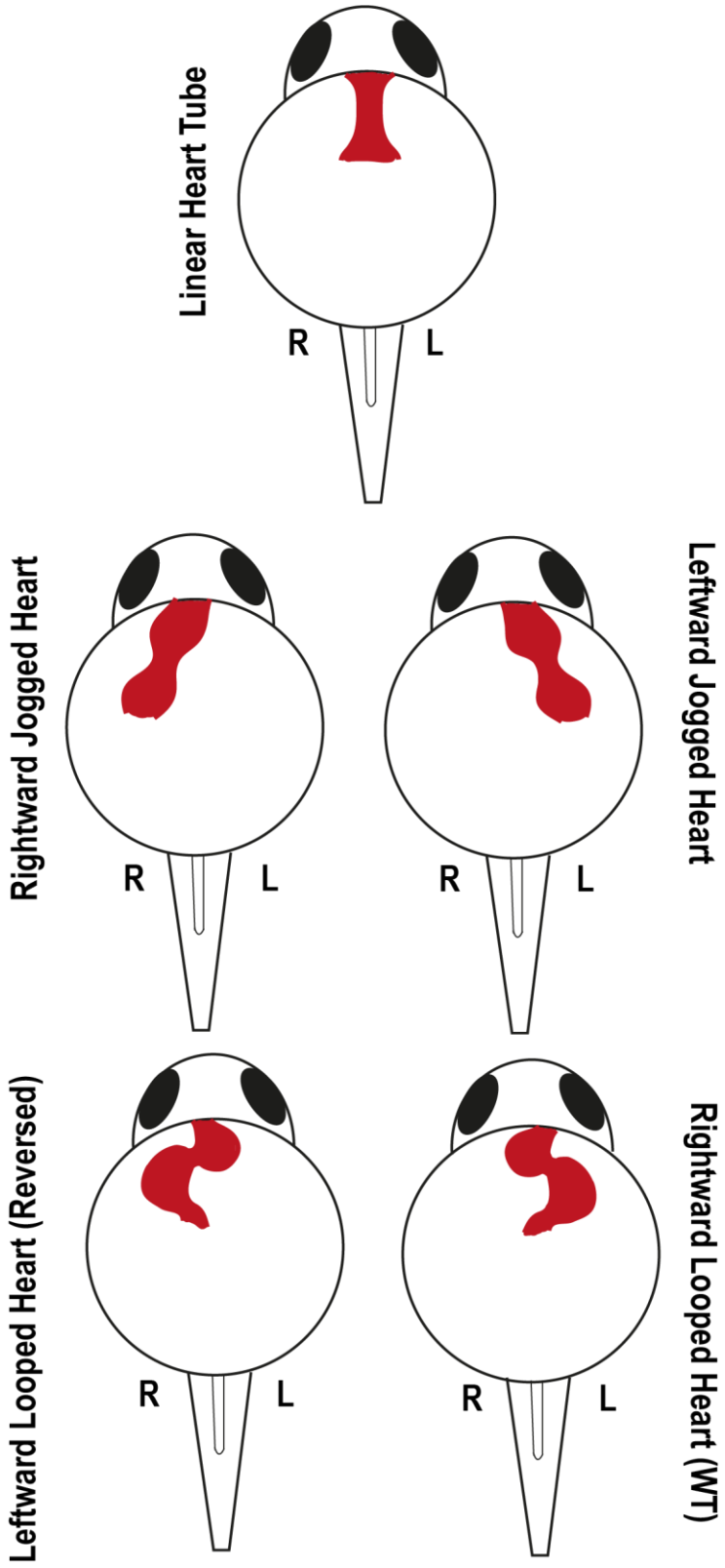

Figure 1.3: Heart Looping in Zebrafish.
Depiction of the zebrafish heart (red) going from linear heart tube to leftward jogged to rightwards looped. Inversed heart jogging and looping is also depicted. Jogging takes place at roughly 24hpf and full looping at roughly 48hpf.

1.2 Cilia

The organelle now known as the cilium was originally described back in the 17th century by Antonie van Leeuwenhoek. Leeuwenhoek was the pioneer of microscopy and microbiology, and upon discovering single celled eukaryotic organisms, was astounded by the “tiny feet” they used to walk and swim (Van Leeuwenhoek, 1932; Mitchell, 2017). It wasn’t until much later that these tiny feet were termed cilia, the singular being cilium - from the latin for eyelash. Although cilia have been known about for the last couple of hundred years, it is only with the relatively recent advances in molecular and cell biology that an understanding of their origin, structure, and function has been pieced together. We now know that cilia are evolutionary conserved microscopic, hair-like, organelles with a microtubule structure enclosed in a ciliary membrane (Satir and Christensen, 2007). Although we now know a significant amount about these fascinating cellular appendages, their origin is less well established. The most common theory is that modern day cilia are derived from a common ancestor which possessed both motility and sensory roles. Interestingly, this original cilium was proposed to be present in the last common ancestor of all eukaryotes (Mitchell, 2017).

1.2.1 Primary and Motile Cilia

Within modern day eukaryotes, cilia are generally defined as either non-motile primary cilia or motile cilia, with each type characterised by the microtubule structure and the motility of the cilium (Ibañez-Tallon et al., 2003; Satir and Christensen, 2007). The microtubule structure within motile cilia tends to consist of a ring of 9 doublet outer microtubules with a pair of single microtubules in the centre – this is termed the 9+2 structure. These outer doublet microtubules possess radial spokes and are decorated with small molecular machines called dyneins, which are the proteins responsible for the motility of the cilium. Conversely, primary cilia do not have these dynein motors or radial spokes and so lack motility. Additionally, primary cilia also lack the central pair of microtubules thus these primary cilia have a 9+0 microtubule arrangement (Satir and Christensen, 2007; Satir et al., 2010). Primary cilia can be found in almost every cell type are involved in multiple types of signal sensing including: mechanosensing of fluid flow, as in the case of the mouse embryonic node, as well as the sensing of morphogens and signalling molecules such as sonic hedgehog. Various receptors can exist within an individual primary cilium at different or the same time, resulting in the primary cilia acting as an antenna like structure for each cell, thus making primary cilia essential to the development and homeostasis of the organism (Rohatgi et al., 2007a; Zhao and Malicki, 2007; Satir et al., 2010). Furthermore, photoreceptors within the retina are derived from primary cilia, with the outer segment of the photoreceptor classed as a highly modified primary cilium (Wheway et al., 2014). The

primary cilium within the photoreceptor, termed the connecting cilium, functions to transport all the necessary components for phototransduction from the inner segment to the outer segment as the outer segment contains no cellular machinery. Due to the essential nature of the connecting cilia in photoreceptors, numerous retinal disorders result from dysfunction of primary cilia (Khanna, 2015).

As discussed, motile cilia possess a 9+2 microtubule structure, however there is an exception to this general classification. Within the L/R organiser of vertebrates, the node in mammals and Kupffer's Vesicle in zebrafish, there exists motile 9+0 cilia which also lack radial spokes (Bellomo et al., 1996). Unlike primary cilia, motile cilia are not found in most cell types but are only found in tissues where locomotion or generation of fluid movement is required. As the cilia beat, or whip in the case of the 9+0 motile cilia, the mechanical force generated moves the fluid within the tissue, a common example being fluid clearance from the airways (Satir and Christensen, 2007). Perturbations in primary or motile cilia function may result in the development of conditions termed ciliopathies with the dysfunction of motile cilia specifically resulting in primary cilia dyskinesia (Roy, 2009; Reiter and Leroux, 2017).

1.2.2 The Intraflagellar Transport System

Until very recently it was thought that cilia lacked the ability to synthesise proteins, thus all proteins that functioned within the cilia had to be transported into the cilia. Although this is not strictly the case, the cilium still requires a method for the transport of proteins from the ciliary base to the tip and back again. This system was discovered in 1993 by the observation of clusters of proteins moving up and down the cilia located between the microtubules and the ciliary membrane and termed the Intraflagellar transport (IFT) system (Kozminski et al., 1993). The particles moving up the cilia from base to tip were termed anterograde IFT complexes and the particles moving down from tip to base were termed retrograde IFT complexes (Anvarian et al., 2019). Subsequent work found that anterograde IFT movement was mediated by heterotrimeric kinesin motors and retrograde IFT movement was mediated by dynein 2 motors (Kozminski et al., 1995; Pazour et al., 1998). Multiple studies have shown that the IFT complexes are indispensable for cilia function within multiple organisms, however, there are minor differences, one being that anterograde IFT movement in zebrafish is also mediated by a semi redundant homodimeric kinesin 2 complex (Zhao et al., 2012; Broekhuis et al., 2013; Anvarian et al., 2019). Further work to characterise these IFT complexes revealed that IFT proteins can be sub-categorised into two classes, the IFT-A and IFT-B complexes, with each responsible for retrograde and anterograde movement respectively (Anvarian et al., 2019). These complexes are so named as they move up or down the A or B microtubules of the axoneme, explaining why they do not collide with each other. The IFT-B complex can be further categorised into IFT-

B1, forming the core part of the IFT-B complex, and IFT-B2 which forms a more peripheral complex that interacts with IFT-B1 (Taschner and Lorentzen, 2016; Kobayashi et al., 2021). There are six IFT proteins which make up the IFT-A complex (IFT144, 140, 139, 122, 121, and 43) and ten that make up the IFT-B1 complex (IFT88, 81, 74, 70, 56, 52, 46, 27, 25 and 22), with a further six making up the IFT-B2 complex (IFT172, 80, 57, 54, 38 and 20) (Taschner and Lorentzen, 2016; Kobayashi et al., 2021). The IFT proteins are highly conserved within eukaryotes which contain cilia, but are absent from eukaryotes which do not i.e. fungi (Avidor-Reiss et al., 2004).

Mutants of proteins found in the IFT-A complex usually result in cilia with bulbous ends as the retrograde function of the IFT-A complex is inhibited thus leading to build up of ciliary cargo at the distal tip (Piperno et al., 1998; Tran et al., 2008; Iomini et al., 2009). In some cases, IFT-A mutants also displayed shortened cilia (Blacque et al., 2006). In contrast, IFT-B component mutants showed severe cilia dysfunction including absent cilia, short cilia and immotile cilia (Pazour et al., 2000; Hou et al., 2007; Tsao and Gorovsky, 2008; Lee et al., 2015). Although the finding that IFT-A and IFT-B complexes function in retrograde or anterograde movement respectively, this directional distinction is not necessarily always the case. Indeed, IFT-B proteins have been implicated in retrograde transport of cargo out of the cilia and IFT-A proteins in the transport of ciliary receptors into the cilia (Mukhopadhyay et al., 2010; Huet et al., 2014). Enforcing the essential nature of these transport complexes to cilia function, critical developmental pathways such as the Hedgehog pathway and other signalling programs are determinately affected in IFT mouse mutants (Huangfu et al., 2003). Additionally, a range of human ciliopathies are directly linked to IFT dysfunction (Huangfu et al., 2003; Wang et al., 2006; Fliegauf et al., 2007).

1.2.3 Primary Cilia and the Hedgehog Pathway

The hedgehog (Hh) signalling pathway is one of a number of intercellular signalling pathways that is critical for organism development. In vertebrates, Hh signalling is involved in the development of almost all internal organs and is mediated through primary cilia (Bangs and Anderson, 2017). The receptor for the Hh ligand is Patched1 (Ptc1) and, when no Hh ligand is bound, Ptc1 repressed Smoothened (Smo) and inhibits Smo from entering the ciliary membrane. Gli transcription factors, the downstream effectors of the Hh pathway, are sequestered to the distal end of the primary cilia without Hh stimulation (Haycraft et al., 2005). When the Hh ligand binds to Ptc1, inhibition of Smo is removed and Smo enters the ciliary membrane, while Ptc1 leaves (Corbit et al., 2005; Rohatgi et al., 2007b). This lack of inhibition on Smo then allows the Gli transcription factors to exit the cilia and translocate to the nucleus to activate transcription of Hh target genes, including *Ptc1* and *Gli,* or repress Hh target genes (Wheway et al., 2018)(Figure 1.4).

In mammals, the translocation of Hh pathway components is dependent upon IFT proteins. IFT proteins were shown to act downstream of the Ptc1 receptor but upstream of Hh target genes, suggesting IFTs are necessary for the translocation of Smo and Gli in and out of the cilia (Huangfu et al., 2003). Loss of IFT proteins in mice leads to the decreased expression of Ptc1 and the build-up of the Gli2 and Gli3 transcription factors at the distal end of the cilium (Beales et al., 2007; Qin et al., 2011). Indeed, loss of IFT80 has been shown to impact canonical Hh signalling in mice due to disrupted Smo localisation (Yuan et al., 2016). The function of primary cilia in the transduction of the Hh pathway can be complex, with primary cilia functioning to regulate Hh signalling both positively and negatively depending on the location within the organism. For instance, loss of IFT proteins results in loss of Hh signalling in the neural tube, where Gli usually activates downstream genes, but gain of function signalling within the limb bud where Gli3 usually represses transcription (Haycraft et al., 2005; Huangfu and Anderson, 2005). Furthermore, FOXJ1 has also been shown to affect Hh signalling within the neural tube of mouse embryos. Increased expression of *Foxj1* artificially increased the length of primary cilia, making them appear more like motile cilia, and resulted in weaker Gli transcriptional activation (Cruz et al., 2010). Further emphasising the role for primary cilia in the Hh pathway, RPGRIP1L, a basal body protein, has been identified in the human ciliopathies Joubert Syndrome and Meckel Syndrome and has been demonstrated to be crucial for the response to Hh signalling, with mouse mutants presenting with limb patterning and neural tube defects (Vierkotten et al., 2007).

Although most of the discussed role for primary cilia in Hh signalling has been in relation to mammals, the role for primary cilia in Hh signalling is conserved in zebrafish (Kim et al., 2010). Indeed, the zebrafish *iguana* mutant which either lacks or has severely stunted primary cilia displays defects associated with dysfunctional Hh signalling (Glazer et al., 2010; Arnold, Lamont, Walker, Spice, C. K. Chan, et al., 2015). Investigation of the expression of *ptc1* in *iguana* mutants revealed that at 24hpf *ptc1* was ectopically expressed, with higher levels of *ptc1* transcript in the neural tube and somites (Wolff et al., 2004). Fitting with this ectopic expression of *ptc1*, expression of Hh target genes including the Gli were expanded in the neural tube and somites (Sekimizu et al., 2004). Overall, however, the expression of downstream genes in response to Hh signalling is generally lower in *iguana* mutants compared to WT both in the neural tube and somites. (Sekimizu et al., 2004). In support of this reduced but expanded mode of Hh signalling zebrafish cilia mutants, knockout of *ift88* resulted in the loss of all cilia but still demonstrated low levels of *ptc1* and *gli1* expression that was expanded into the somites and neural tube (Huang and Schier, 2009).

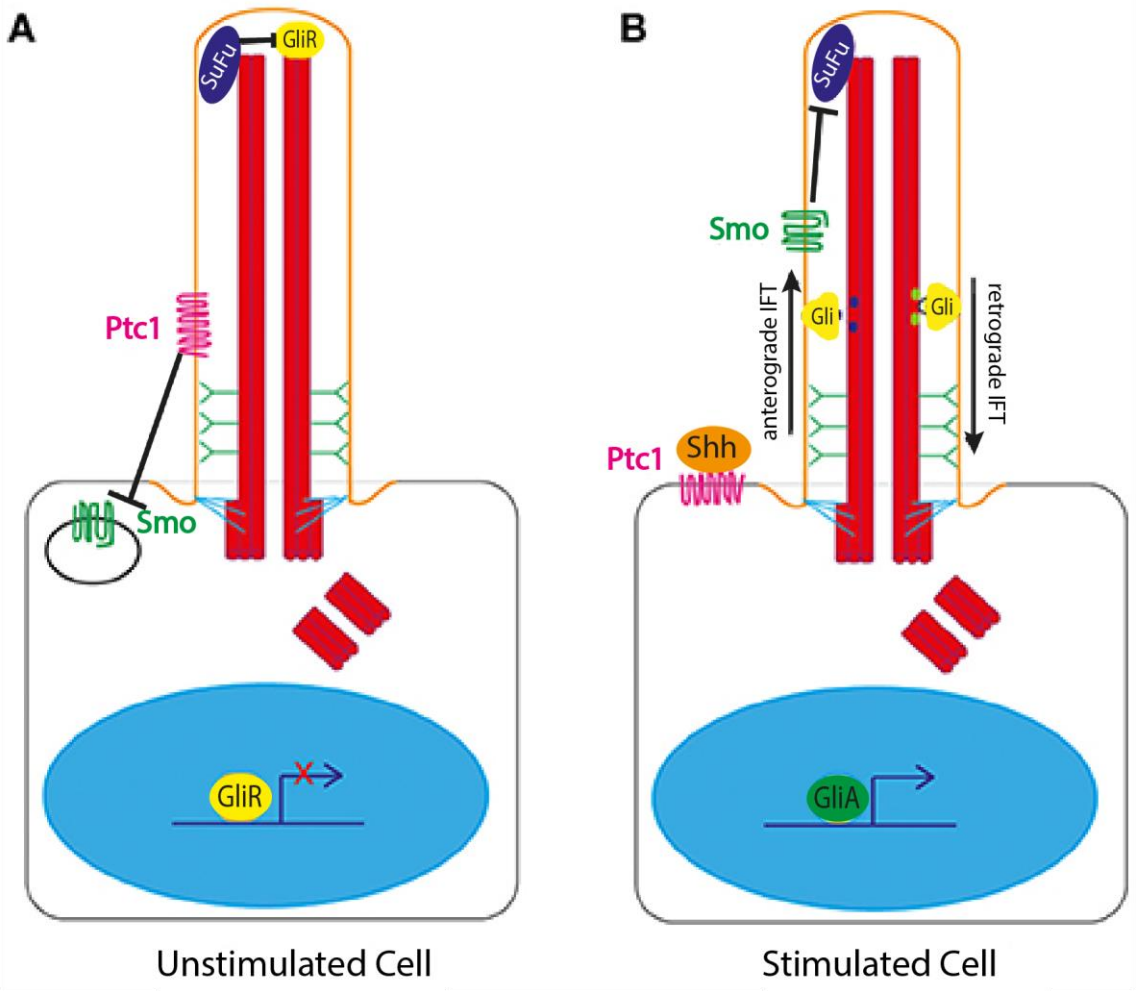

Figure 1.4: Primary Cilia and the Hedgehog Pathway
Depiction of the roll primary cilia play in the functioning of the Hh signaling pathway. **(Left)** The Hh pathway when no Hedgehog ligand is bound to Patched1. Smoothened is inhibited and Gli is sequestered at the ciliary tip by SuFu. Gli target genes are repressed (GliR). **(Right)** The Hh pathway when a Hedgehog ligand is bound to Patched1. Smoothened is no longer inhibited and so inhibits SuFu. This releases Gli which is transported up and down the axoneme by IFTs and is able to active Gli target genes (GliA).
Adapted from Wheway et.al (2018).

1.2.4 Arl13b in Ciliary Trafficking

Arf (ADP-ribosylation factor) family of GTPases act like “molecular switches” within the cell by converting from inactive GDP bound to active GTP bound. Once GTP bound, GTPases alter their interactions with downstream effectors and thus can cause activation of an enzyme, changes in protein localisation, or the effector may also alter its interaction with further cellular proteins (Sztul et al., 2019). These altered interactions are brought about by a conformational change in ARF family GTPases by the hydrolysis of GTP to GDP. As GTP binds spontaneously, the removal of GDP from the active sight is tightly controlled (Sztul et al., 2019). In regards to Arl13b (Arf-like 13b), the loss of GDP is controlled by Arl3, another ciliary enriched Arf-like GTPase (Gotthardt et al., 2015). Interestingly, there are around 30 Arf family GTPases but Arl13b is by far the largest, being almost double the size of the next biggest Arf GTPase. The increased size of Arl13b size is due to a large C-terminal domain of which, other than the presence of a ciliary localisation signal and Proline Rich Domain, the function of is currently unclear (Sztul et al., 2019).

Arl13b, is one of a number of Arf-like GTPases, and is specifically localised to the cilium (Cevik et al., 2010). *Arl13* is predicted to have been present in the last common ancestor of all eukaryotes. Although *Arl13* was lost in non-ciliated organisms, it underwent duplication in vertebrates into *Arl13a* and *Arl13b* (Schlacht et al., 2013; Gigante et al., 2020). Expression patterns of *arl13a* and *arl13b* are significantly different during zebrafish development, with *arl13a* mostly restricted to craniofacial regions, while *arl13b* expression is diffuse throughout the organism but concentrated in highly ciliated structures (Song and Perkins, 2018). This difference in expression suggests the two paralogues have diverged in function. As with most GTPases, Arl13b has multiple functions including membrane trafficking, endocytic trafficking and, importantly for this project, regulating IFT machinery (Cevik et al., 2010; Gigante et al., 2020).

Initial work into understanding the ciliary function of *arl13b* began when *arl13b,* known as *scorpion,* was identified in a zebrafish screen to find genes that result in kidney cysts when mutated (Sun et al., 2004). This screen found that as well as kidney cysts, *scorpion* mutants exhibited curl down body axis and seemed to lack all cilia in the pronephric duct (Sun et al., 2004). Further studies from a mutagenesis screen identified a mouse null mutant of *arl13b* which presented with early embryonic developmental defects including an open neural tube, irregular eyes and increased incidence of heart looping reversal, with embryonic death at around day 13 (Caspary et al., 2007). Investigations into this mutant found that node cilia were significantly shorter than in WT and transmission electron microscopy (TEM) analysis showed that the B microtubule of the outer doublet was only partially connected to the A tubule (Caspary et al., 2007). Unfortunately, cilia motility was not assessed in these mutants so we cannot say whether the observed short cilia also had motility defects which may have caused the reversal of heart looping phenotype. Interestingly, knockout of the IFT-B complex protein *Ift172* results in the loss of cilia and

produced the same open neural tube phenotype seen in knockout *Arl13b* mouse embryos, though heart looping in those mutants was not investigated (Caspary et al., 2007). Furthermore, an *Arl13b* mutant in which the cilia localisation signal was mutated also displayed significantly shorter cilia but neural patterning was indistinguishable from WT and embryos were viable (Gigante et al., 2020).

The link between Arl13b and cilia length is thought to be related to the interaction of ARL13B with the IFT complex. Indeed, mutations in some IFT components in zebrafish and mouse result in short cilia (Pazour et al., 2000; Hou et al., 2007; Krock and Perkins, 2008). Current knowledge suggests that Arl13b regulates the extension of the ciliary membrane with interactions between Arl13b and the IFT complex regulating the growth of the axoneme into the extended membrane, with faster IFT entry into the cilium correlating with increased growth (Engel et al., 2009; Lu et al., 2015). Indeed, in *C. elegans*, a mutation within the large C-terminal domain of *arl-13* (homologous to *Arl13b*) which did not affect cilia localisation resulted in slower IFT movement into and up the cilium (Cevik et al., 2010). Furthermore, overexpression of truncated arl-13 constructs that consist of either the GTPase domain or the C-terminal domain containing the Proline Rich Domain resulted in cilia function defects, suggesting both regions are critical for proper function of Arl13b (Li et al., 2010). Additionally, IFT-B proteins were mis-localised within the cilium of *arl-13* mutants whereas IFT-A proteins were not, however the speed of movement of both complexes within the cilium was affected (Li et al., 2010)

Although the exact function of *arl13b* still remains unclear, it is certainly clear that Arl13b possesses critical roles that affect cilia formation and function through either direct or indirect interactions with IFT complexes as well as numerous other proteins (Cevik et al., 2010; Li et al., 2010; Hor and Goh, 2019).

1.2.5 Structure of Motile Cilia

Motile cilia are used for either locomotion of the organism or for the generation of fluid movement within tissues. The use of motile cilia for locomotion is the case for the majority of prokaryotes, however vertebrates almost exclusively use motile cilia for the production of fluid movement in tissues, with the exception being in sperm cells which utilise a modified motile cilium for locomotion (Ibañez-Tallon et al., 2003; Pazour et al., 2005). Although the majority of motile cilia appear almost identical, they vary in morphology and type of motility produced (Satir and Christensen, 2007). For instance, the motile monocilia within the KV of zebrafish whip in an anticlockwise rotational movement. This is in contrast to other motile cilia, such as in the airway, which beat laterally and are usually found in cells containing hundreds of other motile cilia, termed multiciliated cells (Tilley et al., 2015). These motile cilia are also found within the fallopian tube of mammals, functioning to facilitate the movement of the mature egg, as well in the spinal canal of zebrafish, functioning to produce movement of the cerebrospinal fluid causing straightening of the developing body axis. Dysfunctions within these cilia often lead to infertility as well as scoliosis (Fliegauf et al., 2007; Brooks and Wallingford, 2014; Zhang et al., 2018). Although these 9+2 cilia predominantly function as mechanical drivers of fluid flow, recent work has also demonstrated they may also possess mechanosensory and chemosensory functions (Shah et al., 2009; Scheuer et al., 2012). Nevertheless, the structure of 9+2 motile cilia is well conserved across vertebrates with recent work further elucidating our understanding of these “tiny feet” (Ishikawa, 2017).

Motile cilia structure can be divided into three sections; the axoneme, which makes up the main structure of the protruding cilia, the basal body, which acts as an anchoring point for the axoneme, and the transition zone, which links these two parts together (Ishikawa, 2017). Basal bodies are composed of 9 radially symmetric sets of triplet microtubules arranged in “cartwheel” formation, with the most inner microtubule of a triplet termed the A, the middle termed B and the outer, containing gamma-tubulin, termed C (Bayless et al., 2019). From the basal body forms the 9 doublet microtubules which make up the axoneme. Each pair of microtubules is composed of one complete microtubule ring, termed A tubule, and one incomplete ring (B tubule) which is attached to A-tubule (Broekhuis et al., 2013; Ishikawa, 2017). Each 9+2 cilia also contains inner dynein arms (IDAs) and outer dynein arms (ODAs) which attach to the A-tubule via a dynein docking complex on the inner and outer region of the tubule respectively (Shinohara and Hamada, 2017). Additionally, the outer microtubules are connected by nexin proteins and the central singlet pair of microtubules is connected to the outer doublets by radial spokes (Ishikawa, 2017; Shinohara and Hamada, 2017). The transition zone marks the area where the triplet basal body microtubules become the outer doublet microtubules of the axoneme, the central microtubule pair forms distally to this region (Williams et al., 2011; Broekhuis et al., 2013).

The 9+2 axoneme is enclosed by the ciliary membrane, a modified extension of the cell membrane (Satir and Christensen, 2007; Ishikawa, 2017).

As previously stated, 9+2 is not the only microtubule structure that gives rise to motile cilia. The general architecture of outer doublet microtubules in 9+0 motile cilia remains the same as in 9+2 motile cilia, however 9+0 motile cilia lack the central microtubule pair. Importantly, 9+0 motile cilia also lack inner dynein arms, nexins and the radial spokes that would link the central microtubule pair to the outer doublet microtubules (Ishikawa, 2017; Shinohara and Hamada, 2017)(Figure1.3). Recent work to understand what structural difference gives rise to the rotational motion of the 9+0 motile cilia compared to the planar beating of 9+2 cilia has uncovered some interesting results. Firstly, computer simulations of 9+0 motile cilia structure propose that the outer doublet microtubules are critical for the steady anticlockwise rotational beating (Shinohara et al., 2015). Indeed, microtubule rearrangements induced via administration of Taxol in mice resulted in the random rotation of nodal cilia (Shinohara et al., 2015). Additionally, Shinohara et al. (2015) also demonstrated that the lack of radial spokes is critical for the circular beating of 9+0 cilia. Shinohara et al. (2015) utilised a mouse mutant of the *Rsp4a* gene, which codes for a protein localised to the head of the radial spokes, and showed that loss of this protein induced 9+2 airway cilia to beat radially rather than laterally. Knockout of the *Rsp4a* gene had no effect on 9+0 cilia thus proposing a mechanism whereby the radial beating of motile cilia is translated into planar beating via the radial spokes (Shinohara et al., 2015; Shinohara and Hamada, 2017).

Although this hypothesis requires further investigation, it suggests that the loss of radial spokes is required for the radial beating of 9+0 motile cilia in the node/KV. In support of this, in the developing mouse/zebrafish embryo, the dorsal-ventral and anterior-posterior (A-P) axes are already formed by the time the node/KV develops. As mentioned previously, the pit cells within the node/KV move the basal body of the cilium to the posterior in mouse or anterior in zebrafish of the node/KV. This movement means that the establishment of the L/R axis is dependant of the A-P axis (Hashimoto et al., 2010). If the rotationally beating cilia within the node/KV possessed radial spokes then they would beat laterally in the A-P direction, thus to convert the A-P axis into the L/R axis the cilia need to beat rotationally. Shinohara and Hamada, (2017) speculate that this is the reason 9+0 motile cilia lost their radial spokes during evolution, with the loss of the superfluous central pair shortly after. Indeed, 9+2 motile cilia have been identified within the node and KV (Odate et al., 2016; Gui et al., 2021) suggesting this process is either not yet complete or enough 9+2 cilia have lost their spokes to generate sufficient anticlockwise fluid flow to establish the L/R axis (Shinohara and Hamada, 2017).

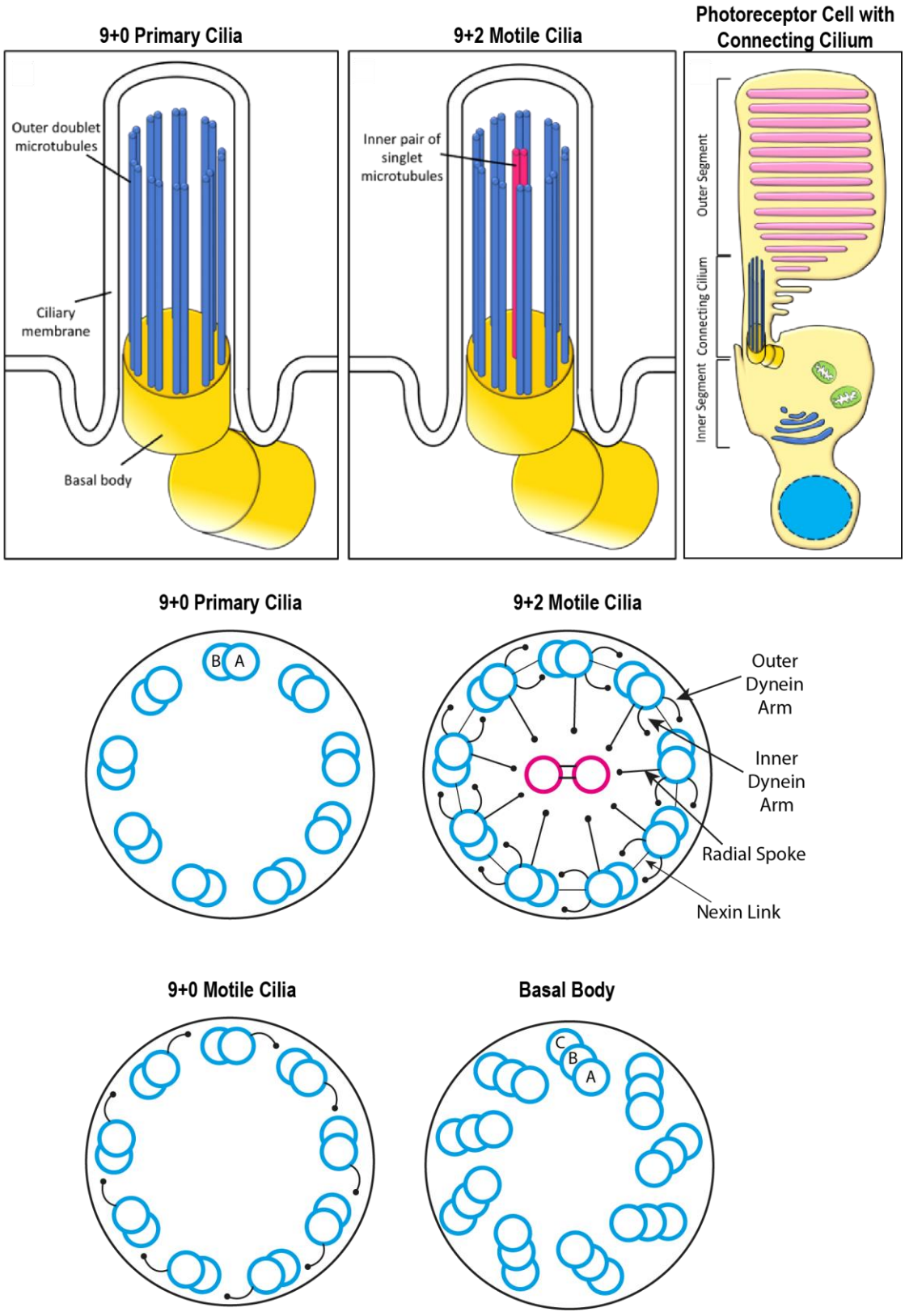

Figure 1.5: Structure of Primary and Motile Cilla.
(A) Structure of a 9+0 primary cilium, 9+2 motile cilium and representation of a photoreceptor cell. Outer doublet microtubules and inner singlet microtubes labelled. Axoneme structure is enclosed in a specialised ciliary membrane. **(B)** Cross section of 9+0 primary and motile cilia as well as 9+2 motile cilia and the basal body. Outer doublet microtubules as well as basal body triplet microtubules are depicted in blue with letters referring to microtubule designations. Inner singlet microtubules are depicted in pink. Outer and inner dynein arms as well as nexin links and radial spokes labelled on the 9+2 motile cilium. Figure adapted from Maxwell, et.al. (2021)

1.2.6 Transcriptional Control of Motile Ciliogenesis

The transcription factor Foxj1 is known to be the master regulator of motile ciliogenesis within vertebrates and is critical for production of motile cilia (Yu et al., 2008). *foxj1* expression has been found in all tissues containing motile cilia such as the zebrafish pronephric duct, KV, nasal placode, floorplate and otic vesicle with increased expression immediately prior to ciliogenesis (Aamar and Dawid, 2008; Stubbs et al., 2008; Yu et al., 2008; Tian et al., 2009). Further confirming the role for Foxj1 in the establishment of motile cilia, mouse mutants null for FOXJ1 functionality were void of motile cilia in the respiratory tract and exhibited a high degree of *situs inversus*, suggesting that both classifications of motile cilia were affected (Chen et al., 1998). Indeed, work by Brody et al., (2000) demonstrated that the 9+2 motile cilia in the respiratory tract were absent in *Foxj1* mutants, but surprisingly found that the 9+0 motile cilia were still present in the node. This raises the question of whether FOXJ1 is indeed required for 9+0 motile ciliogenesis. Knockdown of *foxj1* in zebrafish found that 9+0 KV motile cilia were either absent or significantly reduced in length (Stubbs et al., 2008; Yu et al., 2008). Additionally, ectopic expression of *foxj1* induced the formation of 9+2 motile cilia in cells which do not usually possess motile cilia (Yu et al., 2008). These findings show that *foxj1* drives the formation of motile cilia, including that of 9+0 cilia, suggesting this subtype of motile cilia forms from the same genetic pathway as 9+2 multiciliated cells in mouse and zebrafish (Stubbs et al., 2008). This proposition fits with the previously discussed loss of radial spokes hypothesis, where nodal/KV cilia were originally 9+2 but then diverged as, notably, loss of *foxj1* does not affect 9+0 primary cilia (Brody et al., 2000; Yu et al., 2008).

Loss of FOXJ1 has been shown to inhibit the formation of motile cilia by inhibiting the docking of the basal body with the apical membrane, thus preventing the formation of cilia (You et al., 2004). However latter work demonstrated that *foxj1* acts to upregulate a significant number of motile cilia related genes, such as components of the dynein arms, as well as microtubule structural components, all of which are crucial for the formation of motile cilia (Yu et al., 2008).

1.2.7 Ciliopathies

Ciliopathies are a group of human conditions in which mutations affecting the formation and/or function of cilia is the primary cause of the disease. Due to the presence and essential function of cilia on almost all cells, ciliopathies present with a wide spectrum of phenotypes including renal malformations, situs abnormalities, retinal degeneration, skeletal deformities, obesity and diabetes (Waters and Beales, 2011). More than 25 syndromes have so far been directly linked to defective cilia function including Bardet-Biedl

syndrome (BBS), Usher syndrome (US) and Primary Cilia dyskinesia (PCD) (Reiter and Leroux, 2017) (Table 1.1). Interestingly, a number ciliopathic mutations at a specific loci can produce a range of phenotypic outcomes and, conversely, an array of mutations in different ciliary genes can produce the same phenotypic outcome (Waters and Beales, 2011). Currently over 187 genes have been linked to human ciliopathies with more than 241 proposed as candidate genes (Reiter and Leroux, 2017). Ciliopathies can be categorised as “sensory” ciliopathies, in which the sensing and signalling of the primary cilia is affected, or motile ciliopathies, where the motile cilia are affected, as is the case for PCD. Additionally, in some ciliopathies, all cilia may be affected. Further to this, another classification of ciliopathy has been proposed, termed secondary ciliopathy, which includes non-cilia related proteins in which their dysfunction affects cilia related proteins (Reiter and Leroux, 2017).

Dysfunction of motile cilia typically causes the ciliopathy PCD. Patients with PCD frequently present with severe bronchiectasis, male and female infertility, *situs ambigus* or *situs inversus* and, less commonly, hydrocephalous (Fliegauf et al., 2007; Lucas et al., 2020). PCD tends to be inherited in an autosomal recessive manner, though dominant and X-linked cases do exist (Horani et al., 2016). Genes associated with PCD are usually involved with the formation and function of the dynein arms, radial spokes or microtubule structure of the central pair, with over 45 genes linked to the condition (Reiter and Leroux, 2017; Shoemark and Harman, 2021). While motile cilia have been demonstrated to possess sensory and signalling functions, “sensory” ciliopathies are distinct from that of motile ciliopathies as the aetiology differs. The cause of these ciliopathies is diverse and can include dysfunctional ciliogenesis, impaired ciliary maintenance, aberrant ciliary trafficking causing defective signalling or impaired ciliary targeting and removal of proteins (Reiter and Leroux, 2017). Indeed, BBS is caused by mutations in over 20 different ciliary components including ARL6 (BBS3) and IFT172, one of the IFT-B components required for ciliary trafficking (Bujakowska et al., 2015; Priya et al., 2016). US, BBS as well as other sensory ciliopathies often present with retinal degeneration, termed Retinitis Pigmentosa (RP) (Novarino et al., 2011). The photoreceptor is derived from a primary cilium and so RP can either be a syndromic, in the case of BBS and US, or a non-syndromic ciliopathy. As with other ciliopathies, RP can be caused by dysfunctional IFT trafficking of essential signal transduction components (Pazour et al., 2002; Bujakowska et al., 2015, 2017; Perrault et al., 2015; Xu et al., 2015). Unlike other ciliopathies though, a number of core splicing proteins are also closely linked with the condition, one such protein being PRPF8 (Maxwell et al., 2021).

Ciliopathy	Associated Phenotype/Affected Organs
Alström Syndrome	Childhood obesity, early onset type 2 diabetes, hearing loss, blindness, hypogonadism
Asphyxiating Thoracic Dysplasia	Polydactyly, reduced bone length (especially thoracic bones), kidney and heart dysfunction
Bardet–Biedl Syndrome	Obesity, polycystic kidney disease, polydactyly, hypogonadism, intellectual disability, behavioural dysfunction
Carpenter Syndrome	Craniosynostosis, brachydactyly, supernumerary, polydactyly, congenital heart defects, obesity, intellectual disability
Cone-Rod Dystrophy	Progressive retinal degeneration
Cranioectodermal Dysplasia	Retinitis pigmentosa, craniosynostosis, facial defects, nephronophthisis
Ellis–Van Creveld Syndrome	Skeletal dysplasia, cleft palate, polydactyly, congenital heart defects
Joubert Syndrome	Congenital central nervous system defects, ataxia, intellectual disability, polycystic kidney disease, retinitis pigmentosa, developmental delay
Hydrolethalus Syndrome	Hydrocephalus, cleft palate, heart and lung defects, polydactyly
Leber Congenital Amaurosis	Congenital blindness
Lowe Syndrome	Cataracts, glaucoma, hypotonia, intellectual disability, scoliosis, renal dysfunction and kidney failure
Mckusick–Kaufman Syndrome	Polydactyly, heart defects, genital abnormalities
Meckel–Gruber Syndrome	Central nervous system abnormalities, polydactyly, polycystic kidney disease, pulmonary hypoplasia, retinal degeneration, hydrocephalus
MORM syndrome	Retinal degeneration, micropenis, obesity, intellectual disability
Nephronophthisis	Polyuria, polydipsia, kidney cysts
Occult Macular Dystrophy	Macular dystrophy
Orofaciodigital Syndrome 1	Malformations of the face and oral cavity, intellectual disability, polycystic kidney disease, retinal degeneration, central nervous system defects.
Pallister Hall Syndrome	Polydactyly, hypothalamic hamartoma, kidney dysregulation,
Polycystic Kidney Disease	Cysts within the kidney and renal tube
Primary Ciliary Dyskinesia	Cilia dysmotility in multiple systems and organs affecting brain, respiratory tract resulting in bronchitis and pneumonia, kidney, fallopian tubes, sperm motility resulting in reduced fertility, hearing loss, organism laterality
Retinitis Pigmentosa	Progressive retinal degeneration
Senior–Løken Syndrome	Nephronophthisis, progressive retinal degeneration
Sensenbrenner Syndrome	Microcephaly, hypodontia, kidney failure, brachydactyly, stunted growth, visual defects, kidney cysts
Short Rib Thoracic Dysplasia	Retinitis Pigmentosa, short ribs, thoracic cage constriction
Usher Syndrome	Retinitis pigmentosa, deafness, balance issues
Birt-Hogg Dube Syndrome	Benign skin lesions, skin papules lung cysts, kidney tumours

Table 1.1: List of Ciliopathies and Associated Phenotypes.
Table adapted and complied from:
Badano, J., Mitsuma, N., Beales, P. and Katsanis, N., 2006. The Ciliopathies: An Emerging Class of Human Genetic Disorders. *Annual Review of Genomics and Human Genetics*, 7(1), pp.125-148.
Reiter, J. F. and Leroux, M. R. (2017) 'Genes and molecular pathways underpinning ciliopathies.' *Nature Reviews Molecular Cell Biology*.
Sánchez-Bellver, L., Toulis, V. and Marfany, G., (2021). On the Wrong Track: Alterations of Ciliary Transport in Inherited Retinal Dystrophies. *Frontiers in Cell and Developmental Biology*, 9.
NORD (National Organization for Rare Disorders). 2022. *List of Rare Disease Information - NORD (National Organization for Rare Disorders)*. [online] Available at: <https://rarediseases.org/for-patients-and-families/information-resources/rare-disease-information/>

1.3 The Spliceosome and Prpf8

The spliceosome is a large ribonuclear protein which is involved in the removal of introns within pre-mRNA. The core of the spliceosome is made up of five small protein/RNA complexes called nuclear ribonuclear particles (snRNPs). These snRNPs are termed U1, U2, U4, U5 and U6 with each containing proteins and snRNA that are common or specific to that snRNP and have multiple associated proteins (Wahl et al., 2009). Splicing is initiated by the binding of the U1 snRNP, through snRNA/pre-mRNA interactions, to the 5' splice site (SS). Subsequently, the U2 snRNP recognises and binds to the branch point within the intron thus forming the pre-spliceosome complex. The snRNPs U4 and U6 form a U4/6 di-snRNP and they are usually found bound together. The U5 snRNP associates with this U4/U6 di-snRNP forming a U4/U6.U5 tri-snRNP which binds to the pre-spliceosome complex. Following a number of protein rearrangements in which U1 and U4 exit the complex and U6 binds to the 5' SS, the active splicing complex is formed. At this point the snRNA of U6 interacts with the snRNA of U2, with Prpf8 forming the active site for the transesterification reaction necessary to cleave the 5'SS. Rearrangements within the spliceosome then catalyse the second transesterification reaction resulting in the 3'SS being cleaved and the removal of the intron along with the joining of the two ends of each exon (Grainger and Beggs, 2005) (Figure 1.4) .

Prpf8 is a very large protein of roughly 270kDa and the gene is comprised of 43 exons. Prpf8 is one of the largest proteins in the spliceosome and forms a core component of the U5 snRNP (Stevens et al. 2001). Prpf8 is one of the most highly conserved proteins, with around 97% identity between human and zebrafish and 60% identify between human and yeast ("ClustalW2 EMBL-EBI" 2018). The majority of the research regarding Prpf8 function has been carried out in yeast but due to the high sequence similarity it is presumed the findings also apply to higher organisms. Prp8 (yeast Prpf8) is the only protein within the spliceosome which interacts with the 5'SS, the branch point and the 3'SS in the pre-mRNA as well as the U4, U5 and U6 snRNAs, suggesting that Prp8 function is critical to splicing (Grainger and Beggs, 2005). Indeed, experiments in which Prp8 was knocked down in yeast hindered spliceosome assembly as the U4/U6.U5 tri-snRNP failed to form (Brown and Beggs, 1992).

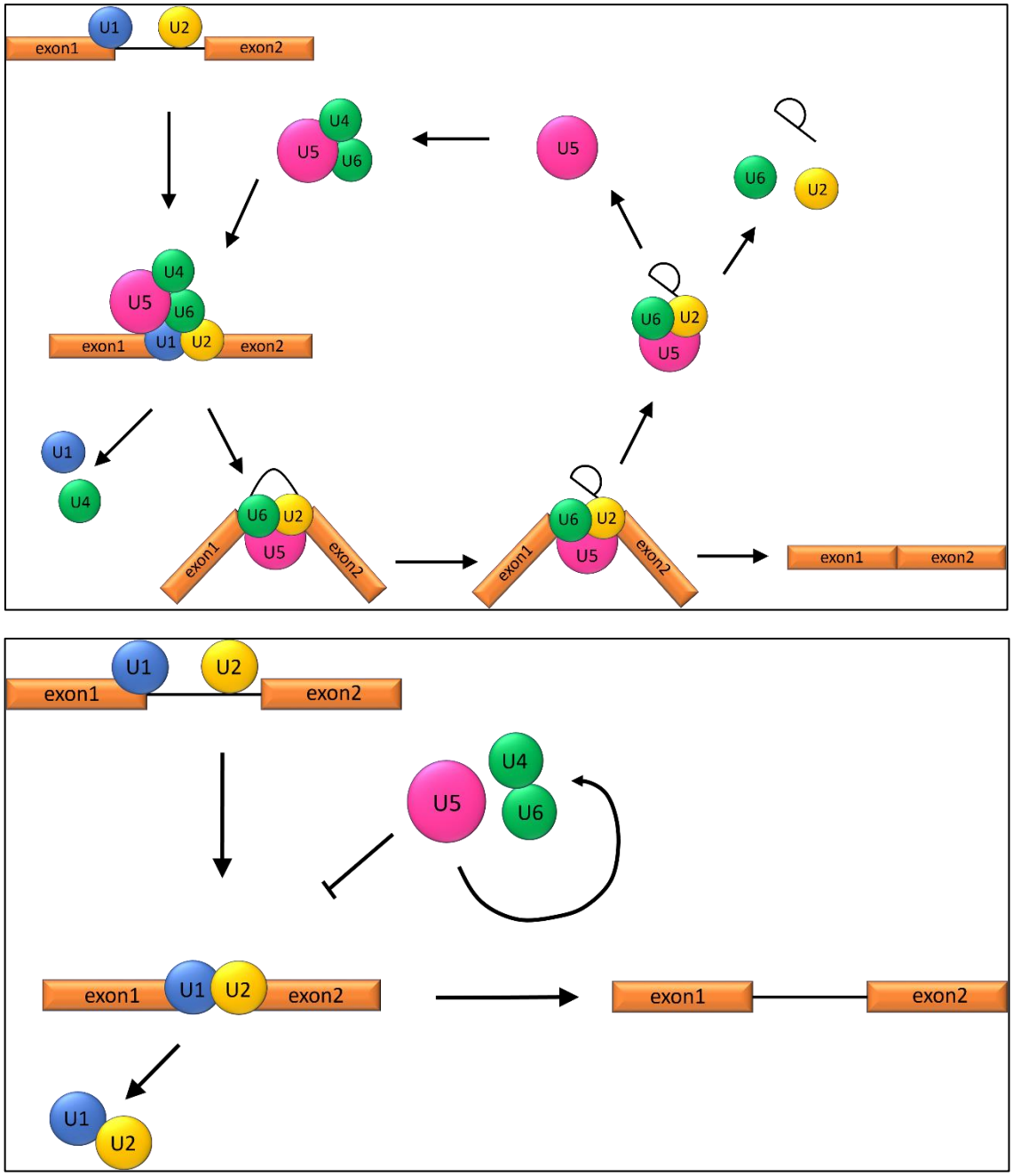

Figure 1.6: Steps of Splicing and Spliceosome Assembly.
Top: Representation of the fundamental steps in the splicing of pre-mRNA. Prpf8 is located in the U5 snRNP (pink). From top left going anticlockwise: Pre-mRNA (orange) 5'SS and BP is recognised and bound by U1 and U2 (blue and yellow) respectively. The tri-snRNP U4/U6.U5 (pink and green) then binds to U1 and U4 inducing complex rearrangements which lead to U5 5'SS binding and the displacement of U1 and U4. Through further complex rearrangements and transesterification reactions, U5 facilitates the splicing out of the intron, resulting in the production of mature mRNA. U5, U6 and U2 then dissociate and are recycled for the next splicing reaction. **Bottom:** Representation of the proposed dysfunction within the splicing process when there are mutations within PRPF8 and other U4/U6.U5 tri-snRNP proteins. U1 and U2 bind the pre-mRNA as normal but, as the tri-snRNP cannot form, the necessary protein binding and transesterification reactions do not occur resulting in mis-spliced mRNA. Figure adapted from Maxwell *et.al.* (2021).

1.3.1 Prp8 Structure and Binding Partners

The majority of biochemical studies into Prp8 have been performed in yeast, but due to the highly conserved nature of Prp8 it is assumed the protein 3D structure and functional domains remain unchanged in zebrafish, mice and humans. Prp8 can be functionally divided into four domains: amino acids (aa) 1-394, 443-770, 771-2170 and 2179-2413 (Boon et al. 2006) (Figure 1.5). Additionally, there is a nuclear localisation signal close to the N-terminus which is crucial for Prp8 transport to the nucleus and thus U4/U6.U5 tri-snRNP formation (Boon et al. 2007). At the C-terminus of Prp8 there is a catalytically inactive Jab1/MPN domain that facilitates interactions with additional spliceosomal proteins (Pena et al., 2007; Zhang et al., 2007; Birol and Echalier, 2014). Arguably the most interesting region for this thesis, since the precursor to this project was the characterisation of the mouse PRPF8^{N1531S} mutant by Michael Boylan (2015), is the functional domain across residues 771-2170. Within this region, work by Galej et al. (2013) revealed that residues 885-1824 can be dissected into three more functional domains consisting of a polymerase like domain, a linker domain and a type-2 restriction endonuclease like domain (aa885-1375, aa1376-1649 and aa1653-1824 respectively) (Galej et al., 2013). Grainger and Beggs (2005) originally proposed an RNA recognition motif at position aa1058-1151 however the work by Galej et.al (2013) suggest this is not the case.

Interestingly, aa1839-2092 of Prpf8 form an adapted RNAse H domain. Rather than breaking down RNA, this RNAse H domain instead appears to bind and manoeuvre the pre-mRNA into position for splicing (Pena et al., 2007; Ritchie et al., 2008; Galej et al., 2013). Furthermore, this domain flips between open and closed configurations which have been demonstrated to correlate with the two phases of splicing respectively (Schellenberg et al., 2013). Initially, it was suggested that the region aa1503-1673 was responsible for splicing co-factor binding as this region is highly conserved and mutations and insertions into this region either inhibited splicing or were lethal (Umen and Guthrie, 1996; Grainger and Beggs, 2005; Turner et al., 2006). However due to the more recent work by Galej et.al (2013), we now know this region corresponds to the linker and endonuclease domains and that contact with the branch point of the intron is made somewhere within residues aa1585-1598 of Prp8 (Galej et al., 2013). This work suggests the catalytically active region may lie within aa1503-1673 and explains why the region is so highly conserved and why mutations are detrimental to organism function. Furthermore, following the first transesterification reaction, this region rotates 30° allowing the accurate placement of exons for the second transesterification reaction when the exons are spliced together (Nguyen et al., 2016). Intriguingly, amino acid 1603 in yeast corresponds to the Prpf8^{N1531S} mutation in mice, giving a possible indication as to which aspects of Prpf8 function the PRPF8^{N1531S} mutation may affect.

There are several protein binding partners crucial to Prp8 function and assembly. The most relevant in terms of the PRPF8^{N1531S} mutant previously characterised in the

Hentges lab are Brr2 and Aar2. Brr2 and Aar2 mutually exclusively bind the C-terminal region of Prp8. Within the cytoplasm Aar2 is bound to Prp8 and, upon translocation of Prp8 to the nucleus, Aar2 is phosphorylated, freeing Aar2 and allowing binding of Brr2 to Prp8 (Boon et al. 2007). Work by Weber et al. (2011) suggests that Aar2 acts to inhibit the activity of Brr2, as only Brr2 and not Aar2 is observed in mature spliceosomes. Structural analysis of Prp8 bound Aar2 found that the C-terminal of Aar2 was crucial for the stabilisation of Prp8 and that Aar2 interacted with several Prp8 domains (Galej *et. al*, 2013). In agreement with the proposition that the function of Aar2 is to inhibit Brr2 activity, Brr2 binding to Prp8 is prevented due to bound Aar2 sequestering the Jab1/MPN domain of Prp8, which is the binding site of Brr2 (Nguyen et al., 2013). Cryo-EM studies show that Brr2 unwinds the U4/U6 snRNA interaction thus causing the release of U4. This U4 release allows the recruitment of other protein complexes, stabilising the RNA interactions between U2, U5 and U6 snRNAs with the pre-mRNA and positioning the 5' splice site and branch point to allow the first transesterification reaction (Galej, *et.al.,* 2016). It is thought that Aar2 also functions in ensuring the U4/U6 di-snRNA binds to Prp8 within the U5 complex following unwinding by Brr2 by inhibiting binding of unwanted RNAs to Prp8 (Weber et al., 2013). Aar2 also has an essential role in in recycling of spliceosomal components with depletion of Aar2 resulting in an increase of unspliced mRNA (Weber et al., 2013). For correct spliceosomal function, the interplay between Aa2r and Brr2 is essential for unwinding and stabilising the U4/U6 di-snRNA to create the catalytically active spliceosome (Raghunathan and Guthrie, 1998).

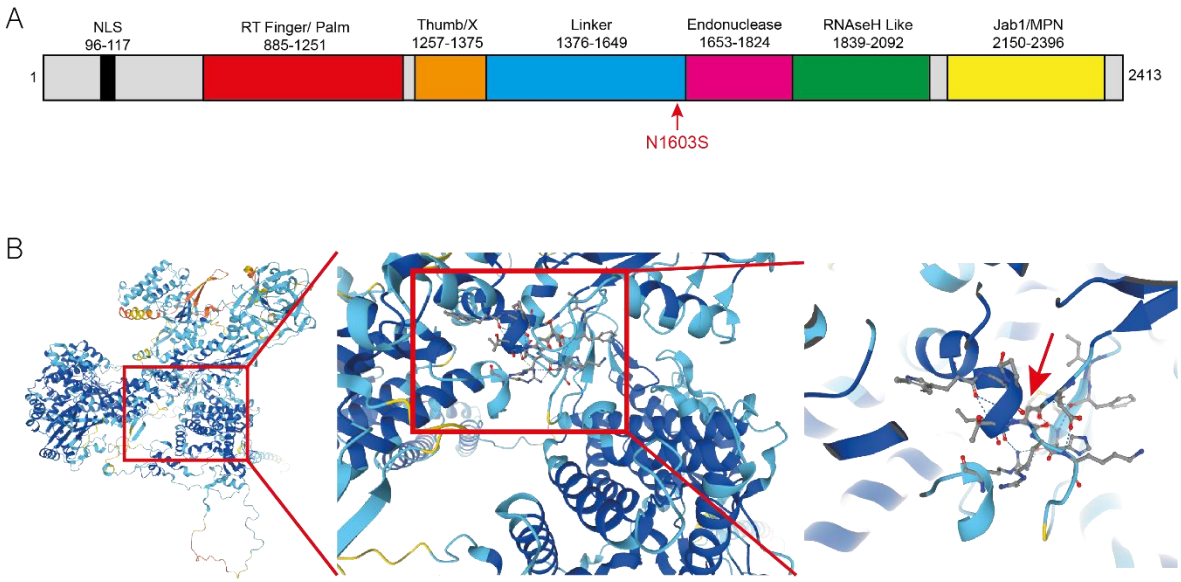

Figure 1.7: Structure of Prp8
(A) Representation the structure of Prp8 depicting all domains and their amino acid position. NLS = nuclear localisation signal. RT=Reverse transcriptase. The red arrow shows the location of the yeast equivalent $PRPF8^{N1531S}$ mutation. **(B)** Protein folding schematic of PRPF8 generated by AlphaFold showing how central the N1531 residue is. From left to right, each panel is a magnified version of the previous panel. Red arrow depicts the location of the N1531 residue.
Adapted from Boylan (2015).
AlphaFold image adapted from: https://alphafold.ebi.ac.uk/entry/Q8T295

1.3.2 Prpf8 in Disease

One of the most common diseases caused by mutations within PRPF8 is Retinitis Pigmentosa (RP). RP affects around 1:4000 people worldwide and is characterised by night blindness and the gradual loss of peripheral vision (Verbakel et al., 2018). RP has been diagnosed in children as young as five, though typical onset is around adolescence (Gao et al., 2019). Around 70-80% of RP cases are non-syndromic with over 80 genes and 3000 mutations identified so far; autosomal dominant mutations account for somewhere between 15-40% of cases (Hartong et al., 2006; Tsang and Sharma, 2018; Daiger, 2021)

As discussed, the retinal photoreceptor cells are highly modified primary cilia, with each cell containing a basal body, connecting cilium and outer segment. Phototransduction occurs within this apical outer segment and, since this segment contains no cellular apparatus, all necessary components for signal transduction have to be transported via the connecting cilium (Roepman and Wolfrum, 2007). Mutations within genes associated with photoreceptor formation and phototransduction can lead to RP, especially genes that are involved in the establishment and function of the connecting cilium. Surprisingly, nine genes associated with the spliceosome have been associated with causing autosomal dominant RP (adRP) when mutated. Of those nine genes, five are core components of the U4/U6.U5 tri-snRNP - PRPF3, PRPF4, PRPF6, PRPF31 and PRPF8 – with others being tri-snRNP splicing co-factors (Fahim et al., 2017) (Figure 1.6).

Within adRP cases, PRPF8 is found to be the second most frequently mutated of the U4/U6.U5 tri-snRNP (Fahim et al., 2017). The vast majority of these RP associated variants were found to be clustered within a 14 codon region in the final exon of PRPF8, with variants in this region accounting for 1% of total RP cases (Towns et al., 2010; Verbakel et al., 2018). However, additional screening has identified PRPF8 adRP causing variants which fall outside of this region, in exons 42 and 39 (Towns et al., 2010; Escher et al., 2018). Nevertheless, over 30 human adRP variants have been identified grouped within the Jab1/MPN C-terminal functional domain (Maxwell et al., 2021). The finding that all adRP PRPF8 mutations are clustered within this functional domain suggest that either this region has increased susceptibility to mutation, or is critically important for PRPF8 function (Towns et al., 2010; Escher et al., 2018).

Analysis of associations between genotype and phenotype in adRP revealed that the three most commonly mutated amino acids in PRPF8 adRP - H2309P, H2309R and R2310K – correlated with patient phenotype severity, with H2309P and H2309R being consistently more severe than R2310K (Towns et al., 2010). Modelling these variants in yeast revealed that the mutations which correlated with patient severity exhibited an increased reduction in yeast growth rate compared to the less severe variants (Towns et al., 2010). As the Jab1/MPN functional domain is highly conserved through Arabidopsis, trypanosomes, yeast to humans (Hoddges et al., 1995) this suggests the region is not highly susceptible to mutation, but is in fact vital for PRPF8 function. The exact mechanism behind

why mutations in the Jab1/MPN domain lead to adRP is currently unknown. It is assumed because the variants are within the last exon, PRPF8 avoids nonsense mediated decay thus allowing for build-up of non-functional protein and reduced levels of functional protein (Gamundi et al., 2008) . In the same vein as this explanation, it is possible that mutated PRPF8 mis-folds causing it to either accumulate and result in cell death, or to be broken down resulting in a decrease of functional PRPF8 (Comitato et al., 2007; Towns et al., 2010).

As previously mentioned, the Jap1/MPN domain of Prp8 interacts with Brr2, SNRNP200 in humans, and causes the unwinding of the U4/U6 di-snRNAs allowing the spliceosome to become catalytically active. Unwinding of the U4/U6 di-snRNA may be affected due to adRP variants within PRPF8 causing inhibition or premature activation of SNRNP200 (Mozaffari-Jovin et al., 2013). Indeed, modelling the PRPF8 adRP variants mentioned, as well as others, in yeast demonstrated interactions between Brr2 and Prp8 were inhibited (Maeder, Kutach, and Guthrie 2009; Boon et al. 2007). A number of these Prp8 adRP variants caused a decrease in unwinding of the U4/U6 di-snRNA while others caused an increase (Mozaffari-Jovin et al., 2013, 2014). Since the charge of the PRPF8 C-terminal tail is only slightly altered by the R2301K variant, the interaction with SNRNP200 is proposed to be only mildly affected. This mild alteration in interaction between PRPF8 and SNRNP200 compared to other adRP PRPF8 variants explains the less severe RP phenotype described previously (Towns et al., 2010; Mozaffari-Jovin et al., 2014). Additionally, mutations within SNRNP200 also cause adRP, giving credence to hypothesis that RP may be caused by splicing dysfunction due to impaired interaction of PRPF8 and SNRNP200 (Escher et al., 2018).

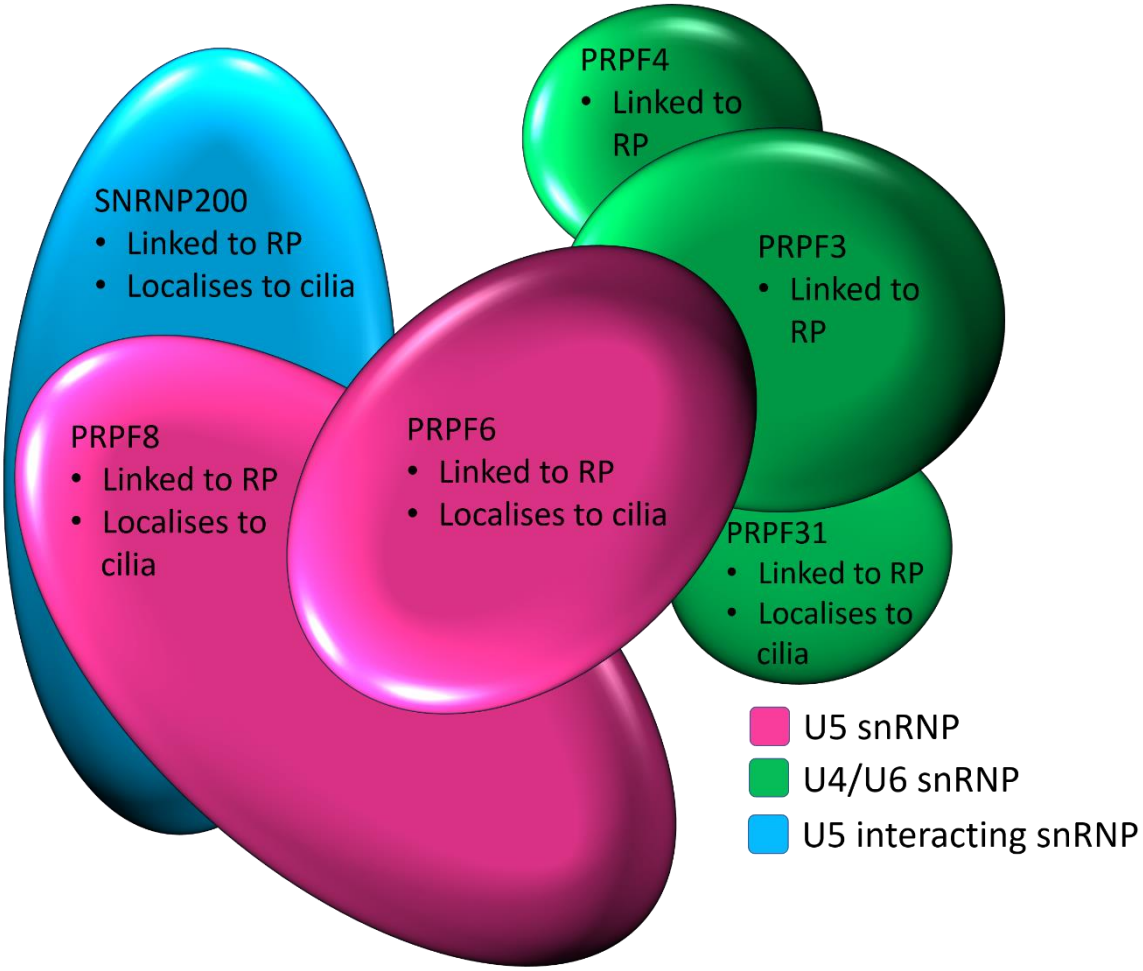

Figure 1.8: Simplified Structure of the U4/U6.U5 tri-snRNP.
All proteins in the U4/U6.U5 tri-snRNP are depicted to scale. All are linked to RP and PRPF8, PRPF6, PRPF31 and SNRNP200 have been found localised to various regions of the cilia in a range of cell types. Image taken from Maxwell, et.al (2021).

1.3.3 Prpf Proteins and Cilia

More recently, investigations aimed at uncovering the link between the U4/U6.U5 tri-snRNP PRPF proteins and RP has suggested that, rather than inhibition of canonical splicing, these proteins are directly required for cilia function. For instance, work by Buskin et al. (2018) found that cilia length and cilia number were significantly decreased in PRPF31 knocked out retinal pigment epithelium (RPE) cells. Furthermore, the number of cilia was also reduced PRP31 RP patient derived photoreceptors. Moreover, Buskin et al. (2018) found that PRPF31 localised to the cilia axoneme within fibroblasts, iPSCs, RPE cells and photoreceptors suggesting PRPF31 does not simply function within the cilia of photoreceptors.

To corroborate the hypothesis that loss of PRPF31 was the cause of the observed cilia defects, Buskin et al. (2018) knocked down *PRPF31* via RNAi in a human ciliated cell line. This knockdown significantly decreased cilia number and disrupted the Hedgehog pathway, confirming cilia functionality was abnormal. Knockdown of *PRPF*31 also caused the mis-localisation of a number of cilia related proteins including IFT88, as well as proteins usually found in the transition zone (Buskin et al., 2018). Similar work utilising an RNAi screen to identify proteins required for ciliogenisis in mouse ciliated cells identified PRPF31 as well as PRPF6, SNRNP200, and PRPF8 (Wheway et al., 2015). Further investigation in RPE cells found that knockdown of PRPF6, PRPF8 and PRPF31 resulted in decreased length and number of primary cilia and that each protein localised to the base of the primary cilium in both a mouse and human ciliated cell line. Additionally, Wheway et al. (2015) showed that PRPF31 RP mutations significantly reduce the length of the photoreceptor connecting cilium and that the length decrease correlates with RP severity. Wheway et al. (2015) also demonstrate that PRPF6 and PRPF8 localise to the connecting cilium axoneme and basal body complex of mouse photoreceptor cells further giving credence to the idea that PRPF proteins cause RP through a splicing independent manner (Wheway et al., 2015). Intriguingly, in a zebrafish model where *prpf31* or *prpf4* was knocked down, the zebrafish displayed pericardial oedema, curled body axis and hydrocephalous, all hallmarks of global motile cilia defects in zebrafish (Linder et al., 2011, 2014; Choksi et al., 2014). Subsequent work also demonstrated that upon up regulation of an equivalent PRPF4 adRP mutation in zebrafish, the embryos also displayed these same morphological phenotypes associated with global motile cilia defects (Chen et al., 2014).

Taken as a whole, these findings would suggest that splicing factor related adRP may not be caused by dysfunctions in the splicing process, but rather dysfunctions within the maintenance and function of the connecting cilium. It is interesting to note that to date, no other non-RP related splicing factors have been found to be localised to the cilia in any model (Johnson and Malicki, 2019) hinting at a specific role for these proteins within cilia. Furthermore, based on the results from *prpf31* and *prpf4* in the zebrafish

model, it could be argued that Prpfs don’t solely function within primary cilia, but are necessary for the function of motile cilia globally.

1.4 Prpf8 Mutant Models

1.4.1 The PRPF8^{N1531S} Project

The PRPF8^{N1531S} mouse line, referred to as K27, was created via an ENU induced mutagenesis screen aimed at isolating mutants on chromosome 11 that possessed developmental defects (Kile et al., 2003; Hentges et al., 2006). This screen utilised a mouse line containing a defined inversion within chromosome 11, termed a balancer chromosome. This balancer chromosome suppresses recombination and so maximises the identification of lethal alleles in trans to the inverted region (Sturtevant, 1921). The specific chromosome 11 balancer used contained an inversion that disrupted the *Wnt3* gene, therefore embryos that were homozygous for the balancer chromosome were embryonic lethal (Liu et al., 1999). The balancer chromosome also carried an *Agouti* transgene marker allowing for easy identification of heterozygotes. These balancer mice were bred to the ENU treated mice to produce offspring that contained a mutation *in trans* to the balancer region. Several rounds of outcrossing and backcrossing were carried out to remove any mutations located outside of the balancer region. This method identified a number of mutations causing developmental defects within the region of chromosome 11 analysed, one of which was the K27 mouse line. Next generation sequencing uncovered several mutations within this K27 line, however only one was found to be in an exon suggesting it was the causative mutation behind the observed developmental defects (Kathryn Hentges, pers comm). This mutation was identified to be an A to G transition within exon 28 of the Prpf8 gene, causing a missense mutation which replaces an asparagine residue with a serine residue at position aa1531. Amino acid 1531 is highly conserved from yeast to humans with modelling of protein dynamics suggesting that this substitution may alter the interaction of Prp8 with the binding partner Aar2 (Choi et al., 2012).

1.4.2 The PRPF8^{N1531S} Phenotype

Work by Boylan (2015) to characterise this PRPF8^{N1531S} mouse mutant revealed some interesting results. These embryos presented with globally delayed development, failure of neural tube closure, failure of embryonic turning and all embryos were lethal around embryonic day 10.5. Most notable was that approximately 50% of mouse PRPF8^{N1531S} embryos presented with reversal of heart looping. This phenotype was found to be caused by global defects within the establishment of the L/R axis, with several known laterality markers, namely *Lefty2* and *Nodal,* displaying absent or ectopic expression. Interestingly, the midline marker *Lefty1* was not expressed in PRPF8^{N1531S} embryos, suggesting that inability to establish the midline may be causing the observed ectopic expression of *Nodal* and *Lefty2*. Notably, the mis-expression of genes associated with

laterality establishment was found to exist in the earliest known marker of laterality, *Cerl2,* before establishment of the midline, suggesting an upstream cause for these observations.

Surprisingly, Boylan (2015) found that 9+0 cilia within the node of PRPF8^{N1531S} embryos, which normally have a circular beat, were completely immotile. This lack of motility correlated with lack of fluid flow, measured by the addition and tracking of small particles in the node. Furthermore, when analysing 9+0 cilia structure within the node cilia, Boylan (2015) found that these cilia were significantly shorter than in WT. Additionally Boylan (2015) also found that node architecture was affected, with the node appearing as a flat depression rather than a concave pit. Transmission electron microscopy of the 9+0 nodal cilia revealed no abnormalities in microtubule structure or absence of dynein arms leaving the cause of the immotility of the 9+0 cilia unknown. In conjunction with uncovering defects in KV cilia, Boylan (2015) and Stephen (2013) also showed that the Prpf8^{N1531S} embryos possessed defects within the Hedgehog pathway. Stephen (2013) found that *Sonic Hedgehog* (*Shh)*, *Gli1* and *Gli2* were slightly upregulated, with *Gli3* slightly downregulated in mutants. Further analysis by Boylan (2015) demonstrated that *Shh* expression was present in the midline of E8.5 embryos, as expected, but expression pattern was interrupted, supporting the findings from Stephen (2013). These findings fit with a proposed cilia specific mechanism for Prpf8, but could also be caused by a reduction in splicing efficiency causing widespread detrimental effects to development. Indeed, Boylan (2015) also demonstrated that splicing efficacy was hindered in a yeast model of the PRPF8^{N1531S} mutation.

Taken as a whole, the work by Boylan (2015) demonstrated that the PRPF8^{N1531S} mutation causes 9+0 KV cilia defects including immotility and decrease in length. This result is proposed to be the cause of the observed defects in expression of laterality markers and the observed heart looping defect. Additionally, *Shh* pathway component expression was dysregulated, but it is unclear whether this links to cilia dysfunction or a result of inhibited splicing fidelity. At this point it is unknown if Prpf8 affects other types of motile cilia because PRPF8^{N1531S} embryos die prior to the development of tissues containing 9+2 motile cilia.

1.4.3 Previous Characterisation of the *cph* Zebrafish

During a genetic screen in zebrafish, Keightley et al. (2013) discovered a missense mutation termed *cephalophŏnus* (*cph*). This G to T transversion was found to cause a premature stop codon in *prpf8* resulting in truncation of the protein at position aa396. This mutation was proposed to result in a null phenotype due to the predicted truncation causing the removal of over 80% of the protein. The *cph* mutation resulted in varied phenotypes including neural degeneration and defects in haematopoiesis. Interestingly, Keightley, *et.al.* (2013) found that *cph* mutants showed aberrant splicing that affected some genes more severely than others. Their analysis showed that several haematopoietic genes were

spliced incorrectly including *gata1*, which displayed exon skipping, as well as signalling molecules such as mapk12. As discussed, Prpf8 is a core protein in the U5 snRNP and is vital for spliceosomal activity. The *cph* mutation was found to cause a failure in the formation of the U4/6.U5 tri-snRNP. Thus, the observation that only a subset of genes in specific cell types showed aberrant splicing was remarkable given the essential nature of the spliceosome. However, Keightley et al. (2013) do concede that the maternal *prpf8* mRNA contribution may function to partially rescue the Prpf8 loss of function phenotype prior to the activation of the zygotic genome. It is possible that the persistence of sufficient maternal *prpf8* transcripts, and thus protein, in some cell types compared to others, as well as the disparity of transcript and protein stability among cell types, may account for the difference seen in splicing within specific cell types of *cph* mutants.

In *cph* mutants, the self-splicing of *prpf8* was also found to be defective, leading to intron 7-8 being retained. This aberrant splicing introduced a stop codon downstream of exon 7 but prior to the stop codon caused by the initial *cph* mutation in exon 9. The fact Prpf8 is involved in its own splicing suggests that Prpf8 may be involved in an auto-feedback loop. As splicing defects are not seen in all pre-mRNAs of a particular cell type, this lack of universal splicing errors may be explained by the reliance on Prp8 to strengthen the exon interaction with U5 in a subset of pre-mRNAs for splicing to be performed correctly (Aronova, *et.al.,* 2007). In light of the discovery by Boylan (2015) that the mouse $PRPF8^{N1531S}$ mutant exhibits defects in cilia motility and L/R axis establishment, it is also conceivable that Prpf8 may have a role independent of spliceosome function which causes aspects of the *cph* phenotype. Indeed, as mentioned, the curl down of the A-P body axis in zebrafish is a hallmark of motile cilia defects. Additionally, preliminary work in the Roy lab suggested that *cph* fish have an increased incidence of heart looping defects (Sudipto Roy, per comm), suggesting problems with laterality establishment.

1.5 Zebrafish as a Model for Studying Cilia Function

Zebrafish are a member of the teleost family of fish, originally from south Asia. Over the last several decades zebrafish have become an invaluable model for studying a range of biological processes. Zebrafish possess orthologues to over 70% of human genes and more than 82% of genes identified in human disease have at least one orthologue in zebrafish (Song et al., 2016). Zebrafish also possess a number of morphological traits which are advantageous to biological research. Firstly, the embryos develop externally allowing for direct visualisation of development under a bright field microscope or by antibody staining or transgenic investigation. Secondly, embryos are naturally transparent up until around 48hpf but pigmentation can be artificially inhibited, or strains can be crossed to the *casper* mutant which completely lacks pigmentation, allowing for visualisation of organogenesis. As well as advantageous morphological characteristics, zebrafish are also incredibly amenable to genetic manipulation. The use of morpholinos to knockdown a gene of interest is widely utilised in zebrafish, as well as the injection of RNA to increase protein levels or introduce a tagged version of the protein of interest.

In terms of research into cilia function, zebrafish have a number of advantages over mice which make them the ideal model for studying cilia function in vivo. Throughout development, motile cilia are present in 44 distinct organs with almost every zebrafish cell possessing a primary cilium (Malicki et al., 2011; Song et al., 2016; Pinto et al., 2021). The KV contains 9+0 rotary beating cilia and by 24hpf 9+2 laterally beating cilia are present in the pronephric duct. Additionally, there are 9+2 motile cilia in the otic vesicle at 24hpf and in the nasal placode at 72hpf. As the PRPF8^{N1531S} mutant mouse embryos die before characterisation of other cilia defects can be carried out, the diverse range of zebrafish ciliated organs along with their transparency make the zebrafish model ideal for studying ciliopathies. Specifically useful for this project is that, unlike mice, during early development zebrafish do not require a functioning circulatory system to survive so defects which detrimentally affect cardiac developmental are more easily investigated (Dooley and Zon, 2000).

In addition to the amenability of zebrafish to genetic manipulation, zebrafish embryos and larvae are ideally suited for high throughput phenotypic screening experiments. Such experiments include chemical screens for compounds which change behaviour or affect disease phenotypes and or progression. Additionally, multiple large scale drug discovery screens have been successfully carried out in genetically modified zebrafish using phenotypic and behavioural readouts (Gehrig et al., 2018). These large-scale screens can relatively quickly and easily identify novel drug or chemical compounds for further testing in clinical trials. For example, zebrafish ciliary *pkd2* and *ift172* mutants displaying renal cysts and A-P body axis curvature were used in a screen of 115 different chemical compounds, with high throughput imaging scoring phenotypic severity. This screen identified Tricostatin A and valpoic acid as compounds which ameliorated ciliopathy disease progression (De

Groh et al., 2010). These findings, along with the anatomical and developmental attributes discussed, highlight the utility of zebrafish as a model organism for studying cilia function

1.6 Aims and Hypothesis

Up to this point the working hypothesis has been that PRPF8^{N1531S} causes splicing dysfunction, possibly through inhibition of spliceosome assembly and/or activation. This explanation does not account for why cilia related functions seem to be predominantly affected in PRPF8^{N1531S} mutants. It is possible that the proposed splicing dysfunction in PRPF8^{N1531S} mutants affects cilia function because cilia related genes possess a common attribute which makes them partially vulnerable to a reduction in splicing fidelity. These attributes could be particularly long/short introns or long/short exons which inhibits the ability for Prpf8 to correctly position the mRNA for splicing.

Another explanation for the observed cilia related defects is that Prpf8 has a yet unknown function in ciliogenisis. This hypothesis is supported by the previously mentioned investigations which localised PRPF8 and other PRPF proteins to the axoneme and basal body of cilia in multiple cell types. Additionally, the finding that multiple other PRPF proteins also produce cilia defects when mutated may provide evidence against the splicing defect hypothesis. If one was to accept the splicing defect hypothesis, one would have to account for why different mutations, as well as differing levels of PRPF protein, across different *PRPF* genes all produce the apparent same mis-splicing of genes which seem to solely affect cilia function (Graziotto et al., 2011; Linder et al., 2011, 2014; Yin et al., 2011; Wheway et al., 2015; Buskin et al., 2018). It is possible that these two hypotheses are not mutually exclusive and that some aspects of the mouse PRPF8^{N1531S} phenotype could be caused by splicing dysfunction and others due to the dysfunction of Prpf8 within the cilium.

My initial aim was to characterise the *cph* mutant, focusing on defects associated with cilia dysfunction. This would reveal if loss of Prpf8 produces similar phenotypes to that of the PRPF8^{N1531S} mutant or whether the observed mouse phenotype is specific to the asparagine to serine mutation. Furthermore, I then aimed to investigate laterality within the *cph* embryo as preliminary data suggested heart looping was defective. I planned to do this by examining expression of a range of laterality markers to deduce whether laterality establishment was affected similarly in the mouse and zebrafish models. Assuming the *cph* mutants did display laterality defects, I investigated the KV to determine if KV cilia motility was affected. I also examined other motile ciliated organs to deduce whether the Prpf8 related cilia defect is specific to 9+0 cilia. In conjunction with this, I aimed to investigate the possible direct link between Prpf8 and cilia by determining the localisation of Prpf8 within *cph* ciliated structures. Additionally, I utilised a translation blocking morpholino to knockdown Prpf8 in WT zebrafish and compare and contrast the observed phenotypes with *cph* mutants to get a clearer understanding of the role of Prpf8 in cilia.

Chapter 2: Materials and Methods

2.1 Common Solutions

Solution	Composition
0.1M PO_4 Buffer	0.2M NaH_2PO_4 - 20 ml, 0.2M Na_2HPO_4 - 80ml, dH_2O - 100ml
5x MAB(T)	11.6g Maleic Acid (Sigma M0375), 8.7g NaCl, 200µl 100% Tween-20 Adjust to pH7.5 with NaOH, H_2O to 200ml
Blocking Buffer (Immunofluorescence)	PBDT, 2% Sheep serum
Blocking Buffer (*in situ*)	1.25g Boeringher blocking reagent, 50ml PBT, pH adjusted to 7.5 with NaOH
Blocking Buffer (Mouse)	3% BSA + 0.2% Tween-20 in H_2O
Blocking Buffer (Western Blot)	5% milk powder in TBST
Blocking Reagent	Blocking reagent (Roche 1096176). 10% stocks made up in MAB (MAB(T) but no tween-20)
Dent's Fix	80% Methanol, 20% DMSO
Egg Water:	0.3g/L NaCl in H_2O
Fish Fix	4% Paraformaldehyde, 4% sucrose, 12 mM $CaCl_2$, 0.1 M PO_4
Hybe A	10ml Hybe B, 50µl 20mg/ml yeast tRNA, 10ul of 50mg/ml heparin, 200µl 10mg/ml salmon sperm.
Hybe B	50% Formamide, 5X Depc SSC, 0.1% Triton X-100, $depcH_2O$, pH adjusted to 5.5 with concentrated HCL
Hybridisation mix (Mouse *in situ)*	25 ml 50% Formamide, 3.25ml 20x SSC pH 7.5, 5ml 0.5M EDTA pH8.0, 25µl 20mg/ml Yeast tRNA (Invitrogen 15401-011), 2.5ml 10% CHAPS (Sigma C5070, dissolved in H2O),100µl 50mg/ml Heparin (Sigma H9399), 1ml 10% Tween-20 (Sigma P1379), 17.5ml $depcH_2O$
Laemmli SDS Buffer	250mM Tris-HCl (pH6.8), 50% glycerol, 25% β-mercaptoethanol,10% SDS, 0.5% bromophenol blue
Lysis Buffer	40mM NaOH
NTMT	1ml 5M NaCl, 2.5ml 2M Tris-HCl pH 9.5, 2.5ml 1M MgCl2, 5ml 10% Tween-20, 39ml H_2O.
PBDT	1% BSA, 1% DMSO, 0.5% Triton-X100, 1X PBS
PBS	1.15g Na_2HPO_4, 0.2g K_2HPO_4, 8g NaCl, 0.2g KCl, To 1L with H2O

PBT	1X PBS, 0.1% TritonX-100
PFA	4% Paraformaldehyde, 1X PBS
PTW	PBS + 0.1% Tween-20
Resolving Gel (8%)	8% acrylamide, 375 mM Tris-HCl (pH 8.8), 0.1% APS, 0.1% SDS, 0.01% TEMED, H_2O
Running Buffer (Western Blot)	25mM Tris, 192mM glycine, 0.1% SDS
Scale 70	4M Urea in H_2O. 10% w/v Triton X-100 (S21414). 70% w/v glycerol (Sigma, 191612).
Scale A2	4M Urea in H_2O.10% w/v Triton X-100 (S21414). 10% w/v glycerol (Sigma, 191612). Adjust pH to 7.7
Scale B4	8M Urea in H_2O.10% w/v Triton X-100 (S21414). Adjust pH to 8.7.
Stacking Gel (4%)	4% acrylamide, 125 mM Tris-HCl (pH 6.8), 1% SDS, 0.06% APS, 0.003% TEMED, H_2O
Staining Solution (*in-situ)*	8.05ml depcH_2O, 1ml 1M TRIS-HCL (pH 9.5), 250µl 4M NaCl, 100µl 10% Triton X-100
TBS (20x Tris-bufferd saline)	400mM Tris, 2.742M NaCl, pH adjusted to 7.6 with HCl
TBST	1X TBS, 0.1% Tween 20
Transfer Buffer (Western Blot)	25mM Tris, 192 mM glycine, 20% methanol

Table 2.1: List of commonly used solutions

2.2: Mouse Husbandry and Embryo Dissection

The *l11Jus27* (Prpf8 mutant) mouse line was maintained on a 129S5 background with the mutation coming from the C57BL/6J (B6) strain. Mouse lines were maintained on a 12 hour light/dark cycle in the Biological Service Facility (BSF) at the University of Manchester in line with Home Office requirements and with BSF ethical approval. Mice were sacrificed using a schedule one method subject to Personal License Number IA4F700D3 conditions. Pregnant female mice were sacrificed according to the desired embryonic developmental time point calculated from when a vaginal plug was noticed. Embryos were then dissected out of their decidua and extra embryonic tissue removed. Embryos were then placed in individual 1.5ml tubes in PBS until dissection was finished. After all embryos were dissected out of the uterus, PBS was removed from each individual tube and embryos were incubated in 4% PFA at room temperature (RT) on a plate shaker for 2 hours. Embryos were then washed twice with PBS. If embryos were not being used immediately they were dehydrated in a 25%, 50%, 75% and 100% methanol gradient before being stored at -20°C in 100% methanol.

2.3: Zebrafish Husbandry

All strains used is this project were maintained by the Institute of Molecular and Cell Biology Zebrafish Facility and are listed in Table 2. The facility sustains a temperature of 28.5°C and a standard light/dark cycle of 14 hours and 10 hours respectively. Zebrafish pair mating method was used to obtain embryos. Embryos were left to develop in egg water containing methylene blue at 28.5°C until the desired stage. Dead embryos were removed periodically.

Zebrafish Strain	Purpose
AB	Wild-type
cph	To assess function of Prpf8
igu	Lacks primary cilia

Table 2.2: List of zebrafish strains used

2.4: Genomic DNA extraction

For DNA extraction of mouse embryos, the yolk sac was removed during dissection and placed in a 1.5ml tube. 100µl 50mM NaOH was then added and the tube placed at 95°C for 30 minutes. 20µl 50mM Tris-HCL was then added to neutralise the solution.

For DNA extraction of adult mouse tissue, the tissue was placed in a 1.5ml tube and 250µl DNA lysis buffer and 2µl of 80µg/ml Proteinase K added. The sample was then incubated at 55°C for 4 hours. Samples were then centrifuged at 13,000RPM for 5 minutes and the supernatant transferred to a fresh tube. 300µl of isopropanol was added to the supernatant and mixed by inversion 8 times. Samples were then centrifuged at 13,00RPM for 20 minutes, the supernatant was removed and the DNA pellet washed in 70% ethanol before being resuspended in 100µl dH_2O.

The method for extraction of genomic DNA from zebrafish was dependant on age. Adult zebrafish (older than 3 months) were anesthetised in Tricaine Mesylate before having a small section of their fin cut off with a sterile blade and it placed in 100µl PBS. The PBS was removed and the fin clip incubated at 95°C for 30 minutes in 40µl of lysis buffer. If the fin clip was not fully dissolved then the tube was vortexed and placed back at 95°C for 10 minutes. For singular zebrafish embryos (<48hpf), they were first dechorionated and washed in PBS. 10µl (40µl if multiple embryos) of lysis buffer was then added and incubated at 95°C for 30 minutes. Both fin clip and embryos lysis solutions could then be used directly in downstream reactions.

2.5: PCR

Manchester University -

All standard PCR reactions were carried out using the following protocol:

2µl 5X MyTaq Red Mix (Bioline 25044)
1µl F&R Primer mix (10mM per primer)
1µl DNA
6µl H_2O

5µl 2X Ultra Taq Red Mix (PB10.33-01)
1µl F&R Primer mix (10mM per primer)
1µl DNA
3µl H_2O

5µl 2X Q5 polymerase (M0492S)
1µl F&R Primer mix (10mM per primer)
1µl DNA
3µl H_2O

The following cycling conditions were used for the majority of PCRs. Annealing temperature was adjusted as required for specific primer pairs as well as extension length depending on size of amplicon.

Heat lid to 112°C
98°C for 5 minutes
Cycle x35 98°C for 30 seconds
60°C for 30 seconds
72°C for 30 seconds
72°C for 10 minutes
Hold 7°C infinite

For Q5 polymerase:

Heat lid to 112°C
Hotstart 98°C
98°C for 2 minutes
Cycle x35 98°C for 10 seconds
60°C for 20 seconds
72°C for 30 seconds
72°C for 10 minutes
Hold 7°C infinite

IMCB -

All standard PCR reactions were carried out using the following protocol:

2x MyFi Mix (Bioline)	5µl
Forward Primer (10mM)	0.5µl
Reverse primer (10mM)	0.5µl
Template DNA	1µl
dH_2O	3µl

The following cycling conditions were used for the majority of PCRs. Annealing temperature was adjusted as required for specific primer pairs.

98°C for 3 minutes
Cycle x35
98°C for 30seconds
60°C for 30 seconds
72°C for 30 seconds
72°C for 5 minutes
Hold 7°C infinite

2.6: Sequencing PCR

Manchester University -

To sequence genomic DNA to confirm the presence of the Prpf8 mutation, or determine the sequence of RT-PCR products, sequencing reactions were set up as follows.

Xµl	DNA
2 µl	Big Dye
2 µl	F or R Primer
4 µl	5x Buffer
X µl	H_2O up to 20µl

DNA and water volumes were adjusted based on the DNA concentration of the PCR product when observed on an agarose gel.

PCR conditions for cycle sequencing were:

Heat lid to 112°C	
96°C for 1 minute	
Cycle x24	96°C for 30seconds
	50°C for 15 seconds
	60°C for 4 minutes
Hold 10°C infinite	

Reactions were then transferred into a 1.5ml tube and 16µl H_2O + 64µl of 95% Ethanol added. Tubes were then briefly vortexed and left at RT for 15 minutes to precipitate products. Tubes were then centrifuged at 13,000RPM for 20 minutes and the supernatant discarded. 250µl of 70% Ethanol was then added and vortexed briefly. Tubes were then spun at 13,000RPM for 10 minutes and supernatant discarded. Tubes were then left open and dried at 90°C before being submitted for sequencing in the FBMH core facility.

IMCB -

All sequencing reactions were carried out using the following protocol:

V3.1 Sequencing Mix	4µl
Forward Primer (10mM)	0.5µl
Template DNA (PCR)	0.5µl
dH_2O	5µl

Cycling conditions for sequencing PCR were as follows:

Heat lid to 112°C	
96°C for 1 minute	
Cycle x25	96°C for 10 seconds
	55°C for 20 seconds
	60°C for 1 minute
Hold 4°C infinite	

Sequencing PCR was then diluted 1:5 in dH_2O and submitted to the sequencing facility.

2.7: Genotyping *cph* Zebrafish

cph zebrafish were initially genotyped using the DNA extraction method and IMCB sequencing method described above. Subsequent genotyping relied on PCR amplification and restriction digest by the following protocol:

PCR amplification of a region of the *prpf8* gene using "*cph"* primers (Appendix1). PCR reaction was cleaned up using QIAGEN PCR Gel Clean up (Cat. No 28104) and a restriction digest using *AccI* enzyme performed as per protocol below using 200-500ng of DNA. Samples were then run on 2% agarose gel. WT will produce one band, Heterozygotes will produce 3 bands and homozygotes will produce 2 bands (see Figure 3.2). Positive control of known mutant was always used to confirm full digestion of PCR product.

2.8: Restriction Digest

All restriction enzymes used in this project were from NEB and were used with 10X Cutsmart buffer and incubated at 37°C for 1 hour. Reaction mixture for genotyping following PCR was as follows:

Template DNA	200ng-1µg
10x Cutsmart buffer	2µl
Restriction enzyme	1µl
dH_2O	up to 20µl

For plasmid linearisation 3µg of template DNA was used and reaction volumes were sometimes adjusted for a 50µl reaction.

2.9: Agarose Gel Extraction

Gel bands were excised from agarose gels by visualising the band on a UV transilluminator and cutting around the band with a clean razor blade. Two alternative methods for agarose gel extraction were used. One utilised the IllustraTM GFX PCR DNA Cel Band Purification Kit" (GE Healthcare 10536295) or the QIAquick Gel Extraction Kit (Qiagen 28704) where the manufacturer's protocols were followed. The alternative method involved piercing a small hole in the bottom of a 0.5ml tube and placing it in a 1.5ml tube. A small amount of glass wool was then inserted into the 0.5ml tube and the cut-out gel band placed on top of the glass wool in the 0.5ml tube. The 1.5ml tube (containing the 0.5ml tube) was then spun at 5,000RPM for 10 minutes. The 0.5ml tube could then be discarded and 1:1 volume of isopropanol added to the filtrate. A 1:10 volume of 3M Na Acetate was then added to the filtrate. Components were then mixed by inversion and incubated at -20°C for

at least 30 minutes. The tube was then centrifuged at 13,000RPM for 10 minutes and the supernatant discarded. Pellet was resuspended in 20µl H2O.

2.10: RNA Isolation from Mouse and Zebrafish Embryos

For extraction of RNA from mouse tissue, the tissue was first placed in a 1.5ml tube and 200µl TRizol Reagent (Sigma T9424) added. Tissue was then homogenised, depending on size of tissue, either with a homogeniser or by repeated suction through a 0.5mm syringe. 20µl of chloroform was then added. Tube was then mixed by inversion a few times before being centrifuged at 14,00RMP at 4°C for 15 minutes. The upper phase of the supernatant was then transferred to a new 1.5ml tube and 50µl isopropanol added. Sample was then mixed by inversion 8 times and left at RT for 10 minutes before being centrifuged at 14,000RMP at 4°C for 10 minutes. Supernatant was then discarded (being careful not to remove the pellet) and 100µl 75% Ethanol (25% depcH_2O) added. Tube was then spun at 14,00RMP at 4°C for 15 minutes. Ethanol was removed and pellet dried before being resuspended in 20µl depcH_2O.

For zebrafish embryos, between 30-60 embryos were transferred from a petri dish to an Eppendorf and washed in PBS. PBS was removed and 1ml of Trizol added. If necessary, embryos could then be kept at -80°C for up to a year. Embryos were lysed in Trizol using a 0.5mm syringe by sucking the embryos back and forth through the needle. 200µl of chloroform was then added to the lysate and mixed by inverting several times. The rest of the protocol was identical to that of mouse RNA extraction except the volume of isopropanol added to the upper phase of the aqueous solution was 500µl rather than 50µl. RNA concentration was measured using a Nanodrop 1000 spectrophotometer. RNA was stored at -80°C.

2.11: cDNA Synthesis

Manchester University –

The Tetro cDNA synthesis kit (Bioline 65042) was used for cDNA synthesis.

X µl	RNA (up to 5µg)
1 µl	Random Hexamer
1 µl	10mM dNTP mix
4 µl	5x Reverse transcriptase buffer
1 µl	Ribosafe RNase inhibitor
1 µl	Tetro Reverse Transcriptase
X µl	DepcH_2O up to 20µl

Volumes of RNA and water were determined for each reaction based on RNA concentration as assessed by nanodrop measurement. The reaction was set up on ice. Reaction components were mixed gently by pipetting then incubated at 25°C for 10 minutes followed

by 45°C for 30 minutes. The reaction was terminated by incubating at 85°C for 5 minutes then rapidly chilling on ice.

IMCB -

The following cDNA synthesis reaction mixture was set up on ice and incubated at 65°C for 5 minutes:

RNA	2µg
Oligo(dT)20 (50 µM)	1µl
dNTPs mix (10 mM)	1ul
DEPC-H_2O	up to 10µl

The reaction was then placed on ice and the following reagents added:

MgCl2 (25 mM)	4µl
10X RT buffer	2µl
DTT (0.1 M)	2µl
RNAse OUT (40 U/µl)	1µl
Superscript III Reverse Transcriptase	1µl

Reaction was incubated at 50°C for 1 hour and then terminated by incubating at 85°C for 5 minutes. 1µl of RNAse H was then added and reaction incubated at 37°C for 30 minutes before being stored at -20°C

2.12: Mouse Embryo Embedding and Sectioning

Embryos that were stored in methanol were rehydrated through a 75%, 50%, 25% and PBS gradient. Embryos were then embedded in OCT. Moulds containing OCT embedded embryos were then placed directly on dry ice to flash freeze the OCT. Moulds were then placed at -80°C until sectioning. Cryostat sectioning was carried out on a Leica 350S. Slides containing sections were stored at -80°C for future use.

2.13: Immunofluorescence of Mouse Sections

Slides were removed from -80°C and dried on a 37°C heat block for 10 minutes. Slides were then washed with PBS (2x 5 minutes) and then, if necessary, subjected to antigen retrieval. Sections were then permeabilised in 0.2% PTW for 1 hour at RT. Slides were then dabbed dry and marked with an oil pen around the sections. Sections were then blocked in Blocking Buffer for 1 hour at RT. Blocking Buffer was then removed and primary antibody diluted in Blocking Buffer was added to sections and incubated overnight at 4°C. Primary antibody was removed and sections washed in 0.1% PTW (3x quick wash, 3x 10 minute washes). Corresponding secondary antibody was then added (either Alexa Flour 488 (1874804) or 647(1959073)) at a 1:500 dilution in Blocking Buffer and incubated at RT in the dark for 1 hour. Secondary antibody was removed and slides washed in 0.1% PTW

(3x quick wash, 3x 10 minute washes). Sections were stained with DAPI (D8417) at a 1:500 dilution in Blocking Buffer for 10 minutes then washed with 0.1% PTW (2x 5 minutes) then washed with H_2O. Slides were then tapped dry, mounted using DPX (06522) and stored at 4°C in the dark.

2.14: Antigen Retrieval of Mouse Sections

300ml 10mM Sodium Citrate pH6 was brought to almost boiling in the microwave. Slides were then put on a rack with sections facing up and submerged in the Sodium Citrate. Slides were microwaved at power 40 for 8 minutes before being allowed to cool back down to room temperature. Slides were removed from Sodium Citrate and washed twice with PBS.

2.15: Mouse Whole Mount Immunofluorescence

Embryos were first permeabilized in 1mL of 0.1%PTW for 2 hours on plate shaker at RT. They were then incubated in 1 mL of Blocking Buffer for 2 hours on a plate shaker at RT. Embryos were then exposed to desired primary antibody at desired dilution (add list of antibodies and dilutions) in Blocking Buffer and incubated at 4°C for 48 hours. Embryos were then washed in PTW (5x 30 minutes) at RT on a plate shaker. Embryos were then exposed to corresponding secondary antibody (either Alexa Flour 488 (1874804) or 647(1959073)) at 1:500 dilution for 48 hours at 4°C. Embryos were then washed in PTW (5x 30 minutes) at RT on a plate shaker. They were then post fixed in 4% PFA for 1 hour at RT on a plate shaker and then washed twice with PBS. Embryos were then stained with DAPI (1:500) diluted in Blocking Buffer for 10 minutes at RT on a plate shaker followed by two PBS washes. Embryos were then cleared in Scale A2 solution, Scale B4 solution and Scale 70 solution each for 48 hours at 4°C on an orbital shaker. Embryos were stored in PBS at 4°C before imaging.

2.16: Zebrafish Embryo Fixation for Immunofluorescence

For embryos 0-23hpf embryos were placed in 1ml of “Fish Fix” (FF) and fixed either at room temperature for 2 hours or at 4°C overnight. Embryos were then dechorionated, washed in PBS multiple times to remove FF and placed in 100% Methanol at -20°C until needed. Embryos older than 23hpf were first dechorionated before fixing in FF then protocol was followed as stated.

For fixation in “Dent’s fix” embryos were dechorionated regardless of HPF and placed in 1ml of Dent’s fix. Embryos were stored overnight at 4°C and used for experiments

the next day. Storage of embryos in 100% Methanol until needed resulted in over fixation of embryos.

2.17: Zebrafish Whole Mount Immunofluorescence

Embryos were transferred into a glass cavity dish and rehydrated from Methanol by washing in consecutively lower Methanol concentrations (75%, 50%, 25%) made up with PBS. Embryos were subsequently washed x3 in PBS at 5 minute intervals. PBS was removed and embryos treated with -20°C acetone and placed at -20°C for 7 minutes (Note – this step was not necessary for embryos fixed with Dent's fix). Embryos were once again washed x3 in room temperature PBS at 5 minute intervals. Embryos were then blocked for 1 hour at room temperature in 2% sheep serum in PBDT on an orbital shaker at 70 rpm. Blocking buffer was removed and primary antibody (see Table 3) diluted in PBDT added. Embryos were then placed on an orbital shaker at 70rpm overnight at 4°C. The following morning the primary antibody was removed and embryos washed in room temperature PBDT x3 at 30 minute intervals on and orbital shaker at 70rpm. PBDT was removed and corresponding secondary antibodies were diluted in fresh PBDT at desired concentration (see Table 4) and placed on an orbital shaker at 70rpm for 5 hours at room temperature. During the last 30 minutes DAPI was added (1:2000). Secondary antibodies were then removed and embryos washed x3 at 30 minute intervals with room temperature PBDT. PBDT was removed and embryos were submerged in 70% glycerol for storage at 4°C.

Primary Antibody	Manufacturer	Dilution
Acetylated-Tubulin (Mouse monoclonal)	Sigma, T6793	1:500
Gamma-Tubulin (Rabbit monoclonal)	Sigma, T5192	1:500
Prpf8 (Rabbit polyclonal)	Abcam, ab79237	1:200

Table 2.3: Primary antibodies for Immunostaining

Secondary Antibody	Manufacturer	Dilution
Alexa Fluor 488 Goat anti-mouse Ab	Invitrogen	1:500
Alexa Fluor 555 Goat anti-Rabbit Ab	Invitrogen	1:500

Table 2.4: Secondary antibodies for Immunostaining

2.18: Measurement of Kupffer's Vesicle (KV) Motile Cilia

14hpf embryos were stained with Ac-tubulin, Gamma-Tubulin and DAPI as per Zebrafish whole mount immunofluorescence protocol. KV was dissected out and mounted on a slide. Carcass was washed and used for genotyping. Mounted KVs were imaged on an Olympus Fluoview 1000 confocal microscope at x100 zoom and a z-stack image taken from the top of the KV to the bottom. Images were processed using ImageJ and a plugin called Simple Neurite Tracer utilised to measure each individual cilium from the base to the tip in 3 dimensions.

2.19: Zebrafish Morpholino Experiments

Morpholinos were designed and synthesized by GeneTools. Morpholinos were reconstituted to 1mM using sterile water upon arrival and stored at room temperature. 1 cell stage AB embryos were initially injected with 0.5nl of 100% morpholino using a Nitrogen gas injector and subsequently 50%, 33%, 25% and 20% etc dilutions until the correct concentration was determined. Correct concentration was determined by more than 75% of embryos surviving as well as the emergence of any phenotype. Injection of water was used as a control to make sure any phenotype was not caused by the injection procedure.

Morpholino	Sequence	Dilution
Prpf8 Translation Blocking (tbMO)	TGGCAGCGTCTAAGTTAAAAGCAGT	20% (1:4)
Prpf8 Splice Blocking (tbMO)	GGAAAGATAATGGTTCCTACCAGGT	33% (1:2)

Table 2.5: Sequence and dilution of morpholinos used

2.20: *In-Situ* Probe Design

The desired gene sequence was viewed on UCSC Genome Browser to determine a region of the gene around 600-800bp suitable for an *in-situ* probe. Usually this was found in the 3'UTR and produced minimal high sequence similarity to other known genes. When a suitable sequence had been decided upon primers were designed to amplify that sequence either from gDNA or cDNA using Primer3 web tool (http://bioinfo.ut.ee/primer3-0.4.0/). RNA polymerase binding sequences were then added to the 5' end of both the forward and reverse primers and a final check for no off-target binding performed. For all

probes – except Hnf3B- T7 polymerase makes the antisense probe and T3 makes the sense probe. This is reversed for Hnf3B.

2.21: *In-Situ* Probe Synthesis

Probes were synthesised by two methods; plasmid linearization and transcription, or PCR of desired region using primers containing RNA polymerase sites.

For zebrafish *lefty2* and zebrafish *dand5* (*Cerl2*), probes were synthesised from plasmids kindly provided by Dr. Sudipto Roy. These plasmids were linearised with the appropriate restriction enzymes and purified into 20ul DEPC-H_2O.

If no plasmid for probe synthesis was available, primers designed to amplify the desired region, and containing the desired RNA polymerase sites, were used in a standard 20µl PCR with gDNA or cDNA as the template. All of the product was run on a 1.5% gel and the desired product was excised and purified. If DNA concentration of product was too low then a second PCR was run using the extracted PCR DNA as template and the process repeated. PCR product was eluted in 20µl of DEPC-H_2O.

Probe	**Enzyme to linearise**	**RNA Polymerase**
lefty2	BamHI	T7
southpaw	N/A (made using primers)	T7
tbx20	N/A (made using primers)	T7
pitx2	N/A (made using primers)	T7
dand5	Supplied pre-linearised	T7
Patched-2	N/A (made using primers)	T7
Dnaaf1	N/A (made using primers)	T7
Gli2	N/A (made using primers)	T7
Gli3	N/A (made using primers)	T7
Hnf3B	N/A (made using primers)	T3
Patched- 1	N/A (made using primers)	T7

Table 2.6: Enzymes required for linearization of plasmid and RNA polymerase required for antisense transcription of probe

To synthesise the probe the following reaction was set up in order on ice:

Purified template DNA	1µg
DIG-RNA labelling mix (Roche)	2µl
10x Buffer (Ambion)	2µl
RNAs Inhibitor (Roche)	2µl
RNA Polymerase	2µl
DEPC-H_2O	up to 20µl

Transcription reaction was incubated at 37°C for 2 hours (longer if less than 1µg of DNA was used). 2µl of DNAse1 (Ambion) was added to reaction and incubated for a further 15 minutes at 37°C. The following was added, in order on ice, to precipitate the RNA:

0.5M EDTA	2µl

4M LiCl	5µl
100% Ethanol	150µl

Solution was incubated overnight at -80°C then centrifuged at 12,000rpm for 30 minutes at 4°C. Supernatant was removed and RNA pellet washed in 70% Ethanol (depcH_2O). Solution was then centrifuged at 12,000rpm for 10 minutes at 4°C before the supernatant was removed and the RNA pellet air dried for 10 minutes. Pellet was dissolved in 20µl DEPC-H_2O and concentration of RNA measured using a Nanodrop 1000 spectrophotometer.

2.22: Mouse Whole Mount *In Situ* Hybridisation

If embryos were previously stored in methanol they were rehydrated through a methanol/PTW gradient (75%, 50%, 25%, PTW) and washed twice in PTW. Embryos were then treated with 10µg/ml Proteinase K (Roche 3115879) in PTW. Mouse embryos E6.5-7.5 were incubated at RT for 5 minutes, for each day of development later, 5 Minutes was added. Proteinase K was removed and embryos fixed for 20 minutes in 4% PFA + 0.1% Glutaraldehyde. Embryos were then rinsed in PTW and transferred to a Nalgene tube. Embryos were then rinsed with a 1:1 dilution of hybridisation mix and PTW followed by a rinse of hybridisation mix. Hybridisation mix was replaced and embryos incubated at 65°C for at least an hour. Hybridisation mix was removed and fresh pre-warmed hybridisation mix added with an appropriate volume of DIG labelled RNA probe. Embryos were then incubated overnight (or weekend) at 65°C. Embryos were then washed twice with prewarmed hybridisation mix (65°C) and 20µg/ml RNase A (Roche 109169) added and incubated at 37°C for 30 minutes. Solution then removed and the embryos washed twice in prewarmed hybridisation mix followed by a wash in 1:1 hybridisation mix and 1x MABT. Two washes in 1x MABT were then carried out followed by one 15 minute wash in 1xMABT. Embryos were then incubated at RT for 1 hour with 1.5ml 5x MABT and 2% Blocking Reagent followed by another 1 hour incubation at RT with 1.5ml 5x MABT, 2% Blocking Reagent and 20% heat treated serum. Embryos were then incubated overnight in fresh 1.5ml 5x MABT, 2% Blocking Reagent, 20% heat treated serum and a 1/2000 dilution of Anti-Digoxigenin-AP (Roche 11093274910). Following the antibody incubation, embryos were washed 3 times in 1x MABT and transferred to a glass scintillation vial. Embryos were then subjected to at least 3x 1 hour washes in 1xMABT (more washes were done if background needed to be reduced). Embryos were then washed twice for 10 minutes in NTMT before being incubated in 3ml NTMT + 1.5µl NBT-BCIP (Roche 11681451 001). Embryos were rocked at RT in the dark for between 30 minutes and 3 days. Once the colour had developed embryos were rinsed in PTW twice and stored in PTW at 4°C.

2.23: Zebrafish Whole Mount *In-situ* Hybridisation

Fixed embryos of the correct stage were removed from -20°C, methanol removed and embryos washed in 50% Methanol/PBS for 5 minutes. 50% methanol was removed and embryos washed x3 in PBT at 5 minute intervals. Following the final wash, PBT was removed and embryos post-fixed with fish fix for 20 minutes before being subjected to another 3x wash with PBT at 5 minute intervals. PBT was removed and 8µl of 1:10 proteinase K (20mg/ml) diluted in 1ml of PBT was added. Embryos less that 24hpf were incubated at room temperature for 30 seconds in the proteinase K solution. Embryos 24hpf-48hpf were incubated for 1 minute. Proteinase K solution was removed and embryos washed x2 in PBT before undergoing another post-fix with fish fix for 20 minutes at room temperature. Embryos were subsequently washed in PBT x3 at 20 minute intervals. PBT was removed and embryos rinsed in 250µl PBT with 250µl 68°C Hybe B. Embryos were then rinsed in 250µl 100% 68°C Hybe B before being transferred into 500µl of 68°C Hybe A and incubated for 4 hours in a 68°C water bath. Hybe A was then removed and 30ul of 68°C Hybe A containing 500-700ng of probe added and incubated overnight in 68°C water bath. Hybe A containing the probe was removed and stored at -80°C if required, embryos were washed in 68°C Hybe B x5 at 30 minute intervals in a 68°C water bath (if *in-situ* produced high background, washes were increased). During the last wash Hybe B was not removed and 500µl of PBT added and left at room temperature for 20 minutes on an orbital shaker at 70rpm. Hybe B/PBT solution was removed and embryos washed in PBT x3 for 10 minutes before being transferred into 500µl blocking buffer and incubated at room temperature for 30 minutes on an orbital shaker at 70rpm. Blocking buffer was removed and fresh 500µl blocking buffer containing anti-DIG AP antibody (1:2000) added and left at 4°C overnight on an orbital shaker at 70rpm. The following morning embryos were subjected to 5x PBT washes at 30 minute intervals (if *in-situ* produced high background, washes were increased). Embryos were transferred to glass cavity dishes, the PBT was removed and embryos were washed in 500µl staining solution x2 for 15 minutes. Staining solution was removed and 1ml staining solution with 20µl of BCIP/NBT to detect alkaline phosphatase activity was added. Embryos were incubated in the dark at room temperature on an orbital shaker at 70rpm for between 30 and 120 minutes until staining was visible. If neccesarry, staining could continue O/N at 4°C. Staining was stopped by washing the embryos in PBT x3 and then kept in fish fix or 70% glycerol at 4°C until imaging.

2.24: Zebrafish Motile Cilia Live Imaging

cph zebrafish embryos were collected and dead/unfertilised embryos removed. Remaining embryos were placed in egg water at 28°C to develop until ~14hpf. A mould designed to hold embryos was made using 2% agarose in egg water and left to set. Once embryos had developed to the correct stage, embryos with well-developed KVs were dechorionated and placed into the mould. Embryos were then covered in egg water and placed on a Ziess live imaging microscope. All embryos were imaged on a x60 water dipping lens at ~150-200fps using Metamorph software. Embryos were then placed into separate wells of a 24 well plate which had been coated with 2% agarose in egg water to stop the embryos sticking to the plastic. Recordings of each embryo were saved according to the well that that embryo was placed in. Embryos were left to develop until the mutant phenotype became apparent and recordings were marked as mutant or WT accordingly. Recordings were analysed using ImageJ and slowed to 15fps.

2.25: CRISPR Design and sgRNA Synthesis

To generate the zebrafish equivalent mutation of the mouse PRPF8^{N1531S} line the corresponding amino acid change had to be determined. Utilising the BLAST Protein Alignment tool this was determined to be PRPF8^{N1538S}. The zebrafish codon for amino acid 1538 is “aac” and so to create the desired amino acid change this codon had to be mutated to either “agc” or “agt”. The zebrafish WT sequence 100bp either side of this codon was pasted into Crispor (http://crispor.tefor.net/) online sgRNA guide designing tool which identified 5 possible protospacer adjacent motifs (PAMs) that could be utilised for sgRNA guides (possible sgRNAs listed in Table 7 in order of ranking in CRISPOR). As this CRISPR/Cas9 system was being used to generate a knock-in rather than knock-out line, a few factors had to be taken into consideration when determining what sgRNA guides to use. Firstly, how close to the desired mutation site the Cas9 cut was going to be. Secondly, whether the PAM site could also be mutated and thirdly, was there any significant risk of off-target cutting. After taking these things into consideration, sgRNA 3 and sgRNA 5 were chosen for synthesis.

sgRNA Guide Ranking	Sequence (PAM)
1	ctaaccgacgattcaccttg (tgg)
2	(cct) aaccgacgattcaccttgtg
3	(cca) tgaatcgtcggttaggaatc
4	accgacgattcaccttgtgg (tgg)
5	(ccg) accaccacaaggtgaatcgt

Table 2.7: sgRNA guide sequences for *prpf8* generated by CRISPOR

These two guide sequences were integrated into a sequence which was used as a forward primer to generate the full length CRISPR guide RNA (gRNA) DNA sequence. Method originally published by Bassett et al., (2013).

Primer name	Sequence
Prpf8 sgRNA 3	GAA ATT AAT ACG ACT CAC TAT A tgaatcgtcggttaggaatc GTT TTA GAG CTA GAA ATA GC
Prpf8 sgRNA 5	GAA ATT AAT ACG ACT CAC TAT A accaccacaaggtgaatcgt GTT TTA GAG CTA GAA ATA GC
Generic Reverse Primer	AAAAGCACCGACTCGGTGCCACTTTTTCAAGTTGATAACGGACTAGCC TTATTTTAACTTGCTATTTCTAGCTCTAAAAC

Table 2.8: Primer sequences used to generate the DNA sequence of gRNA with T7 promoter. Green = T7 promoter sequence. Blue = desired sgRNA sequence. Red = sequence complimentary to the generic reverse primer.

Both primers were purchased from IDT and resuspended to 100µM in sterile water. To generate the full length gRNA the flowing reaction was set up on ice and amplified in a PCR:

5x Phusion buffer	10µl
dNTPs (10mM)	1µl
Guide primer	1µl
Generic reverse primer	1µl
Phusion DNA polymerase	0.5µl
dH_2O	36.5µl

Cycling conditions were as follows:

98°C for 2 minutes
Cycle x35
98°C for 30seconds
55°C for 30 seconds
72°C for 30 seconds
72°C for 5 minutes
Hold 16°C infinite

Upon completion of PCR, 2µl of product was run on a 2% agarose gel to confirm the expected product size of approximately 120bp. Once confirmed, the remaining product was PCR column purified (Qiagen Cat. No. 28104) and eluted in 21µl of DEPC-H_2O. Concentration was measured using a Nanodrop 1000 spectrophotometer. MEGAshortscript T7 kit (Life Technologies) was used to transcribe the full length gRNA from the purified PCR product. Manufacturer's instructions were followed and the following reaction was set up on ice:

PCR product	8µl
10x Buffer	2µl
ATP	2µl
GTP	2µl
CTP	2µl
UTP	2µl
T7 polymerase	2µl

Reaction was mixed thoroughly by pipetting then incubated at 37°C for 3 hours. 1µl of Turbo DNase was added to the reaction and incubated for a further 20 minutes at 37°C. To precipitate the gRNA 115µl of DEPC-H_2O and 15µl of ammonium acetate stop solution were added along with 300µl 100% Ethanol and solution was incubated overnight at -80°C. RNA was precipitated following the same method as in "*in-situ* probe synthesis". Concentration was measured using a nanodrop 100 spectrophotometer and diluted until concentration was ~2000ng/µl.

2.26: CRISPR gRNA Cut Efficiency *In Vitro*

To determine whether or not the gRNAs designed could indeed cut the DNA at the desired location an *in-vitro* test was performed. To do this, a PCR fragment containing the desired cut site in an asymmetric position (e.g 200bp 5' and 100bp 3') was amplified. This meant that that if the guide successfully causes a cut, the one 300bp fragment will become a 200bp and 100bp fragment and can be detected by gel electrophoresis. To establish the efficiency of the chosen guides the following reaction was set up on ice:

PCR template with target site (100ng/µl)	2µl
NEB buffer 3	1µl
10x BSA	1µl
gRNA (700ng/µl)	1µl
Cas9 (500ng/ µl)	1µl
depcH_2O	4.5µl

A positive control reaction which contains a known efficient gRNA and PCR template as well as a negative control reaction which only lacks Cas9 were also set up. All reactions were incubated for 1 hour at 37°C then run on a 2% agarose gel. The relative levels of cleavage between the positive control and the desired guides gave an estimation of cleavage efficiency.

2.27: CRISPR gRNA Cut Efficiency *In Vivo*

If the *in vitro* efficiency for the designed guides was deemed suitable, the next step was to confirm that they could efficiently cause the desired cleavage *in vivo.* To this end, 0.75nl of a 700ng/ul gRNA and 250ng/ul Cas9 reaction mix was injected into the animal pole of roughly 75 single cell stage WT embryos. Injected embryos were incubated at 28.5°C along with un-injected controls until 24hpf at which point 8 embryos of each were taken, lysed, and a PCR carried out using primers designed to amplify the targeted region. Products were then run on a 2% agarose gel to determine if any large deletions had occurred. Products subsequently sequenced to determine if the injected embryos harboured any mosaicism, a clear indication that the gRNAs and Cas9 was successfully cutting at the desired region. The relative ratio of injected embryos which showed mosaicism to those that didn't gave an estimate to *in vivo* cutting efficiency of the designed gRNAs.

2.28: Protein extraction from Embryos

30 embryos of 48hpf were dechorionated, washed in PBS and de-yolked by pipetting up and down. PBS was removed and embryo carcases were washed in PBS multiple times to remove as much of the yolk as possible. PBS was removed and 200µl of Laemmli SDS sample buffer added, embryos were then incubated at 95°C for 15 minutes and vortexed every 5 minutes. Protein sample could then be stored at -80°C if necessary.

2.29: Western Blot

Western blot glass plates were washed with 70% ethanol before being assembled vertically in the gel rack. Water was added to check for leaks. If no leaks were present, water was removed and slides dried with filter paper. 5ml of 8% resolving gel was pipetted between the two plates and then 200ul of ethanol was slowly pipetted onto the gel surface to remove any air bubbles and even out the gel. Gel was left to set and ethanol removed and dried with filter paper. 4% stacking gel was then added until just below the top of the plates, gel comb was inserted and the gel left to set. If protein samples had been frozen, they were thawed and incubated at 95°C for 5 minutes before being centrifuged at 13,000rpm for 5 minutes. 40ul of 48ug protein sample was loaded into each well as resolved by SDS-PAGE electrophoresis for 100 minutes at 160V due to the large size of the protein. Transfer was for 120 minutes at 120V using a wet transfer method onto a methanol

activated PVDF membrane. PVDF membrane was then blocked for 1 hour in blocking buffer at room temperature. Primary antibody was prepared at desired dilution (1:1000 for Prpf8) in blocking buffer and incubated with membrane overnight at 4°C on orbital shaker. Membrane was washed in TBST for 10 minutes x3 and then incubated with corresponding secondary antibody for 1 hour at room temperature. Membrane was once again washed in TBST for 10 minutes x3 before using enhanced chemiluminescence (ECL) reagents in a 1:1 ration for detection. ECL hyper-film (GE healthcare) was used for detection of protein bands.

2.30: Statistical Analysis

GraphPad Prism 9.0 for Windows was used for the statistical analysis of data and the generation of graphs. For statistical comparison of cilia length and number between WT and *cph* or between WT and $p1^{-/-};p2^{-/-}$ embryos, as well as for analysis of protein reduction in the western blot, an un-paired t-test was used. For statistical comparison of reduction in Prpf8 localisation between WT, *cph* and the two tbMO concentrations a one-way ANOVA was used. One-way ANOVA was also used for statistical comparison of cilia length and number for comparison of WT, *cph* and tbMO embryos. For analysis of change in expression between arl13b isoforms, an un-paired t-test was used. Normality was tested for using the Shapiro-Wilk test. All data was normally distributed $p< 0.05$ = * , $p< 0.01$ = ** , $p< 0.001$ = *** , $p< 0.0001$ = ****

Chapter 3: Characterising the *cph* Mutant

3.1.1 Establishing the Left/Right Axis: A Synopsis

During early development of a zebrafish embryo, at around the 6-10 somite stage, a small concave depression forms at the posterior end of the embryo. This structure is referred to as Kupffer's Vesicle (KV) and is responsible for the establishment of the L/R axis (Essner et al., 2005). Within the KV there are monociliated pit cells which develop long motile cilia that whip round in an anticlockwise manner and generate anticlockwise fluid flow that is critical in the creation of the L/R axis (Essner et al., 2005; Hamada, 2016). Additionally, within the KV there are monociliated crown cells, surrounding the pit cells, which possess primary cilia thought to be critical in sensing the anticlockwise fluid flow produced by the motile cilia (Takeda et al., 1999; Yoshiba et al., 2012). The mechanism by which these crown cells sense the anticlockwise fluid flow is still a matter for debate. One hypothesis is the fluid flow transports a signalling molecule or morphogen to the left side of the KV which is sensed by the primary cilia, triggering a downstream signalling cascade. Indeed there is some evidence to support this hypothesis (Tanaka et al., 2005), but the most commonly accepted hypothesis is that the primary cilia act as mechanosensors for the fluid flow (Norris and Grimes, 2012; Hamada, 2020). In a downstream response to the mechanical bending of the primary cilia in the crown cells, and in conjunction with the Pkd2 protein, intracellular Ca^{2+} at the left side of the KV rises and is proposed to elicit downstream gene expression changes, though the intermediatory singling molecules are still unknown (Pennekamp et al., 2002; McGrath et al., 2003; Yoshiba et al., 2012; Yoshiba and Hamada, 2014).

The main effector of this downstream signalling pathway is *dand5* (Schweickert et al., 2010; Shinohara et al., 2012). *dand5* is initially expressed symmetrically around the KV but *dand5* mRNA is degraded specifically on the left in response to anticlockwise fluid flow within the KV (Kawasumi et al., 2011). As Dand5 acts as an inhibitor of the protein Spaw, the higher levels of *dand5* mRNA on the right side of the node result in increased Dand5 protein and thus decreased Spaw activity (Tanaka et al., 2007; Hamada, 2020). As Spaw is not inhibited on the left side, expression of *spaw* is increased through a positive feedback loop resulting in propagation of *spaw* into the left LPM (Saijoh et al., 2003; Marques et al., 2004). To restrict *spaw* expression to the left LPM, *spaw* initiates the expression of *lefty2* in the heart precursor cells in the left anterior LPM as well as *lefty1* in the midline of the embryo. Both *lefty2 and lefty1* acts as inhibitors of *spaw* thus restriction *spaw* expression to the left LPM (Burdine and Schier, 2000). Mis-expression of either *dand5, spaw, lefty1* or *lefty2* can lead to the incorrect establishment of the L/R axis, of which a common feature is reversed or unlooped hearts (Shiratori and Hamada, 2006).

.

3.1.4 The *cph* Zebrafish Phenotype: A Recap

During an ENU induced forward genetic screen Keightley et al., (2013) discovered a zebrafish mutant they termed *cph* that harboured a G to T substitution in *prpf8*. This transversion resulted in a premature stop codon consequently truncating Prpf8 at aa396. As the full length of Prpf8 is 2342 amino acids, this truncation was proposed to result in a null phenotype. Keightley et al., (2013) investigated splicing efficiency in the *cph* mutant and found that *mapk12, gata1* and *p53* mRNA all contained retained introns, as did *prpf8* resulting in an even earlier premature stop codon than the initial *cph* mutation. Additionally, exon skipping was observed for *spi1* mRNA. Further analysis suggested that the lack of full length Prpf8 in *cph* resulted in reduced formation of the U4.U5/U6 tri-snRNP. Keightley et al., (2013) reported that *cph* fish presented with a high degree of CNS cell death starting at around 16-18hpf and becoming severe at 28hpf. Furthermore, the authors report *cph* fish display pericardial oedema and a curled body axis, with preliminary findings from Sudipto Roy identifying an increased incidence of unlooped hearts (Sudipto Roy, Per Comm), suggestive of defects in motile cilia.

3.1.5 Aims for Chapter 3

Within this chapter I aimed to further characterise the *cph* mutant in terms motile cilia defects, focusing on structures known to contain motile cilia. I also aimed to determine whether the establishment of the laterality pathway in the *cph* mutant was defective and, if so, investigate the KV to determine if motile cilia dysfunction could be the root cause. Furthermore, as an indication of possible primary cilia defects, I aimed to determine whether the expression hedgehog pathway genes were affected in the *cph* mutants. Additionally, I also aimed to investigate Prpf8 localisation to gain an insight into the possible relationship between Prpf8 and motile cilia dysfunction.

3.2 Results

3.2.1 *cph* Morphological Characterisation and Genotyping

As Keightley *et.al* (2013) only lightly touch on the possible presence of phenotypes associated with classical motile cilia defects, I decided a more robust analysis of the development of *cph* mutants was required.

cph heterozygotes were crossed and the development of their offspring watched from 12-72hpf (Figure 3.1A). The first observable difference between *cph* homozygotes and their siblings was the slight curl down of the anterior-posterior (A-P) body axis at 24hpf. This phenotype was varied in its penetrance at this stage however was almost fully penetrant by 28-30hpf. As stated by Keightley *et.al* (2013), neural cell death, observed under a light microscope as greying of the affected area, begins at 28hpf however only becomes obvious at around 48hpf. At this stage the curl down of the A-P axis was severe, with most embryos developing some form of kink at the most posterior of their tail. Additionally, homozygous embryos developed an involuntary random twitch, proposed to be a symptom of the continued neural cell death. Pericardial oedema was also very obvious within the *cph* homozygotes at this stage with severity increasing as development continues. Furthermore, by 48hpf kidney cysts start to develop at the most anterior of the pronephric duct. By 72hpf the curl down A-P axis, pericardial oedema and neural cell death were severe with most embryos dying between this stage and 96hpf.

As the curl down of the body axis and pericardial oedema are hallmarks of motile cilia defects, I decided to check whether heart looping was also affected. Homozygous mutants were segregated from the clutch based on observable phenotypes at 48hpf and their heart looping direction visually determined under a light microscope. By this stage all wild type (WT) hearts have completed the looping process and are usually looped to the right. The majority of *cph* embryos displayed unlooped hearts (Figure 3.1B) with a substantial proportion of embryos also showing leftward looping hearts. These observations give a strong indication that motile cilia function is severely affected in *cph* homozygotes.

To confirm that the phenotypes discussed were that of *cph* homozygotes and that there was no dominant effect from heterozygotes, a genotyping method was developed using primers either side of the mutation site to amplify and sequence the embryos (Figure 3.2A and B). As the mutation is a single base pair substitution, sequencing results were not always of sufficient quality to detect this base change so restriction digest using *Acc1* enzyme was employed post PCR amplification. The *Acc1* enzyme cuts at exactly the mutation site allowing for accurate determination of embryo genotype after gel electrophoresis (Figure 3.2C).

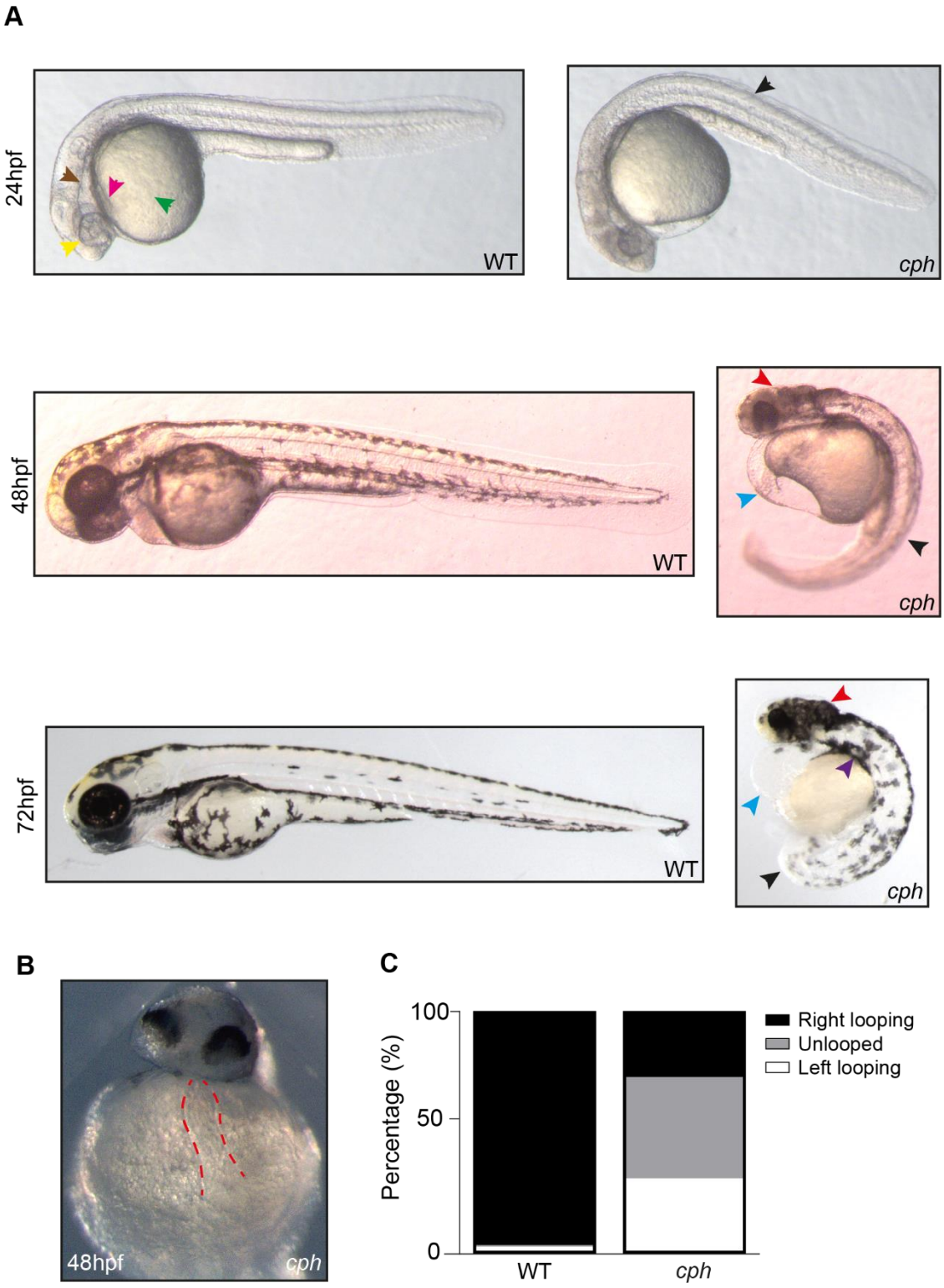

Figure 3.1: Morphological phenotype of *cph* zebrafish. (A) Morphological characteristics of WT and *cph* zebrafish embryos at 24hpf, 48hpf and 72hpf. Black arrows indicate curled down A-P body axis. Blue arrow indicates pericardial oedema. Red arrow indicates neural cell death. Purple arrow indicated kidney cyst. Green and pink arrow indicated yolk sac and heart respectively **(B)** Unlooped heart of a *cph* embryo at 48hpf (**C)** Graph depicting frequency of each looping direction. n=134 WT (97% RL) and n=104 *cph* (27% RL, 42% UL, 31% LL)

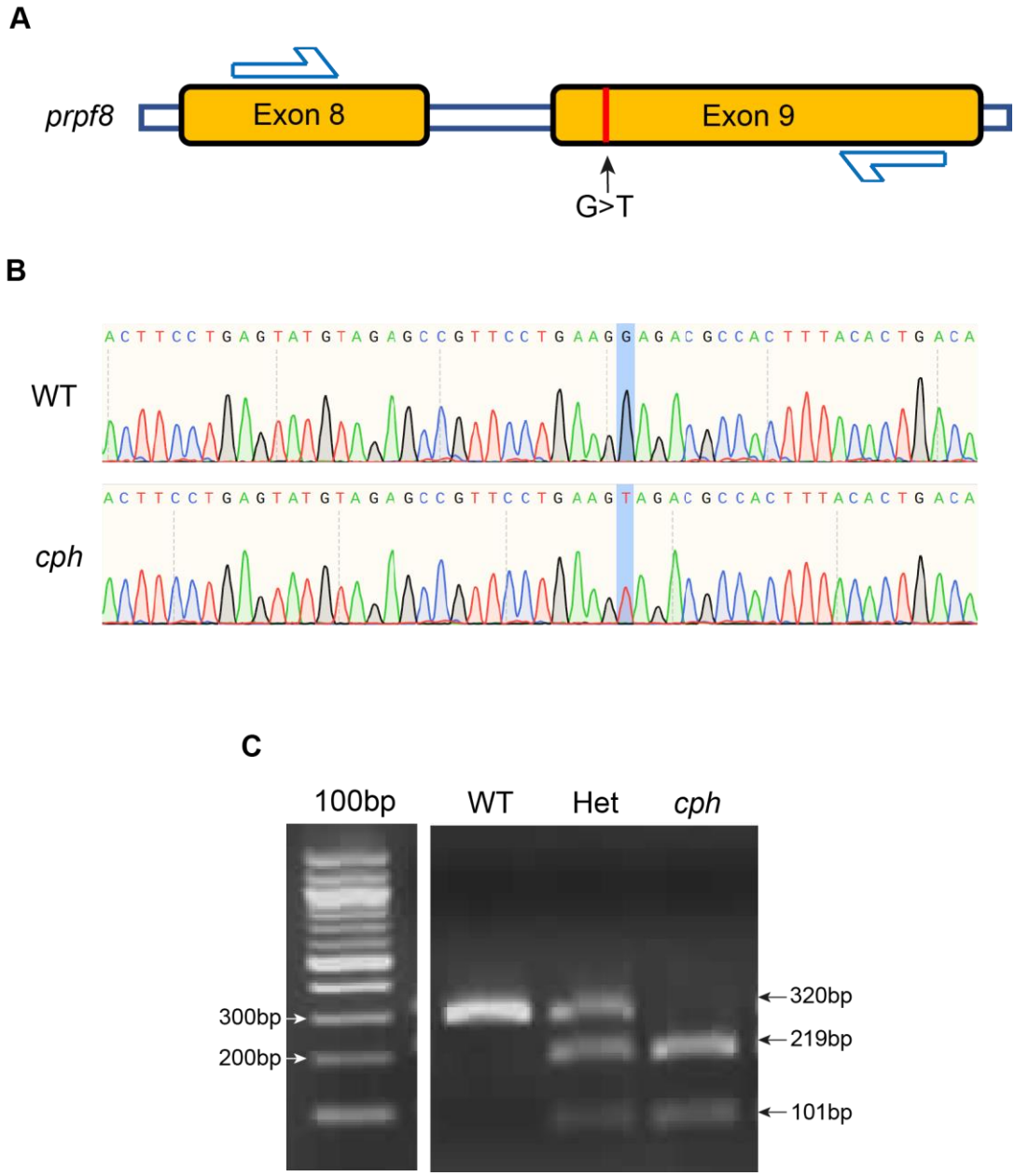

Figure 3.2: Genotyping of *cph.* (A) schematic representation of mutated region of *prpf8* with location of genotyping primers added **(B)** chromatograph from WT and *cph* embryos with mutated base highlighted. **(C)** gel electrophoresis of restriction digest using *AccI* enzyme on PCR reaction using primers from A.

3.2.2 Investigating Left/Right Axis Formation in *cph* Mutants

Although the observation of an increase in unlooped and rightwards looped hearts was indicative of laterality defects, in the case of *cph* homozygotes it may also be due to the gross morphological deformities associated with the phenotype. To confirm whether the heart looping abnormalities were truly associated with defects in the formation of the L/R axis a whole mount *in situ* hybridisation (WISH) for *lefty2 (lft2)* was performed. *lft2* is expressed in the heart precursor cells, which in WT are typically found on the left side of the developing embryo. However, when the WISH was performed on *cph* embryos four expression patterns in various proportions were discovered; left sided, right sided, bilateral and no expression (Figure 3.3A and B). This varying expression pattern is symptomatic of a fault in the establishment of the L/R axis and confirms that the heart looping phenotype was not simply caused by the physical deformities seen in the *cph* embryos.

The next aim was to determine at which point this failure to properly establish the L/R axis occurs. To this end I performed another WISH, this time for *spaw. spaw* is the first gene to be specifically expressed on the left side of the embryo and so acts as a strong indicator for L/R axis establishment at a relatively early developmental time point. As seen with the WISH for *lft2, cph* embryos exhibited four expression patterns of expression; left, right, bilateral and no expression at relatively similar frequencies to that of *lft2 (*Figure 3.3C and D). Although *spaw* is the first gene to be solely expressed on the left, it is not the first gene in the laterality pathway to be expressed. *dand5* is more strongly expressed on the right side of the developing embryo and inhibits *spaw* expression on that side, allowing *spaw* to be expressed on the left. I hypothesised that if there was a cilia defect at the KV *dand5* must also be mis-expressed thus causing the downstream mis-expression of *spaw* and *lft2*. In agreement with this hypothesis, *dand5* was mis-expressed in the same manner as *lft2* and *spaw* though as *dand5* is normally more highly expressed on the right, the staining pattern observed in *cph* mutants showed *dand5* expression higher on the left, as well as bilaterally and reduced *(*Figure 3.3E and F).

lefty1 (*lft1*) is also a key gene in the formation of the L/R axis, and is mainly expressed in the embryo mid-line. Mis-expression of *spaw* and *lft2* in various other zebrafish mutants has been attributed to loss of *lft1* expression (Burdine and Grimes, 2016). Therefore, I decided to confirm whether *lft1* was expressed in the correct pattern in *cph* embryos. Another WISH was carried out and, although mid-line expression of *lft1* was patchy in both WT and *cph* embryos, all WT embryos showed expression in the left developing heart field along with the left diencephalon. *lft1* expression was absent in the heart field and left diencephalon of almost all *cph* mutants (Figure 3.3G).

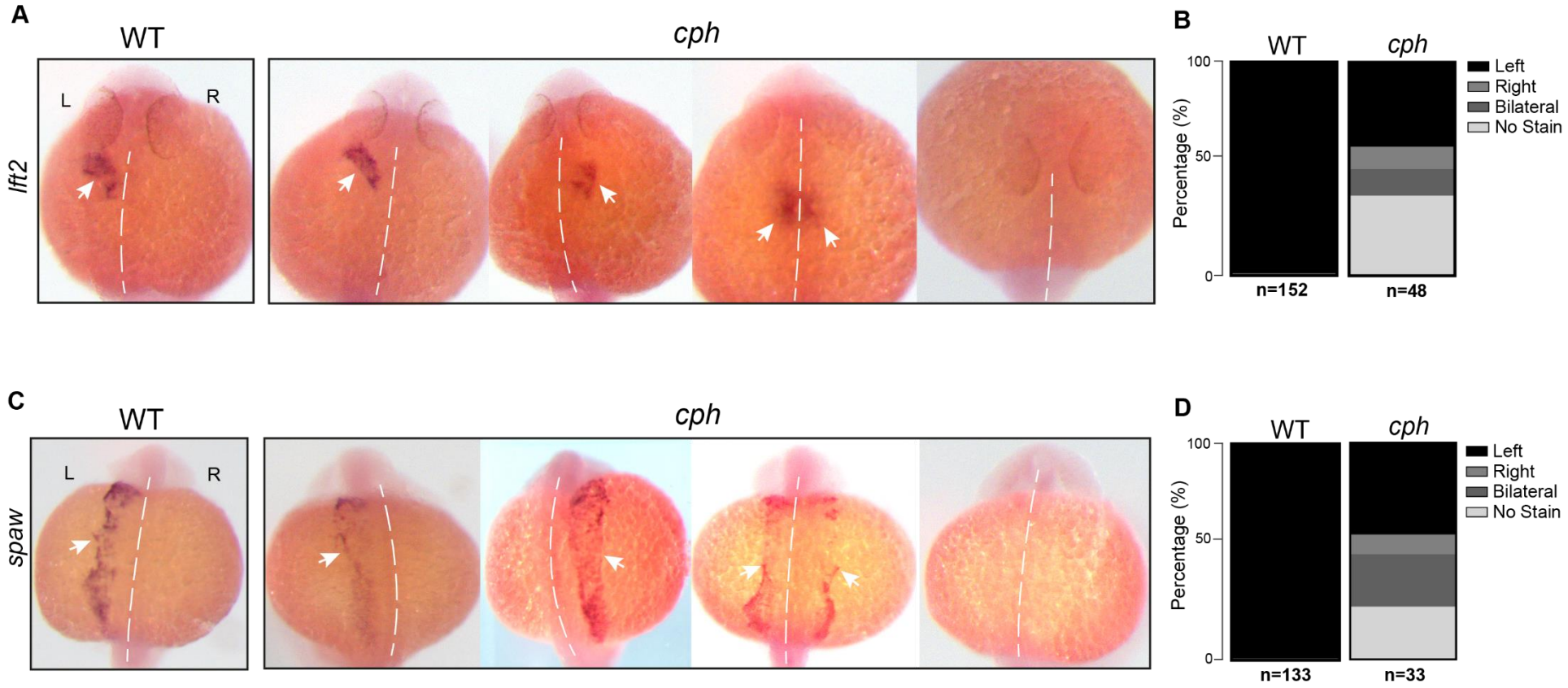
A
WT
cph
lft2
L
R
B
WT
cph
100
50
0
Percentage (%)
Left
Right
Bilateral
No Stain
n=152
n=48
C
WT
cph
spaw
L
R
D
WT
cph
100
50
0
Percentage (%)
Left
Right
Bilateral
No Stain
n=133
n=33

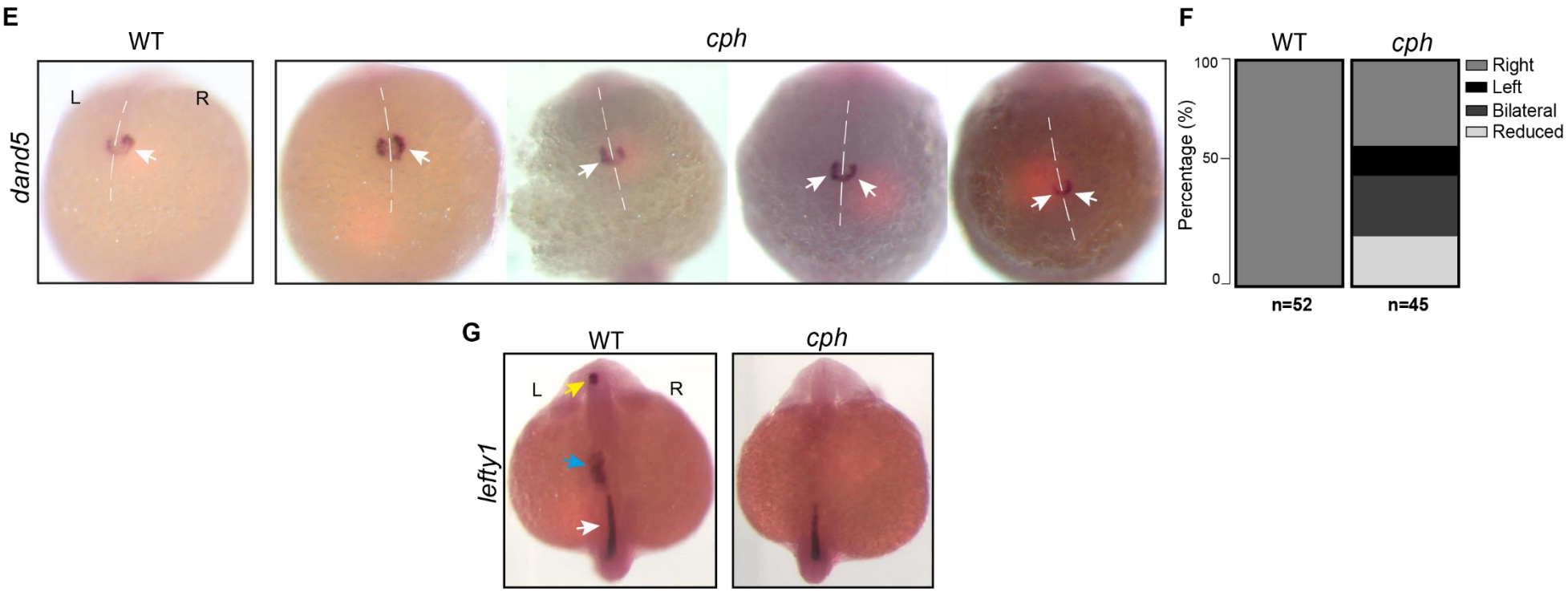

Figure 3.3: Whole mount *in-situ* hybridisation for key laterality genes in *cph* embryos. (A) WISH for *lefty2* on WT and *cph* embryos at 22s stage. **(B)**Graph shows frequency of each of the four phenotypes observed for each genotype (40% L, 12.5%B, 10.5% R, 40% NS). **(C)** WISH for *southpaw* on WT and *cph* embryos at 18s stage. **(D)** Graph shows frequency of each of the four phenotypes observed for each genotype (43% L, 24% B, 9% R, 24% NS). **(E)** WISH for *dand5* on WT and *cph* embryos at 10s stage. **(F)** Graph shows frequency of each of the four phenotypes observed for each genotype (13.3% L, 26.6%B, 37.7% R, 22.2% RS). **(G)** WISH for *lefty1* on WT and *cph* embryos at 18s stage. Blue arrow indicates the staining in the developing heart field and the yellow arrow indicates the staining in the left diencephalon. White arrows indicate areas of observed gene expression. The white dashed line indicates the embryonic midline. n=46

3.2.3 Investigating Cilia Motility in the KV and Other Ciliated Structures

Due to the presence of morphological hallmarks of motile cilia defects as well as confirmed abnormalities in the establishment of the L/R axis, I hypothesised that motile cilia in the KV were affected by the *cph* mutation. To investigate this proposed dysfunction, I performed whole mount immunofluorescence with anti-acetylated tubulin to label cilia axonemes and anti-gamma-tubulin to label the base of the cilium. 10 somite (10s) stage embryos were stained and the KVs of mutants and WT mounted. Due to the KV being a very transient structure, variations within exact developmental stage were minimised by selecting only the most developed and expanded of KVs. Imaging on a confocal microscope revealed that overall structure of the KVs between mutant and WT remained relatively constant with no obvious difference between diameter or depth (Figure 3.4A).

When examining the cilia within the KV, to account for minor variations within KV developmental stage affecting cilia number or size, cilia within an individual KV were analysed and the average value then plotted for that KV. When this analysis was performed on multiple KVs there was no significant difference between the number of cilia in WT (n=18) or *cph* mutants (n=14) (Figure 3.4B). However, when I utilised a program in ImageJ to measure the cilia in 3 dimensions, the motile cilia within *cph* mutants were found to be significantly shorter than in WT (Figure 3.4C).

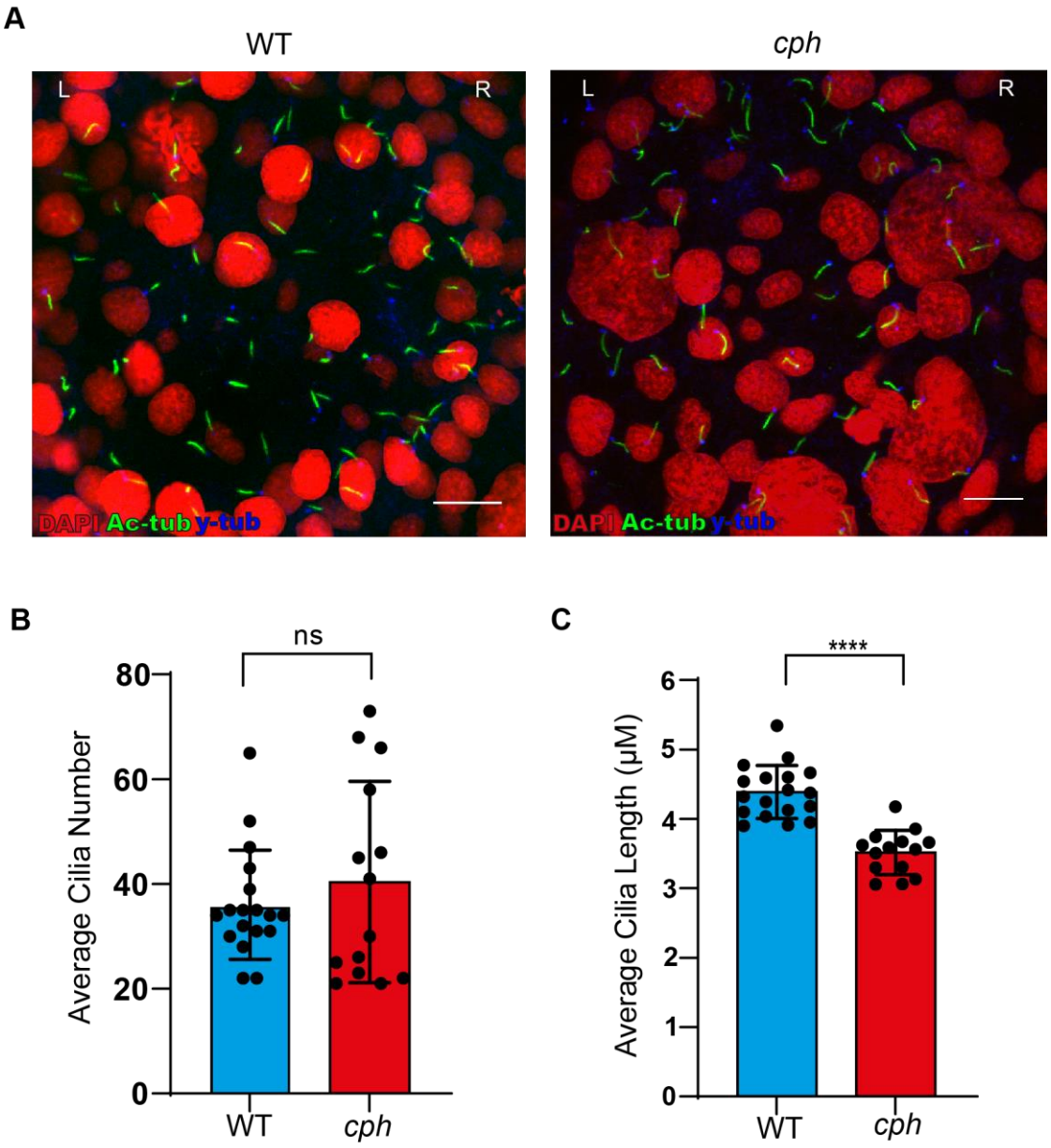

Figure 3.4: Immunofluorescence and Quantification of *cph* KV Cilia.
(A) Immunofluorescence images of the KV in WT and *cph* embryos using antibodies against acetylated tubulin (labelling axonemes), ɣ-tubulin (labelling basal bodies), and DAPI (labelling nuclei). Scale bars are 10μm **(B)** Average cilia number for each KV in WT (n=18) and *cph* embryos (n=14) **(C)** Average cilia length for each KV in WT (n=18) and *cph* embryos (n=14). Data are represented as mean ± SD. Unpaired t test was used to evaluate significance.

The finding that *cph* motile cilia are shorter than that of WT is an interesting discovery but these shorter cilia may still be fully functional and able to generate KV fluid flow. To investigate whether fluid flow in the KV is affected I mounted live 10s WT and *cph* embryos and imaged at high magnification and frame rate. By utilising the presence of naturally occurring particles within the KVs of embryos, I was able to generate videos in which I could track these particles and thus gain an insight into possible abnormal fluid flow. As can be seen from Figure 3.5A, particles within the KVs of WT embryos consistently had a strong anticlockwise rotation around the KV (n=3), in agreement with previous studies and demonstrating that this imaging and tracking method was an accurate readout of fluid flow directionality. In contrast, particles within the KVs of *cph* embryos lacked this strong anticlockwise rotation, instead moving in seemingly random and opposing paths (Figure 3.5B). Interestingly, although these particles did not exhibit the anticlockwise movement I would expect, they did not remain static or exhibit Brownian motion but instead displayed stochastic movements within the KV. This observation suggests that, although general anticlockwise fluid flow was absent, local fluid flows still existed raising the possibility that *cph* KV cilia still possess some motility.

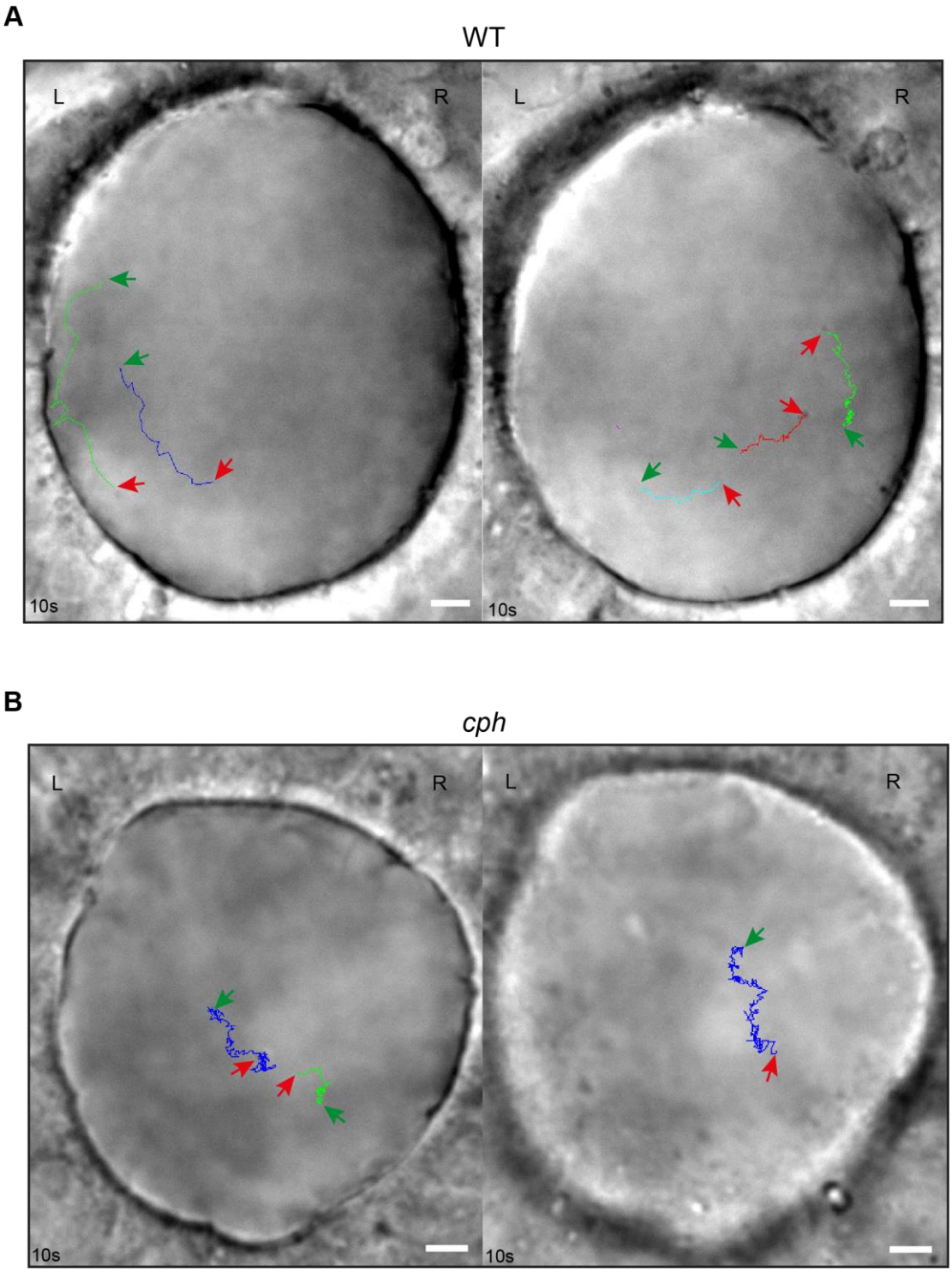

Figure 3.5: KV Fluid Flow in WT and *cph* Embryos. (A) screen capture of a video tracking particle movement in the KV of a WT embryo (n=3). **(B)** screen capture of a video tracking particle movement in the KV of a *cph* embryo (n=3). Lines indicate the path of the tracked particle. Green arrows indicate the beginning of the path and red arrows indicate the end. Videos taken at 600x magnification, 200 frames at 80 fps. Scale bars = 10µm

To get a more precise answer to whether or not *cph* KV motile cilia are functional or not, I altered the high-speed microscope frame rate (~150fps) to capture live KV motile cilia. Videos of WT KVs show many motile cilia “whipping” in an anticlockwise manner (n=10)(Video 3.1) consistent with previously published accounts (Gui et al., 2021) as well as my observations with KV fluid flow. Intriguingly, the motility of motile cilia within the KVs of *cph* embryos were severely disrupted with the “whipping” motion replaced by a twitch like movement (Video 3.2) (n=10). It is interesting to note that not all motile cilia in an individual KV seemed to be affected equally, with cilia motility forming a spectrum of severely dysfunctional to completely WT. In addition, there was a profound heterogeneity of cilia motility dysfunction, not just within *cph* KVs but also between them, with some mutant KVs being almost indistinguishable from WT when imaged in this way.

A possible explanation for this is that due to the imaging being at such high magnification and frame rate, exposure is very low and so it is only possible to see things that are moving in contrast to the background. This limitation of the imaging raises the possibility that within the *cph* KVs there are also completely immotile cilia that cannot be seen by this type of brightfield microscopy. To assess whether this was indeed the case I *in vitro* transcribed *Arl13b*:*gfp* and injected the RNA into WT and *cph* embryos. arl13b is a ciliary specific protein and so when fused to GFP allows for visualisation of motile and immotile cilia. The same imaging parameters were used except this time I imaged the KVs using a GFP fluorescence microscope. As can be seen from Video 3.3, WT GFP KV cilia rotate and whip in the same manner as that seen in Video 3.1 (n=3). However, although *cph* GFP KV cilia also show the same twitching or WT movement as seen in Video 3.3, many completely immotile cilia can also be seen (n=3) (video 3.4). This finding gives credence to the hypothesis that within the *cph* KVs which appeared almost WT under brightfield imaging, there were immotile cilia present which could reduce fluid flow within the KV.

The direct observation of motile cilia defects within the KV of *cph* fish explains the abnormal establishment of the L/R axis, however it does not explain the other motile cilia related phenotypes such as kidney cysts and the curl down phenotype. To establish whether motile cilia were globally affected I mounted live WT and *cph* fish at 24hpf and imaged the motile cilia within the pronephric duct at 600x and 150fps. As can be seen from Video 3.5, rather than whipping around in a circular motion like KV cilia, WT motile cilia within the pronephric duct wave back and forth along the length of the duct (n=3). In contrast, motile cilia within the pronephric duct of *cph* embryos exhibit the same phenotype as seen in the KV, with some cilia twitching and others appearing completely motile (Video 3.6). The same heterogeneous nature of cilia motility both within and between *cph* embryos was also present with some mutant pronephric ducts failing to exhibit any motile cilia. To account for the same imaging limitations discussed previously, the pronephric duct cilia

were imaged using *Arl13b:gfp.* As expected, *cph* pronephric ducts contain a mix of immotile, semi-motile and fully motile cilia (Video 3.7), corroborating the observation within the KV. To further expand on the evidence that motile cilia are globally affected in *cph* embryos, I imaged the otic vesicle of the developing embryo at 24hpf.

WT embryos possess motile cilia within the otic vesicle next to each primary monocilia attached to an otolith – with two otoliths present in each vesicle (Drummond and Austin-Tse, 2013). Imaging of these otoliths in WT showed motile cilia (Video 3.8) (n=3). However, *cph* embryos once again displayed a range of cilia motility; immotile, twitching, fully motile between and within embryos (n=3) (Video 3.9). Taken as a whole, the data from the KV, pronephric duct and otic vesicle demonstrates that *cph* embryos possess dysfunctional motile cilia during laterality determination and up to 24hpf. Unfortunately imaging of motile ciliated structures after this timepoint, such as the nasal placode at 72hpf, was hindered by increasing cell death within the *cph* embryos. At later stages it would have been impossible to deduce if an observed motile cilia dysfunction was due to the *prpf8* mutation or simply a consequence of the embryo dying. However due to the prevalence of phenotypes associated with motile cilia dysfunction at these later stages, I would surmise that cilia immotility persists throughout development.

3.2.4 Primary Cilia Analysis in *cph*

The confirmation that *cph* embryos possess dysfunctional motile cilia suggests it is plausible that primary cilia are also affected by the *cph* mutation. To assess whether this was the case, I decided to investigate the hedgehog pathway within the *cph* embryos. As primary cilia are the organelles at which hedgehog signals are received and transduced into the cell, I reasoned that any structural or functional abnormalities within primary cilia should also affect hedgehog signalling. To this end I performed a WISH for *patched,* the receptor for hedgehog ligands, at 24hpf as at this stage *cph* mutants could be identified while still avoiding the later cell death phenotype which could affect *patched* expression. Upon hedgehog pathway activation, *patched* expression is increased and patched protein localises to the plasma membrane of primary cilia (Rohatgi et al., 2007a; Wheway et al., 2018)). I would expect that if primary cilia were in some way dysfunctional then hedgehog pathway activation would be reduced and thus expression of *patched* would remain low or ectopically expressed. However, as can be seen from Figure 3.6A expression of *patched* remained constant between WT and *cph* embryos (n=40 and n=33 respectively). Notably, although *patched* expression may seem to be increased in the neural region of the *cph* embryo, this was caused by the staining being more diffuse as a result of the beginning of neural cell death.

To further expand on this investigation of the hedgehog pathway, two further WISHs were carried out, on *gli3* and *gli2*. Gli2 and Gli3 are the effectors of the hedgehog pathway and are transcription factors that regulate the expression of downstream hedgehog target

genes, including increasing their own expression (Pietrobono et al., 2019). Results from the WISH for *gli3* (Figure 3.6B) and *gli2* (Figure3.6C) showed no obvious expression difference between WT embryos and *cph* embryos, suggesting that activation and downstream signal transduction of the hedgehog pathway is unaffected. Taken along with the *patched* WISH results, this lack of difference in expression of hedgehog pathway components between WT and *cph* embryos is indicative of functional primary cilia within *cph* embryos.

Additional research into the role of primary cilia in the hedgehog pathway, performed by Arnold et al. (2015), detailed expression changes of genes in both a zebrafish cilia mutant called *iguana,* which has shortened primary cilia*,* and WT zebrafish treated with the hedgehog antagonist cyclopamine. In this work Arnold et al., (2015) analysed the expression pattern of *tbx20,* a transcription factor critical for heart morphogenesis (Chen et al., 2021) and found that the expression of *tbx20* was reduced in *iguana* (*igu)* mutants and absent in the heart of cyclopamine treated fish. As I had access to *igu* mutant embryos I decided to use those as a positive control for embryos I knew had primary cilia defects and compare the expression pattern of *tbx20* between *igu* and *cph* embryos. Embryos were once again fixed at 24hpf, to try and mitigate against the cell death of *cph* hindering the interpretation of the results, and a WISH for *tbx20* carried out. The WT expression pattern of *tbx20* (Figure3.7A) agrees with the expression pattern shown in Arnold *et.al* (2015) with expression in the developing heart field and in the branchiomotor neurons in the hindbrain (white arrows) (n=45). However, the expression pattern of *tbx20* in *igu* mutants looks no different to that of WT, with equally strong expression in both the developing heart field and branchiomotor neurons (Figure3.7B)(n=24). This finding is in disagreement with the results in Arnold *et.al* (2015) who found that expression was reduced. Additionally, *cph* embryos exhibit no obvious difference in expression pattern or intensity for *tbx20* compared to WT or *igu* (n=23) (Figure3.7C) other than one embryo which displayed bilateral staining of *tbx20* in the developing heart field, consistent with the aforementioned disruption to the establishment of the L/R axis (Figure 3.7D).

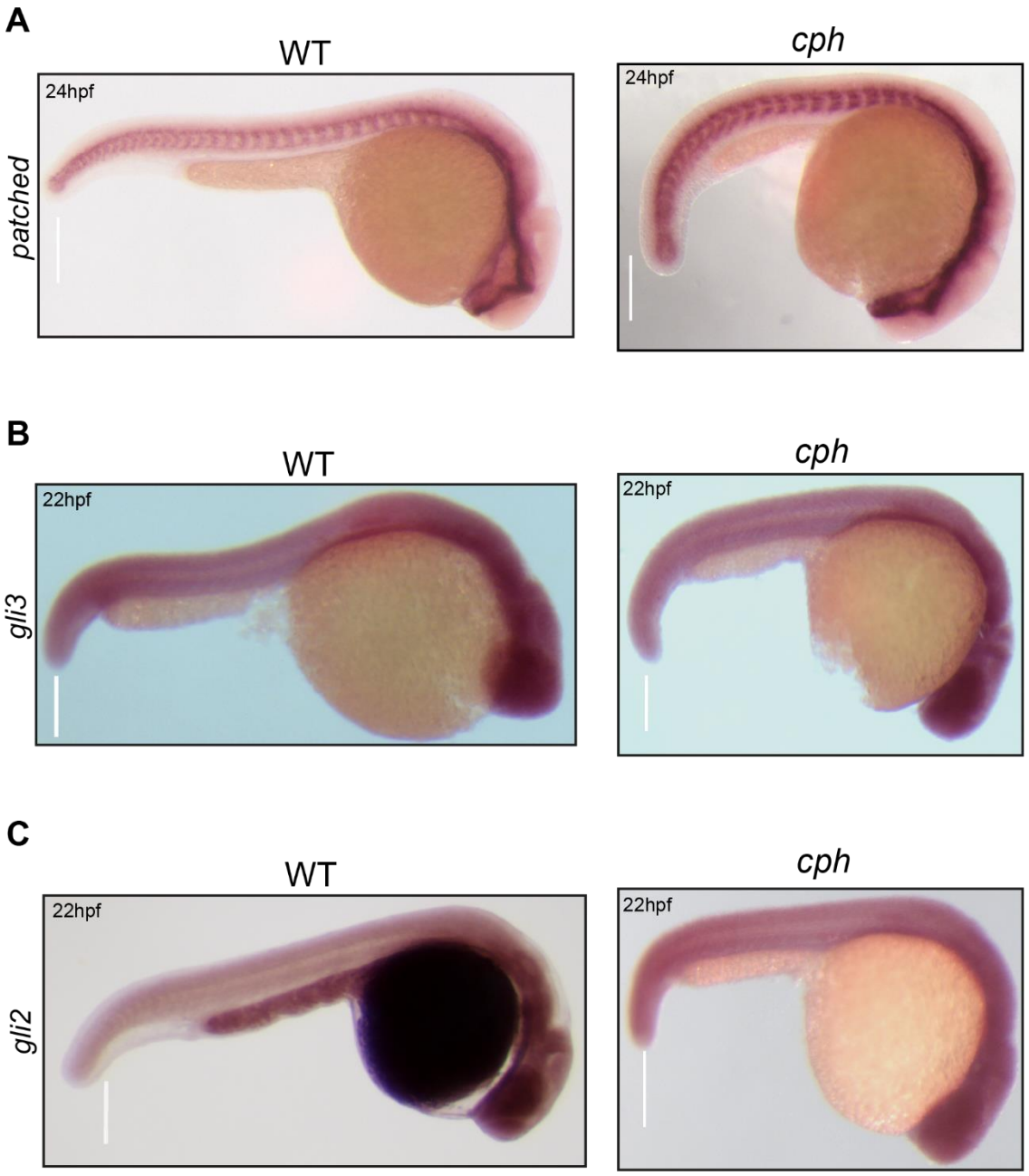

Figure 3.6: Whole Mount *in-situ* Hybridisation for Genes in the Hedgehog Pathway. (A) Representative images for WISH for *patched* on WT (n=42) and *cph (*n=27) embryos at 24hpf. **(B)** Representative images for WISH for *gli3* on WT (n=52) and *cph* (n=23) embryos at 22hpf. **(C)** WISH for *gli2* on WT (n=37) and *cph* (n=31) embryos at 22hpf. All scale bars are 0.2mm.

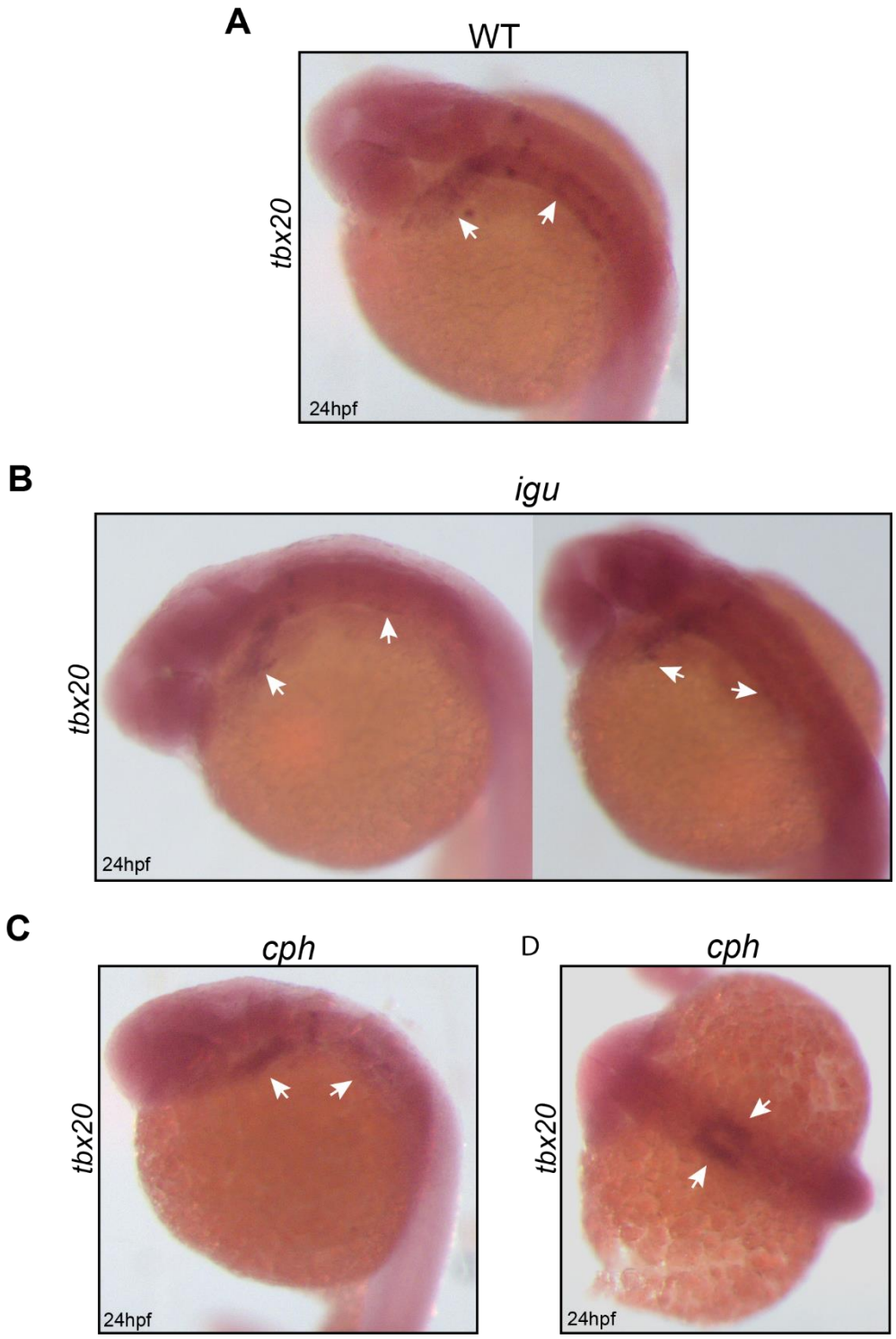

Figure 3.7: Comparing Expression of *tbx20* in Different Cilia Mutants. **(A)** Representative images for WISH for *tbx20* on WT and embryos at 24hpf (n=57). **(B)** Representative images for WISH for *tbx20* on *iguana* embryos at 24hpf (n=21). **(C)** Representative images for WISH for *tbx20* on *cph* embryos at 24hpf (n=38). **(D)** A representative *cph* embryo showing bilateral *tbx20* expression. White arrows indicate areas of gene expression.

3.2.5 Immunofluorescence for Prpf8 in the KV

Why a truncated form of Prpf8 causes global defects in the function of motile cilia in zebrafish is a perplexing question. The standard model for Prpf8 function dictates that prpf8 is a nuclear localised protein, barring the brief period it is in the cytoplasm post translation. However, previous work in the Hentges lab suggests this is not entirely the case, with data proposing that PRPF8 localises to the basal bodies of motile cilia in the mouse embryonic node. To take these initial findings further I carried out an IF for Prpf8 in conjunction with acetylated tubulin on 10s zebrafish and mounted their KVs and imaged on a confocal microscope. Fascinatingly, I found that in WT and *cph* embryos Prpf8 co-localised with acylated-tubulin in the motile cilia of the KV (Figure 3.8A) (Video 3.10). Notably, this co-localisation was not along the full length of the axoneme, but rather Prpf8 staining appeared as punctate clusters seemingly randomly dispersed along the axoneme (white arrows). Additionally, the number of Prp8 clusters in a cilium was not constant, with some cilia having no clusters and others having between one and four.

This finding was unexpected and due to the nature of the protocol I used for Prpf8 antibody staining, along with the fact I did not detect Prpf8 nuclear staining, I decided further control experiments were required. To substantiate my findings, I injected WT zebrafish embryos with a *prpf8* translation blocking morpholino at two concentrations (1:4 and 1:3) creating *prpf8* translation blocking morphants (tbMOs). The aim was to knockdown *prpf8* and repeat the IF for Prpf8. I hypothesised that if the Prpf8/acetylated-tubulin co-localisation persisted then it would suggest that the Prpf8 cilia localisation was caused by the highly modified staining protocol. Astoundingly, the IF for Prpf8 and acetylated-tubulin on *prpf8* tbMO knockdown embryos showed an obvious visual decrease in the abundance of Prpf8 co-localised with cilia (white arrows) as well as cytoplasmic Prpf8 (Figure 3.8A). To quantify the abundance of Prpf8 within cilia of the four models (WT, *cph*, tbMO 1:4 and tbMO1:3), I counted the number of Prpf8 clusters found within cilia and divided by the total number of cilia for each KV to give me average Prpf8 cluster per cilia per KV. This was done for all KVs and the results plotted (Figure 3.8B). As can be seen, there was no difference in Prpf8 localisation between WT and *cph* cilia. However, there was a significant difference between WT Prpf8 localisation and 1:4 and 1:3 tbMO *prpf8* knockdowns. The results show Prpf8 localisation decreases in a concentration dependant manner in tbMO knockdown embryos. As one of the phenotypes of the *cph* embryos is shorter motile cilia, and visually it seemed the same was the case for the tbMO cilia, I wanted to be confident that my results from Figure 3.8B were not being skewed as shorter cilia could mean less Prpf8 protein localised per cilium. To account for this, I re-analysed the numbers of Prpf8 clusters present per µm of cilia (Figure 3.8C). Reassuringly, the trend remains the same with no difference between WT and *cph,* while in tbMO Prpf8 localisation per unit length of cilia decreases as concentration of morpholino increases.

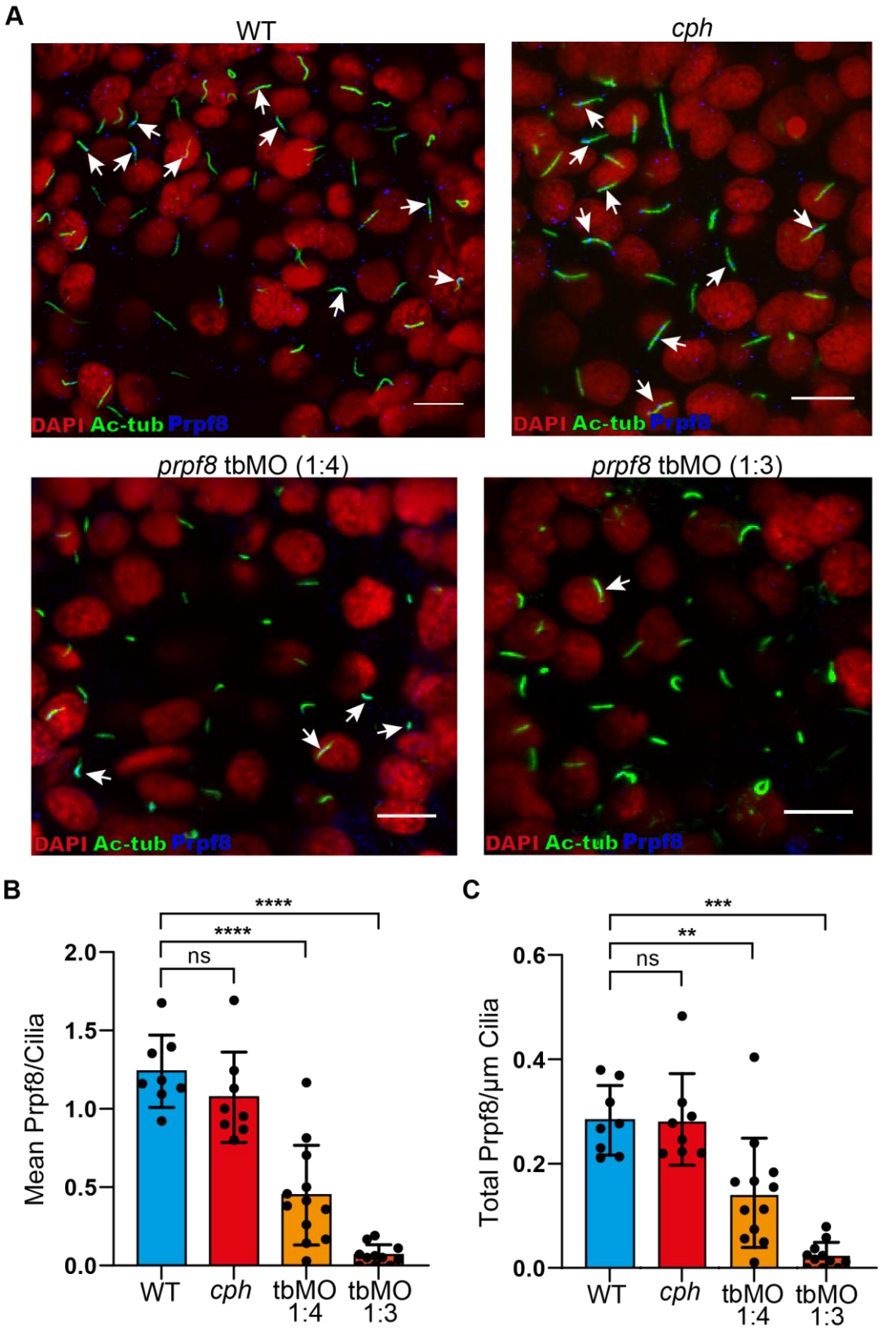

Figure 3.8: Prpf8 Localisation and Quantification in *cph* and Knockdown Zebrafish. (A) Immunofluorescence images of the KV in WT, *cph* and translation blocking knockdown (tbMO) embryos at morpholino concentrations of 1:4 and 1:3. White arrows indicate the location of Prpf8 staining. Scale bars are 10µm **(B)** Quantification of Prpf8 per cilia in the KVs of each model. **(C)** Quantification of Prpf8 per cilia µm in the KVs of each model. Data are represented as mean ± SD. One way ANOVA was used to evaluate significance. WT n=8, *cph* n=8, tbMO1:4 n=12, tbMO1:3 n=11

3.2.6 Quantifying the Prpf8 Morphant KV Cilia Length

As stated in 3.2.5, while investigating Prpf8 localisation I also developed a zebrafish tbMO morphant in which *prpf8* was knocked down. In conjunction with analysing the Prpf8 localisation data, I measured the length of the motile KV cilia of the two concentrations of prpf8 morphant to compare to the *cph* data already presented. KV motile cilia were measured in the same way as previously described and graphed as an average of each KV measured to account for slight differences in developmental stage. From Figure 3.9A we can see that the length of KV motile cilia in tbMO was significantly decreased compared with both WT and *cph* embryos, however there is no significant difference between the two tbMO concentrations. Consistent with the previous results showing no difference in motile cilia number between WT and *cph*, both concentrations of knockdown exhibit no change in KV motile cilia number (Figure 3.9B).

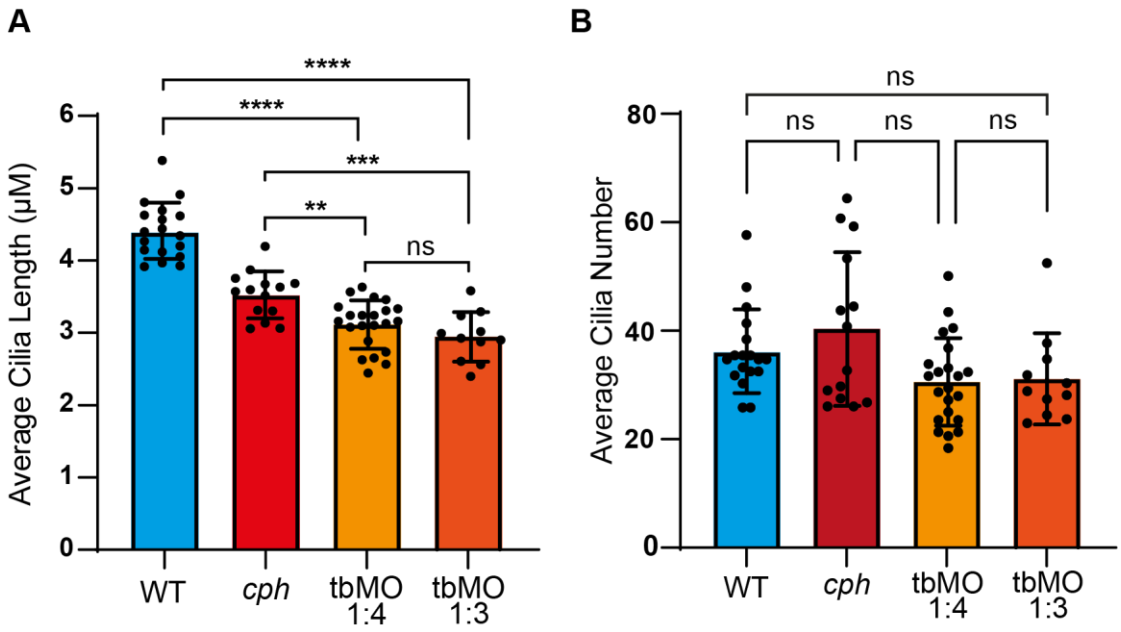

Figure 3.9: Quantification of KV Cilia in WT, *cph* and tbMO. (A) Average cilia length for each KV in WT, *cph,* and tbMO 1:4 and 1:3 embryos **(B)** Average cilia number for each KV in WT, *cph,* and tbMO 1:4 and 1:3 embryos. Data are represented as mean ± SD. One way ANNOVA was used to evaluate significance.

3.3 Discussion

Given that the PRPF8^{N1531S} mouse mutant displays motile cilia defects, the observation that *cph* zebrafish exhibit numerous morphological phenotypes associated with global cilia defects (Choksi et al., 2014), is exciting but not completely unsurprising. As investigations into the PRPF8^{N1531S} mutant were only able to examine the motility of 9+0 cilia of the node due to the early embryonic lethality, the morphological phenotypes associated with the *cph* fish, such as kidney cysts, suggest that 9+2 motile cilia are also affected. The PRPF8^{N1531S} mutant also exhibited heart laterality defects with around 36% of mutant embryos displaying reversed heart looping (Boylan, M. 2015), similar to that of the *cph* mutant embryos. However, the *cph* mutants also displayed a high proportion of unlooped hearts with the frequency of the three looping directionalities almost equal. The observed looping frequencies are consistent with reported looping frequencies of zebrafish mutants with immotile KV cilia (Gui et al., 2021). The additional phenotypes present in the *cph* mutants such as CNS cell death, kink in the posterior of the tail, as well as the myeloid phenotypes reported by Keightley et al. (2013) may or may not have links to cilia defects. Indeed, it is highly likely that, due to the essential nature of Prpf8 in the spliceosome, the array of *cph* phenotypes may be caused by multiple different mechanisms. For example, as prpf8 is involved in mitosis (Hofmann et al., 2010), dysregulation of cell division may be the cause of the CNS degeneration and cell death phenotype. However, Prpf8 may also be affecting cilia through mis-splicing of genes completely unrelated to mitosis, or possibly in an as of yet unknown manner.

Untangling each *cph* phenotype and deducing whether it is related to cilia dysfunction is a challenging task beyond the scope of this thesis. Due to this uncertainty regarding mechanisms underpinning the spectrum of *cph* phenotypes, going forward I will only be discussing the *cph* phenotypes already linked to cilia dysfunction; these are the curled body axis, otolith defects, kidney cysts and heart looping defects (Choksi et al., 2014).

Proper cilia function in the KV is critical for the establishment of the asymmetric gene expression associated with formation of the L/R axis. Disruption of L/R axis formation due to cilia abnormalities in the KV can fall under two categories: the fluid flow within the KV is not produced (due to absence or dysfunction of motile cilia), or the fluid flow within the KV cannot be sensed. Disruption of fluid flow within the KV due to dysfunctional motile cilia is proposed to produce a complex pattern of *dand5*, *spaw* and *lefty2* expression (Hirokawa et al., 2006). Indeed, this complex pattern of laterality gene expression is observed in *cph* embryos, suggesting a KV cilia motility defect. In support of this hypothesis, *pierce1*/*pierce2* zebrafish double mutants, which possess immotile KV cilia, as well as knocked down *foxj1* embryos, which lack the motile KV cilia, also produce this complex pattern of laterality gene expression (Dutta et al., 2015; Gui et al., 2021). Additionally, previous analysis of the PRPF8^{N1531S} mutant uncovered the same complex pattern of expression in the mouse

orthologues of *dand5*, *spaw*, and *lefty2,* (Boylan, M. 2015). However, there are notable differences in the expression of these laterality genes between *cph* and *pierce1*/*pierce2* mutants, as well as in frequency between *cph* and PRPF8^{N1531S}, suggesting that KV motile cilia dysfunction may not be exactly alike in these models.

It is important to note that ectopic expression of *spaw* and *lefty2* can also be caused by loss of the midline expression of *lefty1. lefty1* acts as an inhibitor of *spaw* thus prohibiting *spaw* expression crossing the midline and being ectopically expressed on the right (Meno et al., 1998). As *spaw* induces *lefty2,* right sided *spaw* can induce right sided *lefty2* expression (Burdine and Grimes, 2016; Montague et al., 2018). Although absent or reduced expression of *lefty1* can lead to ectopic expression of *spaw* and *lefty2, lefty1 mis*-expression usually results in bilateral expression of *spaw* and *lefty2*, not the complex patterns of *spaw and lefty2* expression observed in *cph* (Lenhart et al., 2011). Indeed, midline expression of *lefty1* appeared the same in *cph* as in WT suggesting the mis-expression of *spaw* and *lefty2* was not caused by a midline defect in *cph* embryos. However, *cph* usually lacked expression of *lefty1* in the developing heart field and left diencephalon. This result fits with previous findings whereby absent or bilateral *spaw* expression caused loss of *lefty1* in these structures (Long et al., 2003). Additionally, the combined percentage of bilateral and absent expression of *spaw* may be the driving force behind the prevalence of unlooped *cph* hearts (Bakkers et al., 2009).

The finding that there was no change in KV cilia number in *cph* embryos compared to WT embryos, but that *cph* KV cilia were significantly shorter, supports the same finding from PRPF8^{N1531S} mouse mutants (Boylan, M. 2015). It is interesting to note that the relative decreases in cilia length between WT and *cph*/PRPF8^{N1531S} mutants was also comparable, with both exhibiting a decrease of around 20% of total cilium length. This finding supports the notion that there is no correlation between the severity of the Prpf8 mutation and the effect on cilia in *cph* or PRPF8^{N1531S} mutants, and that both mutations may act through the same specific mechanism that is equally affected in both mutants. In contrast to the cilia length similarities between cph and PRPF8^{N1531S} mutants, I found no obvious differences to the structure of the KV, with both WT and *cph* KVs appearing normal.

Additionally, in agreement with the observed shortened motile cilia phenotype within *cph* embryos, the translation blocking morphants also exhibited shortened cilia. As a decrease in WT Prpf8 produced the same cilia phenotype as seen in the *cph* embryos, this suggests that the decrease in length of *cph* KV cilia is not a product of a gain of function mutation. Additionally, the further decrease in length seen in the Prpf8 knockdown embryos compared to that of *cph* embryos is most readily explained by the knockdown of WT maternal *prpf8* mRNA, which would still be present in *cph* embryos at the stages examined thus masking the true null phenotype.

Investigations into the motility of the shorter cilia in *cph* embryos revealed that their motility was indeed severely affected, though not to the same degree as the mouse PRPF8^{N1531S} mutant (Boylan, M. 2015). At this point it is not clear whether the defect in cilia motility is caused by the decrease in length, or whether proteins directly involved in cilia motility are also affected. Investigations into *notch* zebrafish mutants revealed that significantly shorter KV cilia were still fully motile but failed to produce fluid flow, resulting in laterality defects (Lopes et al., 2010) suggesting that the short cilia in *cph* embryos is not the direct cause of the motility dysfunction. Somewhat conversely, the *locke* zebrafish mutant also displays significantly shorter cilia, but does exhibit cilia motility dysfunction (Sullivan-Brown et al., 2008) hinting that there is a link between cilia length and motility. Intriguingly, the cilia motility dysfunction of the *locke* mutant is strikingly similar to that of the *cph* mutant, with some cilia appearing fully functional, some twitching, and others completely immotile. *locke* mutants also show a lack of KV fluid flow and L/R axis defects comparable to that of *cph* mutants, however, the causal mutation in *locke* mutants is in *ccdc40* (Becker-Heck et al., 2010) and causes gross microtubule rearrangements that are not present in PRPF8^{N1531S} mutants (Boylan, M. 2015). Although the microtubule structure has not been determined for *cph* mutants, I see no reason why it should differ from PRPF8^{N1531S} mutants, suggesting that the decrease in motile cilia length may not be the direct cause of the motility dysfunction.

Although I am unsure whether there is direct causality between short motile KV cilia and motility dysfunction, it is clear that the anticlockwise fluid flow of *cph* embryos is disrupted, thus providing convincing evidence that the observed L/R axis defects are due to the observed motile cilia dysfunction. Recent evidence from Wasay Mohiuddin Shaikh Qureshi in the Hentges lab suggests that primary cilia are also significantly shorter in PRPF8^{N1531S} mutants than WT (Pers Comm). Although primary cilia length defects have not been confirmed in *cph* embryos, the results from the PRPF8^{N1531S} mutants open the possibility that the L/R axis disruption is not solely due to lack of KV fluid flow, but may be a combination of both reduced flow and diminished ability to sense it.

As mentioned above, recent data from the PRPF8^{N1531S} mutant suggested that primary cilia in the mutant heart were indeed shorter than WT. In accordance with this, previous findings in the PRPF8^{N1531S} mutant suggested that expression of components of the *Hedgehog* (*Hh*) pathway were dysregulated (Stephen, L. 2013). The finding that there was no change in expression of either *patched, gli2 or gli3* in *cph* mutants was unexpected, given the assumption *cph* embryos would be likely to exhibit primary cilia defects, but not without precedent. Multiple zebrafish mutants with defects in key cilia genes such as *ift172*, *ift57* and *ift88* displayed severe cilia defects but had unaffected hedgehog signalling (Lunt et al., 2009). Notably, these three IFTs are components of the IFT-B protein complex and have been shown to be critical in the transduction of the *Hh* pathway in mice (Huangfu et al., 2003; Houde et al., 2006). The findings by Lunt et.al (2009) introduce the possibility that

the role for cilia in *hh* signalling is not conserved between zebrafish and mice, as is the case with drosophila (Bangs and Anderson, 2017). In disagreement with the findings of Lunt, et.al (2009), Huang, et.al (2009) found that a maternal zygotic (mz) *ift88* mutant showed a slight decrease in *patched* and *gli* expression compared to that of non-mz *ift88* mutant in Lunt et.al (2009), suggesting that cilia are indeed required for the transduction of the *hh* pathway. The conclusions from Huang, et.al (2009) that the *hh* signalling pathway is only slightly reduced in zebrafish mutants lacking primary cilia raises the possibility that in the *cph* mutants *hh* signalling is also reduced, but by such a small amount that it is undetectable by WISH. Further analysis of *hh* pathway component expression by qPCR may reveal if there are any abnormalities comparable to the PRPF8^{N1531S} mutant.

Alternatively, it is possible that as the *cph* mutants still possess primary cilia, albeit possibly shorter, the *hh* pathway is unaffected. An additional explanation given the difference in animal model and mutation is that *cph* mutants differ from the PRPF8^{N1531S} mutant and the primary cilia are completely unaffected. The observation that *tbx20* expression is also normal in *cph* embryos would give credence to the idea that the *hh* pathway is unaffected. However, the finding that *igu* mutants which lack primary cilia also show no difference in *tbx20* expression, in disagreement to results from Arnold, et. al. (2015) which showed reduced *tbx20*, suggest that possibly primary cilia are not as critical to *hh* signal transduction as they are in mammals. As there is contradictory evidence for this suggestion, at this stage I would be more inclined to simply draw the conclusion that, as of yet, *cph* embryos display no abnormalities that can be conclusively linked to primary cilia dysfunction.

The working hypothesis up to this point had been that mutations in Prpf8 cause the mis-splicing of genes related to cilia function, thus causing the observed cilia defects. The result that Prpf8 localises to the axoneme of cilia in WT and *cph* embryos raises questions about this hypothesis. Firstly, what functional role could a splicing factor have directly at the cilia, and secondly, is the observed cilia dysfunction due to the abrogation of Prpf8 function directly at the cilia rather than mis-splicing of cilia related genes. Investigations into whether cilia related genes were mis-spliced in the PRPF8^{N1531S} mutant proved unfruitful, with no obvious mis-splicing detected via RNA-seq or RT-PCR. The apparent lack of a link between mis-spliced cilia genes and the observed cilia dysfunction may support the idea that Prpf8 has a direct role in the cilia. Indeed, additional core U5 splicing components, namely PRPF31, PRPF6, SNRNP200 as well as PRPF8 have all been found localised to either the cilia axoneme or basal body in various cell types (Wheway et al., 2015; Buskin et al., 2018). Notably, the truncated *cph* Prpf8 protein still possesses a putative cilia localisation signal, explaining why no difference in localisation is observed between cph embryos and WT. Interestingly, no core splicing proteins from any other non-U5 snRNP complexes have been found localised to cilia (Johnson and Malicki, 2019) suggesting a specific cilia role for U5

components. Additionally, PRPF6, PRPF8 and PRPF31 have all been implicated in ciliogenesis through siRNA knockdown screens (Kim et al., 2016) with significantly shorter cilia in cells with reduced PRPF8 and PRPF31 (Wheway et al., 2015). Coincidently, Prpf8 and PRPF31 are the two proteins that have been localised to the cilia axoneme. Furthermore, in two studies in zebrafish where either *prpf31* was knocked down or a mutant form of *prpf4* was upregulated, the zebrafish exhibited classic phenotypic hallmarks of motile cilia dysfunction, specifically pericardial oedema and curled down A-P body axis (Linder et al., 2011; Chen et al., 2014). Taking all of the data into consideration, the most parsimonious explanation would be that components of the U5 snRNP have a direct role in ciliogenesis. The alternative hypothesis of mis-splicing of cilia related genes would have to explain why different mutations, as well as decreased expression, in different U5 components all caused the apparent mis-splicing in the same subset of genes. Some evidence leading to rejection of the mis-splicing hypothesis is that no commonality of mis-spliced genes has been identified across the range of U5 snRNP mutants (Towns et al., 2010; Růžičková and Staněk, 2017; Buskin et al., 2018; Wood et al., 2021).

Although the current evidence points to a direct role for Prpf8 in cilia, the two hypotheses are not necessarily mutually exclusive. The idea that prpf8 and the other U5 snRNP components could be involved in the splicing of cilia related genes directly at the cilia is certainly an interesting prospect. In support of this hypothesis, recent work has demonstrated that translation of genes required for ciliogenesis and maintenance occurs within the cilium itself (Hao et al., 2021). In light of this recent discovery, it seems plausible that splicing of cilia genes could also localise within cilia. On the contrary, if localised cilia splicing is indeed the case, why are only U5 snRNP components localised to cilia rather than all of the core spliceosomal machinery required for canonical splicing?

An alternative explanation for the localisation of U5 snRNP proteins to the cilia is that the cilium is the site for U5 snRNP assembly with the U5 snRNA. Initially, snRNAs and snRNP mRNAs are transcribed in the nucleus, snRNP mRNAs are then translated and trafficked to the cytoplasm along with snRNAs for assembly into the U1, U2, U4, U5 and U6 snRNPs. These snRNPs are then trafficked back to the nucleus for spliceosome maturation (Shaw et al., 2008). The cytoplasmic location for this snRNP assembly with snRNAs is currently unknown (Hyjek et al., 2015). This hypothesis may explain why only U5 snRNPs have been localised to the cilia, as U1, U2, U4 and U6. snRNPs may assemble in a different cytoplasmic location.

3.4 Conclusion

In summary, I have established that *cph* mutants display hallmark morphological characteristics of motile cilia defects, including heart laterality defects similar to that of the mouse PRPF8^{N1531S} mutant. Additionally, I have provided strong evidence that laterality defects are present at the whole embryo level and are caused by lack of KV fluid flow, at least in part due to motile cilia defects within KV. At this point in time, it is still not clear whether the shortened KV cilia are the cause of the observed motility defect, or if primary cilia are affected by the *cph* mutation. In contrast to the mouse PRPF8^{N1531S} mutant, no defects in *hh* signalling were observed in *cph* mutants, though future, more precise, investigation may be warranted. Somewhat surprisingly, I found that Prpf8 localised to the KV motile cilia axoneme and there was no difference between location in WT or *cph* embryos suggesting that truncated Prpf8 is still localised correctly but is non-functional. Mutating the putative cilia localisation signal and observing Prpf8 protein sub-cellular localisation, as well as splicing function, may provide further insights into the role of Prpf8 at the cilium.

Chapter 4: Characterising the Prpf8 Knockdown Zebrafish

4.1.1 An introduction to Morpholinos

The first recognised use of a morpholino to inhibit the i*n vivo* translation of mRNA transcripts was by Dr James Summerton (Partridge et al., 1996; Summerton et al., 1997). Morpholinos are usually single stranded oligomers composed of 25 morpholine base pairs which undergo complimentary base pairing to the mRNA target. As Morpholinos are neutrally charged, they strongly bind to RNA and thus efficiently inhibit processing of the RNA transcript (Bill et al., 2009). There are two types of morpholinos used for knockdown of a gene of interest, splice blocking and translation blocking. Splicing blocking morpholinos work by binding to a splice site within the mRNA targeted for knockdown and inhibiting assembly of spliceosome components on that site. This blocking of spliceosome assembly results in the transcript being mis-spliced usually causing a frame shift mutation and premature stop codon. Alternatively a specific exon can be targeted with a splice blocking morpholino to facilitate removal of that exon, possibly to mimic a genetic mutation in another organism (Bill et al., 2009). Translation blocking morpholinos work by binding to the 5' un-translated region (UTR) of the mRNA, near or across the translation start site. Binding at this region inhibits ribosome assembly and thus stops the protein being translated (Summerton, 1999).

Morpholinos are delivered into the yolk of one to four cell stage embryos, with movement into the cells enabled by the neutral backbone of the morpholino inhibiting interactions with RNA binding proteins (Nasevicius and Ekker, 2000). Both types of morpholino can be used in a zebrafish model, with each having advantages and disadvantages. Splice blocking morpholinos only target the zygotic transcripts and so any phenotypes observed due to knockdown may more closely resemble that of a zygotic mutant model (Draper et al., 2001; Bill et al., 2009). Additionally, specific isoforms of a gene can be targeted by splice blocking morpholinos by binding to specific exons within the target transcript (Mably et al., 2003). Conversely, translation blocking morpholinos target both zygotic and maternal mRNA possibly revealing phenotypes early in development that would normally be masked by the presence of functional maternal transcripts (Nasevicius and Ekker, 2000).

The effectiveness of a morpholino is determined by a number of factors. As morpholinos are not degraded by nucleases, they are very stable and are not easily removed from the cell. However, the efficacy of morpholinos during later development is limited because the morpholino is diluted by successive cell divisions, with most morpholino induced phenotypes observed before 3 days post fertilization (Bill et al., 2009). Additionally, as most knockdowns by morpholino not do not completely remove all protein, highly stable proteins that are not regularly degraded may build up in the cell and reach a sufficient level to mask an underlying phenotype even when the morpholino is still readily abundant (Eisen and Smith, 2008).

Although morpholinos have proved successful at elucidating gene function without the need for time consuming and somewhat complicated knockout techniques, there are a number of problems with their use that have no doubt resulted in incorrect results. Firstly, the efficiency of the knockdown needs to be determined and, secondly, the accuracy of knockdown needs to be assessed – that is the possibility that the observed phenotype is due to knockdown of the target gene and not another "off target" gene. Regarding the first problem, when using a splice blocking morpholino, assessing the knockdown efficiency is relatively straightforward. The abundance of full-length mRNA, or mis-spliced mRNA, can be determined through RT-PCR or qPCR and compared to WT controls to give an accurate estimate of knockdown efficiency. For translation blocking morpholinos assessing knockdown efficiency is somewhat harder and relies on the existence of an antibody for the desired target protein. If such an antibody exists, knockdown efficiency can be estimated through either immunofluorescence of the protein in vivo or, more commonly, by western blot (Eisen and Smith, 2008). The drawback of the western blot approach for determining knockdown efficiency is that it usually requires a large number of morpholino injected organisms to generate enough detectable protein and so may not give an accurate estimation on knockdown per organism.

The problem with off- target effects occurring due to the use of morpholinos is much harder to resolve than the efficiency of knockdown. How to determine if the phenotype observed in a knockdown is truly that produced by a lack of the targeted gene requires a number of controls. Notably, previous studies have found that as little as 18 nucleotides of the 25 need to bind mRNA to elicit a knockdown of a gene, thus severely reducing the stringency of the morpholino oligo (Coffman et al., 2004). The main method for determining if any observed morphant phenotype is due to off target effects is to compare the phenotype to a known mutant of the target gene. Examination of similarities and, importantly, differences in phenotype may give clues to whether any off-target effects may be present in the morphant organism. Additionally, it is important to determine whether knockdown of the target gene was successful as inefficient knockdown of the target gene but strong morphant phenotype may indicate an off-target effect. In addition to comparing any observed phenotype to known mutants, comparison of any phenotype between two independent morpholinos targeted to the same gene may also prove useful in determining if either morphant exhibits off-target effect phenotypes. Ideally these two morpholinos would be translation blocking and splice blocking and, at low enough doses, could be used simultaneously to attempt to recapitulate the phenotype observed with each morpholino individually (Eisen and Smith, 2008). Finally, one of the most convincing strategies for demonstrating any morphant phenotype is not due to off target effects is to rescue the phenotype through injection of target RNA that cannot be recognised by the morpholino. This can be achieved by *in vitro* transcribing target RNA that contains synonymous mutations in the region the morpholino binds to. Upon injection of the morpholino with the

transcribed RNA, if the organism does not display the previously observed morphant phenotype then a strong case can be made for that phenotype being a true reflection of target gene knockdown. Notably, this method is not possible for large genes which have a sequence too long to *in vitro* transcribe. This, unfortunately, is the case for *prpf8.*

4.1.3 Aims for Chapter 4

Within this chapter I aim to characterise the zebrafish *prpf8* morpholino knockdown embryos for signs of motile cilia defects. I will compare phenotypes indicative of possible motile cilia defects to those observed in *cph* mutants to find any similarities or differences that may give me an insight into the mechanism by which Prpf8 affects cilia. I will also investigate if this morpholino knockdown model also exhibits laterality defects consistent with the shorter KV cilia observed. Finally, I aim to investigate the original hypothesis that mis-splicing of cilia related genes is the causative mechanism behind the Prpf8 mutant phenotypes by performing RT-PCR on candidate ciliary genes including *arl13b*.

4.2 Results

4.2.1 tbMO Morphological Characterisation

In the previous chapter I utilised a *prpf8* translation blocking morpholino to confirm the localisation of prpf8 in the KV cilia. As this experiment was done at 14hpf, I decided to repeat the tbMO injections and characterise the morphological phenotypes of the morphant to compare to that of the *cph* mutants. From this point forward, all tbMO injections were carried out at 1:4 concentration because the 1:3 concertation caused embryo lethality at around 16hpf.

WT embryos were injected with tbMO at the 1 cell stage and, in the same manner as the morphological characterisation of *cph* embryos, phenotypic abnormalities noted at 12 hour time points until embryo death. The first morphological abnormality was visible at 22-24hpf with the curling down of the A-P body axis (Figure 4.1A). This curling was much more severe in the tbMO fish than the *cph* fish of corresponding age and was present in roughly 90% of injected fish. Additionally, WT fish usually only possess two otoliths within the otic vesicle, however a significant number of tbMO embryos presented of three. Of note is that the *cph* embryos also occasionally possessed three otoliths, however, due to the greying of the CNS, imaging the *cph* fish otic vesicles with a light microscope proved difficult. By 48hpf the morphology of the knockdown morphant fish almost exactly phenocopied the morphology of the *cph* mutants (Figure 4.1B). Both fish models display extensive pericardial oedema (black arrows) as well as a curled A-P body axis of equal severity (red arrows), although there was no kink in the posterior of the tail in the tbMO embryos. Interestingly, the cell death in the CNS of the *cph* embryos and the resultant twitching, which is extensive at 48hpf, does not occur in the tbMO embryos.

Analysing heart looping of 48hpf embryos revealed that tbMO embryos also display heart laterality defects, though there are more leftward and unlooped hearts and less rightward looped hearts than that of *cph* embryos (Figure 4.1C). By 72hpf the pericardial oedema tends to be more severe in *cph* embryos, although still present in tbMO embryos. In tbMO embryos, the curl down of the A-P body axis continues to worsen, though never kinks back on itself as with the tail of *cph* embryos. The tbMO embryos also exhibit kidney cysts by this stage, though upon observation the cysts of the tbMO embryos are generally bigger and more obvious than *cph* (Figure 4.1D). While characterising the morphology of the tbMO embryos in comparison to WT and *cph* embryos, I noticed that the eyes vary in size. Measuring the area of WT, *cph and* tbMO embryo eyes revealed that as development progressed from 24-72hpf the eyes of *cph* and tbMO embryos were much smaller than that of WT (Figure 4.1E). Despite the morphological similarities to *cph* mutants, tbMO embryos survive until around 5 days post fertilisation (dpf) and only seem to die due to starvation caused by an inability to swim and hunt for food.

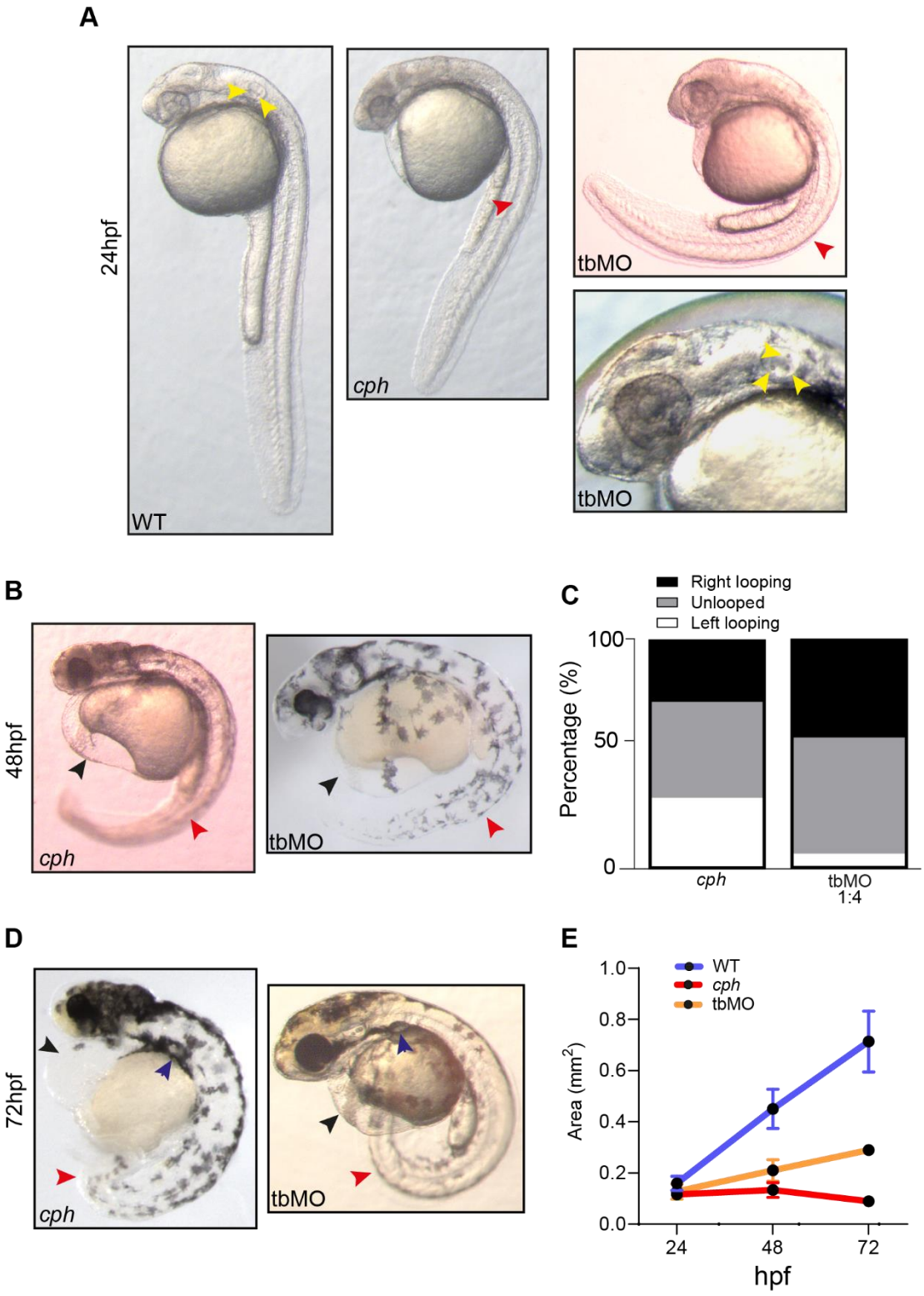

Figure 4.1: Morphological Characterisation of Prpf8 Knockdown Zebrafish Embryos. (A) brightfield images of WT, *cph* and *prpf8* tbMO knockdown embryos at 24hpf. Red arrows indicate the curvature of the A-P body axis. Yellow arrows indicate the otoliths within the otic vesicle. **(B)** Brightfield images of *cph* and *prpf8* tbMO knockdown embryos at 48hpf. Black arrows indicate pericardial oedema. **(C)** Frequency of heart looping directions observed in tbMO embryos compared to *cph* embryos at 48hpf RI = 43% UL = 51% LL = 6%. **(D)** Brightfield images of *cph* and *prpf8* tbMO knockdown embryos at 72hpf. Blue arrows indicate the forming kidney stones. **(E)** Eye size of WT, *cph* and tbMO from 24-72hpf. WT n=13 for all stages. *cph* n=5 for 24hpf, n=3 for 48hpf, n=1 for 72hpf. tbMO n=4 for 24 and 48hpf, n=1 for 72hpf.

4.2.2 tbMO Prpf8 Western Blot

In addition to showing the lack of prpf8 localisation in the cilia of the KV, I wanted to confirm that overall protein levels were reduced in the tbMO embryos. To this end I collected 48hpf WT, *cph* and tbMO embryos and prepared the samples for Western Blot. Equal amounts of protein were loaded and antibodies to detect Prpf8 and acetylated tubulin used. Dr Lu Hao in the Roy lab was instrumental in the optimisation and running of this western. The mass of WT Prpf8 is predicted to be 274kDa, acetylated tubulin 52kDa and the *cph* truncated form of Prpf8 as 48kDa. As can be seen from Figure 4.2A there is a band at roughly 260kDa in WT, with no band in the *cph* lane, and a faint band in the tbMO lane. Although these bands are not at the exact size I would expect, due to the nature of running on a high percentage gel I would predict that these are the correct bands for Prpf8. Additionally, as I would predict to see no band in *cph* at this size due to the truncation removing a large region of the protein, the lack of the high molecular weight band gives further credence to the notion that this 260kDa band is indeed Prpf8. With that being said, quantification of the 260kDa band in WT and tbMO reveals that Prpf8 is knocked down by roughly two thirds (Figure 4.2B). Notably, the tubulin loading control bands for WT and tbMO are of approximately equal intensity indicating that the decrease in Prpf8 band intensity in tbMO is truly due to a lack of Prpf8 rather than a decrease in total protein loaded. Admittedly, the tubulin band in *cph* is noticeably less intense than that of WT and tbMO.

I would not expect to see the truncated form of *cph* Prpf8 at 260kDa, I would expect to see it at roughly 47kDa. As there were no obvious bands in the *cph* Prpf8 lane and the tubulin intensity appeared lower than that of WT and tbMO, I repeated the Western but doubled the protein amount loaded onto the gel. As can be seen from Figure 4.2C*,* as expected the 260kDa band corresponding to Prpf8 and 50kDa band for tubulin in WT increases in intensity. Interestingly we now see a band at around 55kDa in the *cph* lane of the Prpf8 western which is not present in the WT sample. Additionally, tubulin intensity of the *cph* sample also increases compared to that of Figure 4.2A but is still significantly less intense than the corresponding WT tubulin (Figure 4.2C).

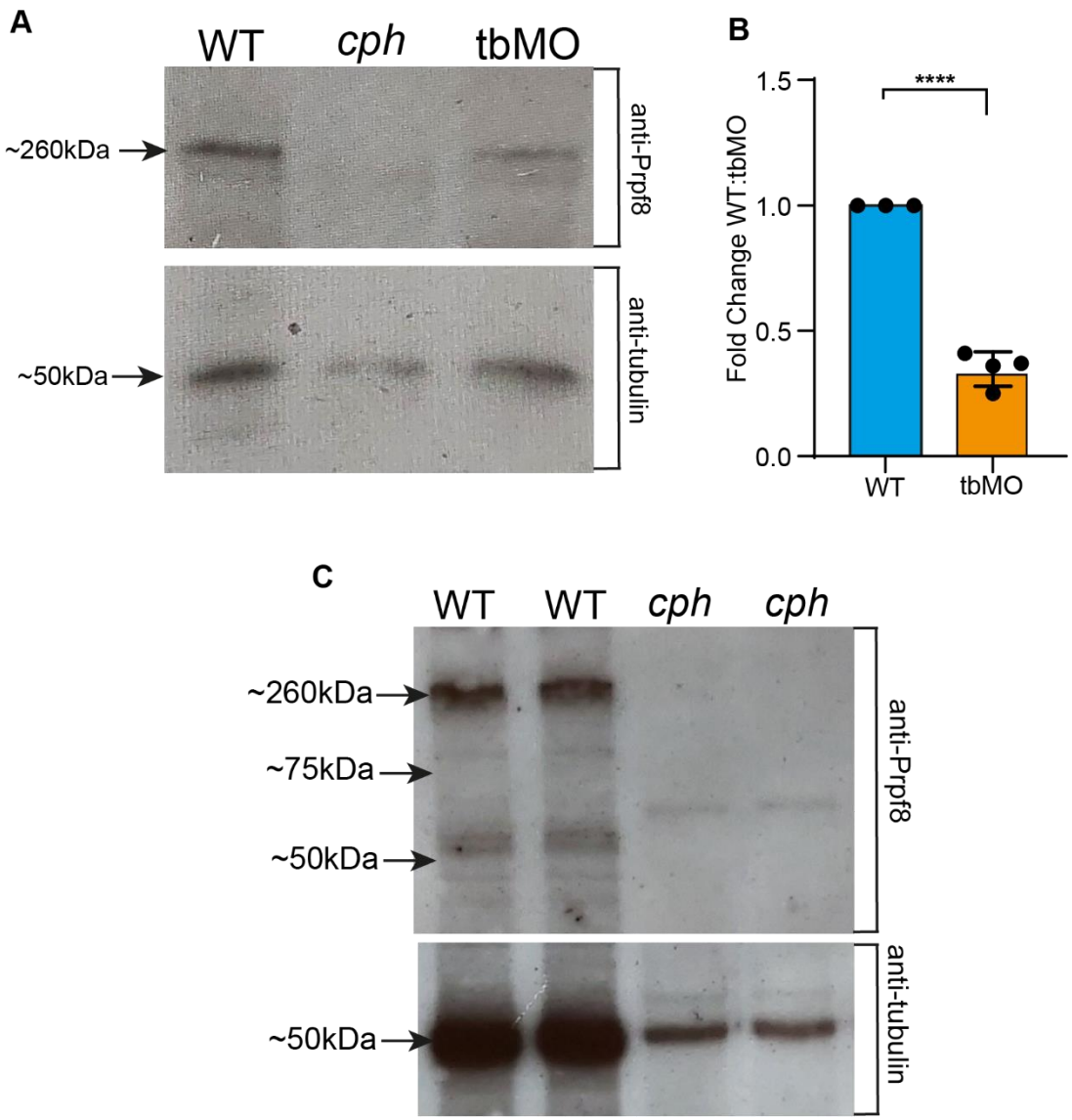

Figure 4.2: Western Blot Showing Relative Levels of Prpf8 in WT, *cph* and tbMO. (A) Protein levels of Prpf8 in WT, *cph* and tbMO with tubulin as loading control. Predicted protein size for Prpf8 is 274kDa. **(B)** Decrease in Prpf8 protein from WT to tbMO measured by optical density **(C)** Protein levels of Prpf8 in WT and *cph* with tubulin as loading control. Predicted protein size for truncated Prpf8 is 47kDa

4.2.3 Characterising Laterality Gene Expression in tbMO Embryos

Since *cph* embryos have heart looping defects and display mis-expression of the genes involved in laterality establishment, to investigate whether the same causation was true for the heart looping defects seen in tbMO embryos I carried out a WISH for *spaw* on 18s embryos.

Intriguingly, only three phenotypes were observed; left, bilateral and right (Figure 4.3 A) in contrast to the *cph* mutant also showing no expression of *spaw.* I quantified these expression frequencies and as can be seen from Figure 4.3B, the most common expression pattern was left followed by bilateral with only a relatively small number of embryos exhibiting right sided expression. As these results did not perfectly match up with what I expected based on the *cph spaw* results I decided to also carry out a WISH for *lefty2*. Strikingly, expression of *lefty2* was only ever present on the left or right, with a large bias for left sided expression (Figure 4.3C). Once again, the patterns and frequency of tbMO *lefty2* expression is in contrast to the expression pattern for *lefty2* seen in *cph* embryos (Figure 4.3D).

Following these perplexing results, I decided to check if midline expression of *lefty1* was also altered in tbMO in comparison to *cph.* As can be seen in Figure 4.3E expression of *lefty1* in the left heart field as well as left diencephalon was absent, in agreement with the expression findings from *cph*. Curiously, although mid-line expression of *lefty1* was variable in WT and *cph* embryos, expression of *lefty1* in the midline of tbMO embryos appeared to be weaker and lack expression in some regions.

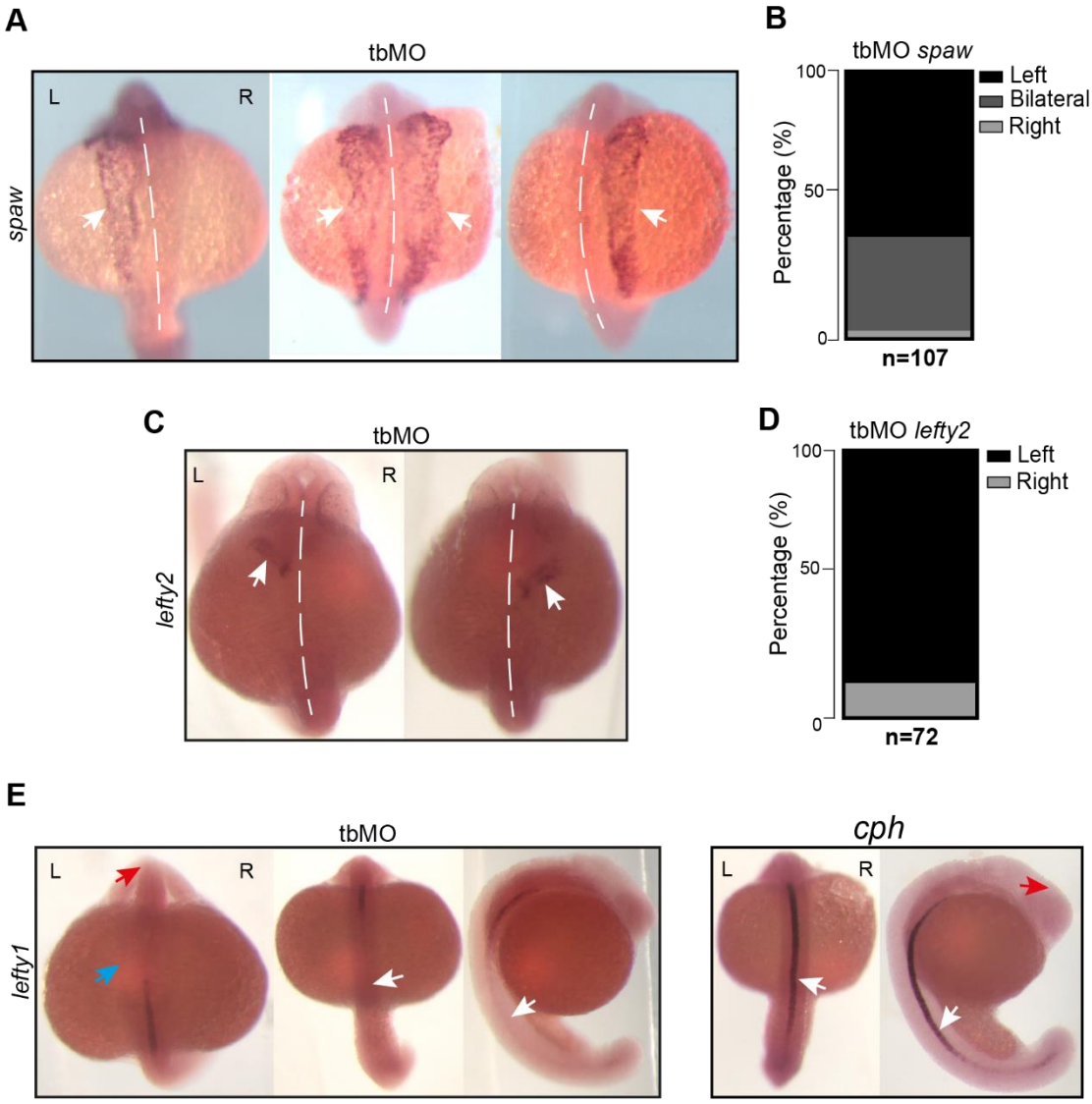

Figure 4.3: Whole Mount *in-situ* Hybridisation for Key Laterality Genes in tbMO. (A) WISH for *southpaw* on tbMO embryos at 18s stage. **(B)** Graph shows frequency of each of the three phenotypes observed L=62%, B=35%, R=3%. **(C)** WISH for *lefty2* on tbMO embryos at 22s stage. **(D)** Graph shows frequency of each of the two phenotypes observed L=87%, R=13%. **(E)** WISH for *lefty1* on tbMO and *cph* embryos at 18s stage. Blue arrow indicates the developing heart field and the red arrow indicates the left diencephalon. White arrows indicate areas of observed gene expression.

4.2.4 Investigating Motile Cilia Abnormalities in tbMO Embryos

As tbMO embryos exhibit defects in the establishment of the L/R axis, but not the same laterality gene expression alterations as *cph* embryos, I decided to investigate the fluid flow and cilia motility in the KV. As with *cph* embryos, I video imaged tbMO KVs and utilised naturally occurring particles to assess fluid flow within the KV. Once again, WT particles move in a strong anticlockwise motion as expected, however, particles in the KV of tbMO embryos have no obvious directionality and follow Brownian motion (Figure 4.4). This observation is in contrast to that of *cph* KVs, in which particles exhibited a small amount of linear movement in random directions.

To assess whether the cause of this disparity was due to a slight differing in the motile cilia phenotype between *cph* and tbMO embryos, I video imaged the cilia of the tbMO KV. Surprisingly the motility of cilia within the KV of tbMO embryos appeared to be identical to that of *cph* embryos, with cilia motility falling into three categories; WT, twitching and immotile (Video 4.1). Notably, the motility of the KV cilia correlated with the severity of the tbMO morphological phenotype, the more stationary or twitching cilia present the worse the pericardial oedema and curl down of the A-P axis. I tracked the particle movements in WT and tbMO KVs and, similar to *cph*, there was a lack of anticlockwise fluid rotation (Figure 4.4). Interestingly, in one video I was able to image cilia motility and particle movement simultaneously. In Video 4.2 we can see that cilia are still motile but that the particle in the KV is still stationary, suggesting lack of cilia motility is not necessarily the reason behind lack of fluid flow as previously stated. Additionally, the particles appear to move a lot less than in *cph* embryos suggesting the cilia immobility phenotype may be slightly stronger.

In addition to video imaging the KV of tbMO embryos, I decided to assess cilia motility in other structures. As the development of kidney cysts is a sign of motile cilia defects in the pronephric duct, I video imaged the pronephric duct of 24hpf tbMO embryos in the same manner as I had *cph* embryos. Surprisingly, tbMO pronephric duct cilia motility looked indistinguishable from WT (Video 4.3) (n=3). All cilia moved in a wave like manner up the entire length of the pronephric duct as well as in the cloaca. As video imaging the fish does not kill them, when these tbMO embryos were left to develop further, surprisingly, they all developed kidney cysts. These results are, as far as I'm aware, the first instance of kidney cysts forming in embryos with the appearance of WT pronephric duct cilia.

As these results were unexpected, and because cell death did not preclude imaging of ciliated structures at later developmental stages, I decided to image the nasal placode of tbMO embryos at 72hpf. In agreement with the finding of fully motile pronephric duct cilia, nasal placode cilia of tbMO embryos were also completely motile and indistinguishable from WT (Video 4.4) (n=3).

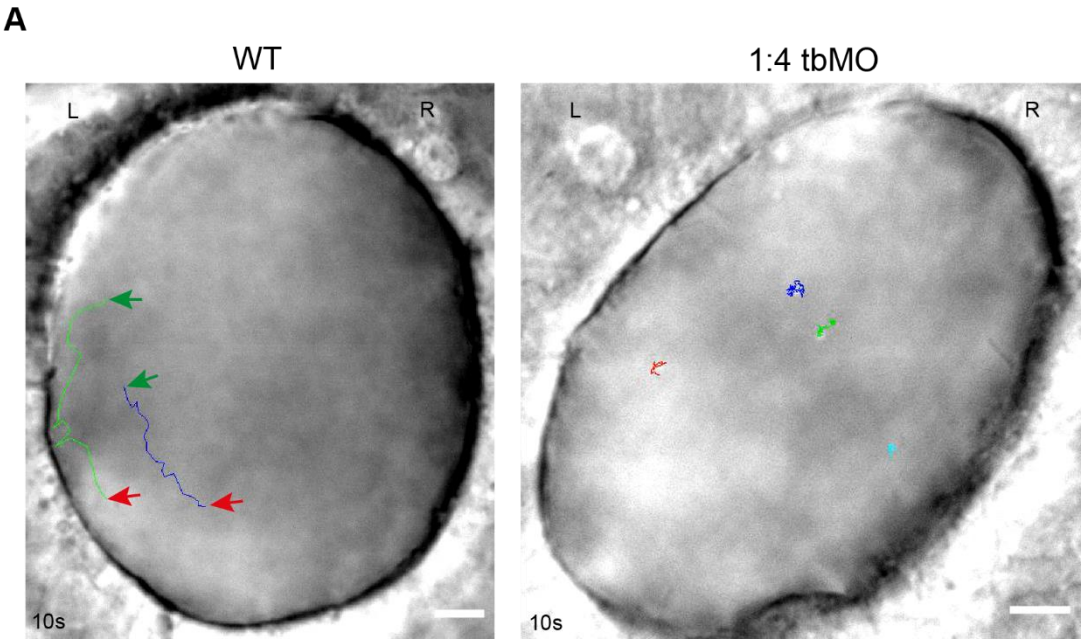

Figure 4.4: KV Fluid Flow in WT and tbMO Embryos. (A) Screen captures of videos tracking particle movement in the KVs of WT (n=3) and tbMO (n=3) embryo. Lines indicate the path of the tracked particle. Green arrows indicate the beginning of the path and red arrows indicate the end. Videos taken at 600x magnification. There are no arrows on the tbMO KV as start and finish of each particle path could not be determined. Scale bars = 10µm

4.2.5 Investigating Mis-splicing of *Arl13b* in *cph,* sbMO and PRPF8^{N1531S}

As Prpf8 is a U5 core spliceosomal protein directly involved in the splicing of introns, we hypothesised that mis-splicing of genes related to cilia function could be the cause of the cilia related phenotypes observed across the Prpf8 mutant models investigated. RNAseq data from the mouse PRPF8^{N1531S} mutant suggested that there was a mis-splicing event in *Arl13b,* a crucial cilia gene*.* The RNA-seq data proposed that exon9 of *Arl13b* was being skipped in PRPF8^{N1531S} mouse mutants. RT-PCR by Wasay Mohiuddin Shaikh Qureshi on this mouse mutant revealed that, as both transcripts were present in WT and PRPF8^{N1531S}*,* this apparent mis-splicing event was in fact a change in levels of isoform usage between WT and PRPF8^{N1531S} (Figure 4.5A). I quantified this shift in isoform usage and found that there was an almost 4-fold increase in the shorter isoform (lower band) in PRPF8^{N1531S} compared to WT (Figure 4.5B). Repeating this RT-PCR on 48hpf WT and *cph* zebrafish revealed the same isoform shift, though the abundance of the shorter isoform appeared visibly less in the zebrafish than mouse models (Figure 4.5C). Quantification of this shift in isoform usage showed a significant increase of around 2 fold compared to WT (Figure 4.5D).

Sequencing of both of these isoforms revealed that exon9 of *arl13b* was perfectly spliced out in the shorter isoform. Figure 4.5E shows the sequencing chromatogram of WT (long isoform) and the short isoform missing the highlighted exon9. Notably, *arl13b* is 10 exons in length and exon 9 is 69 base pairs, so the protein produced from the short isoform is predicted to remain in frame but omit 23 amino acids in the C-terminal region. Providing further evidence for this shift in *arl13b* isoform usage being functionally relevant, RT-PCR of 48hpf zebrafish injected with a splice blocking morpholino (sbMO) also showed this increase in the shorter isoform (Figure 4.5F). This cDNA preparation and MO injection was carried out by a former PhD student (Michael Boylan) a number of years ago, so I did not have enough cDNA to optimise the RT-PCR with equal amounts of cDNA, hence the weaker long isoform band in sbMO. However, as the shorter isoform is stronger in sbMO even with reduced cDNA input, I can conclude that the short isoform is increased compared to WT in this additional *prpf8* morphant.

Since mutations in *PRPF8* are linked to RP, I wondered if this *ARL13B* isoform shift was also present in the retinal cells of RP patients. To investigate this, I was provided with RPE1 cell cDNA by Wasay Mohiuddin Shaikh Qureshi and performed the RT-PCR (Figure 4.5G). However, no short isoform of *ARL13B* was present as the 272 base pair band correlates with the WT long isoform.

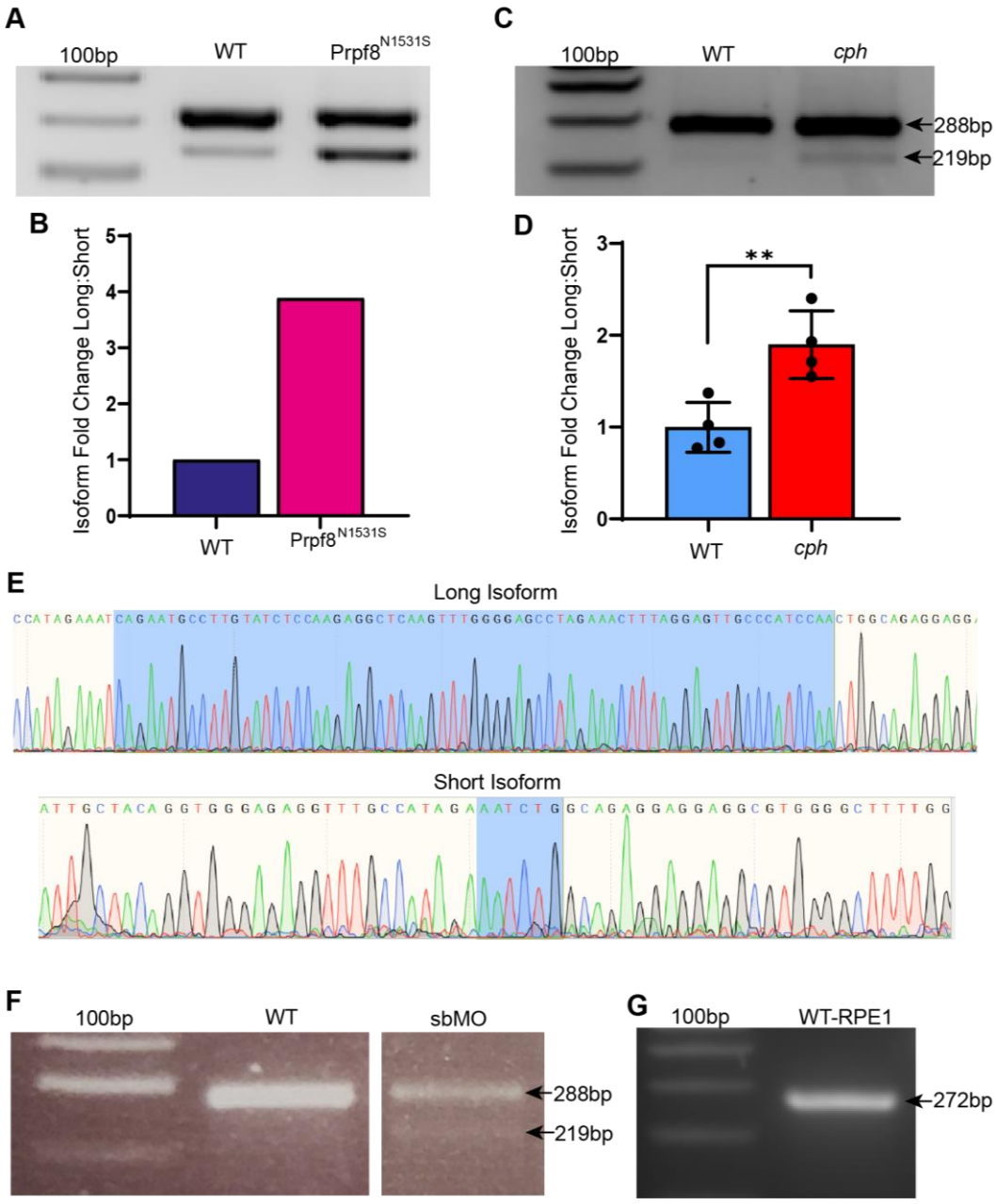

Figure 4.5: Differential Isoform Usage of *arl13b* in Mutants of Prpf8. (A) RT-PCR performed by Wasay Mohiuddin Shaikh Qureshi on exon 8-10 of *Arl13b* in WT and mouse Prpf8^{N1531S} homozygote mouse embryos. **(B)** Graph shows the fold change in the relative optical density of the shorter isoform as a percentage of the longer isoform between WT and Prpf8^{N1531S} homozygote. **(C)** RT-PCR performed *on exon* 8-10 of *arl13b* in WT and *cph* embryos. **(D)** *G*raph shows the fold change in the relative optical density of the shorter isoform as a percentage of the longer isoform between WT and *cph* embryos. Data is represented as mean ± SD. Unpaired t test was used to evaluate significance. **(E)** chromatogram showing highlighted exon 9 in the long isoforms but that exon 9 is spliced out in the shorter isoform of *arl13b.* In the shorter isoform, the last three bases of exon 8 and the first three bases of exon 10 are highlighted. **(F)** RT-PCR performed on exon 8-10 of *arl13b* in WT and sbMO embryos. Both panels are from the same image, I have cropped out lanes that were between WT and sbMO. **(G*)*** RT-PCR performed on exon 8-10 of *ARL13B* in WT RPE1 cells.

4.2.4 Prpf8^{N1531S} Whole Mount *in situ* Hybridisation for Hnf3- *β*

If this shift in *arl13b* isoform usage is indeed the causative mechanism behind the *cph,* sbMO and PRPF8^{N1531S} phenotype, then I hypothesised that the increase in short isoform must have a detrimental impact on downstream protein interactions and gene expression. In *Arl13b* null mice, *Hnf3-β* (*Foxa2*) is not expressed (Caspary et al., 2007), thus I reasoned that a similar phenotype should be observed in the PRPF8^{N1531S} mouse embryos. To this end, a WISH was carried out for *Hnf3-β* on 17s mouse embryos (Figure 4.6). As can be seen, expression of *Hnf3-β* is much reduced in the floorplate of PRPF8^{N1531S} mutants, especially in the cardiac and head region, compared to WT.

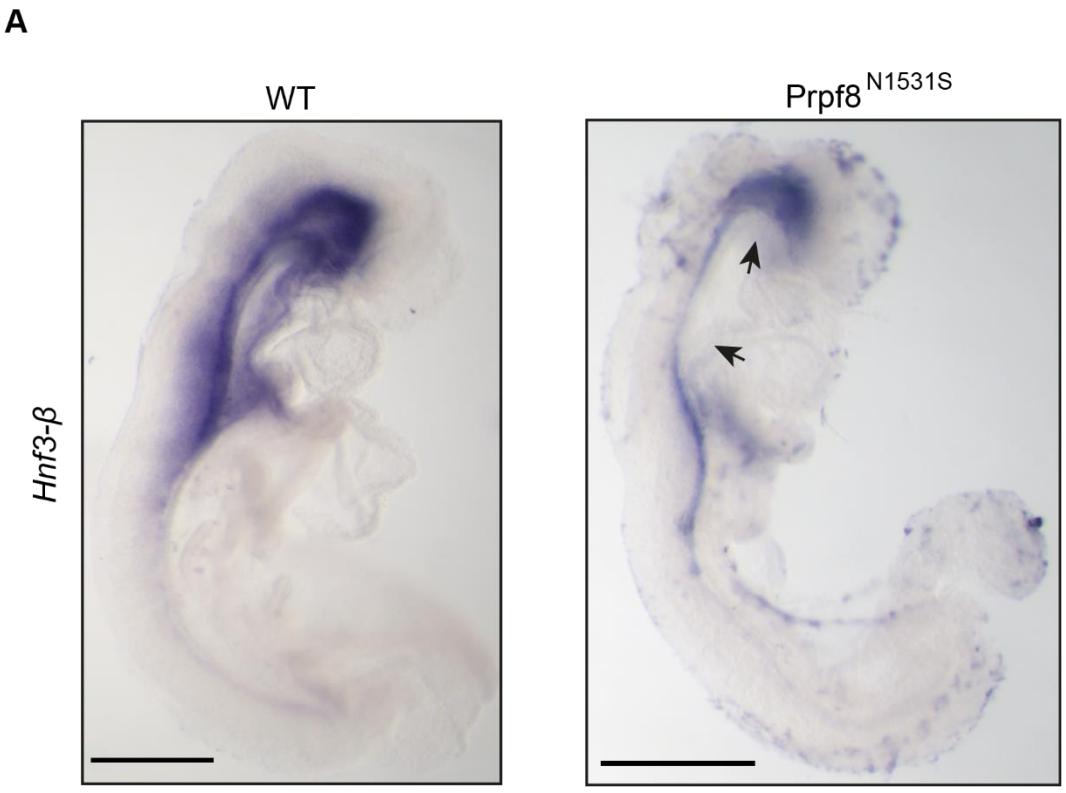

Figure 4.6: Whole mount in situ hybridisation for *Hnf3-β* on Prpf8^{N1531S}. (**A**) WISH on Prpf8^{N1531S} 17 somite mouse embryos (n=2). Scale bars are 0.5mm**.**

4.3 Discussion

The observation that the tbMO zebrafish almost precisely phenocopy the *cph* mutants is an intriguing development. Admittedly there are some minor differences, however all the classical motile cilia defect phenotypes previously discussed are present in both models, including pericardial oedema, kidney cysts and curled body axis. Worth noting is that the curled down body axis was always much more severe in the tbMO embryos than in *cph* embryos at 24hpf. I hypothesise that that the most likely explanation for this observation is that the translation blocking morpholino was not only knocking down the embryonic *prpf8* mRNA, but also the WT maternally contributed mRNA present in all early stage developing zebrafish (Harvey et al., 2013). The knockdown of the WT maternal mRNA would result in a more severe phenotype compared to *cph* embryos as, at 14hpf, the WT maternal *prpf8* mRNA will still be present in *cph* embryos and able to produce functional Prpf8 protein. If this hypothesis is correct, as development continues, I would expect to see the phenotypes within *cph* embryos become more severe as the maternal WT Prpf8 is used up and more truncated zygotic non-functional Prpf8 is translated. Additionally, the tbMO embryos should become less severely affected than *cph* embryos as developmental progresses, because more endogenous WT *prpf8* mRNA is translated as the morpholino is diluted through cell division.

Encouragingly, these predictions are almost exactly what was observed. By 48hpf both *cph* and tbMO were almost equal in the severity of motile cilia dysfunction related characteristics, and by 72hpf *cph* embryos were beginning to die whereas tbMO embryos survive until starvation at 5dpf due to inability to swim caused by the curled body axis. These observations perfectly fit with the hypothesis that Prpf8 functionality in *cph* is initially indistinguishable from WT due to maternal mRNA but slowly deteriorates due to increased translation of zygotic mRNA, while tbMO Prpf8 functionality is initially severely affected but improves as more WT Prpf8 is able to be translated. Further support for this hypothesis comes from the observation that injecting the *prpf8* morpholino into *cph* embryos resulted in severe deformities and lethality at roughly 18s (data not shown). This lethality was presumably due to the maternal *prpf8* mRNA being knocked down and the zygotic non-functional Prpf8 being unable to rescue the phenotype.

Intriguingly, the tbMO embryos do not seem to exhibit any morphological characteristic not directly associated with motile cilia defects. The lack of the neural cell death and tail kink phenotype suggests that these phenotypes may be the result of truncated Prpf8 acting through a cilia independent pathway as previously discussed in chapter **3.3.** Furthermore, as injecting the translation blocking morpholino into *cph* mutants resulted in severe deformities and early lethality, but injection of the same concentration into WT only resulted in motile cilia defects characteristics, an argument could be made that motile cilia have a higher requirement for Prpf8 than other cellular processes. This hypothesis would explain why a ubiquitously expressed protein can manifest as a tissue

specific disease when mutated. Indeed, a similar argument has been made to explain why human heterozygous mutations in PRPF8 cause RP. The argument is that the photoreceptor requires a higher rate of splicing compared to other cell types and so mutations in PRPF8 may reduce the rate of splicing and thus cause the RP phenotype (Maxwell et al., 2021).

This hypothesis could be modified to suggest that motile ciliated cells are also acutely dependant on splicing rate/fidelity, more so than non-motile ciliated cells, thus a small reduction in Prpf8 would result in motile cilia defects due to a reduction in splicing rate/functionality. This hypothesis links back to the previously discussed idea that splicing of cilia related genes may occur within the cilia itself, with this splicing process possibly being more susceptible to fluctuations in the availability of Prpf8. In possible support of this idea the tbMO and *cph* embryos exhibit smaller eyes than that of WT, a phenotype indicative of RP in zebrafish (Yin et al., 2011). This observation suggests a similar mechanism may exists for both RP and motile cilia dysfunction, which may be the increased reliance on splicing fidelity, though it is unclear why photoreceptor cilia and motile cilia would have an increased need for splicing compared to standard primary cilia.

Although characteristics dependant on motile cilia function appeared to be more severe in the tbMO embryos compared to *cph* embryos, surprisingly heart looping directionality frequencies are marginally closer to that of WT. Additionally, the expression patterns and frequencies of tbMO *lefty2 in situs* do not match up with the observed heart looping frequencies, with a large majority of embryos displaying left sided *lefty2* expression but the majority of hearts being unlooped. Furthermore, the observed dissimilarity in expression patterns for *spaw* and *lefty2* between tbMO and *cph* embryos is puzzling. One possible explanation is that due to the *in situ* being carried out at a stage before Prpf8 knockdown can be confirmed, a large proportion of embryos still possess functional Prpf8. Indeed, this is probably the case for a proportion of the left sided expression. However, the knockdown and *in situs* were performed multiple times and controls were used that suggested around 90% of embryos were morphants. Therefore these potential explanations do not fully account for the lack of bilateral *lefty2* expression and lack of absent *spaw/lefty2* expression expected based on *cph* results and previously published expression patterns of *spaw/lefty2* expression in cilia mutants (Dutta et al., 2015; Lin et al., 2017).

As previously discussed, *lefty1* is responsible for forming a midline barrier inhibiting the ectopic expression of *spaw* on the right, with *lefty1* mutants exhibiting high proportions of bilateral *spaw* (Lenhart et al., 2011). The apparent finding that *lefty1* midline expression is reduced in in tbMO embryos compared to *cph* embryos may provide a possible explanation for the high percentage of bilaterally expressed *spaw* in tbMO embryos. However, as the *cph* and tbMO *lefty1 in situs* were not performed together, and thus relative expression levels cannot be definitively compared, this explanation may not hold true.

Furthermore, previous studies find that bilateral *spaw* induces bilateral *lefty2* (Lenhart et al., 2011; Montague et al., 2018) in agreement with the accepted model that *spaw* induces *lefty2* (Meno et al., 1998) thus the finding that *lefty2* is never bilaterally expressed is at odds with the high incidence of bilateral *spaw* expression. Taken together these findings suggest that although the morphological characteristics of tbMO embryos mirror that of *cph* embryos there are differences between the two models at the gene expression level that cannot yet be explained.

As one explanation of the confusing *in situ* results may be that Prpf8 was not efficiently knocked down by the tbMO, a western blot was performed to determine if this was the case. The predicted size of Prpf8 is 274kDa, however the band on the western appears at 260kDa. This apparent discrepancy is explained by the high percentage gel the protein samples were run on. As the percentage, and thus density, of the gel increases it becomes increasingly harder to separate high molecular weight proteins (Sambrooke and Russel, 2001). This drawback results in the top end of the molecular weight scale being incredibly close together and thus a difference of 14kDa being indiscernible. In further support of this 260kDa band being Prpf8, it is missing in the *cph* lane and significantly decreased in the tbMO embryos confirming that Prpf8 was most likely also reduced in the *in situ* embryos. Additionally, previous studies have described Prp8 being detected at roughly 260kDa (Stevens and Abelson, 1999). Notably, acetylated-tubulin appears decreased in *cph* relative to WT and tbMO, however this observation can be explained by the high proportion of cell death (Keightley et al., 2013) and consequently protein degradation seen in *cph* embryos at this stage.

As the Prpf8 localisation results suggest that the truncated Prpf8 protein is still present, I would expect to see a band at around 48kDa corresponding to *cph* Prpf8. When analysing the results from the *cph* western the only band that is present is at roughly 55kDa. As this is the only band present in the *cph* lane and this band seems to be absent in the WT lane, it would seem likely this is the truncated form of Prpf8. However, it is peculiar that no other, possibly non-specific, bands from the WT lane are also present in the *cph* lane. Additionally, unless the truncated form has undergone posttranslational modifications, the proposed Prpf8 protein does not correspond to the predicted molecular weight. I would surmise that the band present in the *cph* lane is not the truncated form of Prpf8. I propose that the severe protein degradation within the *cph* embryos at the stage used for western blot hindered the detection of Prpf8, and other proteins, in *cph* embryos. This idea is backed up by the observation that tubulin abundance also appears to be incredibly low compared to that of WT. Furthermore, the *cph* embryo stage used for KV Prpf8 localisation was 14hpf, long before the cell death phenotype appears (Keightley et al., 2013), explaining why the antibody may detect Prpf8 in IF but not in the western. Repeating the Western blot using *cph* embryos at 14hpf would answer this, though at this stage hundreds of embryos would

need to be genotyped to provide sufficient mutant protein levels for detection.

As *prpf8* knockdown in tbMO embryos appears to be successful, a possible explanation for the difference in laterality gene expression pattern between *cph* and tbMO is that motile cilia within the KV may be less affected in tbMO embryos. The observation that cilia immotility within the KV of tbMO embryos correlates with phenotypic severity is encouraging and suggests that Prprf8 does not act in an all or nothing fashion in regards to motile cilia function. This scale of severity appears akin to that of PRPF31 which causes adRP via a haploinsufficiency mechanism, with less expression resulting in more severe adRP (Vithana et al., 2001; Rivolta et al., 2006; Waseem et al., 2007). Furthermore, mutations in PRPF8 which result in adRP also have a mutation/severity correlation (Towns et al., 2010).

It had been previously hypothesised that due to the PRPF8 adRP mutations mainly occurring in the final exon, the mutated transcript avoided nonsense meditated decay (Gamundi et al., 2008). The absence of this mechanism may permit the accumulation of non-functional PRPF8 and thus result in inadequate levels of functional protein. Alternatively, mutated PRPF8 may undergo aberrant folding thus causing degradation and reduction in functional PRPF8 (Towns et al., 2010; Maxwell et al., 2021). Based on these findings and hypotheses it is plausible to assume that the more motile KV cilia, and thus less severe morphological characteristics (mild curl, no pericardial oedema) seen in some tbMO embryos are due to the increased abundance of Prpf8 compared to that of severe morphological characteristics (severe curl, severe pericardial oedema) seen in other tbMO embryos. Admittedly, this would require Prpf8 protein quantification across the range of phenotypes to be certain.

The proposition that increased knockdown of *prpf8* leads to more severe phenotypes would back up the previous hypothesis that PRPF8 adRP may be caused by a reduction in functional PRPF8 rather than the mis-folding hypothesis. Indeed, embryos injected with tbMO at 1:3 concentration exhibited severe deformities and died at 18hpf, much earlier than that of *cph* and 1:4 tbMO embryos suggesting level of Prpf8 is correlated with embryo phenotypic severity. Taken as a whole, the proposed correlation between Prpf8 abundance and cilia motility once again suggests that motile cilia are acutely dependant on functional Prpf8, possibly more so than the splicing functions of Prpf8.

Within the tbMO embryos that exhibit maximum morphological severity without suffering embryonic lethality, the finding that motile cilia within the KV appear identical in motility to that of *cph* KV motile cilia is somewhat unexpected. Based on previously discussed findings that tbMO embryos exhibit a more severe morphological phenotype early in development compared to *cph,* I would have expected tbMO KV cilia to appear less motile. However, the observation that particle movement within the KV of tbMO embryos was less than that of *cph* particles, even when cilia were observed to still have comparable motility, suggests that tbMO embryos do have increased impartment in fluid flow

establishment. An explanation for this decrease in fluid flow brings us back to the idea that cilia length may be the driving force behind the laterality defect rather than the decreased motility of the KV cilia, which may itself be a product of decreased cilia length. Indeed, KV motile cilia length has been shown to be a critical factor in establishment of fluid flow within the KV with flow rate proportional to cilia length (Smith et al., 2014; Pintado et al., 2017). Additionally, the number of motile cilia within WT KVs vary widely from around 22 to 90, however length is a lot less varied (Gokey et al., 2016) suggesting motile cilia length may have more influence in establishment of KV fluid flow. As we know that tbMO embryos have shorter KV motile cilia than that of *cph* embryos, it is plausible this additional decrease in length is responsible for the further reduction in fluid flow. Again, we still cannot be certain whether the shortening of the cilia is the cause behind the reduction in cilia motility or whether length and motility are two independent characteristics in *cph* and tbMO embryos.

At this point it is impossible to separate the two and it is conceivable both contribute to the lack of fluid flow within the KV. Indeed, previous studies show that the zebrafish KV requires roughly 30 fully motile cilia for correct establishment of the L/R axis (Sampaio et al., 2014), much more than seem to be present in *cph* or tbMO KVs. However, Sampaio et.al (2014) only looked at motile and immotile KV cilia and so the predicted outcome of having motile, semi motile and immotile cilia as we see in *cph* and tbMO cannot be conclusively determined.

A clue to the mechanism by which fluid flow may be affected within the KV comes from the analysis of the pronephric duct cilia in *cph* and tbMO embryos. Similarly to the KV cilia, pronephric duct motile monocilia in *cph* embryos exhibit three types of motility; fully motile, twitching or immotile. It is surprising, given tbMO KV cilia also possess these three categories of motility, that the tbMO pronephric duct motile cilia appear indistinguishable from WT. Furthermore, although the pronephric duct motile cilia appear WT, tbMO embryos still develop kidney cysts. One possible explanation for this is the pronephric duct motile cilia are shorter compared to WT and so cannot generate the fluid flow necessary to prevent the formation of cysts. This explanation would also fit with the hypothesis proposed for reduced KV fluid flow in the tbMO KV. However, as the length of tbMO pronephric duct cilia were never measured I cannot say definitively this is the case. Alternatively, rather than the motility of the cilia in the pronephric duct being affected, it is possible the primary cilia that sense the fluid flow are somehow disrupted. This is the mechanism by which the *pkd2* mutant and morphants develop kidney cysts as the motile pronephric duct cilia are unaffected (Sullivan-Brown et al., 2008).

However, neither of these hypotheses explain why *cph* pronephric duct cilia appear to have a motility defect. I would expect if a decrease in length is causing the motility defect, then both *cph* and tbMO embryos should exhibit pronephric duct cilia motility defects, especially since tbMO embryos display a more severe phenotype at this early stage. It is possible the decrease in length of motile cilia and the motility defect are independent

characteristics. This proposition may explain the slight differences between tbMO and *cph* embryos as cilia motility may be more affected in *cph* and cilia length in tbMO embryos. However, as KV motile cilia exhibit the same motility defect in both tbMO and *cph* embryos, this explanation seems implausible. The *locke* mutant appears to combine all of the motile cilia phenotypes seen in tbMO and *cph* embryos (Zhao and Malicki, 2007; Sullivan-Brown et al., 2008), however no one hypothesis as to how motile cilia could be affected in both tbMO and *cph* embryos seems to explain all observations.

One promising avenue of current investigation does exist that may explain the observed *cph* and tbMO phenotypes. Analysis by Dr Wasay Mohiuddin Shaikh Qureshi into the RNAseq data of the mouse *PRPF*8^{N1531S} mutant revealed the presence of a short *Arl13b* isoform (Figure 4.5A). This short isoform is increased in PRPF8^{N1531S}, *cph* and a *prpf8* splice blocking morphant (sbMO) zebrafish created by Michael Boylan, a previous PhD student, indicating the increase of this abnormal isoform is a direct cause of Prpf8 dysfunction. It is interesting that all of these Prpf8 mutant models contain different mutations within Prpf8, and yet produced the same *arl13b* isoform expression change. The change in *arl13b* isoform expression is the first known example of a common mis-expression/mis-splicing event that directly links to cilia function to occur within multiple models of splicing factor mutations (Maxwell et al., 2021). This observation suggests the central linker region of Prpf8 is critically involved in the spicing of exon 9 of *arl13b* as each model is either missing or contains a mutation within this linker region.

The finding that the short isoform also exists in WT is intriguing as it was previously unknown in mouse and zebrafish (UCSC Genome Browser, 2020 and 2017 assemblies respectively), suggestive of either a functional role for this isoform or that exon 9 contains an increased susceptibility to mis-splicing. As this short isoform is perfectly missing the 69bp exon 9 and remains in frame, I assume the transcript avoids nonsense mediated decay. Interestingly, work by Nozaki et al. (2017) into the function of each ARL13B domain uncovered a specific role for the C-terminal proline rich (PR) region, of which 23 of the 50 amino acids are spliced out in the *arl13b* short isoform. In their work, Nozaki et al. (2017) demonstrated that deletion of the PR region resulted in the loss of binding to IFT-B complex dimer IFT46-IFT56. This finding enforces the idea that ARL13B is involved in the regulation of protein transport via interactions with IFT complexes (Cevik et al., 2010; Li et al., 2010). Further evidence this increased *Arl13b* short isoform may have an effect on our mutants comes from the observation that *Hnf3-β* expression is reduced in the PRPF8^{N1531S} mouse mutant. This result fits with the finding that an *Arl13b* null mouse had completely absent *Hnf3-β* expression (Caspary et al., 2007).

The discovery that *cph,* sbMO and PRPF8^{N1531S} mutants contain an isoform of Arl13b proposed to be less functional, and interactions with the IFT-B complex may be disrupted may explain a number of the observed cilia phenotypes within *cph* and PRPF8^{N1531S} mutants.

Firstly, numerous mutations in different regions within Arl13b are known to cause short cilia (Caspary et al., 2007; Duldulao et al., 2009; Cevik et al., 2010; Li et al., 2010; Gigante et al., 2020), the exact mechanism by which Arl13b regulates cilia length is unknown but is proposed to involve the interaction with the IFT proteins (Engel et al., 2009; Lu et al., 2015; Gigante et al., 2020). As Nozaki et. al (2017) did not measure cilia length of the ARL13B PR region deleted cells we cannot be sure if the lack of a PR region is the cause of the observed short cilia in our models but the link seems plausible given that we know loss of the proline rich region in c.*elegans* resulted in cilia defects as well as disrupted the IFT-B complex functionality (Li et al., 2010).

Secondly, as the level of *arl13b* short isoform expression is relatively low compared to that of WT, this may explain the heterogeneity I observe in cilia motility within individual embryos. Some motile cilia may fully consist of WT Arl13b and thus show normal motility, others may have more of the short isoform and so either twitch or lack motility all together depending on relative levels of short Arl13b.

Thirdly, the observation that there was no change in *hh* pathway component expression fits with the work by Gigante et al. (2020) who found that an ARL13B mutant that lacked cilia localisation had no change in Hh signalling even although primary cilia structure was affected. Since ARL13B could not localise to cilia in the Gigante et.al (2020) study, it seems logical that it could not associate with IFT-B in the cilia, suggesting ARL13B interaction with the IFT proteins is not required for correct Hh signalling. Furthermore, the relationship between IFT proteins and *hh* signalling is not clearly defined and so disruption to the IFT-B complex may not cause changes to *hh* pathway expression even if cilia are dysfunctional (Huang and Schier, 2009; Lunt et al., 2009).

Finally, the dysregulation of the IFT system is one of the main causes of RP (Verbakel et al., 2018) and so, although RP is not confirmed to be a phenotype in our Prpf8 models, the finding of that IFT proteins may be abnormally regulated opens up an explanation for PRPF8 linked RP. Indeed, cilia structure and protein localisation data from collaborators working on PRPF31-associated RP reveal hallmarks of ARL13B/IFT dysfunction within retinal cells (Majlinda Lako, Colin Johnson per com). The fact that WT RPE1 cells do not express this short isoform opens up the possibility that even a small amount of short ARL13B may have deleterious consequences for cilia structure and function.

4.4 Conclusion

In summary, I have developed a *prpf8* knockdown zebrafish model that closely resembles the morphological phenotype of the *cph* mutant. This tbMO also exhibits laterality defects and presents with an almost identical KV motile cilia phenotype. The tbMO zebrafish do possess slight differences in the expression of laterality markers as well as the motility of pronephric duct cilia. However, as these differences are, or produce, phenotypes

associated with motile cilia defects i.e kidney cysts, I can conclude that tbMO embryos are a reliable model for investigating Prpf8 function in relation to cilia. The finding that a short isoform of *arl13b* lacking the PR region exists in multiple models of Prpf8 mutation uncovers a possible mechanism as to how Prpf8 affects cilia function. Currently all data fit with *arl13b* being affected in some way, however further investigation will be required to conclusively confirm this preliminary result.

Chapter 5: Characterising the *pierce1/ pierce2* Double Mutants

5.1.1 Background to *Pierce1/Pierce2* Project

Studies on the gene *pierce1 (p53* induced expression in RB null cells 1) originally identified it as a downstream target of P53 and was upregulated in RB-null embryonic fibroblasts (Sung et al., 2007). *Pierce1* is located on mouse chromosome 2 and codes for a 169 amino acid protein, with the human orthologue of *Pierce1* being 136 amino acids (Anujan, 2018). Clustal analysis revealed that PIERCE1 has a high identity with orthologues in a number of species including; 100% with chimpanzee, 78% to mouse and 44% to zebrafish and also all share the protein domain DUF4490 which possesses unknown function (Anujan, 2018). *Pierce1* has been implicated through a number of high throughput screens in zebrafish and mouse as a potential novel ciliary gene (Hoh et al., 2012; Choksi et al., 2014). Notably, *pierce1* was found to be upregulated by over expression of *Foxj1* (Choksi et al., 2014; Anujan, 2018). Additionally, *PIERCE1* was found to be upregulated through analysis of human PCD samples proving futher evidence that *PIERCE1* may be putative ciliary gene (Geremek et al., 2011, 2014). For these reasons, *Pierce1* was selected for further investigation with the aim of identifying its functional role within ciliogenesis (Anujan, 2018). Analysis of expression of *Pierce1* within an air liquid interface culture of mouse nasal epithelial cells (mNEC), replicating the ciliated cells of the respiratory tract, found that *Pierce1* was upregulated upon mucocillary differentiation. This differential expression pattern corresponded to that of Foxj1 (Anujan, 2018). Additionally, *Pierce1* was expressed in the lung, testes, ovary and brain, all tissues that contain motile cilia. Furthermore, PIERCE1 was localised to the cytoplasm and axoneme of the bronchus and fallopian tube in human samples (Anujan, 2018).

Further analysis of Pierce1 function in zebrafish showed that knockdown of *pierce1* through either translation blocking or splice blocking morpholino resulted in curled A-P body axis, pericardial oedema and hydrocephalus of embryos (Anujan, 2018). Notably, morphants also displayed a high degree of laterality defects, measured by heart looping directionality consistent with mouse models of *Pierce1* knockout (Sung et al., 2016; Gui et al., 2021). The observed laterality defects were proposed to be caused by defects in KV motile cilia. Indeed, imaging showed that KV cilia in both morphants displayed motility defects (Anujan, 2018). These findings suggested that Pierce1 was involved in the function of motile cilia in a number of organs. However, further work by Anujan (2018) in which a zebrafish knockout model of *pierce1* was developed cast doubt on this hypothesis. At least two knockout models were investigated, one with a 29bp insertion in exon2 and another with a 5bp deletion in exon2 both of which resulted in a frameshift and premature stop codon (Anujan, 2018). Neither of these mutants displayed the characteristic motile cilia defects seen in morphants even when bred to be maternally zygotic mutants. These findings cast doubt on the morphant phenotype and suggest the observed defects in cilia motility may be due to off target effects (Anujan, 2018). Notably, confirmation that Pierce1 protein was not

produced in mutants was not possible due to the lack of a zebrafish Pierce1 antibody, meaning the observed lack of phenotype may be due to the existence of functional Pierce1 protein.

To evaluate the disparity between the morphant phenotypes and the knockout phenotypes, Anujan (2018) investigated whether any paralogues to *pierce1* exist in zebrafish. This investigation uncovered a gene called *c15orf56*, now termed *pierce2* (Gui et al., 2021), which also contains the DUF4490 domain (Anujan, 2018). Like Pierce1, Pierce2 function was uncharacterised. Interestingly, *pierce2* expression was also upregulated during air liquid interface cultures of mNEC (Nemajerova et al., 2016). To determine if Pierce2 was compensating for loss of Pierce1 in zebrafish mutants, Anujan (2018) developed a CRISPR strategy to knockout *pierce2* with Yan Ling Chon of the Roy lab finally creating the *pierce2* homozygous mutants. Like the *pierce1* mutants, the *pierce2* mutants exhibited no characteristics redolent of motile cilia defects.

5.1.2 Aims for Chapter 5

Within this chapter I aim to generate *pierce1/pierce2* double mutant zebrafish and characterise any morphological phenotype associated with motile cilia defects. This will include measurement of any heart looping defects as well as observation of any curl down of the A-P body axis. Additionally, I will aim to determine genes required for establishment of the L/R axis are mis-expressed. If laterality defects are observed I will investigate the KV to determine if cilia exhibit any structural or motility defect that may explain the observation of laterality defects. Further to this, I aim to examine the motile cilia within the pronephric duct as well as the nasal placode to determine if cilia motility is affected in other organs. Latterly, I will also try and rescue the *pierce1*/*pierce2* knockout phenotype by injection of sense RNA for each gene.

5.2 Results

5.2.1 Breeding Scheme to Generate Double Mutants

Previous characterisation of the individual mz *pierce1* and *pierce2* (termed *h15c18orf65* prior to this work) mutant zebrafish by Priyanka Anujan and myself, respectively, showed no obvious phenotype. As each protein displays similarity in protein sequence and domains, we hypothesised that Pierce1 and Pierce2 could be compensating for each other. To investigate this, I decided to create double *pierce1* and *pierce2* mutants (hereafter referred to as $p1^{-/-}/p2^{-/-}$). To generate $p1^{-/-}/p2^{-/-}$ double mutants I crossed the homozygous *pierce1* line with the homozygous *pierce2* line. The result of this cross is a clutch of embryos which are all heterozygous for each gene. These fish were viable and were left to develop. After allowing the double heterozygotes to reach sexual maturity, I in-crossed these double heterozygotes with each other and left them to develop. This cross produced 16 genotypes, with 1 in 16 of the fish having the desired double knockout (Figure 5.1A). Because these fish had come from parents which harboured a WT copy of each gene, the $p1^{-/-}/p2^{-/-}$ fish would possess a maternal contribution of WT mRNA for each gene. This maternal contribution could mask the true phenotype associated with double knockout of *pierce1* and *pierce2.* Therefore, the $p1^{-/-}/p2^{-/-}$ fish were in-crossed once more to generate mz $p1^{-/-}/p2^{-/-}$ embryos. Mz $p1^{-/-}/p2^{-/-}$ fish were viable and fertile and the line was kept as $p1^{-/-}/p2^{-/-}$ with out-breeding to AB WT fish stocks every second generation.

The *pierce1* and *pierce2* mutants, generated by Priyanka Anujan and Yan Ling Chong, both contained insertions of 29bp and 34bp in the coding region respectively (Gui et al., 2021). As well as the fact these insertions generated a frame shift resulting in a premature stop codon, they also allow for easy genotyping via PCR and gel electrophoresis. Carrying out the PCR and gel electrophoresis for *pierce1* and *pierce2* in tandem allowed for identification of the genotypes produced from the heterozygous in-cross (Figure 5.1B).

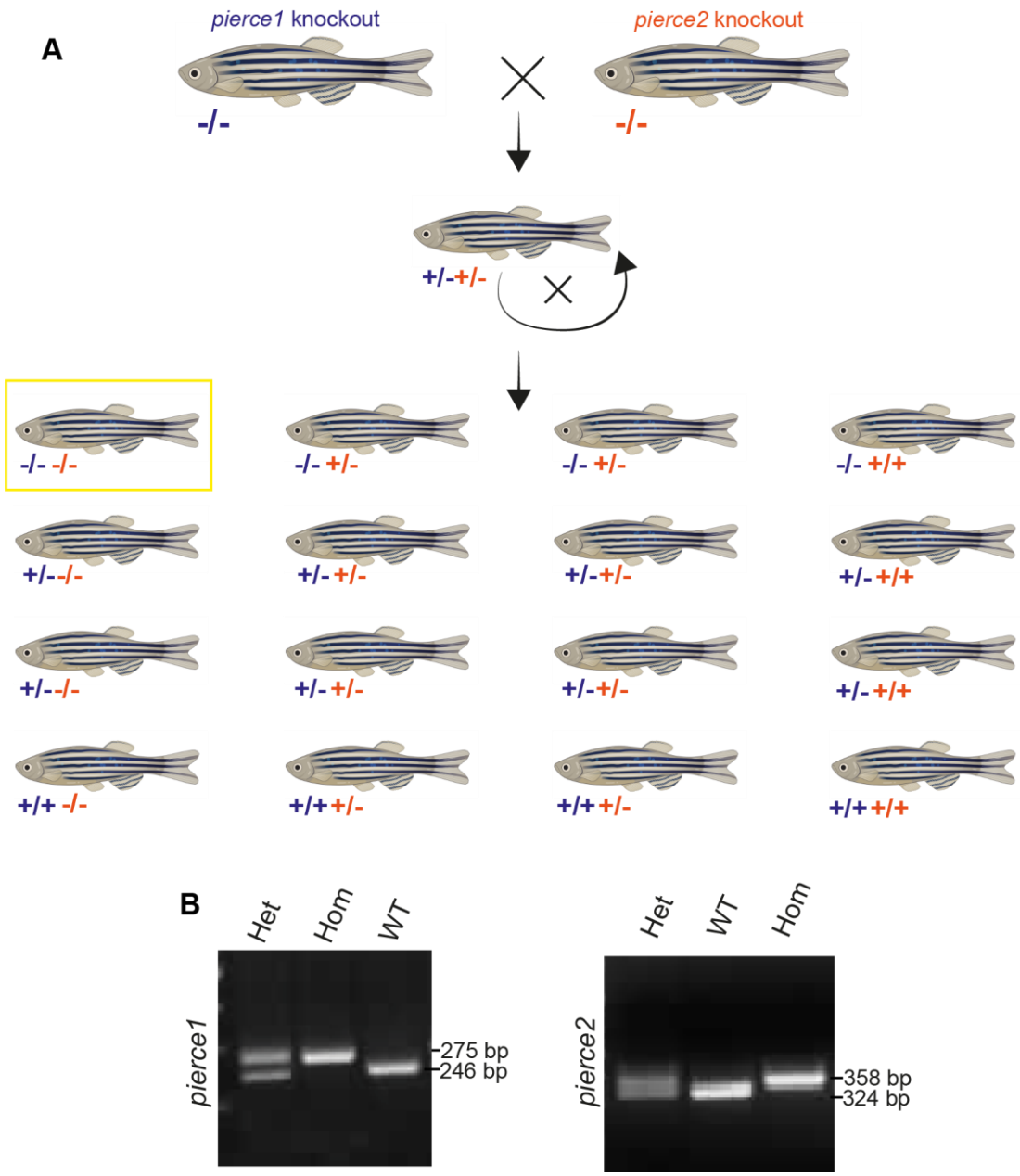

Figure 5.1: Breeding Strategy and Genotyping for *pierce1/pierce2* Double Knockout. (**A**) Schematic demonstrating the breeding strategy used for generation of *p1*$^{-/-}$/*p2*$^{-/-}$ zebrafish. Yellow box highlights the 1/16 double knockout genotype desired **(B)** Genotyping for *pierce1* and *pierce2* knockouts showing band patterns expected for each genotype after PCR and gel electrophoresis

During the process of in-crossing the double heterozygotes to identify *p1*$^{-/-}$/*p2*$^{-/-}$ mutants I noticed that at roughly 48hpf a proportion of embryos displayed varying severities of curling in their A-P body axis. I had assumed that these embryos were possibly the *p1*$^{-/-}$ /*p2*$^{-/-}$ embryos and so I genotyped them to confirm. Although the most severe curled down embryos were indeed *p1*$^{-/-}$/*p2*$^{-/-}$ mutants, puzzlingly, a range of other genotypes also displayed this phenomenon. To investigate, I selected 26 embryos which exhibited defects in their A-P body axis ranging from severe curl to very mild swimming defect. I then scored the severity and of each fish and, after genotyping, noted the number of mutant alleles it possessed. Analysing this data revealed a positive correlation between number of mutant alleles and severity of curl phenotype (Figure 5.2). Unsurprisingly, double heterozygotes displayed a mild phenotype, however, surprisingly *pierce1* mutants with WT *pierce2* background also exhibited a mild defect, and vice versa. This finding was puzzling as these single knockout mutants have the same genetic background as the previously characterised *pierce1* and *pierce2* single mutants which exhibited no phenotypes.

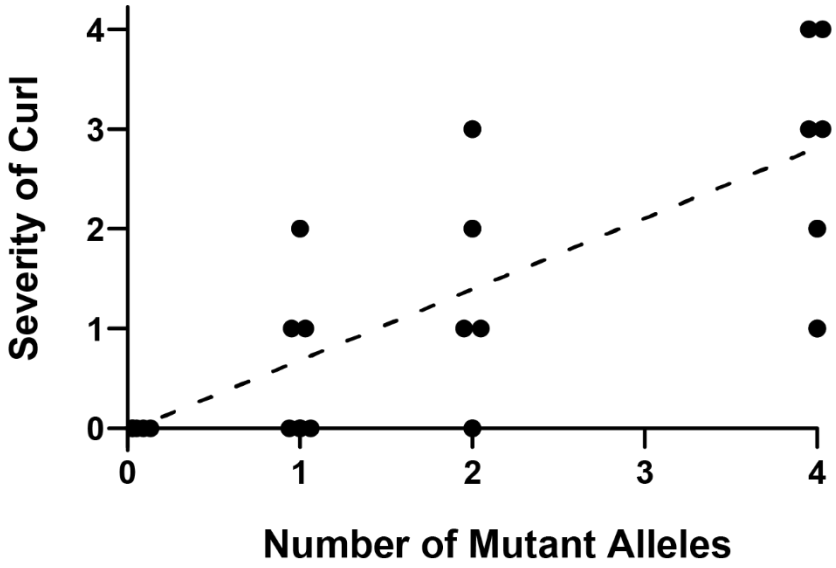

Figure 5.2: Phenotype Severity Matrix for Offspring from *p1/p2* Double Heterozygous In-cross. Spearman Rank correlation between number of mutant alleles in an embryo and the severity of the curled A-P body axis. n=21. Positive correlation with p=<0.0001. No embryos had 3 mutant alleles in this analysis.

5.2.2 *p1*$^{-/-}$*/p2*$^{-/-}$ Morphological Characterisation

Characterisation of the mz *pierce1*/*pierce2* double knockout revealed an increase incidence of heart looping defects. Whole mount IF using A4.1025 antibody, labelling the myosin heavy chain, at 36hpf clearly shows *p1*$^{-/-}$*/p2*$^{-/-}$ embryos with leftward jogged, unlooped and rightwards jogged hearts (Figure 5.3A). Of note is that the hearts of *p1*$^{-/-}$*/p2*$^{-/-}$ embryos never completed looping in either direction, and instead only jogged to the left or right. Quantification of these three jogging phenotypes showed that each looping phenotype accounts for roughly 33% of *p1*$^{-/-}$*/p2*$^{-/-}$ embryos (Figure 5.3B)**.** Interestingly, although I see heart looping dysfunction, only a very small percentage of embryos exhibited curl down of the embryo A-P axis early in development, as observed in *cph* embryos. However, at 72hpf I did observe a curl down at the far posterior of *p1*$^{-/-}$*/p2*$^{-/-}$ embryos compared to WT (Figure5.3C). This curl down persisted throughout larval development and, consistently, adult *p1*$^{-/-}$*/p2*$^{-/-}$ fish displayed a range of severities of scoliotic spines. No other morphological phenotype, such as kidney cysts or pericardial oedema, was observed.

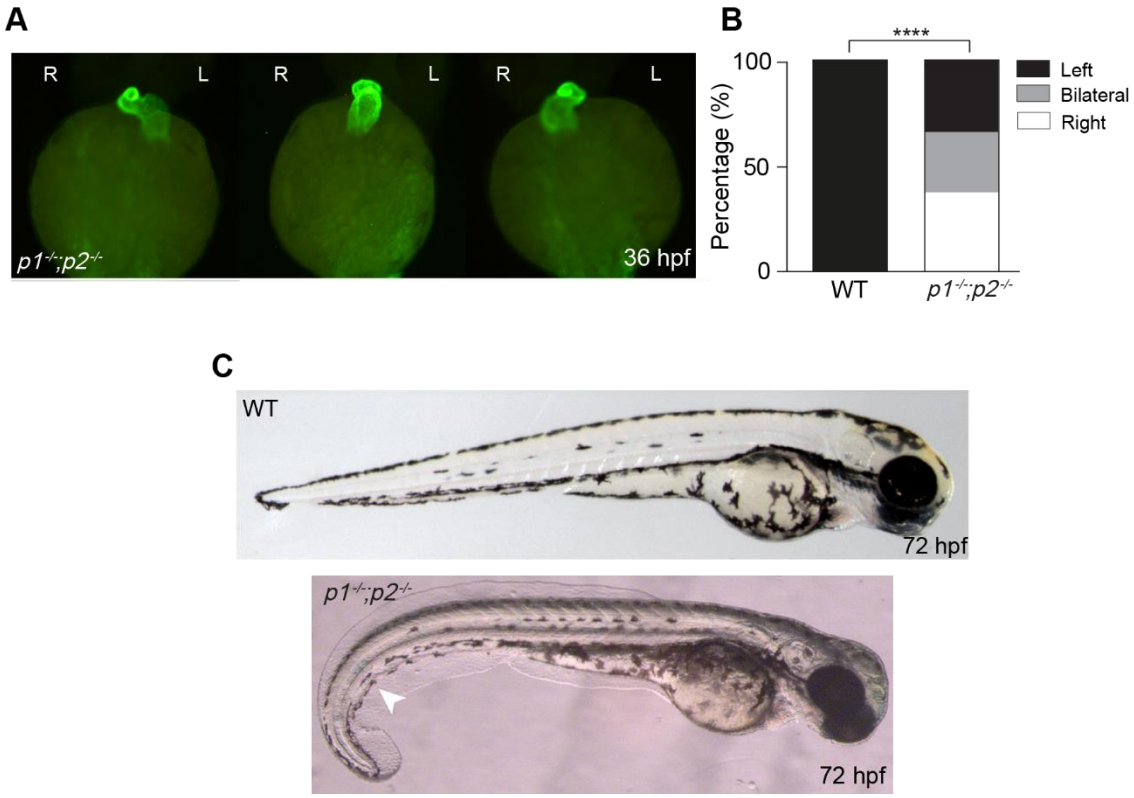

Figure 5.3: Morphological Phenotype of $p1^{-/-}/p2^{-/-}$ Double Mutants. **(A)** Left: Immunofluorescence microscopy showing heart jogging directionality at 36hpf. Images from left to right show the three heart jogging directions observed when observed dorsally: leftward jogging (37.5%), bilateral jogging (29.2%), and rightward jogging (33.3%). Right: quantification of heart jogging directionality in WT (n = 61) and $p1^{-/-}/p2^{-/-}$ (n = 72) embryos **(B)** Bright-field images of WT and $p1^{-/-}/p2^{-/-}$ embryos at 72hpf.

5.2.3 Characterising Laterality Gene Expression in *p1$^{-/-}$/p2$^{-/-}$* Embryos

Following the observation of increased incidence of heart looping defects in *p1$^{-/-}$/p2$^{-/-}$* embryos, indicative of dysfunction in establishment of the L/R axis, I decided to perform a WISH for genes involved in L/R axis formation. Investigating *spaw* expression in *p1$^{-/-}$/p2$^{-/-}$* embryos revealed that, although incredibly weak, four expression patters were present; left, absent, bilateral and right expression (Figure 5.4A). Surprisingly, when these expression patterns were quantified, there was a clear bias towards no *spaw* expression, closely followed by left-handed expression Figure 5.4B). As the observed expression pattern for *spaw* was incredibly weak and unexpected, I decided to perform another WISH for *lefty2* on *p1$^{-/-}$/p2$^{-/-}$* embryos. Interestingly, *lefty2* only displayed three expression patterns; left, absent, and right with a large bias toward absent expression (Figure 5.4C and D). In contrast to *spaw,* the intensity of *lefty2* staining was comparable to that of WT. However, notably, the staining in the heart field never extended out laterality as seen in WT, but instead stayed close to the midline consistent with the observation that *p1$^{-/-}$/p2$^{-/-}$* hearts never fully looped and instead only jogged. Although the observed staining pattern for *spaw* and *lefty2* was different to that seen with *cph*, the mis-expression compared to WT also indicated a dysfunction in establishment of the L/R axis.

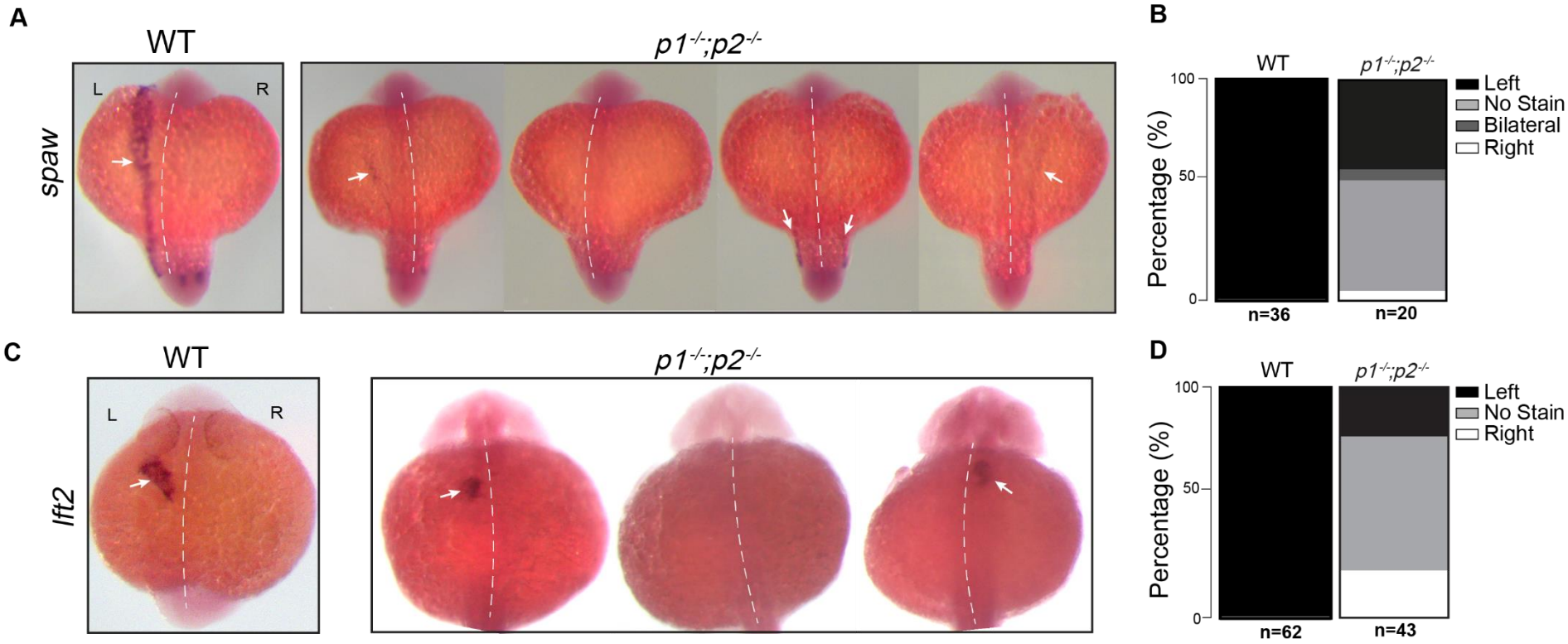

Figure 5.4: Whole Mount *in situ* Hybridisation for Key Laterality Genes in *p1*$^{-/-}$;*p2*$^{-/-}$ Embryos. (A) Left: WISH for *southpaw* on WT and *p1*$^{-/-}$;*p2*$^{-/-}$ embryos at the 18s stage. White arrow indicates the stain. The white dashed line indicates the embryonic midline. For *p1*$^{-/-}$;*p2*$^{-/-}$ embryos, expression on the left, no expression, bilateral and right expression, respectively, are depicted. **(B)** Quantification of *southpaw* expression for WT (n = 36) and *p1*$^{-/-}$;*p2*$^{-/-}$ (n = 20) embryos (L=40%, NS= 50%, R=5%, B=5%). **(C)** Left: WISH for *left2* on WT and *p1*$^{-/-}$;*p2*$^{-/-}$ embryos at the 22s stage. Arrows and labelling are as in (A). **(D)**: Quantification of *lefty2* expression for WT (n = 62) and *p1*$^{-/-}$;*p2*$^{-/-}$ (n = 43) embryos (L=20%, B=60%, NS=20%).

5.2.4 Investigation of KV Motile Cilia in *p1$^{-/-}$/p2$^{-/-}$* Embryos

Since *p1$^{-/-}$/p2$^{-/-}$* embryos exhibited some tell-tale signs of motile cilia dysfunction as well as issues in correct establishment of the L/R axis, I decided to investigate whether the motile cilia within the KV displayed any abnormalities. I performed an IF on 10s WT and *p1$^{-/-}$/p2$^{-/-}$* embryos using acetylated tubulin, gamma tubulin and DAPI. Imaging using confocal microscopy revealed that *p1$^{-/-}$/p2$^{-/-}$* embryos possess no obvious structural abnormality in the KV and still possess KV cilia (Figure 5.5A). Further investigation into the motile cilia within the KV showed that there was no difference in number of cilia between *p1$^{-/-}$/p2$^{-/-}$ (n=5)* embryos and WT (n=10) (Figure 5.5B) as well as no difference in length Figure 5.5C), as had been the case with *cph* embryos. For the number and length of cilia measurements, each datapoint is the average of all the measurements within a single KV. This method of quantification minimises small variations in developmental time point as well as innate developmental differences between embryos.

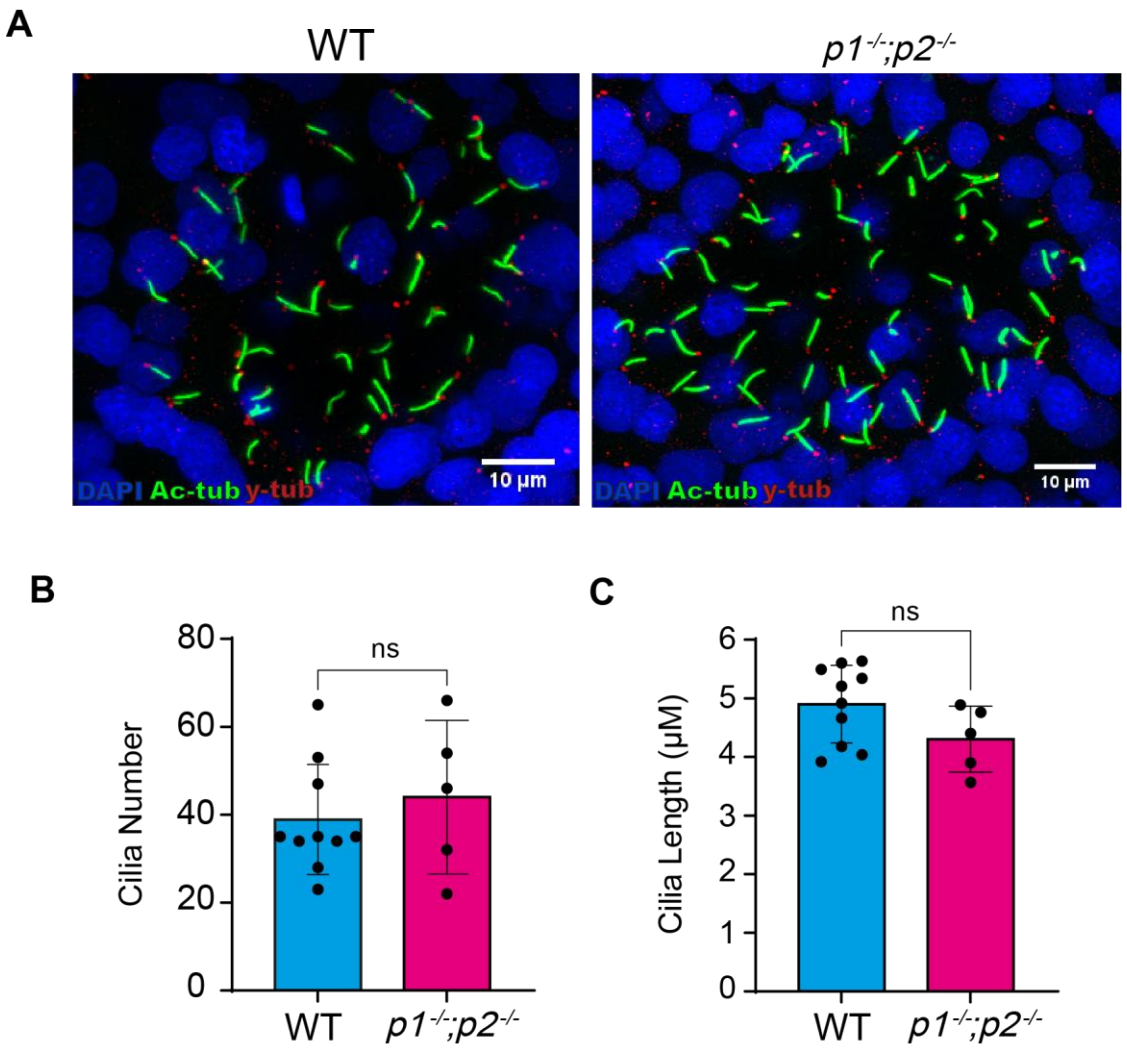

Figure 5.5: Immunofluorescence and quantification of *p1*$^{-/-}$/*p2*$^{-/-}$ KV cilia. (A) IF of KVs of WT and *p1*$^{-/-}$/*p2*$^{-/-}$ embryos using antibodies against acetylated tubulin (labelling axonemes), gamma-tubulin (labelling basal bodies), and DAPI (labelling nuclei). **(B)** Quantification of cilium number per KV in WT and *p1*$^{-/-}$/*p2*$^{-/-}$ embryos. **(C)** Quantification of cilium length per KV in WT and *p1*$^{-/-}$/*p2*$^{-/-}$ embryos. Data are represented as mean ± SD. Unpaired t test was used to evaluate significance.

Due to the presence of laterality defects during heart development, but no observable defects in KV morphology or motile cilia number and structure, I hypothesised that there was likely a dysfunction in the motility of the cilia within the KV. To determine if this was the case, I video imaged the KV of *p1*$^{-/-}$*/p2*$^{-/-}$ embryos. Remarkably, the KV cilia were almost completely immotile (n=5) (Video 5.1). To confirm that this was indeed unique to the *p1*$^{-/-}$*/p2*$^{-/-}$ double mutants I video imaged the *pierce1*$^{-/-}$ and *pierce2*$^{-/-}$ single mutants. Indeed, the cilia within the KV of each single mutant were completely motile (data not shown). The finding that both Pierce1 and Pierce2 need to be knocked out to elicit a motile cilia phenotype suggests each individual protein is functionally redundant. I proposed that if this was the case then complementation of the double mutant with either WT *pierce1* or *pierce2* should rescue the phenotype. I therefore *in vitro* transcribed WT *pierce1* or *pierce2* mRNA and injected each into 1 cell stage *p1*$^{-/-}$*/p2*$^{-/-}$ embryos. Examination of heart looping of injected embryos at 48hpf revealed that heart jogging directionality had been restored to almost WT levels in both *pierce1* rescued and *pierce2* rescued embryos (Figure 5.6), though full looping still not did occur. Video imaging of KV cilia in both *pierce1* injected and *pierce2* injected *p1*$^{-/-}$*/p2*$^{-/-}$ embryos confirmed that this rescue of heart jogging was indeed due to restoration of KV cilia motility (Video 5.2 and Video 5.3)(n=5).

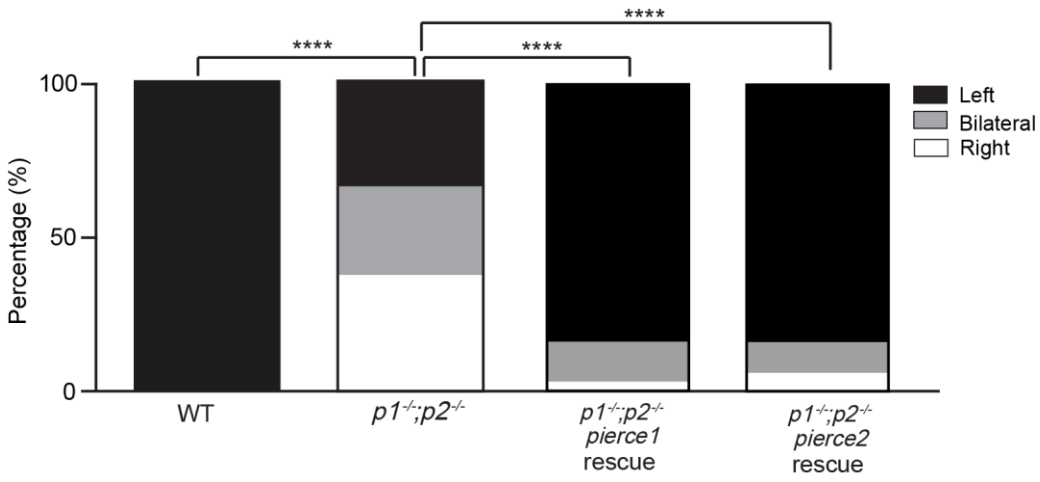

Figure 5.6: Quantification of Heart Jogging Direction of *p1*$^{-/-}$*/p2*$^{-/-}$ Rescue Embryos. (A) Quantification of heart jogging direction in WT (n = 61) and p1$^{-/-}$;p2$^{-/-}$ (n = 72) embryos and p1$^{-/-}$;p2$^{-/-}$ embryos following injection of pierce1 (n = 43) or pierce2 (n = 47) mRNA. One way ANOVA was used to evaluate significance.

5.2.5 Investigation of Cilia Motility in Additional Structures of *p1*$^{-/-}$/*p2*$^{-/-}$ Embryos

As a result of the finding that cilia with the KV of *p1*$^{-/-}$/*p2*$^{-/-}$ embryos were completely immotile, as well as the mild curl down of the A-P body axis at 72hpf, I proposed that other motile cilia in other ciliated structures may also be affected. To investigate this, I video imaged the pronephric duct at 24hpf in *p1*$^{-/-}$/*p2*$^{-/-}$ embryos (n=3) though, surprisingly, cilia motility remained indistinguishable from WT (Video 5.4), consistent with the lack of kidney cyst formation. Further to this, video imaging of the nasal placode at 72hpf in *p1*$^{-/-}$/*p2*$^{-/-}$ embryos also showed no difference compared to WT embryos (n=3) (Video 5.5).

5.3 Discussion

Previous work by Dr Priyanka Anujan demonstrated that knockdown of *pierce1* in zebrafish produced embryos which exhibited classical phenotypes associated with motile cilia defects (Malicki et al., 2011; Anujan, 2018). Knowing this, it was surprising to find that *pierce1,* and the paralogue *pierce2,* knockouts did not exhibit any defects and were indistinguishable from WT. As *pierce1* and *pierce2* are paralogues we hypothesised each protein was compensating for the other. Alternatively, as no antibody was available for either protein, confirmation of knockout by western blot could not be performed and so it was possible Pierce1 and Pierce2 were still translated and functional.

During the process of creating the $p1^{-/-};p2^{-/-}$ double mutants, I found that embryos which were $p1^{-/-};p2^{+/+}$ and $p1^{+/+};p2^{-/-}$ displayed mild characteristics of motile cilia defects i.e curled body axis (Figure 5.3). This finding was puzzling as these embryos should be genetically identical to their mz *pierce1*$^{-/-}$ or *pierce2*$^{-/-}$ grandparents, which showed no signs of cilia defects. I hypothesised that single *pierce* mutants generated from double heterozygous in-cross exhibited mild body axis curl due to the contribution of maternal mRNA consisting of only one WT allele for each gene. This hypothesis suggests that the mild curl down may be the result of a form of haploinsufficiency resulting from insufficient WT maternal mRNA for both genes, in agreement with our hypothesis that the *pierce1* and *pierce2* complement each other. Based on what we now know in relation to Pierce1 and Pierce2 function (Gui et al., 2021), this quasi haploinsufficiency mechanism explains the apparent disparity between *p1*$^{-/-}$*;p2*$^{+/+}$ and mz *pierce1* or *pierce2* mutants. At the time, this discovery was intriguing and provided evidence that knockout of both *pierce1* and *pierce2* cause defects associated with cilia dysfunction. Additionally, due to low sample numbers when scoring phenotypic severity it was not possible to determine if knockout of *pierce1* rather than *pierce2* alleles resulted in a more severe phenotype, as seen in the mouse model (Gui et al., 2021).

Continued morphological analysis of *p1*$^{-/-}$*;p2*$^{-/-}$ revealed a high incidence of heart looping defects. Interestingly, the hearts of *p1*$^{-/-}$*;p2*$^{-/-}$ embryos never fully looped but instead only jogged to the left or right, as well as remaining linear. This finding fits with proposed models of the relationship between heart looping and laterality, where jogging direction is defined by organism laterality but looping is controlled by a heart intrinsic mechanism (Noël et al., 2013; Grimes et al., 2020). Additionally, the presence of jogging and lack of looping is also seen in zebrafish *spaw* mutants where *spaw* expression is initiated but fails to fully propagate to the anterior LPM (Noël et al., 2013). The mis-expression of *spaw* explains the laterality defects exhibited by the heart jogging. Furthermore, the weak and restricted *spaw* expression seen in the *p1*$^{-/-}$*;p2*$^{-/-}$ mutants most likely explains the lack of heart looping. Additionally, the expression patterns of *lefty2* fits with the observed expression of *spaw* with the majority of *p1*$^{-/-}$*;p2*$^{-/-}$ embryos presenting with absent expression, most probably due to the absence of *spaw* to initiate *lefty2* expression. *lefty2* expression is still observed on the

left and right suggesting that some amount of *spaw* must have reached the anterior LPM. However, as this *lefty2* expression remained close to the midline and never extended out laterally as in WT, full heart looping was clearly still hindered in these embryos.

Investigation into the cause of this mis-expression of *spaw* and *lefty2* in *p1*$^{-/-}$;*p2*$^{-/-}$ embryos revealed that KV cilia were completely immotile. Further work demonstrated this immotility was caused by a lack of outer dynein arms within the KV cilia (Gui et al., 2021). This immotility explains the ectopic expression of *spaw*, however it is not clear why *spaw* expression is significantly reduced and spatially restricted. Zebrafish which harbour mutations a dynein assembly factor protein *lrrc50* (*Dnaaf1*) also lack outer dynein arms and possess completely immotile KV cilia. However, these mutants exhibit relatively normal and unrestricted levels of *spaw* expression, but do show the same ectopic expression patterns seen in *p1*$^{-/-}$;*p2*$^{-/-}$ mutants (Sullivan-Brown et al., 2008; Van Rooijen et al., 2008; Loges et al., 2009). The successful rescue of the KV cilia motility by injection of either *pierce1* or *pierce2* proves that the proteins are indeed functionally redundant. Interestingly, mouse mutants of *Pierce1* display KV cilia motility and laterality defects suggesting that PIERCE1 and PIERCE2 are not functionally redundant in mice (Gui et al., 2021). One explanation for this is Pierce1 and Pierce2 possess very similar microtubule protein binding sequences and so Pierce1 could bind the equivalent site for Pierce2 and *vice versa* resulting in functional redundancy. These binding sites may have diverged sufficiently in mice meaning each paralogue cannot function independently resulting in the observed *Pierce1* mouse phenotype. Indeed, there is divergence within the conserved domains of Pierce1 between mouse and zebrafish (Anujan, P. 2018) suggesting this hypothesis could be correct .

Further analysis into cilia motility revealed that the motile cilia of the pronephric duct and nasal placode were fully functional in *p1*$^{-/-}$;*p2*$^{-/-}$ mutants. The curl down of the A-P body axis in *p1*$^{-/-}$;*p2*$^{-/-}$ mutants is usually suggestive of defects in 9+2 cilia, however the spinal cord does contain a number of 9+0 cilia thus explaining the mild nature and late onset of the curl down (Drummond, 2009; Zhang et al., 2018). The reason for this difference in motility between cilia in the pronephric duct and KV in these mutants is unclear. The *lrrc50* zebrafish mutant, which also lacked outer dynein arms exhibited completely immotile pronephric duct cilia (Van Rooijen et al., 2008) and, furthermore, the mouse *Pierce1* mutant displayed motility defects in 9+2 tracheal cilia (Gui et al., 2021). These findings suggest that, either, *pierce1*/*pierce2* have slightly altered functions between mouse and zebrafish, or that *pierce1*/*pierce2* have tissue specific functions within the zebrafish.

5.4 Conclusion

In summary I have demonstrated that Pierce1 and Pierce2 are functionally redundant and the loss of both proteins causes cilia motility defects within the KV of zebrafish. These cilia defects cause downstream disruption of the laterality of the mutant fish, as evidenced by ectopic expression of laterality markers and reversal of heart direction. Further work by Gui et. al (2021) demonstrated loss of Pierce1/Pierce2 resulted in loss of outer dynein arms and that the function of these proteins was conserved in mouse. A full and detailed account of the structure and function of Pierce1/Pierce2 and how these proteins bind to cilia microtubules can be found in Gui et. al (2021). The main finding of our work is that Pierce1 and Pierce2 act to form a docking complex periodically along the microtubule, allowing for binding of the outer dynein arms to the outer doublet microtubules of the cilia axoneme and thus facilitate cilia motility.

6 Final Discussion

6.1 Final Discussion of *prpf8* Phenotype

Within this project, the discovery that a predicted null *prpf8* zebrafish mutant presented with L/R axis defects was an intriguing revelation, though as the PRPF8^{N1531S} mouse mutant also displayed laterality defects, this finding was not without precedent (Boylan, 2015). Nevertheless, the observation that a zebrafish mutant lacking all functionality of such an essential gene is initially viable and only presents with tissue specific phenotypes warranted further investigation.

My initial characterisation of the *cph* revealed that an increase in unlooped and reversed looped hearts was not the only phenotype. Indeed, *cph* embryos presented with curled body axis, pericardial oedema, kidney cysts and otolith defects, all of which are characteristics of motile cilia dysfunction (Drummond, 2009). Additionally, *cph* embryos also displayed a kinked tail severe CNS cell death starting at around 28hpf, though examination by Keightley et al., (2013) found increased cell death throughout the whole embryo at earlier stages. As the morphology of *cph* mutants was grossly malformed at 48hpf (when heart looping direction was analysed), I decided to investigate genes involved in the establishment of the L/R axis to determine if the heart looping phenotype was due to disfiguration of the embryo or truly a laterality defect. Consistent with defects in laterality establishment, *lefty2, spaw,* and *dand5* were either ectopically expressed or absent, in agreement with the PRPF8^{N1531S} mouse mutant.

Furthermore, I found that the motile cilia within Kupffer's Vesicle exhibited motility defects, but unlike the fully stationary motile cilia of the PRPF8^{N1531S} mutant, the KV cilia were either stationary, twitching or appeared comparable to WT. Additionally, the KV motile cilia were also significantly reduced in length. The dysfunctional motile cilia, along with their reduction in length, is most likely the cause of the observed failure to establish the L/R axis. Consistent with the finding that KV cilia displayed aberrant motility, pronephric duct motile cilia displayed the same range of motility dysfunction, most probably the cause of the kidney cysts. Analysis of the motility within the nasal placode was hampered due to the severe cell death of embryos at 72hpf, however the additional phenotypes of otolith defects and curled body axis suggested motile cilia were affected throughout the whole embryo.

The finding that Prpf8 protein localised in distinct clusters to the axoneme of motile cilia within the KV was somewhat surprising given that Prpf8 is thought to act as a nuclear localised protein (Grainger and Beggs, 2005). Consistent with my findings, previous work in the Hentges lab, as well as previously published work by other labs, had suggested PRPF8 may have a direct role in cilia function (Wheway et al., 2015; Buskin et al., 2018). Indeed PRPF8, along with other PRPF proteins, had been localised to the basal body and connecting cilium in photoreceptors as well as the axoneme in a range of other human cell types (Wheway et al., 2015; Buskin et al., 2018). Investigation into the localisation of Prpf8

within other motile ciliated structures in the fish model was hindered due to the IF protocol being specifically optimised for KV staining. Ongoing work, however, aims to fill in this knowledge gap by generating a zebrafish *prpf8*:*gfp* line and analysing Prpf8 localisation in motile ciliated structures as well as primary cilia.

In confirming that Prpf8 does indeed localise to motile cilia in the KV, I generated a translation blocking knockdown zebrafish model of Prpf8. This tbMO zebrafish exhibited heart looping defects as well as all of the additional hallmarks of cilia immotilty as the *cph* mutants, though these phenotypes appeared to be slightly more severe in tbMO embryos. Surprisingly, the tbMO embryos did not display the tail kink or CNS cell death phenotypes, suggesting these two characteristics may be a secondary effect of the *cph* mutation. Consistent with the *cph* phenotype and laterality defects observed, the tbMO embryos displayed ectopic and absent expression of laterality markers. Furthermore, these embryos also exhibited dysfunctional KV motile cilia redolent of the *cph* KV motile cilia phenotype, thus once again explaining the laterality defects. Notably, the expression pattern of *spaw* and *lefty2* did not correlate between *cph* and tbMO embryos though the possible reduction in tbMO *lefty1* midline expression compared to *cph* may contribute to this discrepancy.

The finding that tbMO embryos develop kidney cysts yet pronephric duct cilia appear to be fully motile is somewhat inconsistent with both the *cph* phenotype as well as published literature on cyst formation in embryos with motile cilia defects (Kramer-Zucker et al., 2005; Sullivan-Brown et al., 2008; Van Rooijen et al., 2008). One possible explanation is that the mechanosensing primary cilia within the pronephric duct are also affected by the lack of Prpf8 and thus are unable to sense the fluid flow produced, similar to that of *pkd2* mutants (Sullivan-Brown et al., 2008). This would raise the possibility that primary cilia in the crown cells of the KV are also affected, thus compounding the effect of the KV cilia dysmotility. This hypothesis may also explain the observed differences in laterality gene expression within *cph* and tbMO embryos. If the tbMO embryos had decreased function of both KV motile cilia, due to decreased length, but also decreased primary cilia function, the control of downstream gene expression may diverge from that of *cph.*

Conversely, to explain the formation of kidney cysts in the tbMO embryos which possess motile pronephric duct cilia, it is possible that these cilia are simply shorter than is needed for efficient fluid flow. Indeed, one previously characterised zebrafish mutant possessed significantly shorter pronephric and KV cilia, with motility being apparently unaffected, yet still developed kidney cysts and L/R axis issues (Zhao and Malicki, 2007; Leventea et al., 2016). Since significantly shorter motile cilia is a phenotype of tbMO node cilia, this explanation seems the most plausible, however, it does not explain why *cph* pronephric duct motile cilia exhibit motility dysfunction.

The observation that nasal placode cilia in tbMO embryos appear indistinguishable from WT adds another layer of complexity, though a number of explanations for this finding do exist. Firstly, it is possible that the translation blocking morpholino is sufficiently diluted

by 72hpf not to have an effect on cilia or, secondly, that cilia have recovered their functionality after having been affected at earlier stages. Thirdly, as cilia in multiciliated cells are regulated differently to mono cilia, it is possible Prpf8 plays no role in their function. As no other motile cilia possessing organs were investigated at 72hpf, it is impossible to say if either of these is the case. Alternatively, it is possible that the motile cilia defect seen in tbMO embryos does not affect multiciliated cells. This explanation is plausible as all other motile cilia defects have been observed in monociliated cells. To differentiate between these hypotheses, ideally, I would have compared to the motility of nasal placode cilia in tbMO and *cph* embryos but, due to the severe cell death in the in the head region of *cph* embryos at 72hpf, this comparison was impossible.

While investigating the original hypothesis that mutations in Prpf8 cause the mis-splicing of cilia specific genes, I, in conjunction with Wasay Mohiuddin Shaikh Qureshi, found that an alternate splice isoform of *arl13b* was increased in the PRPF8^{N1531S} mutant, the cph mutant as well as a prpf8 splice blocking knockdown zebrafish model. This increased alternate isoform was found to lack exon 9 of *arl13b* and was termed the “short” isoform. The protein encoded by the short isoform is predicted to lack a large portion of the Proline Rich region at the C-terminal or Arl13b. Work by Nozaki *et al., (*2017*)* demonstrated that the Proline Rich region of ARL13B was critical to facilitate binding of ARL13B to the IFT-B complex, specifically IFT46 and IFT56. Thus, with this finding I hypothesise that the increase in the short isoform of *arl13b* results in attenuated *arl13b* Ift46/56 interactions which causes downstream effects on motile cilia function due to the essential nature of these IFT proteins in the function and maintenance of cilia.

In strong support of this hypothesis, work by Lee et al., (2015) found that knockdown of *ift46* resulted in A-P body axis curvature, kidney cysts and pericardial oedema. Additionally Lee et al., (2015) show the length of motile cilia is significantly reduced in the pronephric duct, otic vesicle, and nasal placode, though they never analysed motility within these organs. Surprisingly, no defects in laterality were observed and investigations showed no decrease in cilia length of KV motile cilia, though the authors suggest this can be explained by the presence of *ift46* maternally contributed mRNA masking the expected phenotype. Indeed, Lee et al., (2015) also generated an *Ift46* mouse mutants which exhibited a high incidence of reversed looped and unlooped hearts, suggestive of laterality defects. Analysis of expression of *Lefty1*/2 confirmed the establishment of the L/R axis was disrupted. Further mirroring the mouse PRPF8^{N1531S} phenotype, *Ift46* mouse mutants also displayed developmental delay, failure of neural tube closure, neural tube kinks, and lethality at embryonic day 10.5.

Interestingly, upon analysis of the node via electron microscopy (EM), (Lee et al., 2015) state that the motile cilia within the *Ift46* mutants were completely absent. This finding is in contrast to the PRPF8^{N1531S} mutant which still possessed cilia in the node albeit immotile. This lack of motile cilia is in contrast to their zebrafish *ift46* knockdown model as

well as other published models of IFT46 mutation which showed motile cilia were present but shorter (Hou et al., 2007; Lee et al., 2015; Shi et al., 2018). However, it is important to note that with my proposed hypothesis, whereby short Arl13b lacks the necessary domain for interaction with Ift46, there is still a high proportion of functioning Arl13b present in the various Prpf8 mutant models I analysed that can carry out the necessary interactions for Ift46 functionality. This distinction would mean that some or all phenotypes observed in Prpf8 mutant models are not as severe as would be expected based on knockout of *Ift46*, thus explaining why *Ift46* knockout mice have no nodal cilia, whereas PRPF8^{N1531S} mice possess non-functioning nodal cilia.

Previous studies had suggested that IFT46 was responsible for the transport of dynein arms from the cytoplasm to the cilia, thus making the finding that PRPF8^{N1531S} mutants possessed dynein arms in the cilia hard to reconcile with IFT46 dysfunction (Hou et al., 2007). However, transmission EM data from the pronephric duct motile cilia of the *ift46* knockdown zebrafish found that they too still possessed dynein arms, suggesting Ift46 is not required for dynein arm transport and thus explaining the presence of dynein arms in the PRPF8^{N1531S} mutant. Possibly the most convincing evidence that Ift46 dysfunction plays a role in the *cph* phenotype is that over expression of *ift46* in zebrafish causes severe CNS cell death, viewed by acridine orange staining (Lee et al., 2015).

Previous work has shown that knockout of *IFT46* causes a significant increase in expression of all other *IFT* genes investigated, including both *IFT-B* and *IFT-A* genes, most likely as a compensatory mechanism (Hou et al., 2007; Taschner and Lorentzen, 2016). This would mean that in *cph* embryos, dysfunctional Ift46, caused by reduced interaction with Arl13b, is causing the increase of IFT gene expression thus resulting in the CNS cell death phenotype observed in Lee et al., (2015). Importantly, this phenotype may not be as attenuated as other *cph* phenotypes as no matter how much more *IFT* gene expression, including *ift46,* there is as a compensatory mechanism, the same proportion of Arl13b still cannot interact with Ift46 thus driving continued increased expression. This explanation fits with the observation that neural cell death still begins to occur at roughly the same stage and at the same intensity in both *cph* and *ift46* knockdown zebrafish embryos (Keightley et al., 2013; Lee et al., 2015).

As all-encompassing as this hypothesis may be to explain the mechanism behind the PRPF8^{N1531S} mouse mutant and the *cph* zebrafish mutant phenotypes, a number of things are left to be explained. Firstly, as I do not see the *arl13b* short isoform in my tbMO embryos, why do they still develop motile cilia defects? My current hypothesis is that at 48hpf, the stage when the RT-PCR for *arl13b* is carried out, the knockdown of *prpf8* is no longer sufficient to result in the mis-splicing of *arl13b.* However, at much earlier stages in tbMO embryos, this *arl13b* short isoform is increased and is causing the motile cilia defects within the KV, otic vesicle, pronephric duct and spinal cord thus resulting in the discussed phenotypes related to these structures. As development continues and the *prpf8*

knockdown becomes less severe, the percentage of WT *arl13b* increases resulting in possibly restored motility to the pronephric duct cilia as well as nasal placode cilia. Admittedly, this is purely speculation and would need further work to demonstrate.

Secondly, if the mis-splicing of *arl13b* is the causative mechanism behind the observed phenotypes, why are Prpf8 and other PRPFs found in the cilia? As previously discussed, it is possible that Prpf8 is involved in splicing of cilia related genes within the cilium itself. One of these genes may be *arl13b,* giving a possible reason for it to be mis-spliced rather than other, possibly nuclear spliced, cilia related genes. However, given that multiple snRNP complexes are required for canonical splicing, yet only U5 snRNPs have been found in cilia, this hypothesis currently seems farfetched. Alternatively, the cilium could be the location for U5 snRNP assembly pre transportation to the nucleus. This would explain why only U5 snRNPs are located in the cilium and, since the location for U5 snRNP assembly is currently unknown, seems a plausible explanation. However, accepting this hypothesis as to the reason for Prpf8 to localise to the cilia would mean the cilia related phenotypes observed in all Prpf8 mutant models described are independent of Prpf8 being localised to the cilium.

6.2 Final Discussion of *p1$^{-/-}$;p2$^{-/-}$* Phenotype

Within this project I have demonstrated that both Pierce1 and Pierce2 function redundantly in the motile cilia of zebrafish. Knockout of both genes results in mild A-P body axis curvature as well as heart looping defects. Interestingly, in generating the *p1$^{-/-}$;p2$^{-/-}$* double knockouts, I noticed that *p1$^{+/+}$;p2$^{-/-}$* and *p1$^{-/-}$;p2$^{+/+}$* embryos displayed mild characteristics of motile cilia defects even although previous characterising of these genotypes revealed no such defects. I proposed that, as the mother was heterozygous for each *pierce* gene, the presence of motile cilia dysfunction phenotypes in these embryos was most likely due to a reduction in functional maternal mRNA for each gene. This proposition is not without precedent, a previous study found that heterozygous mothers for *egfra* were infertile due to the death of fertilized eggs soon after conception. Investigations into this observation revealed that embryo survival depended on a full WT level of maternal *egfra* mRNA (Ciano et al., 2019).

Upon investigation into the laterality effects observed in *p1$^{-/-}$;p2$^{-/-}$* embryos I demonstrated that both *spaw* and *lefty2* were either absent or ectopically expressed. The expression patterns of both genes fit with the current understanding of the generation of the L/R axis (Burdine and Grimes, 2016; Hamada, 2020). For instance, as *spaw* induces *lefty2*, I only ever observe *lefty2* in the left or right LMP where weak *spaw* expression is also observed. As bilateral *spaw* never reaches the LPM it is unable to induce *lefty2*, thus accounting for the lack of bilateral *lefty2* staining. The reason for the weak *spaw* expression

is unknown but most likely relates to a probable lack of *dand5* degradation and so persistent inhibition of Spaw. This proposition is only speculation as *dand5* expression In *p1*$^{-/-}$;*p2*$^{-/-}$ embryos was never investigated. Although *dand5* expression was never analysed, the lack of *dand5* degradation on the left of the KV is entirely consistent with the observation that KV cilia were completely immotile and produced no anticlockwise fluid flow. This finding was especially surprising as morpholino knockdown of *pierce1* had suggested motility of the KV cilia was simply abnormal. As KV cilia motility was found to be completely absent, I hypothesised that Peirce1 and Pierce2 had some function in the assembly or transportation of the outer dynein arms to the cilia. In disagreement with this hypothesis, pronephric duct and nasal placode motile cilia in *p1*$^{-/-}$;*p2*$^{-/-}$ zebrafish appeared indistinguishable from WT. Confirmation that the knockout of Pierce1 and Pierce2 was the causative factor in the immotility of KV cilia, and that each functioned redundantly, was demonstrated by rescue of KV cilia motility by pierce1/2 RNA injection.

In collaboration with the Brown lab at Harvard Medical School we have shown that Pierce1 and Pierce2 function within the ciliary axoneme to link the dynein outer arm complex to the outer doublet microtube. With my zebrafish work on the *p1*$^{-/-}$;*p2*$^{-/-}$ mutant, along with collaborators, we demonstrated that these proteins are crucial in the transduction of the force produced by the outer dynein arm to the microtube axoneme of motile cilia. (Gui et al., 2021). The reason for the tissue specificity in zebrafish is still not clear but does not seem to be the case in mouse models of *PIERCE1* knockout as both KV and respiratory tract cilia exhibit motility defects (Gui et al., 2021).

6.3 Final Conclusion

Although there are still caveats to the proposition, currently the most parsimonious explanation for the findings relating to Prpf8 function is that mutation or reduction of *prpf8* causes the increased mis-splicing of *arl13b,* resulting in the attenuation of the Arl13b/Ift46 interaction thus causing the motile cilia dysfunction phenotypes observed. The function of Prpf8 within the cilium is still unknown, though I would argue the hypothesis that cilia are the location for U5 snRNP assembly is the most reasonable at this point in time.

In regards to pierce1/2 function, I have conclusively demonstrated that the function of both Pierce1 and Pierce2 relates to motile cilia of the KV and their loss causes complete loss of cilia motility. In conjunction with collaborators, we recently published this work in Cell, providing the full structure of both Pierce1 and Pierce2 and how these proteins function within the motile cilia.

The work discussed in this thesis broadens the knowledge of genes involved in motile cilia function and presents candidate genes for the future diagnosis of PCD and linked conditions.

6.4 Limitations

The work presented within this thesis possesses a number of limitations. Firstly, the extensive cell death within the developing *cph* embryos impedes forming any concrete conclusions in regards to Prpf8 function in motile ciliogenesis. Although the CNS cell death only begins to be visible under a brightfield microscope at 28hpf, Keightley et al., (2013) demonstrated that the increased cell death is apparent as early as 10-12hpf and is embryo wide. This increase in cell death means that I cannot determine if the observed cilia defects are truly caused by a truncated Prpf8 or whether the cilia immotility is a feature of the cell dying. The latter would explain the heterogeneity of cilia motility observed within an individual embryo as the cells within the KV and pronephric duct may be at different stages of the apoptotic process. This uncertainty has profound consequences as, if the cilia immotility phenotypes are caused by increased cell death, then the aberrant establishment of the L/R axis, and by extension, heart looping reversal could also be caused by the increased cell death. The same is true for the development of kidney cysts as well as the curl down A-P axis and defects in otolith formation. If this argument is to be believed though, one would have to account for why cell death seems to be preferentially affecting motile ciliated cell types. Indeed, preferential death of motile ciliated cells could be the case, but that leads back to the initial proposition that Prpf8 has functions related to motile ciliogenisis. The observation that tbMO embryos do not exhibit CNS cell death yet still display all the characteristics of motile cilia dysfunction seen in *cph* embryos suggests that the increase in cell death is not the cause of the *cph* cilia immotility, though whole embryo cell death was not investigated.

Secondly, as previously discussed, the use of morpholinos to elucidate gene function presents limitations in and of itself. Due to possible off-target effects, I cannot be certain that the phenotype produced by injection of the translation blocking *prpf8* morpholino is indeed the phenotype one would expect from reduction of Prpf8. Almost every possible precaution was taken to ensure the observed phenotype was accurate and representative of Prpf8 knockdown. These precautions include comparison to known a Prpf8 mutant (*cph)*, comparison to another morphant (sbMO) (Boylan, 2015) and ensuring knockdown efficiency by IF and Western Blot. Although these measures all inferred that the observed tbMO phenotype was due to Prpf8 knockdown, the critical rescue experiment of injecting *prpf8* RNA could not be performed due to the technical limitations of *in vitro* transcribing RNA of several thousand bases. Previous studies have demonstrated that knockdown of Prpf8 does result in cilia defects, suggesting that my observed knockdown phenotype is representative of reduction in Prpf8 (Wheway et al., 2015). However, Wheway et al., (2015) also found that knockdown of other Prpf proteins produced the same phenotype, opening up the possibility that my tbMO may produce the observed cilia immotility phenotypes via off target reduction of a different Prpf protein. Suggesting knockdown of another Prpf protein

is not the case, a BLAST alignment of the translation blocking morpholino sequence only identifies Prpf8 as having sequence similarity to the morpholino.

Thirdly, the Prpf8 antibody used for both IF and Western Blot was not specifically designed for use in zebrafish. According to the manufacturer (Abcam) the Prpf8 antibody used was only tested for compatibility with mouse and human PRPF8. This possible discrepancy in antibody targeting accuracy opens up the possibility that the Prpf8 IF is not actually detecting Prpf8. Additionally, as I had to highly modify the embryo fixation protocol for Prpf8 IF staining, this modification may have affected antibody specificity or produced artifacts in the confocal imaging that were not true representations of Prpf8 localisation. A Western Blot was performed to assess anti-Prpf8 specificity but, as previously discussed, although the Western suggested that anti-Prpf8 detected Prpf8, the band size discrepancy may also be explained by non-specific anti-Prpf8 binding. However, previous work had also demonstrated PRPF8 localisation in the cilium suggesting that my IF results were indeed true representations of Prpf8 localisation (Wheway et al., 2015; Buskin et al., 2018).

These three limitations discussed produce a chain in which the accuracy of one element is reliant on the accuracy of another element. For instance, concluding that the defective motile cilia phenotype is not caused by cell death in *cph* embryos is dependent upon the tbMO knockdown being an accurate representation of Prpf8 knockdown. Furthermore, the Prpf8 knockdown accuracy and efficiency is somewhat dependant on the Prpf8 antibody accuracy, while at the same time the Prpf8 antibody specificity has been somewhat demonstrated through use of the tbMO embryos. Care has been taken to use independent confirmation, such as comparison to other knockdown and mutant models, use of western blot to confirm Prpf8 knockdown, as well as referring to previously published data to increase the reliability of the results herein discussed.

Fourthly, as the *cph* mutation is not equivalent to the mouse PRPF8^{N1531S} mutation, comparisons between the two mutant models may not be justified. Recapitulating the equivalent PRPF8^{N1531S} mouse mutation in zebrafish was attempted through knock-in but was abandoned due to low success rates as well as time constraints. Additionally, due to the presence of maternal mRNA in *cph* embryos, the true null *prpf8* phenotype is masked early in development. This masking would explain why the mouse phenotype appears to be more severe than the *cph* phenotype, with complete loss of cilia motility as well as defects in HH signalling not seen in *cph* embryos. As zygotic *cph* embryos were not viable, it was not possible to produce mz *cph* embryos that may have exhibited a stronger ciliary defect phenotype.

Furthermore, the nature of using animal models to study gene function applicable to human disease throws up its own limitations. Indeed, the reason for the discrepancy between the phenotypes in mouse and zebrafish models of *Prpf8* mutation may solely be

due to the divergence of Prpf8 function through evolutionary time. Although Prpf8 is one of the most highly conserved proteins, conservation in Prpf8 interacting proteins may not be so high thus leading to slight divergence in functionality and observed phenotypes. This divergence in functionality may also extend to humans. Indeed, as of yet no patients have been identified with PRPF8 mutations resulting in *situs* defects*,* though it is important to note that mutations in regions of PRPF8 critical for function may be embryonic lethal. This hypothesis would explain why PRPF8 RP related mutations which are present in humans are so densely clustered together in a single domain.

Possible divergence in gene function between zebrafish, mice and humans is also a limitation of my Pierce1/Pierce2 work. Indeed, we have already demonstrated that there are functional and tissue specific differences in Pierce1 between zebrafish and mouse (Gui et al., 2021). It is possible that the role for Pierce1/Pierce2 as well as Prpf8 in motile cilia has diverged in humans and that my data is not applicable to diagnosis of PCD.

6.5 Future Directions

6.5.1 Linking *arl13b* Short Isoform to *cph* Phenotype

In regards to the Prpf8 project, the majority of the future work will be aimed at confirming whether the increased expression of the short *alr13b* isoform is the reason for the observed cilia defects seen in PRPF8^{N1531S}, *cph,* sbMO, and possibly tbMO. This will be achieved in a number of ways. Firstly, as the short *arl13b* isoform exists naturally in mouse and zebrafish, I hypothesise that it is the relative ratios of long to short *arl13b* isoform that is important in motile cilia function. This hypothesis would mean that overexpression of long *arl13b* in *cph* embryos may rescue the phenotype. To confirm this hypothesis, future work could include cloning full length *arl13b* into a construct suitable for *in vitro* transcription and injecting the long *arl13b* isoform RNA into *cph* embryos. High enough concentrations would be needed so that the *cph* phenotype may be rescued, but low enough concentrations that additional cilia related phenotypes do not manifest. Previous studies on *arl13b* overexpression seem to indicate this concentration will be between 50-300pg/nl (Lu et al., 2015; Pintado et al., 2017). In compliment to this long *arl13b* overexpression, future experiments may include overexpression of the short *arl13b* isoform in WT zebrafish to induce possible motile cilia defects redolent of *cph* and *prpf8* morphant phenotypes. The same technique of cloning of this specific isoform paired with *in vit*ro transcription and injection could be used. Once again careful concentration control may be necessary as to avoid inducing ciliary defects purely due to the over overexpression of *arl13b*.

6.5.2 Arl13b Immunofluorescence and IFT Co-localisation

During these overexpression experiments, it may also be interesting to investigate whether ciliary length in the KV is rescued by long and short *arl13b* isoform overexpression. The outcome of this investigation may demonstrate that the short *arl13b* isoform is the cause of both decreased cilium length and motile cilia defects, as well as provide insights into the mechanism by which *arl13b* regulates ciliary length. Indeed, it is possible that over expression of short *arl13b* does not rescue cilia length due to the abrogated proline rich region no longer interacting with the IFT-B complex. This investigation would involve performing an IF using anti-Acetylated tubulin to mark the axoneme as well as anti-Arl13b to mark the ciliary membrane. It may also be constructive to differentiate between endogenous and exogenous Arl13b and investigate any differences in localisation of the two isoforms. This can be achieved by the addition of a FLAG or MYC epitope tag to the cloned *arl13b* isoforms pre *in vitro* transcription. This experiment would also allow for co-localisation between both Arl13b isoforms and specific IFT-B proteins, namely Ift46. Differences in co-localisation between long and short Arl13b with Ift46 would provide strong evidence that the loss of the Arl13b:Ift46 interaction is the causative mechanism behind the

observed ciliary defects. Elucidating the exact reason for the cilia immotility would be challenging, however further investigation into dynein arm localisation or microtubule structure via IF or TEM of KV motile cilia may provide insights.

6.5.3 Further Investigating Prpf8 Localisation

The finding that Prpf8 localises to the cilia axoneme but that this localisation is not necessarily involved in the proposed mechanism behind the *cph* phenotype is an interesting avenue for future work. As mentioned, further confirmation that the observed Prpf8 IF localisation is accurate is needed. I have identified a putative ciliary localisation signal at the far N-terminal region of Prpf8, consistent with the finding that the *cph* truncated protein isoform of Prpf8 still localises to cilia. Future work aims to generate a tagged version of the *cph* Prpf8 truncation with this ciliary localisation signal mutated. An IF can then be performed using anti-Prpf8 and anti-FLAG or anti-Myc, depending on the tag used, and ciliary localisation for each Prpf8 construct analysed. If the Prpf8 construct containing the mutated ciliary localisation signal is excluded from the cilia then this provides convincing evidence that the staining I observed in my initial investigation was indeed correct. However, it is possible that the putative ciliary localisation signal is not actually a ciliary signal and that this experiment will not be useful. A much more conclusive analysis of Prpf8 localisation is currently underway in the Roy lab where we aim to generate a stable transgenic Prpf8:Gfp line via insertion of a bacterial artificial chromosome containing the *prpf8:gfp* construct. If successful, this experiment should elucidate all locations of Prpf8 and provide insights into the possible localisation of Prpf8 in primary cilia as well as the motile cilia in other ciliated structures.

6.5.4 PRPF proteins in relation to RP

Because preliminary data shared by collaborators working on *PRPF31* RP patient derived RPE cells suggested that *ARL13B* function may be negatively affected, future work should aim to determine if *ARL13B* expression is also affected in these patients as in our Prpf8 zebrafish and mouse models. This can be achieved through cDNA preparation of RP patient derived RPE cells followed by RT-PCR for either whole *ARL13B* or the exon8-10 region. Notably, as the short *ARL13B* isoform does not exist in WT RPE cells, any observed mis-splicing may be clinically relevant to RP development. Additionally, future work may involve bioinformatic analysis of available RNAseq datasets from RP patient IPSCs derived RPE cells to determine if other splicing factor related RP models exhibit aberrant splicing of *ARL13B*. Furthermore, due to the dominant nature of PRPF8 RP mutations, and the fact I see a decrease in eye size in my zebrafish Prpf8 models redolent of an RP phenotype,

measurements of heterozygous *cph* zebrafish may provide further links between our Prpf8 mutant models, cilia, and RP.

6.5.5 Investigating Pierce1/Pierce2 Tissue Specific Functions

Although the function of Pierce1 and Pierce2 in motile cilia has now been determined, future work may seek to understand why there is a tissue specific function for these proteins in zebrafish. As IFs for Pierce1 do not work, most likely as Pierce1 is sequestered within the cilium preventing antibody binding, we are limited in the experimental approaches we can utilise. Further cryo-EM could be performed on the nasal placode cilia to determine if Pierce1 and Pierce2 are present and still functioning to link the dynein arms to the microtubule. This method would be both technically challenging and require a prohibitively high number of zebrafish to generate the required cilia numbers. Alternatively, if we inject Pierce1/Pierce2 tagged with either MYC or FLAG and then dissect out the nasal placode or pronephric duct and perform a western we, may be able to determine if Pierce1 and Pierce2 are present in these cilia. Once again, this may require a prohibitively high number of zebrafish to generate the protein quantities needed for a Western. Overall, it seems there is currently no effective way to investigate the tissue specific nature of Pierce1/Pierce2 and, since mouse models do not exhibit this tissue specific phenotype, one might argue there is not much benefit to this avenue of investigation.

7. Epilogue

Within this thesis I have presented data which contributes new information to the field of motile cilia biogenesis and as well as the relationship between motile cilia and human disease. Through my work investigating Prpf8 I have uncovered a new mechanism which may explain PRPF8 related Retinitis Pigmentosa as well as provided data and hypotheses explaining the role of Prpf8 in the cilia and left/right axis formation. Additionally, through my Pierce1/Pierce2 work I identified the function of these two proteins within motile cilia and advanced the understanding of motile cilia function and structure. Together with collaborators, we published this data in Cell allowing for my work to have a direct impact on future PCD patient diagnosis.

References

Aamar, E. and Dawid, I. B. (2008) 'Isolation and expression analysis of foxj1 and foxj1.2 in zebrafish embryos.' *The International journal of developmental biology*. NIH Public Access, 52(7) p. 985.

Ang, S. L. and Rossant, J. (1994) 'HNF-3 beta is essential for node and notochord formation in mouse development.' *Cell*. Cell, 78(4) pp. 561–574.

Anujan, P. (2018) 'Functional analysis of novel protein , PIERCE1 , in motile ciliogenesis,' (September).

Anvarian, Z., Mykytyn, K., Mukhopadhyay, S., Pedersen, L. B. and Christensen, S. T. (2019) 'Cellular signalling by primary cilia in development, organ function and disease.' *Nature Reviews Nephrology 2019 15:4*. Nature Publishing Group, 15(4) pp. 199–219.

Arnold, C. R., Lamont, R. E., Walker, J. T., Spice, P. J., Chan, C.-K., Ho, C.-Y. and Childs, S. J. (2015) 'Comparative analysis of genes regulated by Dzip1/ *iguana* and hedgehog in zebrafish.' *Developmental Dynamics*, 244(2) pp. 211–223.

Arnold, C. R., Lamont, R. E., Walker, J. T., Spice, P. J., Chan, C. K., Ho, C. Y. and Childs, S. J. (2015) 'Comparative analysis of genes regulated by Dzip1/iguana and hedgehog in zebrafish.' *Developmental Dynamics*. John Wiley & Sons, Ltd, 244(2) pp. 211–223.

Avidor-Reiss, T., Maer, A. M., Koundakjian, E., Polyanovsky, A., Keil, T., Subramaniam, S. and Zuker, C. S. (2004) 'Decoding Cilia Function: Defining Specialized Genes Required for Compartmentalized Cilia Biogenesis.' *Cell*. Cell Press, 117(4) pp. 527–539.

Baker, K., Holtzman, N. G. and Burdine, R. D. (2008) 'Direct and indirect roles for Nodal signaling in two axis conversions during asymmetric morphogenesis of the zebrafish heart.' *Proceedings of the National Academy of Sciences*. National Academy of Sciences, 105(37) pp. 13924–13929.

Bakkers, J., Verhoeven, M. C. and Abdelilah-Seyfried, S. (2009) 'Shaping the zebrafish heart: From left–right axis specification to epithelial tissue morphogenesis.' *Developmental Biology*. Academic Press, 330(2) pp. 213–220.

Bangs, F. and Anderson, K. V. (2017) 'Primary Cilia and Mammalian Hedgehog Signaling.' *Cold Spring Harbor Perspectives in Biology*. Cold Spring Harbor Laboratory Press, 9(5).

Bassett, A. R., Tibbit, C., Ponting, C. P. and Liu, J. L. (2013) 'Highly Efficient Targeted Mutagenesis of Drosophila with the CRISPR/Cas9 System.' *Cell Reports*. Elsevier, 4(1) p. 220.

Bayless, B. A., Navarro, F. M. and Winey, M. (2019) 'Motile Cilia: Innovation and Insight From Ciliate Model Organisms.' *Frontiers in Cell and Developmental Biology*. Frontiers Media S.A., 7, November, p. 265.

Beales, P. L., Bland, E., Tobin, J. L., Bacchelli, C., Tuysuz, B., Hill, J., Rix, S., Pearson, C. G., Kai, M., Hartley, J., Johnson, C., Irving, M., Elcioglu, N., Winey, M., Tada, M. and Scambler, P. J. (2007) 'IFT80, which encodes a conserved intraflagellar transport protein, is mutated in Jeune asphyxiating thoracic dystrophy.' *Nature Genetics 2007 39:6*. Nature Publishing Group, 39(6) pp. 727–729.

Becker-Heck, A., Zohn, I. E., Okabe, N., Pollock, A., Lenhart, K. B., Sullivan-Brown, J., McSheene, J., Loges, N. T., Olbrich, H., Haeffner, K., Fliegauf, M., Horvath, J., Reinhardt, R., Nielsen, K. G., Marthin, J. K., Baktai, G., Anderson, K. V., Geisler, R., Niswander, L., Omran, H. and Burdine, R. D. (2010) 'The coiled-coil domain containing protein CCDC40 is essential for motile cilia function and left-right axis formation.' *Nature Genetics 2010 43:1*. Nature Publishing Group, 43(1) pp. 79–84.

Bellomo, D., Lander, A., Harragan, I. and Brown, N. A. (1996) 'Cell Proliferation in Mammalian Gastrulation: The Ventral Node and Notochord Are Relatively Quiescent.' *DEVELOPMENTAL DYNAMICS*, 205471485.

Bergwerff, M., Gittenberger-de Groot, A. C., Wisse, L. J., DeRuiter, M. C., Wessels, A., Martin, J. F., Olson, E. N. and Kern, M. J. (2000) 'Loss of function of the Prx1 and Prx2 homeobox genes alters architecture of the great elastic arteries and ductus arteriosus.' *Virchows Archiv : an international journal of pathology*. Virchows Arch, 436(1) pp. 12–19.

Bill, B. R., Petzold, A. M., Clark, K. J., Schimmenti, L. A. and Ekker, S. C. (2009) 'A Primer for Morpholino Use in Zebrafish.' *Zebrafish*. Mary Ann Liebert, Inc., 6(1) p. 69.

Birol, M. and Echalier, A. (2014) 'Structure and function of MPN (Mpr1/Pad1 N-terminal) domain-containing proteins.' *Current protein & peptide science*. Curr Protein Pept Sci, 15(5) pp. 504–517.

Blacque, O. E., Li, C., Inglis, P. N., Esmail, M. A., Ou, G., Mah, A. K., Baillie, D. L., Scholey, J. M. and Leroux, M. R. (2006) 'The WD repeat-containing protein IFTA-1 is required for retrograde intraflagellar transport.' *Molecular biology of the cell*. Mol Biol Cell, 17(12) pp. 5053–5062.

Blum, M. and Ott, T. (2018) 'Animal left–right asymmetry.' *Current Biology*. Elsevier, 28(7) pp. R301–R304.

Boon, K.-L., Grainger, R. J., Ehsani, P., Barrass, J. D., Auchynnikava, T., Inglehearn, C. F. and Beggs, J. D. (2007) 'prp8 mutations that cause human retinitis pigmentosa lead to a U5 snRNP maturation defect in yeast.' *Nature Structural & Molecular Biology*, 14(11) pp. 1077–1083.

Boon, K. L., Norman, C. M., Grainger, R. J., Newman, A. J. and Beggs, J. D. (2006) 'Prp8p dissection reveals domain structure and protein interaction sites.' *RNA*. Cold Spring Harbor Laboratory Press, 12(2) pp. 198–205.

Bowers, P. N., Brueckner, M. and Yost, H. J. (1996) 'The genetics of left-right development and heterotaxia.' *Seminars in Perinatology*. W.B. Saunders, 20(6) pp. 577–588.

Boylan, M. (2015) *A Novel Point Mutation in Prpf8 Causes Defects in Left-Right Axis Establishment in the Mouse | Research Explorer | The University of Manchester*. University of Manchester.

Brody, S. L., Yan, X. H., Wuerffel, M. K., Song, S. K. and Shapiro, S. D. (2000) 'Ciliogenesis and left-right axis defects in forkhead factor HFH-4-null mice.' *American journal of respiratory cell and molecular biology*. Am J Respir Cell Mol Biol, 23(1) pp. 45–51.

Broekhuis, J. R., Leong, W. Y. and Jansen, G. (2013) 'Regulation of Cilium Length and Intraflagellar Transport.' *International Review of Cell and Molecular Biology*. Academic Press, 303, January, pp. 101–138.

Brooks, E. R. and Wallingford, J. B. (2014) ‘Multiciliated cells: a review.’ *Current biology : CB*. NIH Public Access, 24(19) p. R973.

Brown, J. D. and Beggs, J. D. (1992) ‘Roles of PRP8 protein in the assembly of splicing complexes.’ *The EMBO Journal*. European Molecular Biology Organization, 11(10) p. 3721.

Bujakowska, K. M., Liu, Q. and Pierce, E. A. (2017) ‘Photoreceptor Cilia and Retinal Ciliopathies.’ *Cold Spring Harbor perspectives in biology*, 9(10) p. a028274.

Bujakowska, K. M., Zhang, Q., Siemiatkowska, A. M., Liu, Q., Place, E., Falk, M. J., Consugar, M., Lancelot, M. E., Antonio, A., Lonjou, C., Carpentier, W., Mohand-Saïd, S., den Hollander, A. I., Cremers, F. P. M., Leroy, B. P., Gai, X., Sahel, J. A., van den Born, L. I., Collin, R. W. J., Zeitz, C., Audo, I. and Pierce, E. A. (2015) ‘Mutations in IFT172 cause isolated retinal degeneration and Bardet-Biedl syndrome.’ *Human molecular genetics*. Hum Mol Genet, 24(1) pp. 230–242.

Burdine, R. D. and Grimes, D. T. (2016) ‘Antagonistic interactions in the zebrafish midline prior to the emergence of asymmetric gene expression are important for left–right patterning.’ *Philosophical Transactions of the Royal Society B: Biological Sciences*. The Royal Society, 371(1710).

Burdine, R. D. and Schier, A. F. (2000) ‘Conserved and divergent mechanisms in left–right axis formation.’ *Genes & Development*. Cold Spring Harbor Laboratory Press, 14(7) pp. 763–776.

Buskin, A., Zhu, L., Chichagova, V., Basu, B., Mozaffari-Jovin, S., Dolan, D., Droop, A., Collin, J., Bronstein, R., Mehrotra, S., Farkas, M., Hilgen, G., White, K., Pan, K.-T., Treumann, A., Hallam, D., Bialas, K., Chung, G., Mellough, C., Ding, Y., Krasnogor, N., Przyborski, S., Zwolinski, S., Al-Aama, J., Alharthi, S., Xu, Y., Wheway, G., Szymanska, K., McKibbin, M., Inglehearn, C. F., Elliott, D. J., Lindsay, S., Ali, R. R., Steel, D. H., Armstrong, L., Sernagor, E., Urlaub, H., Pierce, E., Lührmann, R., Grellscheid, S.-N., Johnson, C. A. and Lako, M. (2018) ‘Disrupted alternative splicing for genes implicated in splicing and ciliogenesis causes PRPF31 retinitis pigmentosa.’ *Nature Communications*. Nature Publishing Group, 9(1) p. 4234.

Caspary, T., Larkins, C. E. and Anderson, K. V. (2007) ‘The Graded Response to Sonic Hedgehog Depends on Cilia Architecture.’ *Developmental Cell*. Elsevier, 12(5) pp. 767–778.

Cevik, S., Hori, Y., Kaplan, O. I., Kida, K., Toivenon, T., Foley-Fisher, C., Cottell, D., Katada, T., Kontani, K. and Blacque, O. E. (2010) ‘Joubert syndrome Arl13b functions at ciliary membranes and stabilizes protein transport in Caenorhabditis elegans.’ *The Journal of Cell Biology*. The Rockefeller University Press, 188(6) p. 953.

Chen, J., Knowles, H. J., Hebert, J. L. and Hackett, B. P. (1998) ‘Mutation of the mouse hepatocyte nuclear factor/forkhead homologue 4 gene results in an absence of cilia and random left-right asymmetry.’ *Journal of Clinical Investigation*. American Society for Clinical Investigation, 102(6) p. 1077.

Chen, Xue, Liu, Yuan, Sheng, X., Tam, P. O. S., Zhao, K., Chen, Xuejuan, Rong, W., Liu, Yani, Liu, X., Pan, X., Chen, L. J., Zhao, Q., Vollrath, D., Pang, C. P. and Zhao, C. (2014) ‘PRPF4 mutations cause autosomal dominant retinitis pigmentosa.’ *Human Molecular Genetics*, 23(11) pp. 2926–2939.

Chen, Y., Xiao, D., Zhang, L., Cai, C. L., Li, B. Y. and Liu, Y. (2021) 'The Role of Tbx20 in Cardiovascular Development and Function.' *Frontiers in Cell and Developmental Biology*. Frontiers Media S.A., 9, January, p. 69.

Choi, Y., Sims, G. E., Murphy, S., Miller, J. R. and Chan, A. P. (2012) 'Predicting the functional effect of amino acid substitutions and indels.' *PloS one*. PLoS One, 7(10).

Choksi, S. P., Babu, D., Lau, D., Yu, X. and Roy, S. (2014) 'Systematic discovery of novel ciliary genes through functional genomics in the zebrafish.' *Development (Cambridge)*. Company of Biologists Ltd, 141(17) pp. 3410–3419.

Ciano, M., Kemp, P. R., Sathyapala, S. A. and Hughes, S. M. (2019) 'Haploinsufficient maternal effect of Epidermal Growth Factor Receptor A mutation in zebrafish.' *bioRxiv*. Cold Spring Harbor Laboratory, August, p. 745018.

ClustalW2 < Multiple Sequence Alignment < EMBL-EBI (n.d.). [Online] [Accessed on 12th January 2022] https://www.ebi.ac.uk/Tools/msa/clustalw2/.

Coffman, J. A., Dickey-Sims, C., Haug, J. S., McCarthy, J. J. and Robertson, A. A. (2004) 'Evaluation of developmental phenotypes produced by morpholino antisense targeting of a sea urchin Runx gene.' *BMC Biology*. BioMed Central, 2(1) pp. 1–9.

Collignon, J., Varlet, I. and Robertson, E. J. (1996) 'Relationship between asymmetric nodal expression and the direction of embryonic turning.' *Nature*. Nature, 381(6578) pp. 155–158.

Comitato, A., Spampanato, C., Chakarova, C., Sanges, D., Bhattacharya, S. S. and Marigo, V. (2007) 'Mutations in splicing factor PRPF3, causing retinal degeneration, form detrimental aggregates in photoreceptor cells.' *Human Molecular Genetics*, 16(14) pp. 1699–1707.

Corbit, K. C., Aanstad, P., Singla, V., Norman, A. R., Stainier, D. Y. R. and Reiter, J. F. (2005) 'Vertebrate Smoothened functions at the primary cilium.' *Nature 2005 437:7061*. Nature Publishing Group, 437(7061) pp. 1018–1021.

Cruz, C., Ribes, V., Kutejova, E., Cayuso, J., Lawson, V., Norris, D., Stevens, J., Davey, M., Blight, K., Bangs, F., Mynett, A., Hirst, E., Chung, R., Balaskas, N., Brody, S. L., Marti, E. and Briscoe, J. (2010) 'Foxj1 regulates floor plate cilia architecture and modifies the response of cells to sonic hedgehog signalling.' *Development*. The Company of Biologists, 137(24) pp. 4271–4282.

Daiger, S. P. (2021) *RetNet: Summaries of Genes and Loci Causing Retinal Diseases*. The University of Texas Health Science Center. [Online] [Accessed on 24th January 2021] https://sph.uth.edu/retnet/sum-dis.htm#B-diseases.

Davidson, B. P., Kinder, S. J., Steiner, K., Schoenwolf, G. C. and Tam, P. P. L. (1999) 'Impact of node ablation on the morphogenesis of the body axis and the lateral asymmetry of the mouse embryo during early organogenesis.' *Developmental biology*. Dev Biol, 211(1) pp. 11–26.

Delling, M., Indzhykulian, A. A., Liu, X., Li, Y., Xie, T., Corey, D. P. and Clapham, D. E. (2016) 'Primary cilia are not calcium-responsive mechanosensors.' *Nature*. Nature Publishing Group, 531(7596) pp. 656–660.

Desgrange, A., Garrec, J. F. Le and Meilhac, S. M. (2018) 'Left-right asymmetry in heart development and disease: Forming the right loop.' *Development (Cambridge)*. Company of Biologists Ltd, 145(22).

Dooley, K. and Zon, L. I. (2000) 'Zebrafish: a model system for the study of human disease.' *Current opinion in genetics & development*. Curr Opin Genet Dev, 10(3) pp. 252–256.

Draper, B. W., Morcos, P. A. and Kimmel, C. B. (2001) 'Inhibition of zebrafish fgf8 pre-mRNA splicing with morpholino oligos: a quantifiable method for gene knockdown.' *Genesis (New York, N.Y. : 2000)*. Genesis, 30(3) pp. 154–156.

Drummond, I. (2009) 'Studying Cilia in Zebrafish.' *Methods in cell biology*. Academic Press, 93, January, pp. 197–217.

Drummond, I. and Austin-Tse, C. (2013) 'Zebrafish cilia.' *In Methods in Enzymology*. Academic Press Inc., pp. 219–244.

Duldulao, N. A., Lee, S. and Sun, Z. (2009) 'Cilia localization is essential for in vivo functions of the Joubert syndrome protein Arl13b/Scorpion.' *Development (Cambridge, England)*. Development, 136(23) pp. 4033–4042.

Dutta, S., Sriskanda, S., Boobalan, E., Alur, R. P., Elkahloun, A. and Brooks, B. P. (2015) 'nlz1 is required for cilia formation in zebrafish embryogenesis.' *Developmental Biology*. Academic Press, 406(2) pp. 203–211.

Eisen, J. S. and Smith, J. C. (2008) 'Controlling morpholino experiments: don't stop making antisense.' *Development*. The Company of Biologists, 135(10) pp. 1735–1743.

Engel, B. D., Ludington, W. B. and Marshall, W. F. (2009) 'Intraflagellar transport particle size scales inversely with flagellar length: Revisiting the balance-point length control model.' *Journal of Cell Biology*. The Rockefeller University Press, 187(1) pp. 81–89.

Escher, P., Passarin, O., Munier, F. L., Tran, V. H. and Vaclavik, V. (2018) 'Variability in clinical phenotypes of PRPF8 -linked autosomal dominant retinitis pigmentosa correlates with differential PRPF8/SNRNP200 interactions.' *Ophthalmic Genetics*, 39(1) pp. 80–86.

Essner, J. J., Amack, J. D., Nyholm, M. K., Harris, E. B. and Yost, H. J. (2005) 'Kupffer's vesicle is a ciliated organ of asymmetry in the zebrafish embryo that initiates left-right development of the brain, heart and gut.' *Development*. The Company of Biologists, 132(6) pp. 1247–1260.

Fahim, A. T., Daiger, S. P. and Weleber, R. G. (2017) *Nonsyndromic Retinitis Pigmentosa Overview*. GeneReviews®. [Online] http://www.ncbi.nlm.nih.gov/pubmed/20301590.

Finnerty, J. R. (2005) 'Did internal transport, rather than directed locomotion, favor the evolution of bilateral symmetry in animals?' *BioEssays* pp. 1174–1180.

Fliegauf, M., Benzing, T. and Omran, H. (2007) 'When cilia go bad: cilia defects and ciliopathies.' *Nature reviews. Molecular cell biology*. Nat Rev Mol Cell Biol, 8(11) pp. 880–893.

Galej, W. P., Oubridge, C., Newman, A. J. and Nagai, K. (2013) 'Crystal structure of Prp8 reveals active site cavity of the spliceosome.' *Nature*. Nature, 493(7434) pp. 638–643.

Gamundi, M. J., Hernan, I., Muntanyola, M., Maseras, M., López-Romero, P., Álvarez, R., Dopazo, A., Borrego, S. and Carballo, M. (2008) 'Transcriptional expression of cis -acting and trans -acting splicing mutations cause autosomal dominant retinitis pigmentosa.' *Human Mutation*, 29(6) pp. 869–878.

Gao, F. J., Li, J. K., Chen, H., Hu, F. Y., Zhang, S. H., Qi, Y. H., Xu, P., Wang, D. D., Wang, L. S., Chang, Q., Zhang, Y. J., Liu, W., Li, W., Wang, M., Chen, F., Xu, G. Z. and Wu, J. H. (2019) 'Genetic and Clinical Findings in a Large Cohort of Chinese Patients with Suspected Retinitis Pigmentosa.' *Ophthalmology*. Elsevier Inc., 126(11) pp. 1549–1556.

Gee, H. (1998) 'The sources of symmetry.' *Nature*. Springer Science and Business Media LLC, August.

Gehrig, J., Pandey, G. and Westhoff, J. H. (2018) 'Zebrafish as a model for drug screening in genetic kidney diseases.' *Frontiers in Pediatrics*. Frontiers Media S.A., 6 p. 183.

Geremek, M., Bruinenberg, M., Ziętkiewicz, E., Pogorzelski, A., Witt, M. and Wijmenga, C. (2011) 'Gene expression studies in cells from primary ciliary dyskinesia patients identify 208 potential ciliary genes.' *Human genetics*. Hum Genet, 129(3) pp. 283–293.

Geremek, M., Ziętkiewicz, E., Bruinenberg, M., Franke, L., Pogorzelski, A., Wijmenga, C. and Witt, M. (2014) 'Ciliary Genes Are Down-Regulated in Bronchial Tissue of Primary Ciliary Dyskinesia Patients.' *PLoS ONE*. Public Library of Science, 9(2).

Gigante, E. D., Taylor, M. R., Ivanova, A. A., Kahn, R. A. and Caspary, T. (2020) 'Arl13b regulates sonic hedgehog signaling from outside primary cilia.' *eLife*. eLife Sciences Publications Ltd, 9, March.

Glazer, A. M., Wilkinson, A. W., Backer, C. B., Lapan, S. W., Gutzman, J. H., Cheeseman, I. M. and Reddien, P. W. (2010) 'The Zn Finger protein Iguana impacts Hedgehog signaling by promoting ciliogenesis.' *Developmental Biology*. Academic Press, 337(1) pp. 148–156.

Glicman Holtzman, N., Schoenebeck, J. J., Tsai, H. J. and Yelon, D. (2007) 'Endocardium is necessary for cardiomyocyte movement during heart tube assembly.' *Development*. The Company of Biologists, 134(12) pp. 2379–2386.

Gokey, J. J., Ji, Y., Tay, H. G., Litts, B. and Amack, J. D. (2016) 'A Kupffer's vesicle size threshold for robust left-right patterning of the zebrafish embryo.' *Developmental dynamics : an official publication of the American Association of Anatomists*. NIH Public Access, 245(1) p. 22.

Gotthardt, K., Lokaj, M., Koerner, C., Falk, N., Gießl, A. and Wittinghofer, A. (2015) 'A G-protein activation cascade from Arl13B to Arl3 and implications for ciliary targeting of lipidated proteins.' *eLife*. eLife Sciences Publications Ltd, 4(NOVEMBER2015).

Grainger, R. J. and Beggs, J. D. (2005) 'Prp8 protein: At the heart of the spliceosome.' *RNA*. RNA, 11(5) pp. 533–557.

Grant, M. G., Patterson, V. L., Grimes, D. T. and Burdine, R. D. (2017) 'Modeling Syndromic Congenital Heart Defects in Zebrafish.' *Current Topics in Developmental Biology*. Academic Press, 124, January, pp. 1–40.

Graziotto, J. J., Farkas, M. H., Bujakowska, K., Deramaudt, B. M., Zhang, Q., Nandrot, E. F., Inglehearn, C. F., Bhattacharya, S. S. and Pierce, E. A. (2011) 'Three gene-targeted mouse models of RNA splicing factor RP show late-onset RPE and retinal degeneration.' *Investigative Ophthalmology and Visual Science*, 52(1) pp. 190–198.

Grimes, D. T., Patterson, V. L., Luna-Arvizu, G., Schottenfeld-Roames, J., Irons, Z. H. and Burdine, R. D. (2020) 'Left-right asymmetric heart jogging increases the robustness of dextral heart looping in zebrafish.' *Developmental Biology*. Academic Press, 459(2) pp. 79–86.

De Groh, E. D., Swanhart, L. M., Cosentino, C. C., Jackson, R. L., Dai, W., Kitchens, C. A., Day, B. W., Smithgall, T. E. and Hukriede, N. A. (2010) 'Inhibition of Histone Deacetylase Expands the Renal Progenitor Cell Population.' *Journal of the American Society of Nephrology*. American Society of Nephrology, 21(5) pp. 794–802.

Gui, M., Farley, H., Anujan, P., Anderson, J. R., Maxwell, D. W., Whitchurch, J. B., Botsch, J. J., Qiu, T., Meleppattu, S., Singh, S. K., Zhang, Q., Thompson, J., Lucas, J. S., Bingle, C. D., Norris, D. P., Roy, S. and Brown, A. (2021) 'De novo identification of mammalian ciliary motility proteins using cryo-EM.' *Cell*. Elsevier, 184(23) pp. 5791-5806.e19.

Hamada, H. (2016) 'Roles of Motile and Immotile Cilia in Left-Right Symmetry Breaking.' *Etiology and Morphogenesis of Congenital Heart Disease: From Gene Function and Cellular Interaction to Morphology*. Springer Japan, January, pp. 57–65.

Hamada, H. (2020) 'Molecular and cellular basis of left-right asymmetry in vertebrates.' *Proceedings of the Japan Academy Series B: Physical and Biological Sciences*. The Japan Academy pp. 273–296.

Hamada, H. and Tam, P. P. L. (2014) 'Mechanisms of left-right asymmetry and patterning: Driver, mediator and responder.' *F1000Prime Reports*. Faculty of 1000 Ltd, 6, December.

Hao, K., Chen, Y., Yan, X. and Zhu, X. (2021) 'Cilia locally synthesize proteins to sustain their ultrastructure and functions.' *Nature Communications 2021 12:1*. Nature Publishing Group, 12(1) pp. 1–16.

Hartong, D., Berson, E. and Dryja, T. (2006) 'Retinitis pigmentosa.' *Lancet*, 368 pp. 1795–1809.

Harvey, S. A., Sealy, I., Kettleborough, R., Fenyes, F., White, R., Stemple, D. and Smith, J. C. (2013) 'Identification of the zebrafish maternal and paternal transcriptomes.' *Development (Cambridge)*. Development, 140(13) pp. 2703–2710.

Hashimoto, M., Shinohara, K., Wang, J., Ikeuchi, S., Yoshiba, S., Meno, C., Nonaka, S., Takada, S., Hatta, K., Wynshaw-Boris, A. and Hamada, H. (2010) 'Planar polarization of node cells determines the rotational axis of node cilia.' *Nature Cell Biology 2010 12:2*. Nature Publishing Group, 12(2) pp. 170–176.

Haycraft, C. J., Banizs, B., Aydin-Son, Y., Zhang, Q., Michaud, E. J. and Yoder, B. K. (2005) 'Gli2 and Gli3 Localize to Cilia and Require the Intraflagellar Transport Protein Polaris for Processing and Function.' *PLOS Genetics*. Public Library of Science, 1(4) p. e53.

Hentges, K. E., Nakamura, H., Furuta, Y., Yu, Y., Thompson, D. M., O'Brien, W., Bradley, A. and Justice, M. J. (2006) 'Novel lethal mouse mutants produced in balancer chromosome screens.' *Gene expression patterns : GEP*. Gene Expr Patterns, 6(6) pp. 653–665.

Hirokawa, N., Tanaka, Y., Okada, Y. and Takeda, S. (2006) 'Nodal Flow and the Generation of Left-Right Asymmetry.' *Cell*. Cell Press, 125(1) pp. 33–45.

Hoddges, P. E., Jackson, S. P., Brown, J. D. and Beggs, J. D. (1995) 'Extraordinary sequence conservation of the PRP8 splicing factor.' *Yeast*, 11(4) pp. 337–342.

Hoffman, J. I. E. and Kaplan, S. (2002) 'The incidence of congenital heart disease.' *Journal of the American College of Cardiology*. J Am Coll Cardiol, 39(12) pp. 1890–1900.

Hofmann, J. C., Husedzinovic, A. and Gruss, O. J. (2010) 'The function of spliceosome components in open mitosis.' *Nucleus*. Taylor & Francis, 1(6) p. 447.

Hoh, R. A., Stowe, T. R., Turk, E. and Stearns, T. (2012) 'Transcriptional Program of Ciliated Epithelial Cells Reveals New Cilium and Centrosome Components and Links to Human Disease.' *PLOS ONE*. Public Library of Science, 7(12) p. e52166.

Hor, C. H. and Goh, E. L. (2019) 'Small GTPases in hedgehog signalling: emerging insights into the disease mechanisms of Rab23-mediated and Arl13b-mediated ciliopathies.' *Current Opinion in Genetics & Development*. Elsevier Current Trends, 56, June, pp. 61–68.

Horani, A., Ferkol, T. W., Dutcher, S. K. and Brody, S. L. (2016) 'Genetics and biology of primary ciliary dyskinesia.' *Paediatric Respiratory Reviews*. W.B. Saunders, 18, March, pp. 18–24.

Hou, Y., Qin, H., Follit, J. A., Pazour, G. J., Rosenbaum, J. L. and Witman, G. B. (2007) 'Functional analysis of an individual IFT protein: IFT46 is required for transport of outer dynein arms into flagella.' *The Journal of cell biology*. J Cell Biol, 176(5) pp. 653–665.

Houde, C., Dickinson, R. J., Houtzager, V. M., Cullum, R., Montpetit, R., Metzler, M., Simpson, E. M., Roy, S., Hayden, M. R., Hoodless, P. A. and Nicholson, D. W. (2006) 'Hippi is essential for node cilia assembly and Sonic hedgehog signaling.' *Developmental biology*. Dev Biol, 300(2) pp. 523–533.

Huang, P. and Schier, A. F. (2009) 'Dampened Hedgehog signaling but normal Wnt signaling in zebrafish without cilia.' *Development (Cambridge, England)*. Company of Biologists, 136(18) p. 3089.

Huangfu, D. and Anderson, K. V. (2005) 'Cilia and Hedgehog responsiveness in the mouse.' *Proceedings of the National Academy of Sciences*. National Academy of Sciences, 102(32) pp. 11325–11330.

Huangfu, D., Liu, A., Rakeman, A. S., Murcia, N. S., Niswander, L. and Anderson, K. V. (2003) 'Hedgehog signalling in the mouse requires intraflagellar transport proteins.' *Nature*. Nature, 426(6962) pp. 83–87.

Huet, D., Blisnick, T., Perrot, S. and Bastin, P. (2014) 'The GTPase IFT27 is involved in both anterograde and retrograde intraflagellar transport.' *eLife*. Elife, 3(3).

Hyjek, M., Wojciechowska, N., Rudzka, M., Kołowerzo-Lubnau, A. and Smoliński, D. J. (2015) 'Spatial regulation of cytoplasmic snRNP assembly at the cellular level.' *Journal of Experimental Botany*. Oxford Academic, 66(22) pp. 7019–7030.

Ibañez-Tallon, I., Heintz, N. and Omran, H. (2003) 'To beat or not to beat: roles of cilia in development and disease.' *Human molecular genetics*. Hum Mol Genet, 12 Spec No 1(REV. ISS. 1).

Iomini, C., Li, L., Esparza, J. M. and Dutcher, S. K. (2009) 'Retrograde intraflagellar transport mutants identify complex A proteins with multiple genetic interactions in Chlamydomonas reinhardtii.' *Genetics*. Genetics, 183(3) pp. 885–896.

Ishikawa, T. (2017) 'Axoneme Structure from Motile Cilia.' *Cold Spring Harbor Perspectives in Biology*. Cold Spring Harbor Laboratory Press, 9(1).

Johnson, C. A. and Malicki, J. J. (2019) ‘The Nuclear Arsenal of Cilia.’ *Developmental Cell*.

Kathiriya IS, S. D. (200AD) ‘Left-right asymmetry and cardiac looping: implications for cardiac development and congenital heart disease - PubMed.’ *American Journal of Medical Genetics*, 97(4) pp. 271–279.

Kawasumi, A., Nakamura, T., Iwai, N., Yashiro, K., Saijoh, Y., Belo, J. A., Shiratori, H. and Hamada, H. (2011) ‘Left-right asymmetry in the level of active Nodal protein produced in the node is translated into left-right asymmetry in the lateral plate of mouse embryos.’ *Developmental biology*. Dev Biol, 353(2) pp. 321–330.

Keightley, M. C., Crowhurst, M. O., Layton, J. E., Beilharz, T., Markmiller, S., Varma, S., Hogan, B. M., De Jong-Curtain, T. A., Heath, J. K. and Lieschke, G. J. (2013) ‘In vivo mutation of pre-mRNA processing factor 8 (Prpf8) affects transcript splicing, cell survival and myeloid differentiation.’ *FEBS Letters*, 587(14) pp. 2150–2157.

Khanna, H. (2015) ‘Photoreceptor Sensory Cilium: Traversing the Ciliary Gate.’ *Cells*. Multidisciplinary Digital Publishing Institute (MDPI), 4(4) p. 674.

Kile, B. T., Hentges, K. E., Clark, A. T., Nakamura, H., Salinger, A. P., Liu, B., Box, N., Stockton, D. W., Johnson, R. L., Behringer, R. R., Bradley, A. and Justice, M. J. (2003) ‘Functional genetic analysis of mouse chromosome 11.’ *Nature*. Nature, 425(6953) pp. 81–86.

Kim, H. R., Richardson, J., van Eeden, F. and Ingham, P. W. (2010) ‘Gli2a protein localization reveals a role for Iguana/DZIP1 in primary ciliogenesis and a dependence of Hedgehog signal transduction on primary cilia in the zebrafish.’ *BMC Biology*. BioMed Central, 8, April, p. 65.

Kim, J. H., Ki, S. M., Joung, J.-G., Scott, E., Heynen-Genel, S., Aza-Blanc, P., Kwon, C. H., Kim, J., Gleeson, J. G. and Lee, J. E. (2016) ‘Genome-wide screen identifies novel machineries required for both ciliogenesis and cell cycle arrest upon serum starvation.’ *Biochimica et Biophysica Acta (BBA) - Molecular Cell Research*, 1863(6) pp. 1307–1318.

Kobayashi, T., Ishida, Y., Hirano, T., Katoh, Y. and Nakayama, K. (2021) ‘Cooperation of the IFT-A complex with the IFT-B complex is required for ciliary retrograde protein trafficking and GPCR import.’ *Molecular Biology of the Cell*. American Society for Cell Biology, 32(1) pp. 45–56.

Kozminski, K. G., Beech, P. L. and Rosenbaum, J. L. (1995) ‘The Chlamydomonas kinesin-like protein FLA10 is involved in motility associated with the flagellar membrane.’ *The Journal of cell biology*. J Cell Biol, 131(6 Pt 1) pp. 1517–1527.

Kozminski, K. G., Johnson, K. A., Forscher, P. and Rosenbaum, J. L. (1993) ‘A motility in the eukaryotic flagellum unrelated to flagellar beating.’ *Proceedings of the National Academy of Sciences of the United States of America*. Proc Natl Acad Sci U S A, 90(12) pp. 5519–5523.

Kramer-Zucker, A. G., Olale, F., Haycraft, C. J., Yoder, B. K., Schier, A. F. and Drummond, I. A. (2005) ‘Cilia-driven fluid flow in the zebrafish pronephros, brain and Kupffer’s vesicle is required for normal organogenesis.’ *Development*. The Company of Biologists Ltd, 132(8) pp. 1907–1921.

Krock, B. L. and Perkins, B. D. (2008) 'The intraflagellar transport protein IFT57 is required for cilia maintenance and regulates IFT-particle–kinesin-II dissociation in vertebrate photoreceptors.' *Journal of Cell Science*. The Company of Biologists, 121(11) pp. 1907–1915.

Lee, M. S., Hwang, K. S., Oh, H. W., Ji-Ae, K., Kim, H. T., Cho, H. S., Lee, J. J., Yeong Ko, J., Choi, J. H., Jeong, Y. M., You, K. H., Kim, J., Park, D. S., Nam, K. H., Aizawa, S., Kiyonari, H., Shioi, G., Park, J. H., Zhou, W., Kim, N. S. and Kim, C. H. (2015) 'IFT46 plays an essential role in cilia development.' *Developmental biology*. Dev Biol, 400(2) pp. 248–257.

Van Leeuwenhoek, A. (1932) 'Antony van Leeuwenhoek and his "Little Animals": being some Account of the Father of Protozoology and Bacteriology and his Multifarious Discoveries in these Disciplines.' *Nature 1932 130:3288*. Nature Publishing Group, 130(3288) pp. 679–680.

Lenhart, K. F., Lin, S. Y., Titus, T. A., Postlethwait, J. H. and Burdine, R. D. (2011) 'Two additional midline barriers function with midline lefty1 expression to maintain asymmetric Nodal signaling during left-right axis specification in zebrafish.' *Development*, 138(20) pp. 4405–4410.

Leventea, E., Hazime, K., Zhao, C. and Malicki, J. (2016) 'Analysis of cilia structure and function in zebrafish.' *Methods in Cell Biology*. Academic Press, 133, January, pp. 179–227.

Li, Y., Wei, Q., Zhang, Y., Ling, K. and Hu, J. (2010) 'The small GTPases ARL-13 and ARL-3 coordinate intraflagellar transport and ciliogenesis.' *The Journal of cell biology*. J Cell Biol, 189(6) pp. 1039–1051.

Lin, C. Y., Tsai, M. Y., Liu, Y. H., Lu, Y. F., Chen, Y. C., Lai, Y. R., Liao, H. C., Lien, H. W., Yang, C. H., Huang, C. J. and Hwang, S. P. L. (2017) 'Klf8 regulates left-right asymmetric patterning through modulation of Kupffer's vesicle morphogenesis and spaw expression.' *Journal of Biomedical Science*. BioMed Central Ltd., 24(1) pp. 1–14.

Linder, B., Dill, H., Hirmer, A., Brocher, J., Lee, G. P., Mathavan, S., Bolz, H. J., Winkler, C., Laggerbauer, B. and Fischer, U. (2011) 'Systemic splicing factor deficiency causes tissue-specific defects: a zebrafish model for retinitis pigmentosa†.' *Human Molecular Genetics*, 20(2) pp. 368–377.

Linder, B., Hirmer, A., Gal, A., Rüther, K., Bolz, H. J., Winkler, C., Laggerbauer, B. and Fischer, U. (2014) 'Identification of a PRPF4 Loss-of-Function Variant That Abrogates U4/U6.U5 Tri-snRNP Integration and Is Associated with Retinitis Pigmentosa.' Buratti, E. (ed.) *PLoS ONE*, 9(11) p. e111754.

Liu, C., Liu, W., Lu, M. F., Brown, N. A. and Martin, J. F. (2001) 'Regulation of left-right asymmetry by thresholds of Pitx2c activity.' *Development*, 128(11) pp. 2039–2048.

Liu, P., Wakamiya, M., Shea, M. J., Albrecht, U., Behringer, R. R. and Bradley, A. (1999) 'Requirement for Wnt3 in vertebrate axis formation.' *Nature genetics*. Nat Genet, 22(4) pp. 361–365.

Loges, N. T., Olbrich, H., Becker-Heck, A., Häffner, K., Heer, A., Reinhard, C., Schmidts, M., Kispert, A., Zariwala, M. A., Leigh, M. W., Knowles, M. R., Zentgraf, H., Seithe, H., Nürnberg, G., Nürnberg, P., Reinhardt, R. and Omran, H. (2009) 'Deletions and Point Mutations of LRRC50 Cause Primary Ciliary Dyskinesia Due to Dynein Arm Defects.' *The American Journal of Human Genetics*. Cell Press, 85(6) pp. 883–889.

Long, S., Ahmad, N. and Rebagliati, M. (2003) 'The zebrafish nodal-related gene southpaw is required for visceral and diencephalic left-right asymmetry.' *Development*, 130(11) pp. 2303–2316.

Lopes, S. S., Lourenço, R., Pacheco, L., Moreno, N., Kreiling, J. and Saúde, L. (2010) 'Notch signalling regulates left-right asymmetry through ciliary length control.' *Development*. The Company of Biologists, 137(21) pp. 3625–3632.

Lu, H., Toh, T., Narasimhan, V., Thamilselvam, S. K., Choksi, S. P. and Roy, S. (2015) 'A function for the Joubert syndrome protein Arl13b in ciliary membrane extension and ciliary length regulation.'

Lucas, J. S., Davis, S. D., Omran, H. and Shoemark, A. (2020) 'Primary ciliary dyskinesia in the genomics age.' *The Lancet Respiratory Medicine*. Lancet Publishing Group pp. 202–216.

Lunt, S. C., Haynes, T. and Perkins, B. D. (2009) 'Zebrafish ift57, ift88, and ift172 intraflagellar transport mutants disrupt cilia but do not affect hedgehog signaling.' *Developmental Dynamics*. John Wiley & Sons, Ltd, 238(7) pp. 1744–1759.

Mably, J. D., Mohideen, M. A. P. K., Burns, C. G., Chen, J. N. and Fishman, M. C. (2003) 'heart of glass regulates the concentric growth of the heart in zebrafish.' *Current biology : CB*. Curr Biol, 13(24) pp. 2138–2147.

Maeder, C., Kutach, A. K. and Guthrie, C. (2009) 'ATP-dependent unwinding of U4/U6 snRNAs by the Brr2 helicase requires the C terminus of Prp8.' *Nature Structural & Molecular Biology*, 16(1) pp. 42–48.

Mahaffey, J. P., Grego-Bessa, J., Liem, K. F. and Anderson, K. V. (2013) 'Cofilin and Vangl2 cooperate in the initiation of planar cell polarity in the mouse embryo.' *Development (Cambridge, England)*. Development, 140(6) pp. 1262–1271.

Malicki, J., Avanesov, A., Li, J., Yuan, S. and Sun, Z. (2011) 'Analysis of Cilia Structure and Function in Zebrafish.' *Methods in Cell Biology*. Academic Press, 101, January, pp. 39–74.

Marques, S., Borges, A. C., Silva, A. C., Freitas, S., Cordenonsi, M. and Belo, J. A. (2004) 'The activity of the Nodal antagonist Cerl-2 in the mouse node is required for correct L/R body axis.' *Genes & development*. Genes Dev, 18(19) pp. 2342–2347.

Maxwell, D. W., O'Keefe, R. T., Roy, S. and Hentges, K. E. (2021) 'The role of splicing factors in retinitis pigmentosa: links to cilia.' *Biochemical Society Transactions*. Biochem Soc Trans, 49(3) pp. 1221–1231.

McGrath, J., Somlo, S., Makova, S., Tian, X. and Brueckner, M. (2003) 'Two populations of node monocilia initiate left-right asymmetry in the mouse.' *Cell*. Cell Press, 114(1) pp. 61–73.

Medeiros De Campos-Baptista, M. I., Holtzman, N. G., Yelon, D. and Schier, A. F. (2008) 'Nodal signaling promotes the speed and directional movement of cardiomyocytes in zebrafish.' *Developmental Dynamics*. John Wiley & Sons, Ltd, 237(12) pp. 3624–3633.

Meno, C., Shimono, A., Saijoh, Y., Yashiro, K., Mochida, K., Ohishi, S., Noji, S., Kondoh, H. and Hamada, H. (1998) 'lefty-1 is required for left-right determination as a regulator of lefty-2 and nodal.' *Cell*. Cell, 94(3) pp. 287–297.

Meno, C., Takeuchi, J., Sakuma, R., Koshiba-Takeuchi, K., Ohishi, S., Saijoh, Y., Miyazaki, J. I., Ten Dijke, P., Ogura, T. and Hamada, H. (2001) 'Diffusion of nodal signaling activity in the absence of the feedback inhibitor Lefty2.' *Developmental cell*. Dev Cell, 1(1) pp. 127–138.

Mitchell, D. R. (2017) 'Evolution of Cilia.' *Cold Spring Harbor Perspectives in Biology*. Cold Spring Harbor Laboratory Press, 9(1) p. a028290.

Montague, T. G., Gagnon, J. A. and Schier, A. F. (2018) 'Conserved regulation of Nodal-mediated left-right patterning in zebrafish and mouse.' *Development*. The Company of Biologists, 145(24).

Mozaffari-Jovin, S., Wandersleben, T., Santos, K. F., Will, C. L., Luẖrmann, R. and Wahl, M. C. (2014) 'Novel regulatory principles of the spliceosomal Brr2 RNA helicase and links to retinal disease in humans.' *RNA Biology*. Taylor and Francis Inc., 11(4) pp. 298–312.

Mozaffari-Jovin, S., Wandersleben, T., Santos, K. F., Will, C. L., Lührmann, R. and Wahl, M. C. (2013) 'Inhibition of RNA Helicase Brr2 by the C-Terminal Tail of the Spliceosomal Protein Prp8.' *Science*, 341(6141) pp. 80–84.

Mukhopadhyay, S., Wen, X., Chih, B., Nelson, C. D., Lane, W. S., Scales, S. J. and Jackson, P. K. (2010) 'TULP3 bridges the IFT-A complex and membrane phosphoinositides to promote trafficking of G protein-coupled receptors into primary cilia.' *Genes & development*. Genes Dev, 24(19) pp. 2180–2193.

Nasevicius, A. and Ekker, S. C. (2000) 'Effective targeted gene "knockdown" in zebrafish.' *Nature genetics*. Nat Genet, 26(2) pp. 216–220.

Nemajerova, A., Kramer, D., Siller, S. S., Herr, C., Shomroni, O., Pena, T., Suazo, C. G., Glaser, K., Wildung, M., Steffen, H., Sriraman, A., Oberle, F., Wienken, M., Hennion, M., Vidal, R., Royen, B., Alevra, M., Schild, D., Bals, R., Dönitz, J., Riedel, D., Bonn, S., Takemaru, K. I., Moll, U. M. and Lizé, M. (2016) 'TAp73 is a central transcriptional regulator of airway multiciliogenesis.' *Genes and Development*. Cold Spring Harbor Laboratory Press, 30(11) pp. 1300–1312.

Nguyen, T. H. D., Galej, W. P., Bai, X. C., Oubridge, C., Newman, A. J., Scheres, S. H. W. and Nagai, K. (2016) 'CryoEM structure of the yeast U4/U6.U5 tri-snRNP at 3.7 Å resolution.' *Nature*. Europe PMC Funders, 530(7590) p. 298.

Nguyen, T. H. D., Li, J., Galej, W. P., Oshikane, H., Newman, A. J. and Nagai, K. (2013) 'Structural Basis of Brr2-Prp8 Interactions and Implications for U5 snRNP Biogenesis and the Spliceosome Active Site.' *Structure(London, England:1993)*. Elsevier, 21(6) p. 910.

NIH (2015) *Situs inversus | Genetic and Rare Diseases Information Center (GARD) – an NCATS Program*. [Online] [Accessed on 15th January 2022] https://rarediseases.info.nih.gov/diseases/4883/situs-inversus#ref_8997.

Noël, E. S., Verhoeven, M., Lagendijk, A. K., Tessadori, F., Smith, K., Choorapoikayil, S., Den Hertog, J. and Bakkers, J. (2013) 'A Nodal-independent and tissue-intrinsic mechanism controls heart-looping chirality.' *Nature Communications 2013 4:1*. Nature Publishing Group, 4(1) pp. 1–9.

Nonaka, S., Shiratori, H., Saijoh, Y. and Hamada, H. (2002) 'Determination of left–right patterning of the mouse embryo by artificial nodal flow.' *Nature 2002 418:6893*. Nature Publishing Group, 418(6893) pp. 96–99.

Nonaka, S., Tanaka, Y., Okada, Y., Takeda, S., Harada, A., Kanai, Y., Kido, M. and Hirokawa, N. (1998) 'Randomization of left-right asymmetry due to loss of nodal cilia generating leftward flow of extraembryonic fluid in mice lacking KIF3B motor protein.' *Cell*. Elsevier B.V., 95(6) pp. 829–837.

Nonaka, S., Yoshiba, S., Watanabe, D., Ikeuchi, S., Goto, T., Marshall, W. F. and Hamada, H. (2005) 'De Novo Formation of Left–Right Asymmetry by Posterior Tilt of Nodal Cilia.' *PLOS Biology*. Public Library of Science, 3(8) p. e268.

Norris, D. P. and Grimes, D. T. (2012) 'Cilia Discern Left from Right.' *Science*. American Association for the Advancement of Science, 338(6104) pp. 206–207.

Novarino, G., Akizu, N. and Gleeson, J. G. (2011) 'Modeling Human Disease in Humans: the Ciliopathies.' *Cell*. NIH Public Access, 147(1) p. 70.

Nozaki, S., Katoh, Y., Terada, M., Michisaka, S., Funabashi, T., Takahashi, S., Kontani, K. and Nakayama, K. (2017) 'Regulation of ciliary retrograde protein trafficking by the Joubert syndrome proteins ARL13B and INPP5E.' *Journal of Cell Science*. Company of Biologists Ltd, 130(3) pp. 563–576.

Ocaña, O. H., Coskun, H., Minguillón, C., Murawala, P., Tanaka, E. M., Galcerán, J., Muñoz-Chápuli, R. and Nieto, M. A. (2017) 'A right-handed signalling pathway drives heart looping in vertebrates.' *Nature*. Nature, 549(7670) pp. 86–90.

Odate, T., Takeda, S., Narita, K. and Kawahara, T. (2016) '9 + 0 and 9 + 2 cilia are randomly dispersed in the mouse node.' *Microscopy (Oxford, England)*. Microscopy (Oxf), 65(2) pp. 119–126.

Okada, Y., Nonaka, S., Tanaka, Y., Saijoh, Y., Hamada, H. and Hirokawa, N. (1999) 'Abnormal nodal flow precedes situs inversus in iv and inv mice.' *Molecular cell*. Mol Cell, 4(4) pp. 459–468.

Partridge, M., Vincent, A., Matthews, P., Puma, J., Stein, D. and Summerton, J. (1996) 'A simple method for delivering morpholino antisense oligos into the cytoplasm of cells.' *Antisense & nucleic acid drug development*. Antisense Nucleic Acid Drug Dev, 6(3) pp. 169–175.

Pazour, G. J., Agrin, N., Leszyk, J. and Witman, G. B. (2005) 'Proteomic analysis of a eukaryotic cilium.' *The Journal of cell biology*. J Cell Biol, 170(1) pp. 103–113.

Pazour, G. J., Baker, S. A., Deane, J. A., Cole, D. G., Dickert, B. L., Rosenbaum, J. L., Witman, G. B. and Besharse, J. C. (2002) 'The intraflagellar transport protein, IFT88, is essential for vertebrate photoreceptor assembly and maintenance.' *Journal of Cell Biology*. The Rockefeller University Press, 157(1) pp. 103–114.

Pazour, G. J., Dickert, B. L., Vucica, Y., Seeley, E. S., Rosenbaum, J. L., Witman, G. B. and Cole, D. G. (2000) 'Chlamydomonas IFT88 and its mouse homologue, polycystic kidney disease gene tg737, are required for assembly of cilia and flagella.' *The Journal of cell biology*. J Cell Biol, 151(3) pp. 709–718.

Pazour, G. J., Wilkerson, C. G. and Witman, G. B. (1998) 'A dynein light chain is essential for the retrograde particle movement of intraflagellar transport (IFT).' *The Journal of cell biology*. J Cell Biol, 141(4) pp. 979–992.

Pena, V., Liu, S., Bujnicki, J. M., Lührmann, R. and Wahl, M. C. (2007) 'Structure of a multipartite protein-protein interaction domain in splicing factor prp8 and its link to retinitis pigmentosa.' *Molecular cell*. Mol Cell, 25(4) pp. 615–624.

Pennekamp, P., Karcher, C., Fischer, A., Schweickert, A., Skryabin, B., Horst, J., Blum, M. and Dworniczak, B. (2002) 'The ion channel polycystin-2 is required for left-right axis determination in mice.' *Current biology : CB*. Curr Biol, 12(11) pp. 938–943.

Perrault, I., Halbritter, J., Porath, J. D., Gérard, X., Braun, D. A., Gee, H. Y., Fathy, H. M., Saunier, S., Cormier-Daire, V., Thomas, S., Attié-Bitach, T., Boddaert, N., Taschner, M., Schueler, M., Lorentzen, E., Lifton, R. P., Lawson, J. A., Garfa-Traore, M., Otto, E. A., Bastin, P., Caillaud, C., Kaplan, J., Rozet, J. M. and Hildebrandt, F. (2015) 'IFT81, encoding an IFT-B core protein, as a very rare cause of a ciliopathy phenotype.' *Journal of Medical Genetics*. BMJ Publishing Group Ltd, 52(10) pp. 657–665.

Pietrobono, S., Gagliardi, S. and Stecca, B. (2019) 'Non-canonical hedgehog signaling pathway in cancer: Activation of GLI transcription factors beyond smoothened.' *Frontiers in Genetics*. Frontiers Media S.A., 10(JUN) p. 556.

Pintado, P., Sampaio, P., Tavares, B., Montenegro-Johnson, T. D., Smith, D. J. and Lopes, S. S. (2017) 'Dynamics of cilia length in left–right development.' *Royal Society Open Science*. The Royal Society Publishing, 4(3).

Pinto, A. L., Rasteiro, M., Bota, C., Pestana, S., Sampaio, P., Hogg, C., Burgoyne, T. and Lopes, S. S. (2021) 'Zebrafish motile cilia as a model for primary ciliary dyskinesia.' *International Journal of Molecular Sciences*, 22(16) pp. 1–17.

Piperno, G., Siuda, E., Henderson, S., Segil, M., Vaananen, H. and Sassaroli, M. (1998) 'Distinct mutants of retrograde intraflagellar transport (IFT) share similar morphological and molecular defects.' *The Journal of cell biology*. J Cell Biol, 143(6) pp. 1591–1601.

Priya, S., Nampoothiri, S., Sen, P. and Sripriya, S. (2016) 'Bardet–Biedl syndrome: Genetics, molecular pathophysiology, and disease management.' *Indian Journal of Ophthalmology*. Wolters Kluwer -- Medknow Publications, 64(9) p. 620.

Qin, J., Lin, Y., Norman, R. X., Ko, H. W. and Eggenschwiler, J. T. (2011) 'Intraflagellar transport protein 122 antagonizes Sonic Hedgehog signaling and controls ciliary localization of pathway components.' *Proceedings of the National Academy of Sciences of the United States of America*. National Academy of Sciences, 108(4) pp. 1456–1461.

Ramsdell, A. F. (2005) 'Left–right asymmetry and congenital cardiac defects: Getting to the heart of the matter in vertebrate left–right axis determination.' *Developmental Biology*. Academic Press, 288(1) pp. 1–20.

Reiter, J. F. and Leroux, M. R. (2017) 'Genes and molecular pathways underpinning ciliopathies.' *Nature Reviews Molecular Cell Biology*.

Ritchie, D. B., Schellenberg, M. J., Gesner, E. M., Raithatha, S. A., Stuart, D. T. and MacMillan, A. M. (2008) 'Structural elucidation of a PRP8 core domain from the heart of the spliceosome.' *Nature Structural & Molecular Biology 2008 15:11*. Nature Publishing Group, 15(11) pp. 1199–1205.

Rivolta, C., McGee, T. L., Frio, T. R., Jensen, R. V., Berson, E. L. and Dryja, T. P. (2006) 'Variation in retinitis pigmentosa-11 (PRPF31 or RP11) gene expression between symptomatic and asymptomatic patients with dominant RP11 mutations.' *Human Mutation*, 27(7) pp. 644–653.

Roepman, R. and Wolfrum, U. (2007) 'Protein networks and complexes in photoreceptor cilia.' *Sub-cellular biochemistry*. Springer New York, 43, May, pp. 209–35.

Rohatgi, R., Milenkovic, L. and Scott, M. P. (2007a) 'Patched1 regulates hedgehog signaling at the primary cilium.' *Science*. American Association for the Advancement of Science , 317(5836) pp. 372–376.

Rohatgi, R., Milenkovic, L. and Scott, M. P. (2007b) 'Patched1 regulates hedgehog signaling at the primary cilium.' *Science*. American Association for the Advancement of Science , 317(5836) pp. 372–376.

Van Rooijen, E., Giles, R. H., Voest, E. E., Van Rooijen, C., Schulte-Merker, S. and Van Eeden, F. J. (2008) 'LRRC50, a Conserved Ciliary Protein Implicated in Polycystic Kidney Disease.' *Journal of the American Society of Nephrology : JASN*. American Society of Nephrology, 19(6) p. 1128.

Roy, S. (2009) 'The motile cilium in development and disease: emerging new insights.' *BioEssays*. John Wiley & Sons, Ltd, 31(7) pp. 694–699.

Růžičková, Š. and Staněk, D. (2017) 'Mutations in spliceosomal proteins and retina degeneration.' *RNA Biology*, 14(5) pp. 544–552.

Saijoh, Y., Oki, S., Ohishi, S. and Hamada, H. (2003) 'Left-right patterning of the mouse lateral plate requires nodal produced in the node.' *Developmental biology*. Dev Biol, 256(1) pp. 161–173.

Sambrooke, J. and Russel, D. (2001) 'Molecular cloning: a laboratory manual.' *In Molecular cloning: a laboratory manual*. 3rd ed., Cold Spring Harbor Laboratory Press, p. 2344.

Sampaio, P., Ferreira, R. R., Guerrero, A., Pintado, P., Tavares, B., Amaro, J., Smith, A. A., Montenegro-Johnson, T., Smith, D. J. and Lopes, S. S. (2014) 'Left-right organizer flow dynamics: how much cilia activity reliably yields laterality?' *Developmental cell*. Dev Cell, 29(6) pp. 716–728.

Satir, P. and Christensen, S. T. (2007) 'Overview of structure and function of mammalian cilia.' *Annual Review of Physiology*. Annual Reviews pp. 377–400.

Satir, P., Pedersen, L. B. and Christensen, S. T. (2010) 'The primary cilium at a glance.' *Journal of cell science*. J Cell Sci, 123(Pt 4) pp. 499–503.

Schellenberg, M. J., Wu, T., Ritchie, D. B., Fica, S., Staley, J. P., Atta, K. A., Lapointe, P. and Macmillan, A. M. (2013) 'A conformational switch in PRP8 mediates metal ion coordination that promotes pre-mRNA exon ligation.' *Nature structural & molecular biology*. Nat Struct Mol Biol, 20(6) pp. 728–734.

Scheuer, C., Boot, E., Carse, N., Clardy, A., Gallagher, J., Heck, S., Marron, S., Martinez-Alvarez, L., Masarykova, D., Mcmillan, P., Murphy, F., Steel, E., Ekdom, H. Van and Vecchione, H. (2012) 'Sensory functions of motile cilia and implication for bronchiectasis.' G. Balint, Antala, B., Carty, C., Mabieme, J.-M. A., Amar, I. B., and Kaplanova, A. (eds) *Frontiers in Bioscience - Scholar*. Frontiers in Bioscience, 4 S(3) pp. 1088–1098.

Schlacht, A., Mowbrey, K., Elias, M., Kahn, R. A. and Dacks, J. B. (2013) 'Ancient complexity, opisthokont plasticity, and discovery of the 11th subfamily of Arf GAP proteins.' *Traffic (Copenhagen, Denmark)*. Traffic, 14(6) pp. 636–649.

Schweickert, A., Vick, P., Getwan, M., Weber, T., Schneider, I., Eberhardt, M., Beyer, T., Pachur, A. and Blum, M. (2010) 'The nodal inhibitor Coco is a critical target of leftward flow in Xenopus.' *Current biology : CB*. Curr Biol, 20(8) pp. 738–743.

Sekimizu, K., Nishioka, N., Sasaki, H., Takeda, H., Karlstrom, R. O. and Kawakami, A. (2004) 'The zebrafish iguana locus encodes Dzip1, a novel zinc-finger protein required for proper regulation of Hedgehog signaling.' *Development (Cambridge, England)*. Development, 131(11) pp. 2521–2532.

Shah, A. S., Yehuda, B. S., Moninger, T. O., Kline, J. N. and Welsh, M. J. (2009) 'Motile cilia of human airway epithelia are chemosensory.' *Science (New York, N.Y.)*. Science, 325(5944) pp. 1131–1134.

Shaw, D. J., Eggleton, P. and Young, P. J. (2008) 'Joining the dots: Production, processing and targeting of U snRNP to nuclear bodies.' *Biochimica et Biophysica Acta (BBA) - Molecular Cell Research*. Elsevier, 1783(11) pp. 2137–2144.

Shi, L., Shi, X. and Shen, Y. (2018) 'Intraflagellar transport 46 (IFT46) is essential for trafficking IFT proteins between cilia and cytoplasm in Paramecium.' *Scientific Reports 2018 8:1*. Nature Publishing Group, 8(1) pp. 1–14.

Shinohara, K., Chen, D., Nishida, T., Misaki, K., Yonemura, S. and Hamada, H. (2015) 'Absence of Radial Spokes in Mouse Node Cilia Is Required for Rotational Movement but Confers Ultrastructural Instability as a Trade-Off.' *Developmental Cell*. Cell Press, 35(2) pp. 236–246.

Shinohara, K. and Hamada, H. (2017) 'Cilia in left–right symmetry breaking.' *Cold Spring Harbor Perspectives in Biology*, 9(10).

Shinohara, K., Kawasumi, A., Takamatsu, A., Yoshiba, S., Botilde, Y., Motoyama, N., Reith, W., Durand, B., Shiratori, H. and Hamada, H. (2012) 'Two rotating cilia in the node cavity are sufficient to break left-right symmetry in the mouse embryo.' *Nature Communications*, 3.

Shiratori, H. and Hamada, H. (2006) 'The left-right axis in the mouse: from origin to morphology.' *Development*. The Company of Biologists, 133(11) pp. 2095–2104.

Shoemark, A. and Harman, K. (2021) 'Primary Ciliary Dyskinesia.' *Seminars in Respiratory and Critical Care Medicine*, 42(4) pp. 537–548.

Smith, D. J., Montenegro-Johnson, T. D. and Lopes, S. S. (2014) 'Organized chaos in Kupffer's vesicle: How a heterogeneous structure achieves consistent left-right patterning.' *Ceased*. Taylor & Francis, 4(3) pp. 119–125.

Song, P. and Perkins, B. D. (2018) 'Developmental expression of the zebrafish Arf-like small GTPase paralogs arl13a and arl13b.' *Gene expression patterns : GEP*. NIH Public Access, 29, September, p. 82.

Song, Z., Zhang, X., Jia, S., Yelick, P. C. and Zhao, C. (2016) 'Zebrafish as a Model for Human Ciliopathies.' *Journal of Genetics and Genomics*. Elsevier, 43(3) pp. 107–120.

Stainier, D. Y. R., Lee, R. K. and Fishman, M. C. (1993) 'Cardiovascular development in the zebrafish. I. Myocardial fate map and heart tube formation.' *Development*. The Company of Biologists, 119(1) pp. 31–40.

Stephen, L. A. (2013) *Identification and characterisation of cardiac defects in mouse models isolated from a random chemical mutagenesis screen*. University of Manchester.

Stevens, S. W. and Abelson, J. (1999) 'Purification of the yeast U4/U6·U5 small nuclear ribonucleoprotein particle and identification of its proteins.' *Proceedings of the National Academy of Sciences of the United States of America*. National Academy of Sciences, 96(13) p. 7226.

Stevens, S. W., Barta, I., Ge, H. Y., Moore, R. E., Young, M. K., Lee, T. D. And Abelson, J. (2001) 'Biochemical and genetic analyses of the U5, U6, and U4/U6[bull]U5 small nuclear ribonucleoproteins from Saccharomyces cerevisiae.' *RNA*. Cambridge University Press, 7(11) pp. 1543–1553.

Stubbs, J. L., Oishi, I., Izpisúa Belmonte, J. C. and Kintner, C. (2008) 'The forkhead protein Foxj1 specifies node-like cilia in Xenopus and zebrafish embryos.' *Nature Genetics 2008 40:12*. Nature Publishing Group, 40(12) pp. 1454–1460.

Sturtevant, A. H. (1921) 'A Case of Rearrangement of Genes in Drosophila.' *Proceedings of the National Academy of Sciences of the United States of America*. National Academy of Sciences, 7(8) p. 235.

Sulik, K., Dehart, D. B., Inagaki, T., Carson, J. L., Vrablic, T., Gesteland, K. and Schoenwolf, G. C. (1994) 'Morphogenesis of the murine node and notochordal plate.' *Developmental Dynamics*. John Wiley & Sons, Ltd, 201(3) pp. 260–278.

Sullivan-Brown, J., Schottenfeld, J., Okabe, N., Hostetter, C. L., Serluca, F. C., Thiberge, S. Y. and Burdine, R. D. (2008) 'Zebrafish mutations affecting cilia motility share similar cystic phenotypes and suggest a mechanism of cyst formation that differs from pkd2 morphants.' *Developmental Biology*. Academic Press, 314(2) pp. 261–275.

Summerton, J. (1999) 'Morpholino antisense oligomers: the case for an RNase H-independent structural type.' *Biochimica et biophysica acta*. Biochim Biophys Acta, 1489(1) pp. 141–158.

Summerton, J., Stein, D., Huang, S. Ben, Matthews, P., Weller, D. and Partridge, M. (1997) 'Morpholino and phosphorothioate antisense oligomers compared in cell-free and in-cell systems.' *Antisense & nucleic acid drug development*. Antisense Nucleic Acid Drug Dev, 7(2) pp. 63–70.

Sun, Z., Amsterdam, A., Pazour, G. J., Cole, D. G., Miller, M. S. and Hopkins, N. (2004) 'A genetic screen in zebrafish identifies cilia genes as a principal cause of cystic kidney.' *Development*. The Company of Biologists, 131(16) pp. 4085–4093.

Sung, Y. H., Baek, I. J., Kim, Y. H., Gho, Y. S., Oh, S. P., Lee, Y. J. and Lee, H. W. (2016) 'PIERCE1 is critical for specification of left-right asymmetry in mice.' *Scientific Reports 2016 6:1*. Nature Publishing Group, 6(1) pp. 1–8.

Sung, Y. H., Kim, H. J. and Lee, H. W. (2007) 'Identification of a novel Rb-regulated gene associated with the cell cycle.' *Molecules and Cells*. The Korean Society for Molecular and Cellular Biology, 24(3) pp. 409–415.

Sztul, E., Chen, P. W., Casanova, J. E., Cherfils, J., Dacks, J. B., Lambright, D. G., Lee, F. J. S., Randazzo, P. A., Santy, L. C., Schürmann, A., Wilhelmi, I., Yohe, M. E. and Kahn, R. A. (2019) 'ARF GTPases and their GEFs and GAPs: concepts and challenges.' *Molecular Biology of the Cell*. American Society for Cell Biology, 30(11) p. 1249.

Takeda, S., Yonekawa, Y., Tanaka, Y., Okada, Y., Nonaka, S. and Hirokawa, N. (1999) 'Left-right asymmetry and kinesin superfamily protein KIF3a: New insights in determination of laterality and mesoderm induction by KIF3A(-/-) mice analysis.' *Journal of Cell Biology*. J Cell Biol, 145(4) pp. 825–836.

Tanaka, C., Sakuma, R., Nakamura, T., Hamada, H. and Saijoh, Y. (2007) 'Long-range action of Nodal requires interaction with GDF1.' *Genes & development*. Genes Dev, 21(24) pp. 3272–3282.

Tanaka, Y., Okada, Y. and Hirokawa, N. (2005) 'FGF-induced vesicular release of Sonic hedgehog and retinoic acid in leftward nodal flow is critical for left–right determination.' *Nature 2005 435:7039*. Nature Publishing Group, 435(7039) pp. 172–177.

Taschner, M. and Lorentzen, E. (2016) 'The Intraflagellar Transport Machinery.' *Cold Spring Harbor Perspectives in Biology*. Cold Spring Harbor Laboratory Press, 8(10).

Tian, T., Zhao, L., Zhao, X., Zhang, M. and Meng, A. (2009) 'A zebrafish gene trap line expresses GFP recapturing expression pattern of foxj1b.' *J. Genet. Genomics*, 36 p. 581589.

Tilley, A. E., Walters, M. S., Shaykhiev, R. and Crystal, R. G. (2015) 'Cilia dysfunction in lung disease.' *Annual review of physiology*. Annu Rev Physiol, 77, February, pp. 379–406.

Towns, K. V., Kipioti, A., Long, V., McKibbin, M., Maubaret, C., Vaclavik, V., Ehsani, P., Springell, K., Kamal, M., Ramesar, R. S., Mackey, D. A., Moore, A. T., Mukhopadhyay, R., Webster, A. R., Black, G. C. M., O'Sullivan, J., Bhattacharya, S. S., Pierce, E. A., Beggs, J. D. and Inglehearn, C. F. (2010) 'Prognosis for splicing factor PRPF8 retinitis pigmentosa, novel mutations and correlation between human and yeast phenotypes.' *Human Mutation*. Hum Mutat, 31(5) pp. E1361–E1376.

Tran, P. V., Haycraft, C. J., Besschetnova, T. Y., Turbe-Doan, A., Stottmann, R. W., Herron, B. J., Chesebro, A. L., Qiu, H., Scherz, P. J., Shah, J. V., Yoder, B. K. and Beier, D. R. (2008) 'THM1 negatively modulates mouse sonic hedgehog signal transduction and affects retrograde intraflagellar transport in cilia.' *Nature genetics*. Nat Genet, 40(4) pp. 403–410.

Tsang, S. H. and Sharma, T. (2018) 'Autosomal Dominant Retinitis Pigmentosa.' *In Atlas of Inherited Retinal Diseases. Advances in Experimental Medicine and Biology*. Springer New York LLC, pp. 69–77.

Tsao, C. C. and Gorovsky, M. A. (2008) 'Different effects of Tetrahymena IFT172 domains on anterograde and retrograde intraflagellar transport.' *Molecular biology of the cell*. Mol Biol Cell, 19(4) pp. 1450–1461.

Turner, I. A., Norman, C. M., Churcher, M. J. and Newman, A. J. (2006) 'Dissection of Prp8 protein defines multiple interactions with crucial RNA sequences in the catalytic core of the spliceosome.' *RNA*. Cold Spring Harbor Laboratory Press, 12(3) p. 375.

UCSC Genome Browser Gateway (2002) Genome Research. [Online] [Accessed on 10th January 2022] https://genome.ucsc.edu/cgi-bin/hgGateway.

Umen, J. G. and Guthrie, C. (1996) 'Mutagenesis of the yeast gene PRP8 reveals domains governing the specificity and fidelity of 3' splice site selection.' *Genetics*. Genetics, 143(2) pp. 723–739.

Verbakel, S. K., van Huet, R. A. C., Boon, C. J. F., den Hollander, A. I., Collin, R. W. J., Klaver, C. C. W., Hoyng, C. B., Roepman, R. and Klevering, B. J. (2018) 'Non-syndromic retinitis pigmentosa.' *Progress in Retinal and Eye Research*. Pergamon, 66, September, pp. 157–186.

Vierkotten, J., Dildrop, R., Peters, T., Wang, B. and Rüther, U. (2007) 'Ftm is a novel basal body protein of cilia involved in Shh signalling.' *Development*. The Company of Biologists, 134(14) pp. 2569–2577.

Vithana, E. N., Abu-Safieh, L., Allen, M. J., Carey, A., Papaioannou, M., Chakarova, C., Al-Maghtheh, M., Ebenezer, N. D., Willis, C., Moore, A. T., Bird, A. C., Hunt, D. M. and Bhattacharya, S. S. (2001) 'A Human Homolog of Yeast Pre-mRNA Splicing Gene, PRP31, Underlies Autosomal Dominant Retinitis Pigmentosa on Chromosome 19q13.4 (RP11).' *Molecular Cell*, 8(2) pp. 375–381.

Wahl, M. C., Will, C. L. and Lührmann, R. (2009) 'The spliceosome: design principles of a dynamic RNP machine.' *Cell*. Cell, 136(4) pp. 701–718.

Wang, Q., Pan, J. and Snell, W. J. (2006) 'Intraflagellar transport particles participate directly in cilium-generated signaling in Chlamydomonas.' *Cell*. Cell, 125(3) pp. 549–562.

Waseem, N. H., Vaclavik, V., Webster, A., Jenkins, S. A., Bird, A. C. and Bhattacharya, S. S. (2007) 'Mutations in the Gene Coding for the Pre-mRNA Splicing Factor, PRPF31 , in Patients with Autosomal Dominant Retinitis Pigmentosa.' *Investigative Opthalmology & Visual Science*, 48(3) p. 1330.

Watanabe, D., Saijoh, Y., Nonaka, S., Sasaki, G., Ikawa, Y., Yokoyama, T. and Hamada, H. (2003) 'The left-right determinant Inversin is a component of node monocilia and other 9+0 cilia.' *Development*. The Company of Biologists, 130(9) pp. 1725–1734.

Waters, A. M. and Beales, P. L. (2011) 'Ciliopathies: an expanding disease spectrum.' *Pediatric Nephrology (Berlin, Germany)*. Springer, 26(7) p. 1039.

Weber, G., Cristão, V. F., Santos, K. F., Jovin, S. M., Heroven, A. C., Holton, N., Lührmann, R., Beggs, J. D. and Wahl, M. C. (2013) 'Structural basis for dual roles of Aar2p in U5 snRNP assembly.' *Genes & Development*. Cold Spring Harbor Laboratory Press, 27(5) pp. 525–540.

Weber, G., Cristõo, V. F., Alves, F. de L., Santos, K. F., Holton, N., Rappsilber, J., Beggs, J. D. and Wahl, M. C. (2011) 'Mechanism for Aar2p function as a U5 snRNP assembly factor.' *Genes & Development*. Cold Spring Harbor Laboratory Press, 25(15) pp. 1601–1612.

Wheway, G., Nazlamova, L. and Hancock, J. T. (2018) 'Signaling through the primary cilium.' *Frontiers in Cell and Developmental Biology*. Frontiers Media S.A., 6(FEB) p. 8.

Wheway, G., Parry, D. A. and Johnson, C. A. (2014) 'The role of primary cilia in the development and disease of the retina.' *Organogenesis*. Landes Bioscience, 10(1) pp. 69–85.

Wheway, G., Schmidts, M., Mans, D. A., Szymanska, K., Nguyen, T.-M. T., Racher, H., Phelps, I. G., Toedt, G., Kennedy, J., Wunderlich, K. A., Sorusch, N., Abdelhamed, Z. A., Natarajan, S., Herridge, W., van Reeuwijk, J., Horn, N., Boldt, K., Parry, D. A., Letteboer, S. J. F., Roosing, S., Adams, M., Bell, S. M., Bond, J., Higgins, J., Morrison, E. E., Tomlinson, D. C., Slaats, G. G., van Dam, T. J. P., Huang, L., Kessler, K., Giessl, A., Logan, C. V., Boyle, E. A., Shendure, J., Anazi, S., Aldahmesh, M., Al Hazzaa, S., Hegele, R. A., Ober, C., Frosk, P., Mhanni, A. A., Chodirker, B. N., Chudley, A. E., Lamont, R., Bernier, F. P., Beaulieu, C. L., Gordon, P., Pon, R. T., Donahue, C., Barkovich, A. J., Wolf, L., Toomes, C., Thiel, C. T., Boycott, K. M., McKibbin, M., Inglehearn, C. F., Stewart, F., Omran, H., Huynen, M. A., Sergouniotis, P. I., Alkuraya, F. S., Parboosingh, J. S., Innes, A. M., Willoughby, C. E., Giles, R. H., Webster, A. R., Ueffing, M., Blacque, O., Gleeson, J. G., Wolfrum, U., Beales, P. L., Gibson, T., Doherty, D., Mitchison, H. M., Roepman, R. and Johnson, C. A. (2015) 'An siRNA-based functional genomics screen for the identification of regulators of ciliogenesis and ciliopathy genes.' *Nature Cell Biology*, 17(8) pp. 1074–1087.

Williams, C. L., Li, C., Kida, K., Inglis, P. N., Mohan, S., Semenec, L., Bialas, N. J., Stupay, R. M., Chen, N., Blacque, O. E., Yoder, B. K. and Leroux, M. R. (2011) 'MKS and NPHP modules cooperate to establish basal body/transition zone membrane associations and ciliary gate function during ciliogenesis.' *Journal of Cell Biology*. The Rockefeller University Press, 192(6) pp. 1023–1041.

Wolff, C., Roy, S., Lewis, K. E., Schauerte, H., Joerg-Rauch, G., Kirn, A., Weiler, C., Geisler, R., Haffter, P. and Ingham, P. W. (2004) 'iguana encodes a novel zinc-finger protein with coiled-coil domains essential for Hedgehog signal transduction in the zebrafish embryo.' *Genes & Development*. Cold Spring Harbor Laboratory Press, 18(13) pp. 1565–1576.

Wood, K. A., Eadsforth, M. A., Newman, W. G. and O'Keefe, R. T. (2021) 'The Role of the U5 snRNP in Genetic Disorders and Cancer.' *Frontiers in Genetics*. Frontiers, 12, January, p. 20.

Xu, M., Yang, L., Wang, F., Li, Huajin, Wang, X., Wang, W., Ge, Z., Wang, K., Zhao, L., Li, Hui, Li, Y., Sui, R. and Chen, R. (2015) 'Mutations in human IFT140 cause non-syndromic retinal degeneration.' *Human Genetics 2015 134:10*. Springer, 134(10) pp. 1069–1078.

Yin, J., Brocher, J., Fischer, U. and Winkler, C. (2011) 'Mutant Prpf31 causes pre-mRNA splicing defects and rod photoreceptor cell degeneration in a zebrafish model for Retinitis pigmentosa.' *Molecular neurodegeneration*, 6, July, p. 56.

Yokoyama, T., Copeland, N. G., Jenkins, N. A., Montgomery, C. A., Elder, F. F. B. and Overbeek, P. A. (1993) 'Reversal of left-right asymmetry: a situs inversus mutation.' *Science (New York, N.Y.)*. Science, 260(5108) pp. 679–682.

Yoshiba, S. and Hamada, H. (2014) 'Roles of cilia, fluid flow, and Ca2+ signaling in breaking of left–right symmetry.' *Trends in Genetics*. Elsevier, 30(1) pp. 10–17.

Yoshiba, S., Shiratori, H., Kuo, I. Y., Kawasumi, A., Shinohara, K., Nonaka, S., Asai, Y., Sasaki, G., Belo, J. A., Sasaki, H., Nakai, J., Dworniczak, B., Ehrlich, B. E., Pennekamp, P. and Hamada, H. (2012) 'Cilia at the node of mouse embryos sense fluid flow for left-right determination via Pkd2.' *Science (New York, N.Y.)*. Science, 338(6104) pp. 226–231.

You, Y., Huang, T., Richer, E. J., Schmidt, J. E. H., Zabner, J., Borok, Z. and Brody, S. L. (2004) 'Role of f-box factor foxj1 in differentiation of ciliated airway epithelial cells.' *American Journal of Physiology - Lung Cellular and Molecular Physiology*. American Physiological Society, 286(4 30-4) pp. 650–657.

Yu, X., Ng, C. P., Habacher, H. and Roy, S. (2008) 'Foxj1 transcription factors are master regulators of the motile ciliogenic program.' *Nature Genetics 2008 40:12*. Nature Publishing Group, 40(12) pp. 1445–1453.

Yuan, X., Cao, J., He, X., Serra, R., Qu, J., Cao, X. and Yang, S. (2016) 'Ciliary IFT80 balances canonical versus non-canonical hedgehog signalling for osteoblast differentiation.' *Nature Communications 2016 7:1*. Nature Publishing Group, 7(1) pp. 1–13.

Zhang, L., Shen, J., Guarnieri, M. T., Heroux, A., Yang, K. and Zhao, R. (2007) 'Crystal structure of the C-terminal domain of splicing factor Prp8 carrying retinitis pigmentosa mutants.' *Protein Science*. John Wiley & Sons, Ltd, 16(6) pp. 1024–1031.

Zhang, X., Jia, S., Chen, Z., Chong, Y. L., Xie, H., Feng, D., Wu, X., Song, D. Z., Roy, S. and Zhao, C. (2018) 'Cilia-driven cerebrospinal fluid flow directs expression of urotensin neuropeptides to straighten the vertebrate body axis.' *Nature Genetics 2018 50:12*. Nature Publishing Group, 50(12) pp. 1666–1673.

Zhao, C. and Malicki, J. (2007) 'Genetic defects of pronephric cilia in zebrafish.' *Mechanisms of Development*. Elsevier, 124(7–8) pp. 605–616.

Zhao, C., Omori, Y., Brodowska, K., Kovach, P. and Malicki, J. (2012) 'Kinesin-2 family in vertebrate ciliogenesis.' *Proceedings of the National Academy of Sciences of the United States of America*. Proc Natl Acad Sci U S A, 109(7) pp. 2388–2393.

Zhu, L., Belmont, J. W. and Ware, S. M. (2006) 'Genetics of human heterotaxias.' *European Journal of Human Genetics 2006 14:1*. Nature Publishing Group, 14(1) pp. 17–25.

Appendix 1 – Primer Sequences

Gene Name	Purpose	Species	Forward	Reverse
ARL13B	Amplification of ARL13B Exon 8-10	Human	CCACCGGGTAGAACCACTTA	AATGTCCCAGTTCACCTTGC
Prpf8	Amplification of Prpf8 mutation site	Mouse	CTCTGCCCCAACTACCTGAG	GACCTGCCAAGAAAGAGACG
MIT35	K27 genotyping	Mouse	AGTAACATGGAACATCGACGG	TGCTCAGCTCTGGAGTGCTA
Hnf3B	Hnf3B in situ	Mouse	CCTTCAACCACCCCTTCTCT	TTTCTCCTGGTCCGGTACAC
Gli2	Gli2 in situ	Mouse	CCCCCGGGATATTGTAGTCT	GGATACGCACATGTCTGTGG
Gli3	Gli3 in situ	Mouse	TGACCAAGGGGTAACAGGTC	GTATCCAGTTGTGGGCTGCT
Patched-1	Patched-1 in situ	Mouse	GGCGGTGGACGTTGGG	GGTCACACGAACAATGGGTCT
rps18	Housekeeping gene for loading control	Zebrafish	TGCAGAACCCTCGCCAGTACAA	ACGCAGACCCCAGAAGTGACG
arl13b	Amplification of ARL13B Exon 8-10	Zebrafish	GAAGAAGCAGCACCCAAAAG	GCCCGTGCTTGAAGATAAGA
southpaw	*southpaw* in situ	Zebrafish	TTGCGTGTGGATCGATAAAA	ACTCCTCCACGATCATGTCC
gli2	*gli2* in situ	Zebrafish	CCTCAGGTCCCAGAATGGTA	CGTTTGGCTGAACCATACCT
gli3	*gli3* in situ	Zebrafish	GGGATCTGAACCTCACTCCA	TACTCCCTCTTGGTGCTGCT
lefty1	*lefty1* in situ	Zebrafish	ATGTGCTGCAGGGAACAGTA	CCCGTGCTATATGCTCAAAA
patched-2	*patched-2* in situ	Zebrafish	TGCCTCCTCCTATGAACCAC	AACTTCCCAAAACAGCCAGA
prpf8	*cph* genotyping	Zebrafish	ATCCTGATCTACCCGCCTTC	ATCAATGGCTCGTCTGGTTC
tbx20	*tbx20* in situ	Zebrafish	CTTACTCCATCCGCCCTCG	TGGACTGATTTTGTTAACCACCG
FLAG_*arl13b*	Insertion of FLAG into N-term *arl13b* construct	Zebrafish	gatgatgataaaTTCAATCTGATGGCGAAC	atctttataatcCATTTCCCCCCTAAATGC
arl13b	Amplificaiton of full length *arl13b*	Zebrafish	CCCCAGTGAAAGCATTTAGG	GGGGTTGGGGAAGTAGAGGT
arl13b	Inverse primers for removal of exon9	zebrafish	ATTTCTATGGCAAACCTCTCC	CTGGCAGAGGAGGAGG
MYC	Amplificaiton of MYC for *arl13b* construct insertion	Zebrafish	gcaTCTAGATCGACGGTATCGCGATTTA	AaaCTCGAGGAGTCGAAATTCAAGTCCTC